School of Molecular and Life Sciences

Zn–based chalcogenide 1D semiconductor nanocrystals: synthesis and applications

Wei Chen

This thesis is presented for the Degree of
Doctor of Philosophy
of
Curtin University

September 2020

Declaration

To the best of my knowledge and belief this thesis contains no material previously published by any other person except where due acknowledgement has been made.

This thesis contains no material which has been accepted for the award of any degree or diploma in any university.

Signature:
Date: 8th September 2020

Abstract

Zinc–based chalcogenide semiconductor nanocrystals, including ZnS, ZnSe and ZnTe quantum dots are of great importance owing to their potential for optical, photoelectric and biomedical applications. The work in this thesis presented novel colloidal synthesis methods for high–quality ZnS and ZnSe nanoparticles with controlled crystal structure and morphology. The growth mechanisms of the uniform zero–dimensional (0D) ZnSe(S) nanodots and one–dimensional (1D) ZnSe(S) nanorods were elucidated. A novel heterostructure composed of Au noble metal tips and ZnSe nanorods in nanoscale was synthesized and the anisotropic growth nature between the Au nanoparticle domain and the ZnSe nanorods domain was revealed. The Au–tipped ZnSe nanorods were used as catalysts for H_2 evolution reaction (HER) by photocatalytic water splitting.

In the first part of the thesis in relation to my research project, a new hot–injection method for the facile shape and size control of ZnSe nanocrystals in a phosphine–free system was presented. By employing super hydride as reductant to tailor the activity of Se precursor, uniform ZnSe nanodots or nanorods with tunable diameter were obtained. A detailed investigation on the special role of super hydride in the phosphine–free synthesis of ZnSe nanocrystals was demonstrated, along with a proposed mechanism that was responsible for the formation of ZnSe nanodots and nanorods. By combing the calculated Gibbs free energies of the reaction between Se and super hydride and the experiment results, we concluded that selenium precursor in oleylamine can be reduced to Se_2^{2-} or Se^{2-} depending on the amount of super hydride added. With the increase of super hydride, Se^0 was reduced to Se_2^{2-} then Se^{2-}, and the reaction activity of different Se species are: $Se^{2-} > Se_2^{2-} > Se^0$. ZnSe nanodots of zinc blende phase were obtained if active Se^{2-} was employed as Se precursor, while ZnSe nanorods of wurtzite phase were obtained if less active Se_2^{2-} was employed as Se precursor.

In the second part of the thesis in relation to my research project, I developed a one–pot heat–up method for synthesis of ZnS, ZnSe and annoyed ZnS_xSe_{1-x} nanoparticles. Compared with the hot–injection method, this method has advantages such as higher production yields and feasible operation procedures. By adopting 1–dodecanethiol (DDT) as the co–ligand in combination with oleylamine (OLA) for the synthesis of ZnS, ZnSe and ZnS_xSe_{1-x} nanoparticles, I successfully synthesized monodisperse 1D ZnS, ZnSe and ZnS_xSe_{1-x} nanorods using the one–pot heat–up method. The studies of the effect of DDT on the synthesis of ZnSe, ZnS and ZnS_xSe_{1-x} nanorods indicated that DDT could improve the reaction activity of Se or S powder precursor in OLA and bind preferably on some facets of nanocrystals. This allows the

nanocrystals grow faster along other specific facets, leading to the formation of 1D nanorods. The control experiments in the absence of the DDT only produced nanodots using similar synthetic route. Au nanoparticles further selectively grew on the obtained ZnSe nanorods, constituting Au–ZnSe nanorods heterostructures with the Au nanoparticles being deposited on one tip, two tip and side facets of the ZnSe nanorods. Cation exchange reactions were further applied to Au–ZnSe nanorods to produce Ag_2S–ZnS heterostructures.

In the last part of the thesis in relation to my research project, we employed the synthesized ZnSe nanorods in the aforementioned heat–up method for Au–ZnSe hybrid nanorods growth and studied the performance of the hybrid nanorods in photocatalytic H_2 evolution reaction by water splitting. The research results showed that Au tips were found to grow on the apices of ZnSe NRs non–epitaxially to form an interface with no preference of orientation between Au (111) and ZnSe (001). Density functional theory (DFT) calculations reveal that the Au tips on ZnSe hybrid NRs gain enhanced adsorption of H compared to pristine Au, which favors the hydrogen evolution reaction. Photocatalytic tests reveal that the Au tips on ZnSe NRs effectively enhance the photocatalytic performance in hydrogen generation, in which the single Au–tipped ZnSe hybrid NRs show the highest photocatalytic hydrogen production rate of 437.8 $\mu mol \cdot h^{-1} \cdot g^{-1}$ in comparison with a rate of 51.5 $\mu mol \cdot h^{-1} \cdot g^{-1}$ for pristine ZnSe NRs. An apparent quantum efficiency of 1.3% for hydrogen evolution reaction for single Au–tipped ZnSe hybrid NRs was obtained, showing the potential application of this type of cadmium (Cd)–free metal–semiconductor hybrid NPs in solar hydrogen production. This work opens an avenue towards Cd–free hybrid nanoparticle (NP)–based photocatalysis for clean fuel production.

Acknowledgements

I would like to thank my supervisor Dr. Guohua Jia sincerely for his continues support and patient supervision, including offer and scholarship application, experiments operation guidance, data analysis, co–operation with other groups, manuscripts revising and so on. He has so much profound knowledge of chemistry and abundant research experiences in nanomaterials that he can always give me professional suggestions when I meet research problems in lab or get confused of experimental data. His great passion and energy in doing research also motivates me a lot to work in nano area.

I would like to express my appreciation to my supervisor Dr. Mark Buntine. He has given me a lot freedom to choose my research project during PhD. And when I met difficulty, he is always there to help me work out. His excellent qualification in research and project management ensured the smooth accomplishment of my PhD career step by step.

It's such a good experience to study overseas, especially in beautiful Perth, Australia. I would like to give my thanks to the lovely people I work with, Shaghraf, Fei Wang, Jiayi Chen and Rundong Mao, working in lab has much more fun when working with them. I will miss the common but unforgettable days we spent in lab, having lunch or tea together, with hearty laughter. I also want to express my thanks to my lovely housemates, Xiu and Mi, we met at the first beginning when I arrived in Perth, their smiles are as sunny as the sunshine in November, which warmed my heart a lot from home sickness. My thanks also go to all the friends I had fun with in Australia and China during my PhD study period.

I would like to express my sincere appreciation to the staff and students who gives me help when I need in School of Molecular and Life Sciences, Curtin Universit. I want to thank Dr. Ching Yong Goh, Grant Cope and Peter Chapman for their effective assistance in chemical ordering, experimental setup and UV–Vis, TGA analysis, Kelly Merigot, Dr. Aaron. Dodd, Veronica Avery, Dr. Jean–Pierrie Vedar and Dr. Zakaria Quadir from the Microscopy and Microanalysis Facility in the John de Laeter Centre for their assistance during TEM, XRD and XPS characterization. I would like to give my special thanks to the co–authors for their outstanding effort in the collaborative work, especially Xiaojie Li for his strong support in photocatalysis testing.

I want to acknowledge the scholarship from China Scholarship Committee and Curtin University, without the provided scholarship I would not even start PhD.

Last but not least, I would like to give my deepest thanks and love to my parents, my sister and great family, without them I can never enjoy so much happiness in my life. They always have

my back and give me endless love whenever and wherever. I would like to thank my Right Man, Yihe Wang for his love, accompany and support during the past years no matter when we are in China or Australia.

“Life is like a box of chocolates. You never know what you're gonna get.” (Forrest Gump)

As long as we see life as chocolate, we can always find the sweet part.

List of Publications and Presentations

Peer–reviewed journal articles

1. **Wei Chen**, Xiaojie Li, Fei Wang, Shaghraf Javaid, Yingping Pang, Jiayi Chen Zongyou Yin, Shaobin Wang, Yunguo Li, Guohua Jia, Non–epitaxial Gold–Tipped ZnSe Hybrid Nanorods for Efficient Photocatalytic Hydrogen Production, *Small* 2020, 16, 1902231
2. **Wei Chen**, Amir Karton, Tanveer Hussian, Shaghraf Javaid, Fei Wang, Yingping Pang and Guohua Jia, Spontaneous shape and phase control of colloidal ZnSe nanocrystals by tailoring Se precursor reactivity, *CrystEngComm*, 2019, 21, 2955
3. Shaghraf Javaid, **Wei Chen**, Guohua Jia, Franca Jones, Spontaneous Formation of a Hybrid Heterotrimer of Fe3O4–Ag2S–ZnS by Seeded–Growth Method. *Aust. J. Chem.*, 2020, in press. DOI: 10.1071/CH19545
4. Shaghraf Javaid, Xiaojie Li, Fei Wang, **Wei Chen**, Yingping Pang, Shaobin Wang, Guohua Jia, Franca Jones, Synthesis of magnetically separable Fe3O4–Au–CdS kinked heterotrimers incorporating plasmonic and semiconducting functionalities, *J. Mater. Chem. C*, 2019, 7(46): 14517–14524.
5. Yingping Pang, Md Nasir Uddin, **Wei Chen**, Shaghraf Javaid, Emily Barker, Yunguo Li, Alexandra Suvorova, Martin Saunders, Zongyou Yin, Guohua Jia, Colloidal Single–Layer Photocatalysts for Methanol–Storable Solar H2 Fuel. *Adv. Mater.* 2019, 31(49): 1905540.
6. Shaghraf Javaid, Yunguo Li, Dechao Chen, Xiaomin Xu, Yingping Pang, **Wei Chen**, Fei Wang, Zongping Shao, Martin Saunders, Jean–Pierre Veder, Guohua Jia, Franca Jone, Spontaneous Formation of Heterodimer Au–Fe7S8 Nanoplatelets by a Seeded Growth Approach, *J. Phys. Chem. C* 2019, 123, 10604–10613
7. Yingping Pang, Minyi Zhang, Dechao Chen, **Wei Chen**, Fei Wang, Shaghraf Javaid, Martin Saunders, Matthew R. Rowles, Lihong Liu, Shaomin Liu, Amit Sitt, Chunsen Li, Guohua Jia, Why Do Colloidal Wurtzite Semiconductor Nanoplatelets Have an Atomically Uniform Thickness of Eight Monolayers? *J. Phys. Chem. Lett.*2019, 10, 12, 3465–3471
8. Guohua Jia , Fei Wang , Mark Buntine , Minyi Zhang , **Wei Chen** , Shaghraf Javaid , Chunsen Li , Lai Chang Zhang , Xuyong Yang , Sheng Wang and Heng Yang, Atomically thin cadmium–free ZnTe nanoplatelets formed from magic–size nanoclusters, Nanoscale Advances (2020), In press, DOI: 10.1039/D0NA00409J

9. Ren Cai, Yaping Du, Dan Yang, Guohua Jia, Bowen Zhu, Bo Chen, Yifan Lyu, Kangfu Chen, Dechao Chen, **Wei Chen**, Lu Yang, Yuliang Zhao, Zhuo Chen, Weihong Tan, Free–standing 2D nanorafts by assembly of 1D nanorods for biomolecule sensing, *Nanoscale*, 2019, 11, 12169–12176
10. Aixiang Wang, Wenjie Wang, Jiayi Chen, Rundong Mao, Yingping Pang, Yunguo Li, **Wei Chen**, Dechao Chen, Derek Hao, Bing-Jie Ni, Martin Saunders, and Guohua Jia, Dominant Polar Surfaces of Colloidal II–VI Wurtzite Semiconductor Nanocrystals Enabled by Cation Exchange, *J. Phys. Chem. Lett*. 2020, 11, 13, 4990–4997

Oral presentations

- Spontaneous Shape and Phase Control of Colloidal ZnSe nanocrystal by tailoring Se precursor reactivity at the *20th International Union of Materials Research Societies International Conference in Asia (IUMRS)* Sep 2019, Perth, Australia.
- Non–epitaxial Gold–tipped ZnSe Hybrid Nanorods for Efficient Photocatalytic Hydrogen Production, 5 min flash presentation, *School of Molecular and Life Sciences, HDR symposium*, Dec 2019, Curtin University, Perth, Australia.

Poster presentations

- Selective Growth of Au onto ZnSe Nanorod Couples for photocatalysis Quantum Dots (QD) Jun 2018, 10th International Conference on Quantum Dots (QD 2018), Toronto, Canada
- Non–epitaxial Gold–tipped ZnSe Hybrid Nanorods for Efficient Photocatalytic Hydrogen Production, poster presentation, *School of Molecular and Life Sciences, HDR symposium*, Dec 2019, Curtin University, Perth, Australia.

Contents

List of Figures

List of Tables

List of Abbreviations

Definition	Abbreviation
Zero–dimensional	0D
One–dimensional	1D
Two–dimensional	2D
H2 evolution reaction	HER
1–dodecanethiol	DDT
Oleylamine	OLA
Octylamine	OA
Hexadecylamine	HDA
Trioctylphosphine	TOP
Trioctylphosphine oxide	TOPO
Diphenylphosphine	DPP
Thiophenol	SPH
Nanocrystals	NCS
Quantum dots	QDS
Valence band	VB
Conduction band	CB
Energy gap	EG
Density of electronic states	DOS
Zinc diethyl dithiocarbamate	$ZN(DDTC)_2$
Dodecylamine	DDA
Triphenyl phosphine	PPH_3
1–octadecene	ODE
Nanoplateles	NPLs
Wurtzite	WZ
Zinc blende	ZB
Octadecylamine	ODA
Transmission electron microscopy	TEM
Scanning electron microscope	SEM
Magic–sized clusters	MSCs
Selected area electron diffraction	SAED
High–angle annular dark–field scanning transmission electron microscopy	HAADF–STEM
Small–angle X–ray scattering	SAXS
Trioctylamine	TOA
Nanorods	NRs
Transmission electron microscopy	TEM
High–resolution transmission electron microscopy	HRTEM
Fast Fourier transform	FFT
Density functional theory	DFT
Scanning transmission electron microscope	STEM
Energy dispersive X–ray	EDX
Didodecyldimethylammoniumbromide	DDAB
Normal hydrogen electrode	NHE
Mercaptoundecanoic acid	MUA
2–mercaptoethanesulfonic acid	MSA

Mercaptopropionic acid	MPA
Polyethylenimine	PEI
Poly(styrene–co–maleic anhydride)	PSMA
Thermal gravimetric analysis	TGA
X–ray Diffraction	XRD
X–ray photoelectron spectroscopy	XPS
Inductively coupled plasma mass spectrometry	ICP–MS
Photoluminescent	PL
Ultraviolet–visible spectroscopy	UV–Vis
photodynamic therapy	PDT
reactive oxygen species	ROS

Chapter 1. Thesis Overview

1.1 Background

One–dimensional (1D) semiconductor nanorods have remarkable electronic properties such as narrow fluorescence, low lasing threshold and ultrafast exciton dynamics. As the benchmark materials with two–dimensional quantum confinement effect, CdX (X=Se, S and Te) nanorods were widely studied as light emitting diode[1–3], and photo catalyst for H_2 generation [4, 5]. Following the pioneer work of Peng et al. on the first synthesis of CdSe nanorods,[6] the synthetic approaches of uniform CdX (X=Se, S and Te) nanorods are greatly developed.[7, 8] On the other hand, controlled synthesis of monodisperse ZnX (X=Se, S and Te) nanorods is still a challenge. A few studies reported the successful control of shape and phase of one–dimensional ZnSe nanorods[9–13] and ZnS nanorods[14–16] in which the synthetic procedures involve tedious steps and are not easy to control. Some of them used toxic and expensive ligand such as TOP (trioctylphosphine), TOPO (trioctylphosphine oxide), diphenylphosphine (DPP), thiophenol (SPh) which are not "green" and not convenient to handle during syntheses.

As a very important representative of II–VI nanomaterials, Zn–based nanocrystals have received tremendous attention due to their wide band gap and non–toxicity, as well as their applications in bio–imaging, sensor, photovoltaics and photocatalytic H_2 energy evolution. The successful synthesis of ZnS, ZnSe nanorods and nanodots with controlled shape and size alongside their growth mechanisms laid a firm foundation for their stimulation applications.

In addition, metal–semiconductor hybrid nanoparticles combining separate components in a single nano–object have remarkable optical and electronic properties, and find promising applications in optoelectronics, photocatalysis and biomedicine. As benchmark catalysts, cadmium (Cd)–based hybrid nanoparticles have been extensive investigated for photocatalytic H_2 production through water splitting. However, the high toxicity and the carcinogenicity of Cd–based materials is the main obstacle that restricts their widespread applications. In this sense, Cd–free hybrid nanoparticles possessing photocatalytic performance comparable to Cd–based hybrid materials are highly demanded and of significant importance. Zinc–based semiconductor nanocrystals are less or non–toxic and environmental–friendly. These merits make them potential alternatives to the Cd–based materials in photocatalysis and biomedical applications.

1.2 Research objectives

The aim of this research is to develop facile and effective approaches to synthesize Zn–chalcogenide nanoparticles with controlled size, crystal structure, morphology, including 0–0D nanodots and 1D nanorods, and expand these nanomaterials to hybrid nanomaterials, such as noble metal–semiconductor hybrids. The studies on the growth mechanism of Zn–chalcogenide nanoparticles and hybrid nanoparticles are highlighted. The potential of the obtained hybrid nanoparticles like Au–ZnSe hybrid nanorods for clean fuel H_2 generation is also investigated and evalutated. The special objectives of the project are listed below.

a) Summarize the progress and challenges on Zn–chalcogenide nanoparticles synthesis, especially for 1D nanorods synthesis, use noble metal–semiconductor, such as Au–CdSe or Pt–CdS heterostructures as photocatalysts to investigate their potential in photocatalytic water splitting.
b) Develop effective colloidal hot–injection methods for the synthesis of ZnSe nanodots or nanorods. Study the effect of precursor activity on the crystal structure, phase and morphology by using Se precursor with diverse activity.
c) Develop general heat–up methods to synthesize ZnSe, ZnS and ZnS_xSe_{1-x} nanorods and study the synthetic conditions that affect the nanoparticle morphology.
d) Selectively grow noble metal (Au) nanoparticles on the obtained ZnSe, ZnS and ZnS_xSe_{1-x} nanorods.
e) Use the synthesized Au–ZnSe hybrid nanorods as photocatalysts towards hydrogen production through water splitting.

1.3 Thesis organization

The thesis has 7 chapters.

Chapter 1 is the introduction of the thesis, which includes a brief introduction of zinc chalcogenides and zinc chalcogenide hybrid nanoparticles alongside the research objectives.

Chapter 2 is the literature review, which includes four major parts. Part 1 introduces the basic physical and chemical properties of zinc chalcogenide nanoparticles. Part 2 reviews the main colloidal synthetic approaches of ZnS, ZnSe and ZnTe nanoparticles, includes 0D nanodots, 1D nanowires or nanorods and 2D nanosheet or nanoplatelets. Part 3 focuses on the synthesis of noble metal, such as Au and Pt hybridized II–VI semiconductor nanomaterials. Considering that there were only very limited research reports on Au/Pt– zinc chalcogenide (ZnS, ZnSe or ZnTe), I expanded this topic to cadmium chalcogenide nanoparticles as they all belong to II–

VI semiconductors. The application of these hybrid nanomaterials is summarized in the final part, which includes photocatalytic pollute degradation and H_2 generation, as well as reactive oxygen species in biomedical area.

Chapter 3 details the information of facilities used for nanoparticles synthesis and characterization in this work, which involves an introduction of experimental set–up, Schleck line, glove box and analysis equipment such as TEM, XRD, XPS, ICP and TGA.

Chapter 4–6 is the research outputs based on aforementioned research objectives.

Chapter 4 and 5 focus on developing facile synthesis approaches for Zn–chalcogenide nanoparticles, including the hot–injection method and the one–pot heating–up method. Chapter 6 studied the growth of noble metal Au onto ZnSe nanorods and their performance on photocatalytic H_2 evolution reaction.

Specifically, chapter 4 reports a novel hot–injection method developed in this work for controlled synthesis of ZnSe nanoparticles. As the new founding is published on Royal Chemical Society (2019), we reused the main manuscript (Spontaneous shape and phase control of colloidal ZnSe nanocrystals by tailoring Se precursor reactivity) and the Supporting Information with some modification as the main part of Chapter 4.

Chapter 5 introduces a one–pot heat–up method for the synthesis of ZnSe, ZnS and $ZnSe_xS_{1-x}$ nanorods and nanodots, in which I found that the proper choice of ligand like oleylamine and dodecanethiol has significant influence on the final morphology and crystal phase of the obtained nanoparticles. A manuscript in relation to this research finding is being prepared and will be submitted for publication shortly.

Chapter 6 is based on the objective of photocatalytic application study. As the research finding is published on Wiley (2019), we reused the main manuscript (Non–Epitaxial Gold–Tipped ZnSe Hybrid Nanorods for Efficient Photocatalytic Hydrogen Production) and supporting information with some modification as the main part of Chapter 6.

Chapter 7 is the conclusion of the research projects and recommendation for readers.

The appendix A is Copyright and Permission for reusing figures in published articles.

Appendix B is the statement of contribution to Co–authored paper, which refer to Chapter 4 and Chapter 6.

Appendix C, D, E is supporting information for Chapter 4, Chapter 5 and Chapter 6.

Chapter 2. Literature review

2.1 Introduction

Colloidal semiconductor nanocrystals (NCs) constituted of hundreds to thousands of atoms are also named as "quantum dots (QDs)" or "artificial atoms" because these nanoparticles build the bridge between molecules and bulk materials. The size of colloidal semiconductor nanocrystals is usually within 100 nm (typically less than 10 nm in diameter) in at least one dimension. Organic surfactants serve as passivating ligands, which stabilize the tiny nanoparticles from aggregation in spite of their high surface energy. Since the early report from A Henglein[1] in 1982 and a later report from R. Rossetti and L. E. Brus *et al.* [2] of the successful synthesis of CdS semiconductor QDs with a diameter of 4.5 nm in aqueous solution in 1983, massive research has been conducted on the study of the novel and unique optoelectronic properties and applications of these quantum size nanoparticles.

As one of the most unique characteristic, the quantum confinement effects of colloidal semiconductor nanoparticles attracted extensive attention. To be specific, the bandgap of semiconductor nanocrystals is size–dependent and can be tailored when the size of nanoparticles is smaller than or comparable with the Borh radius of the semiconductor materials. For example, when the size of QDs decreases, the bandgap gets larger and the energy levels becomes discrete which results in the change of their electric and optical properties[3, 4]. Owing to these excellent optical and electronic properties[5], such as size–dependent wavelength absorption and emission, good stability and high luminescent quantum efficiency, colloidal semiconductor nanocrystals find many applications in light emitting diode (LED),[6, 7] photocatalysts,[8–10] and photodetector[11,12], biomedical imaging probe[13, 14] and cancer treatment[15].

The most common colloidal semiconductor NCs can be simply classified into several types based on their compositions, such as II–VI semiconductor NCs (CdSe, CdS, CdTe, ZnSe, ZnS, ZnTe),,[16] III–V semiconductor NCs (InP, GaAs, InAs), [17] I–III–VI semiconductor NCs ($CuInS_2$ or $AgInS_2$), [18] IV–VI semiconductor NCs (PbSe, PbS, or PbTe),[19] , or single element group IV element semiconductor (Si, C, or Ge and oxide semiconductor like TiO_2),[20 21]. The growth of another component onto the initial semiconductor QDs forms hybrid semiconductor nanoparticles, such as CdSe/ZnS[22], CdSe/CdS[23] core/shell nanorods and Pt–CdSe[24]

nanoplatelets, which expands the palette of hybrid nanoparticles and provides a solid basis for their stimulating applications.

Other than element–based classification, the semiconductor nanoparticles could be also classified based on the quantum confinement in different dimensions. To be specific, QDs could be classified into three classes, including zero–dimensional (0D) spherical dots, one–dimensional (1D) nanorods or nanowires and two–dimensional (2D) nanoplates or nanoplatelets. For 0D spherical dots, the diameter of these nanoparticles are smaller than the material's Borh radius which means the excitons are confined in three dimensions. In 1D nanocrystals such as nanowires or nanorods, the electrons and holes are confined in two dimensions except for the length directions. For 2D nanocrystals such as nanoplates, nanofilms or nanoplatelets, the excitons are only exhibits confined in one dimension, namely the thickness direction [25, 26]. It is well known that the energy levels of semiconductor bulk materials consist two continuous bands, a fully occupied lower valence band (VB) and a higher empty conduction band (CB). The vacancy energy level between VB and CB forms an energy gap (E_g), also known as bandgap. A schematic diagram on the quantum confined nanoparticles is shown as **Figure 2.1**. As seen in **Figure 2.1**, the energy band structures changes from continuous to discrete energy levels and the bandgap increases as the size of QDs decreases. Due to these unique characteristics, semiconductor nanocrystals have interesting size and shape dependent optical and electronic properties.

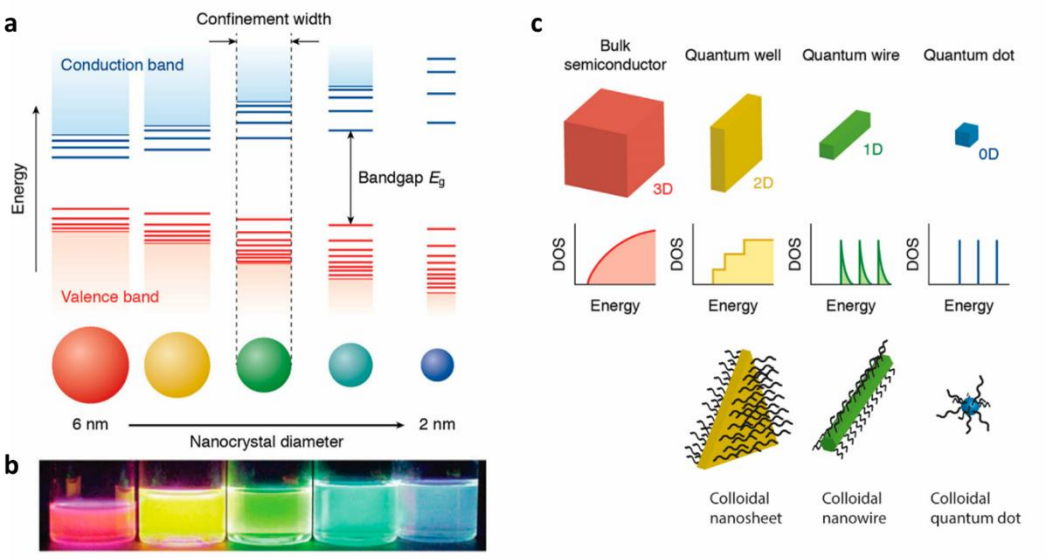

Figure 2.1 (a) Schematic illustration of quantum confinement effects of NCs. (b) Photos of CdSe NCs with varied size dispersed organic solutions (e.g. toluene) under UV irradiation. (c) Schematic illustration of typical morphology and the energy level structure of 3D (bulk), 2D, 1D and 0D semiconductor NCs.[25]

Group II–VI semiconductor nanomaterial is an important part of semiconductor nanomaterials. As the earliest studied quantum dots, Cd–based II–VI semiconductor nanoparticles like CdSe and CdS are extensively and thoroughly studied in term of syntheses, properties and applications. Uniform nanodots, nanorod or nanowires and thin nanoplatelets are successfully synthesized by various synthetic approaches, while on the other side, Zn–based semiconductor nanocrystals gained less progress on synthesis and application because of the difficulties in synthesizing these nanocrystals. Even though Zn–based II–VI semiconductor nanoparticles are less studied than Cd–based nanoparticles in the past decades, the advantages of Zn–based chalcogenide nanoparticles, such as heavy metal–free, environmental friendly and earth abundant make them great potential for a wide range of applications. Therefore developing new synthetic approaches that are capable of producing size and shape controlled zinc chalcogenide nanocrystals is a worthwhile research project.

2.2 Fundamental characteristics of Zn–chalcogenide semiconductor materials: ZnS, ZnSe and ZnTe

ZnS, ZnSe and ZnTe are typical Cd–free II–VI semiconductor materials. As one of the earliest found semiconductor material, bulk ZnS has a wide band gap of 3.7 eV.[27] From the aspect of crystallography, there are two main crystalline forms of ZnS, namely zinc blende (ZB) structure and wurtzite (WZ) structure. Bulk ZnS with zinc blende structure is more stable at low temperature while at elevated temperature (~1020°C), it could transfer to wurtzite structure.[28] **Figure 2.2** depicts these two different crystal structures., For zinc blende phase is based on a face–centred cubic (fcc) stacking, with Zn and S atoms tetrahedrally coordinated and stacked in a ABCABC pattern. [29] While for a wurtzite structure, the atoms are stacked hexagonally in a ABABAB pattern.[30] **Table 2.1** listed the crystal structure parameter details about the space group, lattice constant of ZnS, ZnSe and ZnTe of both zinc blende and wurtzite structures.[31, 32]

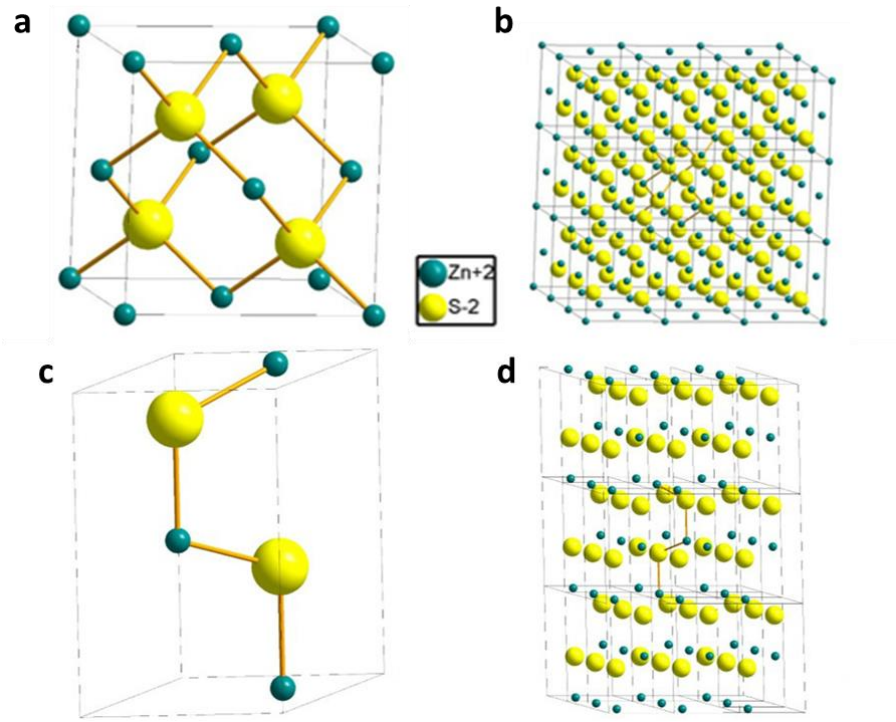

Figure 2.2 A schematic diagram of ZnS of zinc blende and wurtzite structures. (a) A single unit cell of zinc blende ZnS; (b) 3x3x3 lattice of zinc blende ZnS; (c) A single unit cell of wurtzite ZnS; (d) 3x3x3 lattice of wurtzite ZnS.

Table 2.1 Crystal structure parameters of ZnS, ZnSe and ZnTe

	Structure	Space Group	Lattice constant
ZnS	zinc blende	Z = 4, F4–3 m	a = b = c = 5.41 Å
	wurtzite	Z = 2, P63mc	a = b = 3.81 Å, c = 6.23 Å,
ZnSe	zinc blende	Z = 4, F4–3 m	a = b = c = 5.65 Å
	wurtzite	Z = 2, P63mc	a = b = 3.99 Å, c = 6.63 Å
ZnTe	zinc blende	Z = 4, F4–3 m	a = b = c = 6.07 Å
	wurtzite	Z = 2, P63mc	a = b = 4.32 Å, c = 6. Å

The bandgap structures of ZnS, ZnSe and ZnTe were shown in **Figure 2.3**. The wide bandgap enables ZnS semiconductor nanoparticles absorb ultraviolet (UV)–light which makes it good candidate for UV–based devices such as UV light detector or electroluminescence device. Zinc selenide (ZnSe), with similar properties to ZnS in the aspect of crystal structure, has narrower band gap compared with ZnS (3.54 eV for ZB, 3.91 eV for WZ). For bulk ZnSe, the band gap of ZnSe is 2.72 eV.[33, 34] When size is tuned down to the nanoscale, the bandgap of ZnSe quantum dots enlarged, which make its absorption covers a spectral range from 350nm to 450 nm due to the quantum confinement effect. Zinc blende ZnTe has narrowest band gap of 2.26 eV among these three zinc–based chalcogenide semiconductors.[34] For ZnSe and ZnS

nanocrystals, it's quite stable at ambient environment while ZnTe nanocrystals is very sensitive to air because they could be oxidized to form Te metal easily.

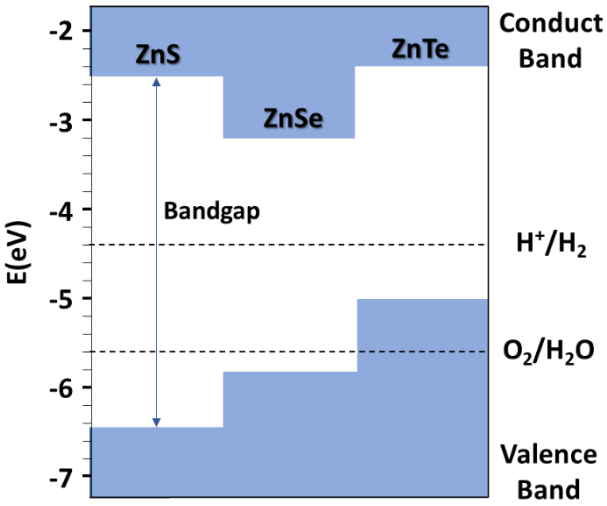

Figure 2.3 Schematic of band structures of ZnS, ZnSe and ZnTe.

2.3 The development of colloidal synthesis of Zn based II–VI quantum dots

For colloidal semiconductor synthesis, hot–injection method [35, 36] and heat–up method [37, 38] are widely reported in the controlled growth of nanoparticle. In the past decades, uniform nanoparticles have been synthesized by hot–injection method in which a precursor solution is injected into another precursor solution or solvent at elavated temperature. The classic nucleation and growth mechanism theory indicates that the decreasing of the temperature due to the room–temperature precursor injection can help separate the nucleation stage and crystal growth stage which is conventionally considered beneficial for the formation of homogeneous colloidal nanoparticles.

In a one–pot heat–up synthesis approach, all chemical precursors are mixed together with solvent and ligand at the firstly beginning and heated up to a pre–determined temperature. This method is quite straightforward comparing with a hot–injection method because no further addition of a second precursor is required. The obvious superiority of the heat–up method is the operation convenience and the reliability on synthesizing nanomaterials on a large scale while the drawback is that the formed nanoparticles are not as uniform as the nanoparticles prepared by the hot–injection method because of the less control on the crystal nucleation stage and growth stage.

Bases on the classic LaMer model, ideally, the formation of nanocrystal could be separated into three stages including monomers formation, nucleation and growth process, as shown in

Figure. 2.4a. [39] At first stage I, the monomer concentration increases gradually as the reaction evolves until a point of supersaturation (S) is obtained. In the next stage II, the supersaturation finally achieves a critical value (Sc), which provides enough energy for the system to overcome the energy barrier of nucleation. Thus, homogeneous nucleation throughout the entire reaction solution can be found at the stage II. As a result of fast nucleation process, the monomers are massively consumed which leads to the monomer concentration decreased rapidly below the critical value. Ttherefore the entire system enters into the stage III. At final stage III, no new nuclei formed but nuclei formed at stage II grow simultaneously into large nanoparticles. [39, 40]

For the hot injection method, after the rapid injection of organometallic reagents (precursor) into a hot solvent, the concentration of monomers increased rapidly and reached the critical value of Sc which caused the simultaneous nucleation. As the nucleation consumed monomers, the remaining supersaturation value decreased below Sc, thus the nucleation step was stopped and the growth step started. Because the nuclei's growth progress is similar, the nanoparticles will end up with an exceptionally narrow size distribution.

As for the heat–up method, all chemicals are put in the reactor together, the monomer concentration continuously increased along with the heating up stage. After it reaches the critical value of Sc, the nucleation procedure occurred followed by the later growth of nuclei, as seen in Figure. 2.4b.[37] The distinct difference between the hot–injection method and the heat–up method is the burst nucleation induced by the hot injection.

Some new methods or reactors were also developed and reported on zinc based nanoparticle synthesis. For example, Guidelli *et al.* [41] developed a novel continuous–flow microfluidic reactor for ZnSe nanodots synthesis wherein the low temperature (160 °C) at the beginning part of the fluid could lead to nucleation and the later part with a higher temperature (340 °C) helped ZnSe nanocrystals growth. This new approach is capable of synthesizing large amount nanocrystals.

A typical set–up of colloidal nanoparticles synthesis by the hot–injection method involves a three–neck flask in which the precursor is injected into a solvent at an elevated temperature. The heat–up synthesis could also use the same set–up as that for the hot injection method except all chemicals are put in the reacting flask together at the first beginning of the synthesis and no further injection is needed.

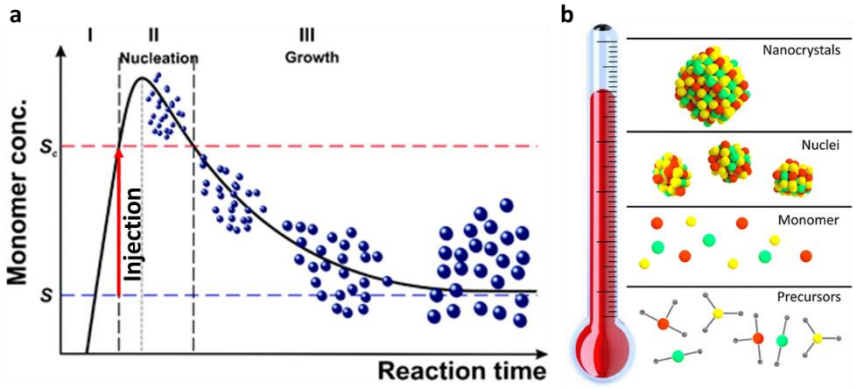

Figure 2.4 (a) Schematic illustration of the nucleation and growth stage for the synthesis of nanocrystals according to the LaMer model. The red arrow shows the concentration increase by a hot injection of precursor.[39] (b) Schematic illustration of a typical heat–up synthesis. The precursors are stable at room temperature, as the temperature increases, the cation and anion precursors react with each other to generate monomers then nucleate to form small nuclei, which eventually grow into nanoparticles.[37]

2.3.1 ZnS quantum dots synthesis

2.3.1.1 0D ZnS spherical dots and 1D ZnS nanorods or nanowires.

In the past decades, much research has been done on the controlled synthesis of 0D ZnS spherical dots and 1D nanorods or nanowires. The first report on synthesis of ZnS spherical dots dated back to 1985 when R. Rossetti and and L. E. Brus *et al.* [42] synthesized ZnS spherical dots with a diameter of 1.5~3 nm in water and methanol at a very low temperature (–77 °C) by using Na_2S and $Zn(ClO_4)_2$ as the precursors. This research finding initiated the synthesis methods study of ZnS semiconductor quantum dots. Later on, the research focused more on developing mild experimental conditions for synthesis, such as mild temperatures, extended choice of surface coating ligands or precursor chemicals for replacement of unstable $Zn(ClO_4)_2$.

Ligand controlled growth.

Ligands play multiple roles during the nanoparticle nucleation and growth ranging from the regulation of the solubility and activity of precursor preparation to the guidance of growth orientation for crystals morphology-controlled growth. For instance, the binding energy between ligand and different facets of the nucleus is different. After the form of the nuclei, the remaining monomers in the solution will deposit much faster on the facets with lower binding energy than those with higher binding energy which consequently producing elongated anisotropic 1D NCs.

For low dimensional ZnS nanocrystals synthesis, amines with varied alkyl chains and phosphines were widely used as ligand to control the NC growth. Li *et al.* [43] reported a ligand controlled synthesis of ZnS spherical dots and nanorods with varied morphologies and crystal phases between 150°C to 200°C (**Figure 2.4 a–d**). These results indicated that ligand played vital roles on the morphology control by single source thermal decomposition method. Specifically, with octylamine (OA) and hexadecylamine (HDA) as the capping ligands, hexagonal ZnS nanorods were obtained while the employment of trioctylphosphine (TOP) and HDA ligand for synthesis led to the formation of spherical zinc blende ZnS spherical dots . Another case of ligand controlled synthesis of ZnS was presented by Thupakula *et al.* [44] who employed zinc ethylxanthate dissolved in TOP as the single source precursor and injected it into the mixture of TOP and HDA at 200°C. The final products were spherical dots with a diameter of ~3.5 nm if TOP was replaced by OA to dissolve zinc ethylxanthate and the mixture was injected into HDA, whereas the final products were nanorods or nanowires with different aspect ratios determined by the annealing temperature and time.

Growth condition in single source decomposition.

Thermal decomposition of the single–source precursor in an organic solvent could result in the formation of the uniform nanoparticles. Pradhan *et al.* [45] reported a single source precursor approach for the synthesis of ZnS nanodots, using zinc thiocarbamates or thiocarbonates in HDA as both the reaction medium to promote thermal decomposition of the precursor and as ligand to stabilize nanoparticles. The spherical ZnS nanoparticles started to grow at 90 °C and after the reaction evolved at 150 °C for some time, uniform ZnS spherical dots with an average size of 4.5 nm in diameter were obtained. Apart from the effect of ligand and precursor on ZnS nanoparticles synthesis, experimental parameter, such as the heating rate was found to play a role on the morphology and phase control. For example, when the precursors were heated up by a high rate, spherical ZnS nanodots of zinc blende phase were obtained while lower heating rate led to the formation of wurtzite nanorods (Figure 2.4 e–h).[46]

Zhu *et al.* [47] synthesized ultrathin and long ZnS nanowires with a diameter of 2 nm by the thermal decomposition of zinc diethyl dithiocarbamate ($Zn(DDTC)_2$) in a mixture of dodecylamine (DDA) and triphenyl phosphine (PPh3) at 280°C. The control experiments revealed that the co–existing of organophosphine and organoamine was essential for the formation of ultrathin and long ZnS nanowires. In the absence of PPh_3, only shorter ZnS nanorods of cubic structure were obtained whereas without addition of DDA, only spherical ZnS nanodots were obtained from nearly isotropic growth due to the strong binding ability of

PPh_3. It was found out that the ultrathin nanorwires were formed by the oriented attachment from tiny nanocrystals formed at the early stage of the reaction.

Soft template and oriented attachment.

Other than the ligand mediated synthesis of ZnS nanoparticles at elevated temperatures (>150 °C) from the single source precursor, Li and co–workers [48] successfully synthesized single–unit–cell ZnS quantum wires at a relatively low temperature (100 °C~140 °C) by using OLA as the soft template. OLA is amphiphilic molecular with a hydrophobic long alkyl chain and a hydrophilic headgroup, when it binds to metal ions (e.g. Zn ions) at a range of temperature, and it could assemble into crossed lamellar structures (Zn–OLA). The ultranarrow interlayer and intralayer spacings of Zn–OLA lamellar structure can work as a double–lamellar template for cluster or extremely small nanoparticle growth.[49, 50] When OLA was adopted as the soft template for ZnS growth at a relatively low temperature, extra thin nanowires with a diameter of 0.8 nm to 2.2 nm and a length from 70 nm to 340 nm were obtained through the oriented attachment mechanism (**Figure 2.4 i–l**).

Another example of oriented attachment leading to ZnS nanorods growth was reported by Yu *et al.* [51] in which ZnS nanorods were synthesized by the hot injection of diethylzinc into S precursor dissolved in an HDA solvent. With detailed analysis of TEM images on the intermediate aliquots, they confirmed that the elongated ZnS nanorods were formed from 5 nm–sized spherical ZnS nanodots via oriented attachment, with the long axis of being the (111) direction.

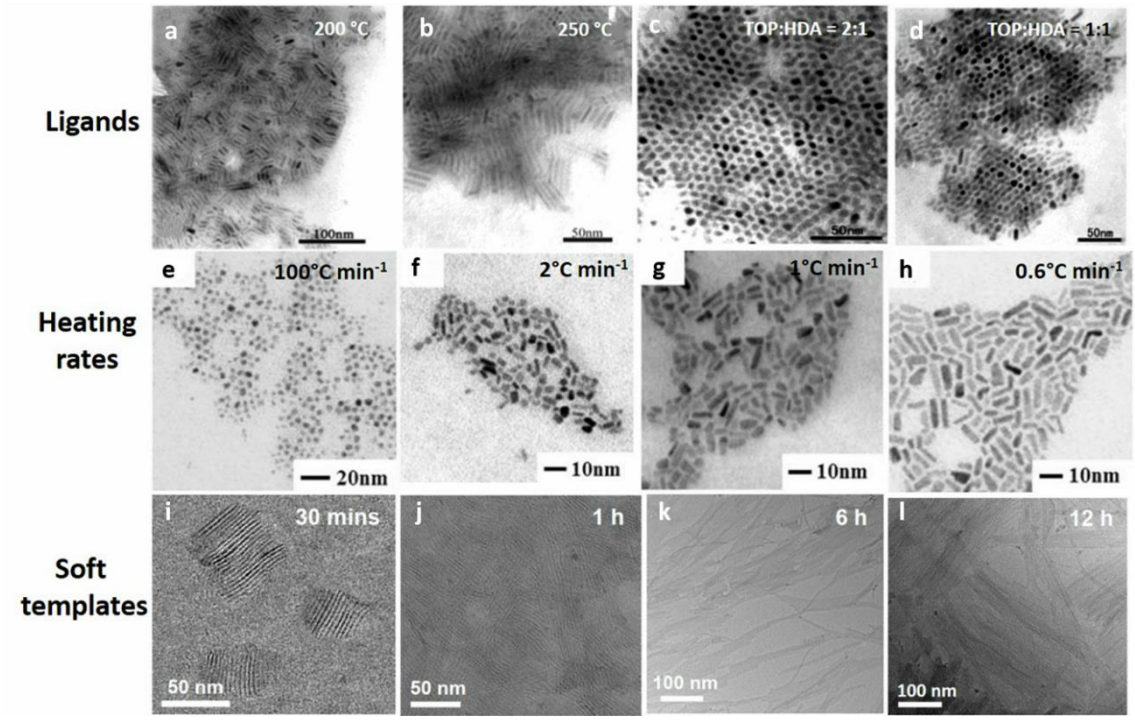

Figure 2.5 (a,b) Transmission Electron Microscopy (TEM) images of ZnS nanorods prepared from a single–source precursor, with OA and HDA as ligand; (c,d) ZnS nanodots synthesized with a solution of TOP and HDA[43]; (e–h) TEM images ZnS nanodots and nanorods synthesized at different heating rates. (e) by 100°C min^{-1}, (f) by 2°C min^{-1}, (g) by 1°C min^{-1}, and (h) by 0.6°C min^{-1}. A higher heating rate resulted in the formation of spherical nanodots while nanorods were obtained at the lower heating rate. [46] (i–l) TEM images of ZnS ultrathin semiconductor nanowires wherein OLA works as the soft templates for oriented attachment. [48]

Based on above research results, it can be summarized that the choice of precursors (single–source precursor or separate precursor), organic ligands (organophosphine or organoamine), synthesis approach (hot injection or heat–up method) and growth rate or temperature all play important roles in the synthesis of ZnS nanodots and nanowires or nanorods. Appropriate combination of these factors could lead to the successful synthesis of ZnS nanodots or nanorods with controlled size, structure and morphology.

2.3.1.2 2D ZnS nanoplateles.

Compared with the massive research of the colloidal 0D or 1D ZnS nanoparticles synthesis, there is less progress in the synthesis of 2D ZnS nanosheet or nanoplateles. For 2D nanocrystals, the excitons are strongly confined along the thickness direction, thus the synthesis of 2D NCs with controlled uniform thickness is important for tuning the geometry of the nanoparticles and

the optical and electronic properties that underpin their applications in optoelectronics, sensors and lasers.

Cation exchange.

Cation exchange is one of the approaches for the synthesis of 2D ZnS nanosheets from other 2D NCs. Fenton *et al.* [52] reported a successful synthesis of ZnS nanoplateles from $Cu_{1.8}S$ by cation exchange. For a cation exchange method, one principle for choosing the sacrificed synthon is that the high quality sacrificed NCs could be obtained by a facile synthesis route. Meanwhile, the cation of NCs used for later cation exchange should have high mobility that facilitate partial or complete exchange with other cations.[53] In the cation exchange for 2D ZnS nanosheets formation,[52] $Cu_{1.8}S$ with hexagonal shape and uniform thickness were used as sacrificed NCs due to the well–developed synthesis route for $Cu_{1.8}S$ nanoplateles in OLA, ODE and DDT and the high mobility of Cu^{2+} which could be exchanged by Zn^{2+}. By employing Zn–OLA complex as the zinc source for cation exchange at 50 °C, 2D ZnS hexagonal nanoplateles or $Cu_{1.8}S$–ZnS hybrid hexagonal nanoplateles could be obtained depending on the degree of cation exchange completion, shown as **Figure 2.6 (a–g).**

Single–source precursor decomposition.

Another method for 2D ZnS NCs synthesis is through a solvothermal process in which sealed teflon–lined stainless steel autoclave is used as the reaction containers so the temperature in the autoclave can exceed the boiling point of the solvents and provide enough energy for the reaction. Zhou *et al.* [54] reported the synthesis of wurtzite ZnS nanoplates based on a solvothermal method using $ZnS(EN)_{0.5}$ complex (EN=Ethylenediamine) as the single source precursor through the thermal decomposition in carbon disulphide solution at 180 °C. SEM images confirmed that the final products of decomposition from $ZnS(EN)_2$ complex were ZnS consisted of rectangle nanoplates with lateral dimensions ranging from 1 to 2 μm, as seen in **Figure 2.6** (h,i). The solvothermal method could produce NCs with a large quantity and higher yield. However, the ZnS nanoplates synthesized by the solvothermal method were much larger and thicker than the ZnS nanoplates synthesized by the cation exchange. The extent of the morphology and uniformity control of ZnS nanoplates is not as good as that of ZnS nanoplates synthesized through colloidal approaches.

Soft template and oriented attachment.

Being similar to 1D ZnS nanowires or nanorods, ZnS nanoplateles could also be synthesized via oriented attachment. Pang *et al.* [55] reported a synthesis of wurtzite ZnS nanoplateles (NPLs)

by a one–pot synthetic approach in which $Zn(NO_3)_2$ and sulfur were mixed in OA and OLA and the reaction was kept at 170 °C for 6 h. The obtained ZnS rectangular NPLs were 1.4 nm in thickness which corresponds to eight monolayers and showed a very narrow emission band. Mechanistic studies on the formation of ZnS NPLs indicated that the extra thin ZnS nanowires were firstly formed at 150 °C which then transformed to small NPLs by oriented attachment and finally formed ZnS NPLs with uniform thickness. The transformation from lamellar mesostructure ZnS to ZnS NPLs was also verified by Dai and coworkers [56] who proposed the ultrathin ZnS NPLs were synthesized under the template–guided methods. An interesting result from increasing the amount of sulfur precursor used in the reaction of ZnS nanoparticle synthesis showed that when excessive S precursor was used, the morphology of final ZnS product was nanorods instead of ZnS NPLs, as seen in **Figure 2.6 (l–o).** This is because that a high concentration of monomers could fascinate the anisotropic growth of 1D ZnS nanorods.

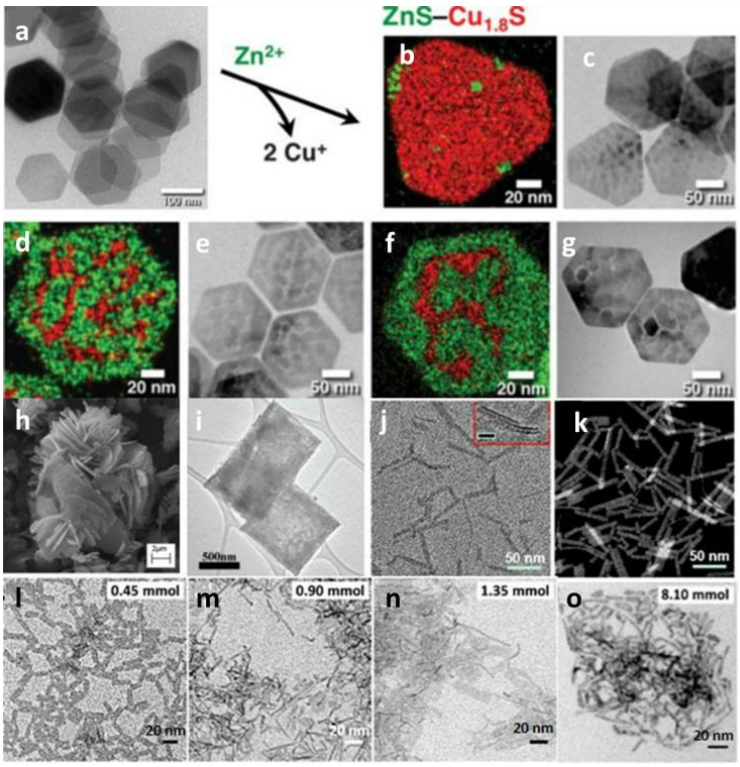

Figure 2.6 (a) TEM image of $Cu_{1.8}S$ hexagonal plates; (b–g) ZnS–$Cu_{1.8}S$ marbled plates obtained by partial cation exchange from $Cu_{1.8}S$ hexagonal plates.[52] (h–i) Scanning Electron Microscope (SEM) and TEM image of wurtzite–type ZnS with quasi–square or rectangle nanoplate–like morphology.[54] (j–k) TEM and STEM images of ZnS nanoplateles with a uniform thickness of ~1.4 nm obtained from oriented attachment of small ZnS nanoplateles. [55] (l–o) TEM images of ultrathin ZnS NCs synthesized with different amounts of sulfur: (l) ZnS NPLs (0.45 mmol) (m,n) a mixture of ZnS NPLs and NRs (0.90, 1.35 mmol), (o) ZnS NRs (8.10 mmol). [56]

2.3.2 Synthesis of ZnSe quantum dots

2.3.2.1 0D ZnSe spherical dots and 1D ZnSe nanorods or nanowires.

Coprecipitation and reverse micelles as soft template.

The early synthesis of colloidal ZnSe spherical dot was reported by a coprecipitation method in which $Zn(ClO_4)_2$ and H_2Se were used as the precursors at low temperatures (–80°C to room temperature) in isoproponal and methonal solution[57]. The obtained ZnSe nanocrystals from the coprecipitation method showed a large blue shift of absorption than the bulk material which indicated strong quantum effect and the tiny size (~2 nm diameter) of the products.

Apart from the coprecipitation in alcohol solvent developed in the early stage of quantum dot synthesis, soft template techniques which employ reverse micelles or normal micelles as the templates or micro–reactors were also used for ZnSe nanoparticle synthesis. For instance, Yang *et al.* [58] used water/Triton X–100/2–propanol/cyclohexane as the reverse micro emulsion templates (water–in–oil) for zinc blende ZnSe nanodot synthesis and concluded that the particle size (diameter ranging from 2.86 to 3.76 nm) depended on the amount of 2–propanol co–surfactant and the ratio of water to surfactant. Beside the aforementioned methods, a hot–injection method which aims at separating the nucleation phase and growth phase gained much attention in the synthesis of colloidal ZnSe nanoparticles.[59]

Hot–injection and oriented attachment.

Cozzoli *et al.* [60] gained the shape and phase control of ZnSe nanocrystals by a hot–injection method. In their research, active diethylzinc was used as the zinc precursor and selenium powder was used as the selium precursor while different surfactants such as phosphonic acids, amines and carboxylic acids were employed as ligand to control phase and morphology of the products. As a result, the hot injection rate and temperature determined the final shape of ZnSe nanoparticles, as seen in (**Figure 2.7 a–c**). For the synthesis of spherical ZnSe nanodots, Zn/Se precursor were prepared in TOP or Trinbutylphosphine (TBP) solution and then rapidly injected to HDA which was heated to 300°C~340°C. When the injection of the precursor changed to dropwise addition at a high temperature (345°C), twisty ZnSe nanorods with an aspect ratio from 2–3 to 7–8 were obtained. While the volume of precursor for hot injection increased, branched ZnSe nanorods were synthesized. These findings indicated that the injection rate, temperature and precursor volume played key roles in shape and phase control of nanoparticles while keeping other factors such as ligand and solvent in the reaction system the same.

The hot injection method was also successfully applied to synthesize 1D ZnSe nanowires or nanorods in which the oriented attachment of 0D nanodots to 1D nanorods contributed to the anisotropic growth. It is well known that in a process of the oriented attachment, the final nanoparticles were obtained by the fusion of original nanocrystals by sharing their common crystallographic orientation. And the driving force of oriented attachment is the weak interactions between the components such as hydrogen bonds and Van der Waals force, and the reduction of interfacial energy by the diffusion of surface planes could also promote the oriented attachment. Sarkar *et al.* [61] presented a synthesis approach of 1D ZnSe nanowires with wurtzite (WZ) structure from 0D ZB ZnSe nanodots by an oriented attachment mechanism. In the case of 1D ZnSe nanowires with wurtzite structure formed from 0D ZnSe nanodots with zinc blende (ZB) structure by oriented attachment, the DFT calculation results conformed the less formation energy of the WZ rod (–2.663 eV) than the coupled ZB dots (–2.320 eV), which means the formation of WZ ZnSe nanorods is more energetically favourable than the assembled quantum dots with the ZB phase.

Apart from the hot injection method, a new approach aiming at separating the nucleation stage and growth stage for colloidal synthesis of ZnSe quantum dots was reported by Guidelli, *et al.* who used a continuous–flow microfluidic reactor to divide nuclei and growth stage at 160°C and 340°C separately.[41] The synthesized ZnSe nanodots showed sharp excitation absorption and emission which indicates the formation of monodisperse ZnSe quantum dotss.

Ligand mediated growth.

The final morphology of ZnSe nanocrystals largely depended on the choice of ligand for 1D ZnSe nanowires or nanorods growth. Organic amines like Octadecylamine (ODA), HDA can promote the formation of 1D ZnSe nanowires or nanodots while organic phosphines or oxide phosphines like TOP or TBP promote the formation of ZnSe 0D nanodots. For example, if single amine such as ODA was used as both the ligand and solvent for ZnSe nanocrystal synthesis, short ZnSe nanorods were self–assembled while only polydisperse rods were obtained when ODA and TOPO were used as the ligands,.[62] Jia and Banin[63] reported the synthesis of ZnSe nanorods with controlled aspect ratios through a ripening mechanism. In this approach, long ZnSe nanowires were firstly synthesized by the hot injection of Se–OLA to zinc precursor. Then the formed long ZnSe nanowires were cleaned from the crude solution and were dispersed into pure OLA again. The mixture was gradually heated to 280 °C. The annealing of ZnSe nanowires at this temperature triggered the ripening process in which the

long and thin ZnSe nanowires transferred into shorter and thicker ZnSe nanorods by a thermaldynamically controlled material diffusion process (**Figure 2.7** d–f).

One–pot heat–up method.

Apart from injecting the hot–injection method, non–injection one–pot method was also used to synthesize ZnSe quantum dots. Yao *et al.*[64] reported the synthesis of a families of magic–sized ZnSe quantum dots by a one–pot heat–up method. In a typical synthesis, $NaBH_4$ was employed to reduce Se to H_2Se in OA and OLA which worked as the Se precursor. Heating Zn precursor and above–mentioned Se–precursor together in ODE and OLA up to 230°C resulted in the formation of a series of magic–sized ZnSe quantum dots with the first exciton absorption peaks ranging from 280 nm to 347 nm. Another heat–up method was reported by Ning *et al.* [65] who introduced a well–defined molecular clusters ($[Zn_4(SPh)_{10}](Me_4N)_2$, Zn_4 clusters) to change the ZnSe magic–sized clusters (MSCs) template and guide the growth of ZnSe nanorods or nanodots. The molar ratio of Zn_4 clusters to the ZnSe precursor determined the final products in which ZnSe nanodots were obtained when more Zn_4 clusters was added while nanorods with tuneable aspect ratios were synthesized when less Zn_4 clusters were added (**Figure 2.7 g–l**).

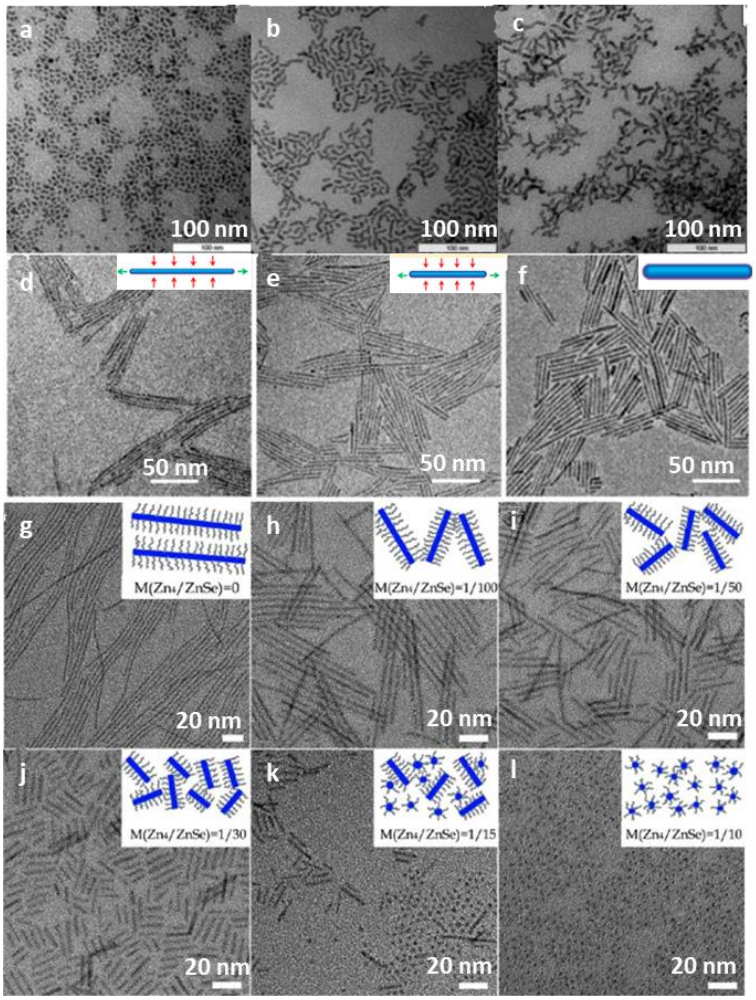

Figure 2.7 (a–c) TEM images of ZnSe nanoparticles obtained from hot–injection method. (a) Spherical dots by rapid injection. (b) Nanorods by dropwise addition. (c) Branched NCs by increasing the total volume of injected precursors.[60] (d–f) A ripening procedure showing ZnSe nanowires (d) evolved into the ZnSe nanorods after 5 min (e) and 15 min (f) at 280 °C.[63] (g–l) TEM images of ZnSe NCs synthesized with Zn_4 clusters as template. (g) nanowires synthesized without Zn_4 clusters; (h–l) ZnSe nanoparticles of various aspect ratio owing to varied molar ratio of Zn_4/ZnSe; (h–j) ZnSe nanorods with varied length of 60 nm, 45 nm and 21 nm as the ratio of Zn_4 to ZnSe varied from 1:100, 1:50 to 1:30 respectively. (k) A mixture of ZnSe nanorods and spherical dots, M(Zn_4:ZnSe) = 1:15. (l) ZnSe spherical dots, M(Zn_4:ZnSe) = 1:10.[65]

2.3.2.2 2D ZnSe nanoplateles.

Unlike the abundant research and progress on the synthesis of 0D and 1D ZnSe quantum dots, 2D ZnSe nanoparticles received much less attention. Park *et al.* [66] reported a facile one–pot heat–up approach for the synthesis of 1.4–nm–thick ZnSe nanosheets by using zinc nitrate and selenium as the precursors and OA and OLA as the ligands at a relatively low temperature (170°C for 6h), as seen in **Figure 2.8** (a–d). The absorption of the formed wurtzite ZnSe nanosheets shows a narrow peak which indicated the very uniformity of thickness of ZnSe nanosheets. Pang *et al.* [55] further studied the mechanism of for the formation of the ultrathin ZnSe nanoplateles both experimentally and theoretically based on the first–principle calculations. They found that the ultrathin ZnSe nanosheets were composed of eight monolayers of the (110) layer. Because of the large energy barrier for the growth of the ninth layer growth onto the eighth layer, it is unlikely for the obtained eight–layer thick ZnSe nanosheets to grow thicker.

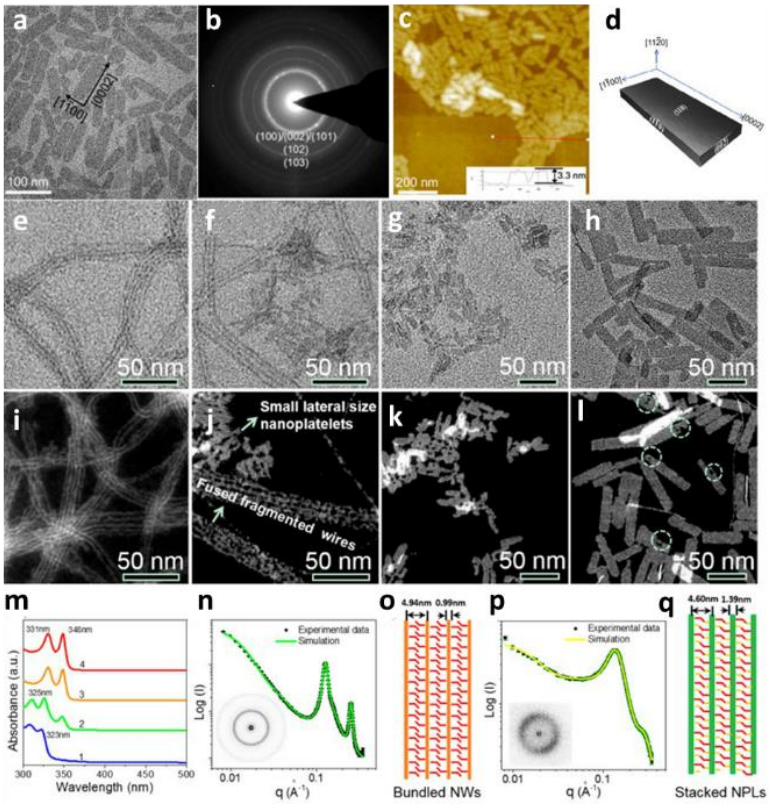

Figure 2.8 (a) TEM image of single–layered ZnSe nanosheets synthesized by the one–pot heat–up method; (b) Selected Area Electron Diffraction (SAED) pattern showing the identical lattice planes (002), (100) and (101) of wurtzite ZnSe.(c) AFM image of ZnSe nanosheets, indicating a typical thickness of 3.3 nm. (d) crystallographic orientation of a ZnSe nanosheet;66 (e–i) TEM (e–h) and High–Angle Annular Dark–Field Scanning Transmission Electron Microscopy (HAADF–STEM) (i–l) images of ZnSe aliquots taken at 150 °C for (e and i) 2 min, (f and j) 4 min, (g and k) 30 min, and (h and l) 2 h. (m) Absorption spectra of ZnSe nanocrystals corresponding to (e) to (h), showing the red shift of wavelength absorption. (n) Small–angle X–ray scattering (SAXS) patterns and (o) Schematics of bundled NWs. (p) SAXS patterns and (q) schematics of stacked NPLs. Red and orange lines in panels o and q correspond to OLA and OA, respectively.[55]

2.3.3 Synthesis of ZnTe quantum dots

ZnTe, with the narrowest bandgap among zinc–based chalcogenide (2.26 eV for the bulk material) and a Bohr exciton diameter of 6.2 nm,[67] could absorb visible green light at around 550 nm which could be good candidates for optical devices and photocatalysis study.[68] However, compared with ZnS or ZnSe, high quality ZnTe nanoparticles are even harder to synthesize because of the stronger metallicity of Te which makes ZnTe very unstable under ambient environment and easy for Te^{2-} to be oxidized to Te metal. The first step for ZnTe nanoparticles synthesis is the activation of Te precursor. To obtain Te precursor with increased

activity, several research groups had employed different ligands or strong reducing agents like superhydride to gain further control of the growth of the ZnTe nanocrystals.

Ligand mediated growth.

Lee *et al.* [69] employed TOP or TBP to activate Te powder for the synthesis of ZnTe nanocrystals. It was found that the addition of phosphine formed a TOP–Te (or TBP–Te) complex which could work as active Te precursor for ZnTe nanoparticle synthesis. With certain amine as the ligand, the morphology of final ZnTe nanoparticles could be controlled. For example, when ODE was used as the solvent, ZnTe nanoflowers were obtained after growth at 270°C while if TOP–Te (or TBP–Te) was used as the Te precursor, ZnTe nanoflowers would decompose into smaller nanodots. When OA, DDA or octadecylamine (ODA) were used as the ligands for the synthesis, only ZnTe nanodots were obtained. However, if the aforementioned primary amines were replaced by a branched amine such as trioctylamine (TOA), ZnTe nanoflowers were obtained again. These results indicate that alkyl chains showed a steric effect which disturbed the formation of ZnTe nanoflowers under similar synthetic conditions. The effect of ligands on the final morphology of ZnTe nanoparticles was compared in **Figure 2.9**.

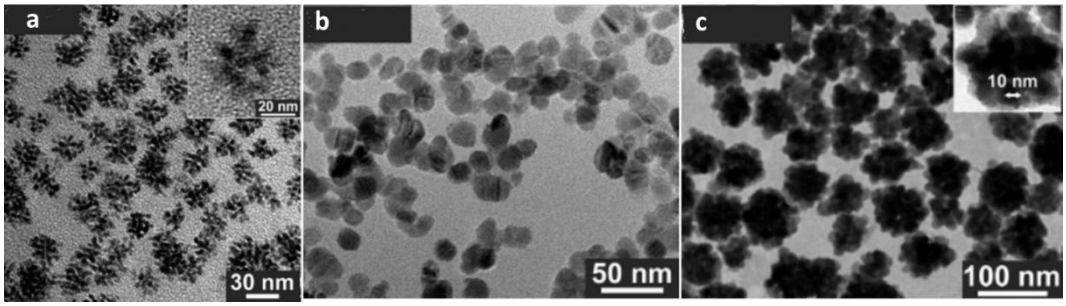

Figure 2.9 TEM images of ZnTe nanocrystals synthesized with various ligands. (a) Nanoflower synthesized with Zn/TOP; (b) Spherical nanodots synthesized using ODA; (c) Plump nanoflowers synthesized with TOA. [69]

Superhydride activated Te–TOP for ZnTe growth.

Lithium triethylborohydride ($LiBH(CH_2CH_3)_3$) also known as superhydride, is a very strong reducing agent used in organometallic and organic chemistry. Zhang *et al.* [70] employed superhydride as the reducing reagent to prepare poly–tellurium precursors for the synthesis of ZnTe nanoparticles and found that the morphology of obtained ZnTe nanocrystals strongly related to the growth temperature. Typically, at a low temperature (150 °C), kinetic growth dominated the growth process which resulted in ZnTe nanorods through an anisotropic growth approach while at an elevated temperature (250°C), quasispherical ZnTe nanodots were

obtained due to thermodynamic growth. They further used superhydride–reduced Te dissolved a mixture of TOP and OLA solutions to ZnTe nanoparticles.[71] They found that the addition of superhydride as the strong reducing agent was capable of reducing Te(0) to Te^{2-}, Te_2^{2-}, Te_3^{2-} or polytellurides in TOP and oleylamine depending on the amount of super hydride added. Compared with Te (0) in TOP and oleylamine, superhydride reduced Te precursor showed much higher activity in the reaction with Zn precursor. It was found that with increased the amount of the superhydride addition, Te (0) was firstly reduced to Te_2^{2-}, followed by Te^{2-}, and finally to Te^{2-}. Te^{2-} is more active than Te_2^{2-} which makes the growth rate different for the nucleation and growth of ZnTe nanocrystals. This research provided a facile method that adopting strong reducing agent to produce active polytellurides as a tellurium precursor for the synthesis of high–quality ZnTe nanodots or nanorods, as seen in **Figure 2.10**.

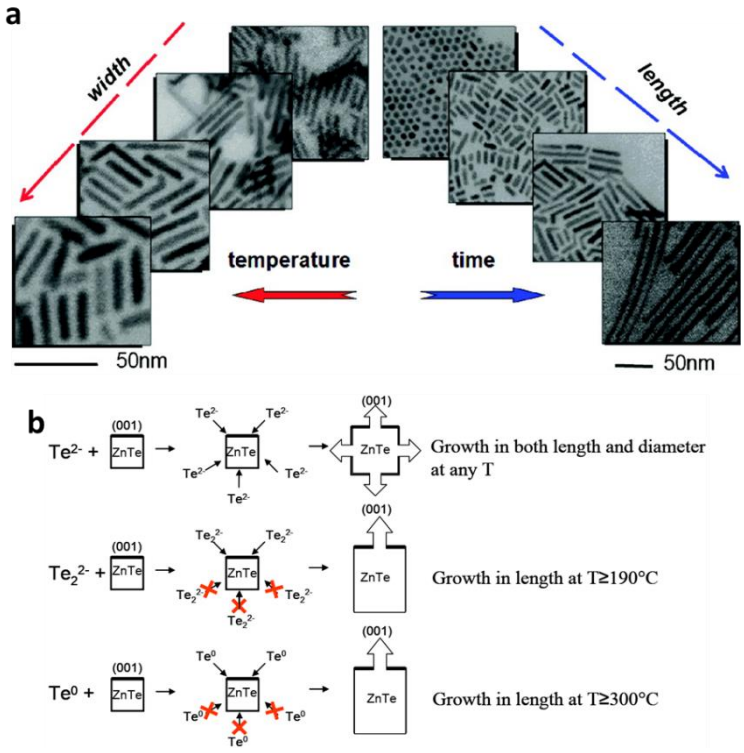

Figure 2.10 (a) TEM images of ZnTe nanorods showing that temperature increased from 190ºC to 300ºC leading to the width/diameter increased from 3.5nm to 7.0nm. ZnTe nanodots obtained by decreasing to half amount of reactant. The length of ZnTe nanorods increased from 21 nm for short nanorods to 150 nm long nanorods resulted from growth time extension from 10 min to 90 min. (b) Scheme of shape controlling growth mechanism of ZnTe nanorods, indicating the varied react activity of Te species on ZnTe nanocrystal facet growth.[71]

2.3.4 Zinc–based semiconductor–semiconductor hetero–nanoparticles

2.3.4.1 Core/shell hybrids.

Core/shell structure is a very common type of hybrid semiconductor nanocrystals. According to the alignment of band gap offset, core/shell structure of two different semiconductor nanoparticles could be classified into two typical types, namely type I and type II. A type I heterostructure has a straddling gap offset in which the valence of one semiconductor is lower than the other's valence band while its conduction band is higher in energy than the other's conduction band. For a type II structure, both valence band and conduction band of one semiconductor are lower or higher than those of the other semiconductor, which leads to a staggered gap offset. For core/shell structure zinc chalcogenide semiconductor nanoparticles, both type I and type II structure were synthesized for different applications.

As ZnS has a large band gap, it is usually applied as the shell material for the synthesis of type I hybrid semiconductor nanoparticles. Because of the straddling valence band and conduction band alignment, the excited electrons and holes are confined in the core material which has a narrow bandgap than ZnS. For example, ZnSe/ZnS core/shell hybrid structure quantum dots synthesis was reported from Wang *et al.* [72] and Lee *et al.* [73] by using diethylzinc and Se–TOP as precursors. In these cases, bare ZnSe dots were synthesized firstly, then cleaned ZnSe quantum dots were transferred to HDA for ZnS overcoating. Typically, Et_2Zn and $(TMS)_2S$ (hexamethyldisilathiane) in TOP slowly were dropped into the HDA solution containing ZnSe quantum dots by a dropping funnel. Then the reaction was kept at 80°C for 24 h for growth. ZnS shell epitaxially grew onto ZnSe core due to the small lattice different between these two semiconductor materials.

Another core/shell structure quantum dots composed of ZnTe and ZnSe semiconductor materials with type II bandgap offset was reported by Bang *et al.* [74] The products showed a broaden wavelength absorption band and the offset of ZnTe and ZnSe enables more efficient charge (electron and hole) separation, which enhanced the solar conversion efficiency by 11 times compared to the bare ZnSe quantum dot–based device. Jang *et al.* [75] demonstrated a synthesis of double–shelled ZnSeTe/ZnSe/ZnS heterostructures which could be used as bright, colour–pure blue emitters. The growth of exquisite ZnSe and ZnS double shell greatly enhanced the optical properties as blue light emitter and this double–shelled ZnSeTe/ZnSe/ZnS heterostructures recorded the highest device performances to date among the non–Cd blue–emitting QLEDs, as seen in **Figure 2.11 (a–d).** Compared with bare ZnSe nanodots, the obtained ZnSe/ZnS core/shell nanodots have stronger luminescence because of the passivation

of ZnS shell. This epitaxial growth of high–quality ZnSe/ZnS core/shell nanorods was further developed by Ji *et al.* [76] ZnS shell of manifold morphology, such as flat–shell, islands–shell and helical–shell could be grown onto core 1D ZnSe nanorods. And the transformation of shell morphology was a strain–controlled transformation which resulted from the changing of shell growth rates via tuning the precursors' reactivity, as seen in **Figure 2.11 (e–h)**.

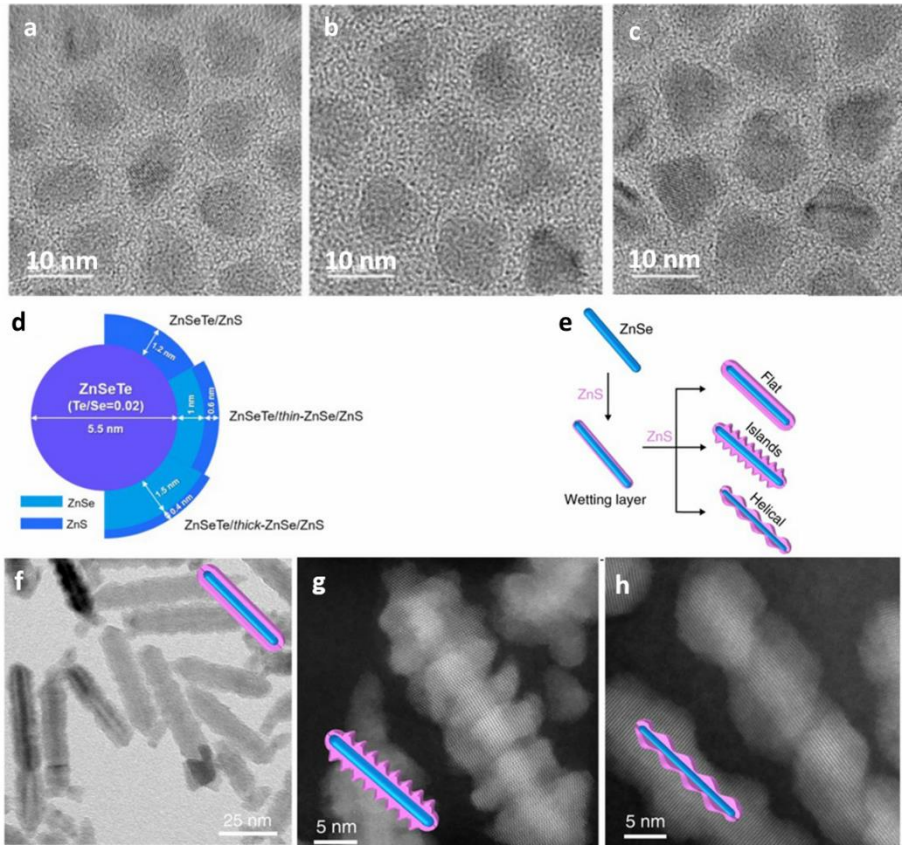

Figure 2.11 TEM images of (a) ZnSeTe/ZnS QDs with single ZnS shell, (b) ZnSeTe/ZnSe/ZnS QDs with thin double shells, and (c) ZnSeTe/ ZnSe/ZnS QDs with thick double shells. (d) Schematic illustration of ZnSeTe/ZnS or ZnSeTe/ZnSe/ZnS heterostructures with varied shell.[75] (e) Schematic of the controlled shell growth of ZnS on a ZnSe nanorod. (f–h) TEM or STEM images of ZnSe/ZnS hybrid nanorods with flat–, islands– or helical–shells. [76]

2.3.4.2 Dot in rod hybrids by cation exchange.

Li and Manna *et al.* [77] also reported a ZnSe/ZnS dot in rod core/shell structure synthesised by cation exchange from CdSe/CdS dot–in–rod core/shell nanocrystals. They synthesized CdSe/CdS core shell nanorods firstly, then exchanged Cd^{2+} to Cu^{+}, followed by exchanged Cu^{+} to Zn^{2+}. After two steps of cation exchange, blue–UV fluorescent ZnSe(core)/ZnS(shell) nanorods (NRs) with type I bandgap alignment were obtained, as shown in **Figure 2.12**. This cation exchange method fulfilled the bandgap tuning and the obtained ZnSe/ZnS nanorods

showed enhanced photoluminance efficiency and optical stability than bare ZnSe nanoparticles owing to more confined carrier in the core region. The drawback of the increased defects caused by multiple cation exchange in the ZnSe/ZnS dot in rod core/shell hybrid has limited this hybrid core/shell structure from high photo luminance efficiency.

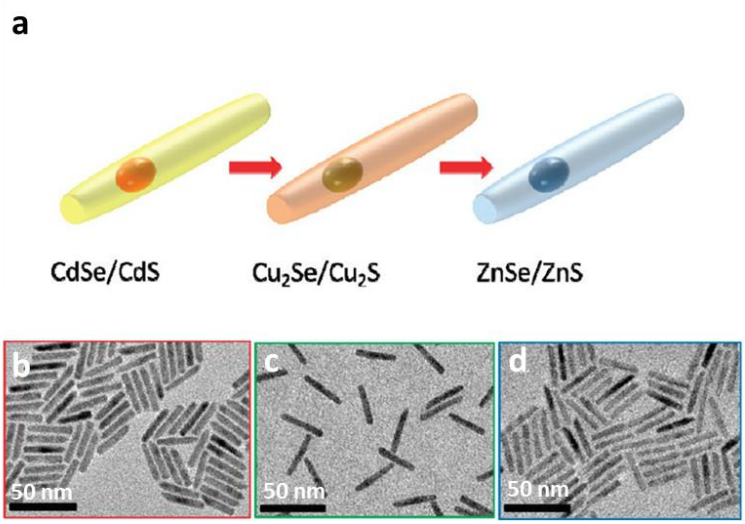

Figure 2.12 (a) Schematic illustration of ZnSe/ZnS dot–in–rod hybrid nanoparticle synthesized from two–step cation exchange reactions starting from CdSe/CdS dot–in–rods core–shell NRs.(b–d) TEM images of the starting CdSe/CdS NRs, later Cu^{2+} exchanged Cu_2Se/Cu_2S NRs and final Zn^{2+} exchanged ZnSe/ZnS NRs.[77]

2.3.4.3 Segmented hybrids.

Another typical hybrid nanostructure is segmented hybrid in which the second nanomaterial grown onto the first one on specific directions and the original nanoparticle is not fully covered by the other one. For Zn–based chalcogenide, a unique dumbbell–like segmented ZnTe and ZnSe hybrid nanorods is reported by Ji and co–workers [78] where they selectively grew ZnSe tips onto the apexes of ZnTe rods, as seen in **Figure 2.13**. The hybrid nanostructures were obtained via a layer–by–layer growth method in which Zn and Se precursors were added to the pre–synthesized ZnTe nanorods. The small (6.4%) lattice mismatch between ZnTe and ZnSe is quite helpful for the epitaxial growth of ZnSe onto ZnTe. Changing the amount of Zn and Se precursor for ZnSe tip growth could manipulate the monolayers of ZnSe which resulted in the formation of ZnSe with different size. Compared with bare ZnTe nanorods, the fluorescence of the obtained type II ZnSe–ZnTe semiconductor nanodumbbells can be tuned between ~500 and 585 nm by changing the tip size of ZnSe.

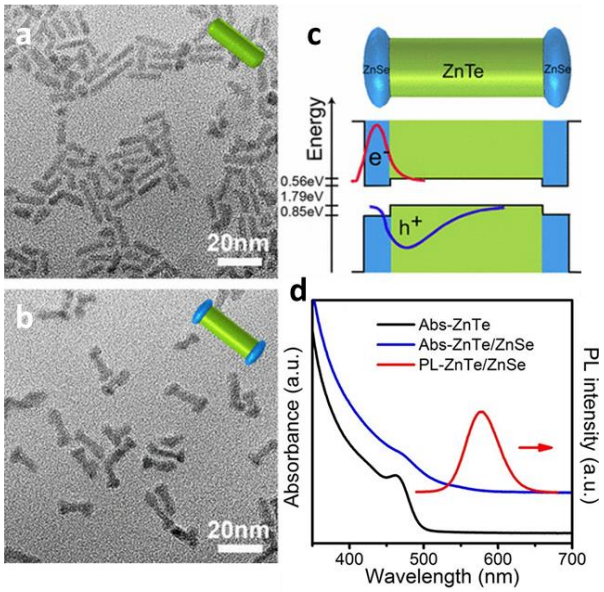

Figure 2.13 (a) TEM images of ZnTe nanorods synthesized with TOP–Te–Superhydride; (b) ZnTe/ZnSe hybrid dumbbell–shaped nanorods formed by selectively growing ZnSe on the apexes of ZnTe rods; (c) Scheme of Type II band offset in ZnTe/ZnSe nanorods, indicating the spatially charge separation; (d) UV–vis absorption and photoluminescence spectra of ZnTe and ZnTe/ZnSe hybrid nanodumbbells.[78]

2.4 Synthesis of noble–metal–semiconductor hybrid nanoparticles

The integration of noble metal like Au and Pt onto semiconductor nanocrystals enables novel properties of nanoparticles such as enhanced electron and hole separation ability. The Femi energy level of Au and Pt is 5.1 eV and 5.7 eV respectively which is within the bandgap of semiconductors like CdSe and ZnSe. This energy alignment makes the light induced charge separation more efficient because the hot electron could be transferred to the metal part of the hybrid nanoparticles. In the past several decades, many noble metal–semiconductor nanoparticles were synthesised, and their applications were demonstrated.

2.4.1 Synthesis of noble–metal–zinc based II–VI hybrid nanoparticles

Although there are many effective methods for the synthesis of ZnSe, ZnS and ZnTe nanoparticles, the integration of noble metal and Zn based II–VI semiconductor nanoparticles are not fully developed. This could be as associated with the difficulty in Zn–based semiconductor nanocrystal synthesis, such as limited choice on ligand and precursor and harsh experimental conditions (precise precursor concentration and reaction temperature control and multiple procedures). Meanwhile, the large lattice mismatch of Au and ZnSe increased the

difficulty on hybrid interface formation. There are only a few reports on the synthesis of noble metal– zinc–based chalcogenide semiconductor hybrid nanoparticles.

Pradhan *et al.* [79] reported the synthesis of Au–ZnSe hybrid nanoparticles in which Au nanoparticles embedded in the long ZnSe nanowires constituted of giant ZnSe nanospheres. They found that Au has strong affinity of thiol which snatches the thiol promptly from the surface of ZnSe semiconductor nanocrystals and promoted the agglomeration of ZnSe nanocrystals. Later on, they [80] investigated an Au–ZnSe heterostructure with Au nanodots as the head and the snaky ZnSe nanorods as the tail. The formation of the hybrid structure was found to be a heteroepitaxial growth mechanism where large Au nanodots of 10 nm grew on zinc–blende ZnSe nanocrystals via coincidence site epitaxy. Specifically, snaky ZnSe nanorods were synthesized firstly, then Au nanoparticles and Se precursor were introduced into the pre–synthesized ZnSe nanorod solution and annealed at an elevated temperature (~250°C). The characterization of High–Resolution Transmission Electron Microscopy–Fast Fourier Transform (HRTEM–FFT) and Density functional theory (DFT) calculation indicated that the heterojunction at the interface of face–center cubic Au and zinc blende ZnSe nanoparticles is 3 × 3 surface unit cells of ZnSe with 4 × 4 surface unit cells of Au (**Figure 2.14 a–d**) which could reduce the lattice mismatch from 35% to 6%. This research indicated the possibility of the formation of Au–ZnSe hybrid nanoparticles with fcc Au and zinc–blende ZnSe despite the large crystal lattice mismatch between them.

Apart from the external interface junction of Au with ZnSe, Au–ZnTe core/shell nanodots are synthesized and applied in fluorescence imaging of cancer cell by Dunpall *et.al.* [81] The water–soluble Au–ZnTe nanodots were synthesized under inert environment with citrate capped Au nanoparticles as the seeds and L–cysteine ethyl ester hydrochloride as the ligand. (**Figure 2.14 e–j**), Scanning Transmission Electron Microscope–Energy Dispersive X–Ray (STEM–EDX) elements mapping data showed that Au element localised in the centre while Zn and Te were found to be mainly concentrated at the particle out surfaces which resulted in Au–ZnTe core–shell structure. Fluorescence and phase–contrast light microscope characterizations demonstrated the potential use of such nanoparticles in bio–labelling wherein the blue light emissions within the PL45 cell line corresponded to the emission from ZnTe nanoparticles.

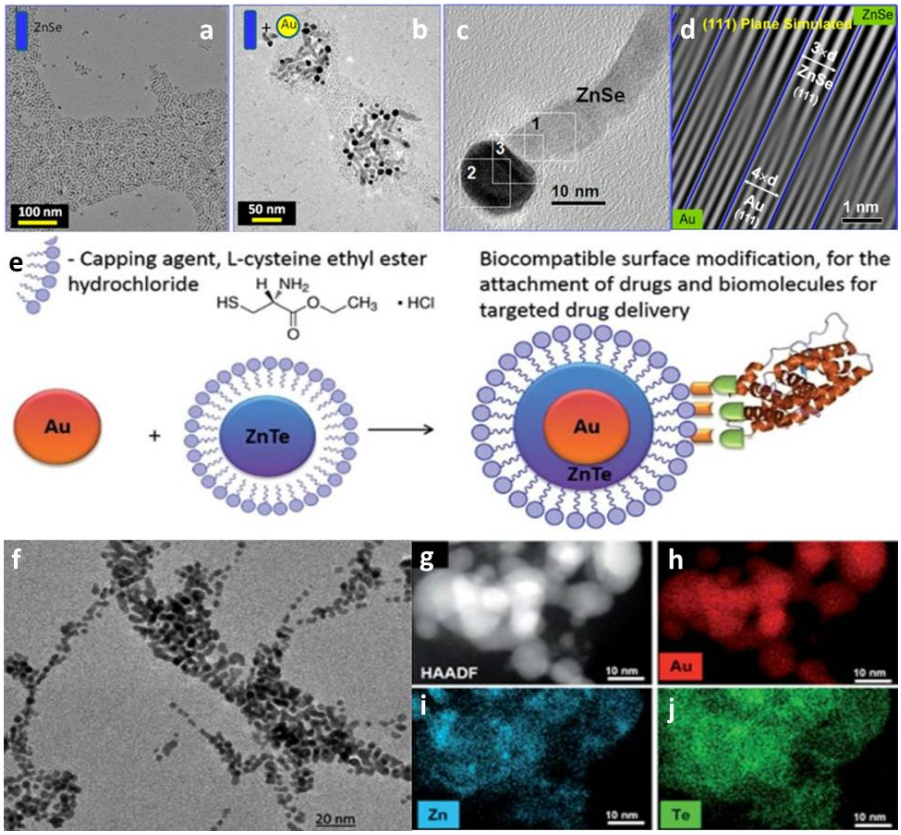

Figure 2.14 (a–c) Morphological characterization of the curly ZnSe nanorods and Au–ZnSe hybrid nanorods with 10 nm Au nanoparticle head obtained at 250 °C by annealing. (d) Simulated HRTEM images from the FFT corresponding to Au (111) and ZnSe (200) planes, which indicates that three unit cells of Au match with four unit cells of ZnSe periodically. [80] (e) Schematic illustration of the synthesis procedure of Au–ZnTe core–shell hybrid nanodots. (f) TEM images of Au–ZnTe core–shell nanoparticles using TEM. (g–j) STEM–EDX mapping of Au–ZnTe core–shell nanoparticles, showing Au in the particle centre with Zn and Te on the surface.[81]

In summary, there are limited research reports on noble metal–Zn chalcogenide hybrid nanoparticles synthesis and applications. One reason could be the synthesis of high–quality Zn–chalcogenide nanoparticles has not been achieved as Zn–chalcogenide nanoparticles were usually employed as original nanoparticles for the further noble metal growth. Meanwhile, the large lattice mismatch could also leads to the increased difficulty on the interface junction formation. The previous investigation, however, demonstrated the formation possibility of noble–metal–ZnSe or ZnTe hybrids despite the large lattice mismatch. The application of Au–ZnTe core–shell nanoparticles as biolabel showed the potential of these hybrid Cd–free Zn–based nanoparticles in biomedical applications.

On the other side, owing to the fully developed synthetic routes of Cd–chalcogenide nanoparticles, noble metal–Cd chalcogenide heterostructures with exquisite morphology and

composition were extensively reported and applied in various fields. Considering that Zn chalcogenide quantum dots have some similar properties because Zn and Cd belong to the IIB class, the synthesis methods and applications for Cd–based chalcogenide quantum dots can be used as the reference and the guidance for Zn–based chalcogenide quantum dots. So we also summarized some research outputs of Cd–based chalcogenide quantum dots which could shed light on the study of Zn–based chalcogenide quantum dots.

2.4.2 Synthesis of Cd–based noble–metal–II–VI hybrid nanoparticles

2.4.2.1 Nobel metal nanoparticle growth onto low dimensional quantum dots.

Noble metal growth onto Cd–chalcogenide nanoparticles.

a) Au precursor concentration.

Growth of noble metal onto Cd–base chalcogenide quantum dots is much more widely studied compared with Zn–based chalcogenide quantum dots. The first report of the selective growth of metal nanoparticle on quantum dots can be traced back to 2004 wherein Banin group developed a synthetic route for gold nanoparticle growth onto CdSe quantum rods and tetrapods .[82] Au tips of tuneable size were found anisotropically deposited onto CdSe nanoparticles and the novel structure showed strong coupling between gold and semiconductor components (**Figure 2.15 a–c**). For this hybrid structure synthesis, CdSe nanorods or tetrapods were firstly synthesized and cleaned for later Au growth, with $AuCl_3$ as the gold precursor. Didodecyldimethylammoniumbromide (DDAB) and DDA were employed as the ligand and reduction agent for Au^{3+}. With a low Au precursor concentration, small Au tips were found to grow onto one or two ends of CdSe nanorods. With increased Au precursor concentration, larger Au tips were deposited on both two ends of CdSe nanorods. Further increasing Au precursor concentration led to the growth of both ends alongside the body growth of CdSe nanorods. Similar phenomenon can be found in the case of CdSe tetrapods where Au tips grew onto the four ends of tetrapods. This pioneer work opened an avenue for compositing noble metal–II–VI semiconductor hybrid structures.

b) Ripening of the Au domains.

Other than controlled deposition of Au nanoparticles on CdSe and/or CdS nanorods thourgh concentration mediation of the Au precursor, a ripening mechanism which resulted in the size increase of Au domains was studied. Banin *et. al.* reported a synthesis of asymmetric one–sided Au–tipped CdSe rods with precisely controlled large Au domains (**Figure 2.15 d–f**).[83]

Generally, with a low Au precursor concentration, Au prefers to grow onto one tip onto CdSe nanorods followed by double–tip growth and body growth. However, Banin *et al.* [83] observed a one–sided growth and formation of "nano–bell–tongues" when the Au concentration was increased remarkably. The experimental analysis and theoretical modelling by DFT indicated that one–side growth was formed after a ripening procedure as the magnitude of these density fluctuations increased from the increased Au concentration which provided the driving force for ripening.

c) Defects under ambient atmosphere.

Besides CdSe nanorods, Au nanoparticles can be also selectively grown onto CdS nanorods by manipulating reaction conditions such as the growth conditions. Saunders and co–workers [84] reported the synthesis of Au–CdS hybrid nanoparticles and they found that the growth atmosphere played an important role on the growth of Au. Within air atmosphere Au nanocrystal formed at both nanorod tips, then grew onto defect sites on the nanorod surface, and finally experienced a ripening process where one Au tip grew at the expense of the other Au tip on the nanorods. (**Figure 2.15 g–l**). The characterization of HRTEM and measurement of angle between the (002) plane of the CdS nanorods and the (111) plane of the Au nanocrystals indicated that the angles varied among the statistic samples which indicated that the Au nanocrystals randomly grew onto CdS nanorods and the growth was non–epitaxial growth. These findings showed that the defect of semiconductor nanorods can also play an important part in Au nanoparticle deposition on semiconductor nanocrystals and the ripening process which was observed in the growth of Au onto CdSe nanorods, was commonly found in the growth process of Au–CdS hybrid nanorods.

d) UV light irradiation.

Being different from the ripening process for large Au nanocrystals growth on CdSe or CdS nanorods, a photoreduction strategy for large gold domains in hybrid nanoparticles (diameter up to 15 nm) was reported by Carbone *et al.* [85]. They conducted the control experiments to investigate the effect of UV light on Au metal growth on CdS nanorods. Experiment results showed that without UV light irradiation, small size Au domains could be found on both ends of CdS nanorods. While with UV light irradiation, large Au domains can be found on one end of CdS nanorods and small size Au domains were found on the other end. The size of the Au domains was obviously larger than the diameter of CdS nanorods. This founding proved that not only largely increased Au precursor concentration and prolonged growth time but also UV

light irradiation can promote the deposition of large Au nanoparticles on the one side of CdS nanorods.

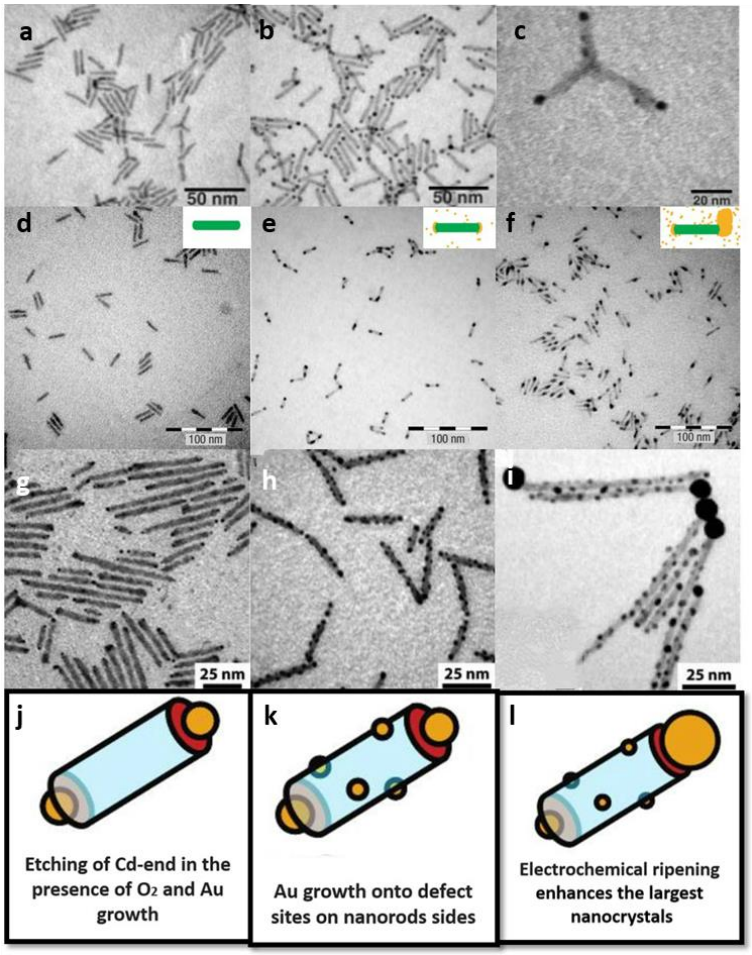

Figure 2.15 (a–c) TEM images of the original CdSe nanorods and Au–CdSe hybrid nanorods showing the controlled growth of Au tips onto CdSe nanorods and tetrapods.[82] (d–f) TEM images of CdSe nanorods and Au–CdSe hybrid nanorods, indicating the large increase of Au/rod molar ratio leads to two–sided growth followed by one–sided ripening growth which finally formed a nano–bell–tongues Au–CdSe hybrid.[83] (g–i) TEM images showing Au growth on CdS nanorods in air after 30 min, 150 min and 3 days. At early stage of the growth, Au nanocrystals nucleated and grew preferentially at the nanorod apexes. Later, Au nanoparticles were found further grown at defect sites. With a longer growth time, a ripening process caused the large Au nanoparticles formation on the apex of CdS nanorods. (j–l) Schematic diagram corresponding to g to i.[84]

e) Au/Pt selective growth on CdSe/CdS seeded rods.

In addition to pure CdSe or CdS nanorod, Menagen and co–workers [86] reported selective growth of Au nanoparticles on CdSe seeded CdS hybrid nanorods. Specifically, firstly high quality dot–in–rod CdSe–CdS nanorods with adjustable optical properties were synthesized, then the synthesized rods were used as the starting materials for Au growth. As a result, Au

was selectively grown onto the location of CdSe seeds inside the CdS nanorods which showed a different habit from the previous reports wherein Au preferred growing on the end of pure CdSe or CdS nanorods. This phenomenon is caused by an electrochemical Ostwald ripening process where CdSe seed works as a sink for electrons, thereby the $AuCl_3$ precursor could be reduced on the spot and Au nanoparticles growth is promoted in this area.

The mechanism for the selective Au growth at one end or two ends or alongside the body of CdSe–seeded CdS nano–heterostructures was revealed by Chakrabortty and co–workers.[87] They proposed a hierarchical order of reactivity of the CdS nanorods end facets and the sides facets, to be special, the higher surface energy at the end facet than body side facets induced the prior Au deposition onto the apex of CdS nanorods and the growth habit could be expanded to Ag growth on the seeded CdSe/CdS nanorods in which similar morphology changes to that of Au–CdSe/CdS nanorods is observed despite some cation exchange from CdS to Ag_2S was observed.

Another typical noble metal platinum (Pt) was used to prepare noble metal–semiconductor hybrid nanoparticle synthesis to improve their electric property such as conductivity and electron transfer. The selective growth of Pt metal and PtNi– and PtCo– binary metal onto CdS nanorods with controllable metal size and composition was successfully synthesized by the reduction of Pt precursor.[88] The face–centred cubic Pt tip size can be adjusted from 4.3 nm to 5.7 nm and the growth location can be adjusted by controlling the relative concentration of metal precursor to CdS nanorods. Specifically, at a low Pt precursor concentration, Pt only grew on the S rich facet of the CdS nanorods while at a high Pt precursor concentration, Pt grew onto two end facets of the CdS nanorods which is similar to that of Au metal growth onto CdS nanorods. By adding Ni or Co acetate with Pt acetylacetonate as the multiple metal precursors to a solution containing CdS nanorods, binary metal like PtNi– and PtCo– combined CdS hybrid nanorods were synthesized. This research represented a new class of hybrid materials which are of great interest for further applications studies.

The aforementioned studies presented multiple approaches to control the growth of Au and Pt onto Cd–chalcogenide nanoparticles, by manipulating the Au growth conditions like Au precursor ratio, growth temperature, growth time and growth atmosphere.

Noble metal as seed for quantum dots growth.

a) Sulphuration and cation exchange.

Other than depositing Au tips onto CdSe or CdS NCs to synthesize noble–metal–semiconductor hybrid NCs, the use of noble metal as the core or seed for semiconductor NCs growth could also form hybrid NCs. For example, Au/CdS core/shell structure was fabricated by multiple steps of cation exchange reaction.[89] The synthesis of Au/CdS core/shell structure involves 4 main steps: (1) Au nanodots were synthesized by reducing $AuCl_3$ with OLA as reduction agent and ligand at 100°C ; (2) A silver shell was grown onto Au seeds by introducing $AgNO_3$; (3) Sulphur powder was used as the S source for sulphuration of Ag to Ag_2S; (4) After the formation of Au/Ag_2S core/shell structure, $Cd(NO_3)_2$ was used to conduct cation exchange from Ag_2S to CdS which led to the final Au/CdS core/shell structure. It's concluded that less energy losses on defects were observed for this core/shell Au/CdS hybrids compared to metal–semiconductor Au–CdS nanorods formed by reduction growth method because the hybrid nanoparticles synthesized using the cation exchange reaction had fewer interfacial defects and traps. But the potential barrier at the Au/CdS interface hindered the transfer of excitons from CdS to Au domains. This method opened an avenue to investigate noble metal–semiconductor nanoparticles core/shell structure like Au/CdS core/shell structure and provided a basis for their applications in photocatalysis and electronic devices.

b) Sequential growth and core transformation.

Other than synthesis by cation exchange reactions, a novel Au@CdS/Pt hybrid structure was reported by sequential growth approach from Ma and coworkers.[90] For the sequential growth method, Au nanotriangle was firstly synthesized and used as the seed, then Pt tips were grown onto the vertex of Au triangle and a CdS layer was grown along the sides of Au triangle. Owing to the direct contact of each component in this special structure, it showed good photocatalytic performance for H_2 generation. For Au/Pt seeded semiconductor hybrids, an interesting finding is that when employing Pt–Au heterodimer as seeds for metal sulfide like Cu_xS_y or PdS hybrid growth, the metal sulfide nanoparticles domain grew exclusively on the exposed Au, not Pt which proved that Au may have stronger affinity to sulphide than Pt does.[91] Because CdS nanoparticles were usually grown at a high temperature (>270°C), the Au–Pt heterodimer seeds was converted to Pt/Au core shell seeds, thus a (Pt@Au)–CdS heterostructure was obtained, as seen in **Figure 2.16 (a–i)**. Another chemical transformation from Au–CdS tipped heteronanorods to AuS/Cd core/shell nanoparticles was reported by Huis *et al.* [92] In this work, composition and morphology transformations from Au–CdS nanorods into AuS/Cd core/shell nanoparticles were induced by the electron irradiation. (**Figure 2.16 j–n**)

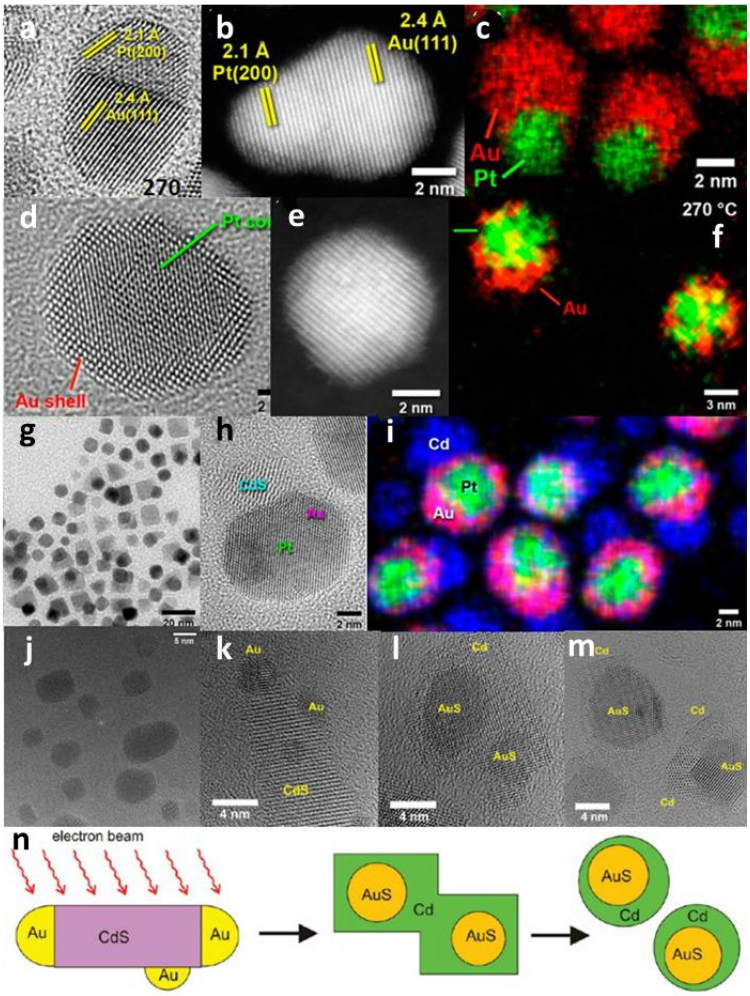

Figure 2.16 (a–c) Pt–Au heterodimers. (d–f) Pt–Au heterodimers transformed into Pt/Au core/shell structure after annealing at 270 °C. (g–i) (Pt@Au)–CdS heterostructures after CdS grown onto Pt@Au core/shell nanoparticles.[91](j–m) TEM images showing the transformation of CdS–Au rod–tip nanoparticles into AuS/Cd core/shell nanostructures under high–intensity electron beam irradiation. (n) Schematic diagram of the radiation–induced chemical transformation.[92]

c) Multiple Shapes.

Noble metal–CdSe or CdS heterostructures of diverse shape have been obtained by employing Au or Pt as the seeds for semiconductor growth. The change of growth temperature, concentration of Cd and Se or S precursor could promote the formation of Au–CdSe hybrid with different shape. Haldar and coworkers reported the seeded synthesis of Au–CdSe hybrid nanoflowers, nanotetrapods and core/shell structure.[93] With Au nanoparticles as the seeds, CdSe nanocrystals of different shapes grew epitaxially onto the (001) facet of the Au seed. Here Au–CdSe hybrid nanostructure was used as an illustrative example. Au nanoparticles with a diameter of about 6 ± 2 nm had been synthesized using $HAuCl_4$ and $NaBH_4$ as precursor and

reducing agent, respectively. The obtained Au nanoparticles were then used as seed for the growth of CdSe with different shapes. The growth of CdSe with different shapes dependeded on the growth parameters like temperature and molar ratios and concentration of Cd and Se precursors. Flower–shaped hybrid Au–CdSe nanostructures were obtained at a reaction temperature of 240 °C while increasing the reaction temperature to 280°C led to tetrapod–shaped nanostructures. Furthermore, conduction the synthesisat 240°C with decreased concentration of Cd and Se precursors produced half formed Au–CdSe core–shell structure instead, as seen in **Figure.2.17 (a–d)**. These results also illustrated the heteroepitaxy at the junction of the (111) facets of fcc Au and the (0001) of wurtzite CdSe.

The seeded–growth approach could also be employed to integrate magnetic, metal and semiconductor components into a one–particle system to obtain Fe_3O_4–Au–CdS heterotrimers, as seen in **Figure.2.17 (e–k)**, [94] Au–CdSe nanoflowers as shown in Figure.2.15 (l–o) were obtained by controlling the growth time [95] while Au_xCd_y–CdSe crooked hybrid nanowires were produced by the diffusion of Cd into Au nanoparticle at a high temperature.

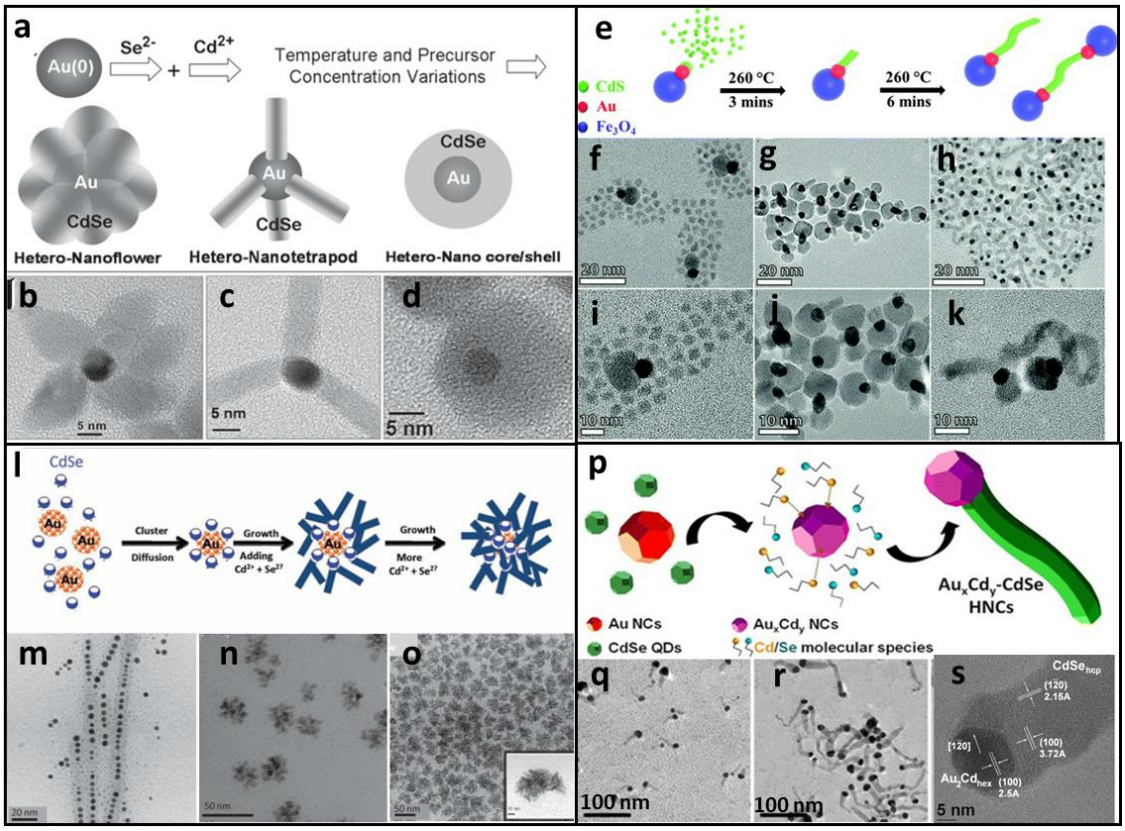

Figure 2.17 (a) Stepwise schematic illustration of the formation of flower–, tetrapod–, and core/shell–shaped Au–CdSe hybrid nanoparticles, starting with Au core. (b–d) TEM images of three different shapes of Au–CdSe hybrid nanostructures.[93] (e) Schematic diagram presenting the formation of Fe_3O_4–

Au–CdS trimer at 260 °C after the injection of Fe_3O_4−Au seed (f, i) 3 min (g, j) and 6 min (h, k) respectively.[94] (L) Scheme of the formation of Au–CdSe nanoflowers. (m–o) TEM images of hybrid Au–CdSe nanocrystals obtained at 150 °C for 5 min, 25 min, and 40 min. (m) Au nanoparticles surrounded by small CdSe cluster. (n) Au nanoparticles covered by rodlike CdSe. (o) Au−CdSe nanoflowers. [95] (p) Growth protocol of Au−CdSe hybrid nanocrystals. (q–s) TEM and HRTEM images showing the obtained Au−CdSe (q,r) hybrid nanocrystals at 250 °C in dibenzyl ether after 5 min, 1 h and Au_xCd_y–CdSe (s) hybrid nanocrystals in ODE at 300 °C for 2 h.[96]

2.4.2.2 Nobel metal growth onto two–dimensional quantum dots.

For two–dimensional quantum dots like nanosheets or nanoplatelets, the photo–generated excitons are confined along the thickness direction while the length and width direction exhibit no or weak quantum confinement properties. The growth of noble metal onto two–dimensional quantum dots provides new types of hybrid nanoparticles with different morphology and optoelectronic properties.

Naskar and co–workers[24] reported a synthesis of two–dimensional noble metal–CdSe hybrid nanoplatelets. A series of noble metal like Au, Pt and Pd were site–selectively grown onto CdSe nanoplatelets, **seen in Figure 2.18**. Typically, CdSe nanoplatelets of 5 monolayer thickness were firstly synthesized by a method described by Tessier et.al, [97] then the purified nanoplatelets were placed together with noble metal precursor stock solution and ligand like OLA and ODE for metal growth at the room temperature or enhanced temperature depending on the metal species. It is found that Au and Pt tend to grow into spherical shape while quasi rectangular and flat Pd domains tend to grow onto CdSe nanoplatelets. Au domains were easier to grow onto CdSe nanoplates compared with Pt or Pd since Au domains could grow at the room temperature while Pt and Pd can only grow at elevated temperatures (~130 °C). This research expanded types of low dimensional nanoparticles like tips–on–rod Au–CdS nanorods to two–dimensional Cd–based noble metal–hybrid nanoplatelets with novel morphologies and could be used as advanced materials for photocatalysis or sensing and other applications.

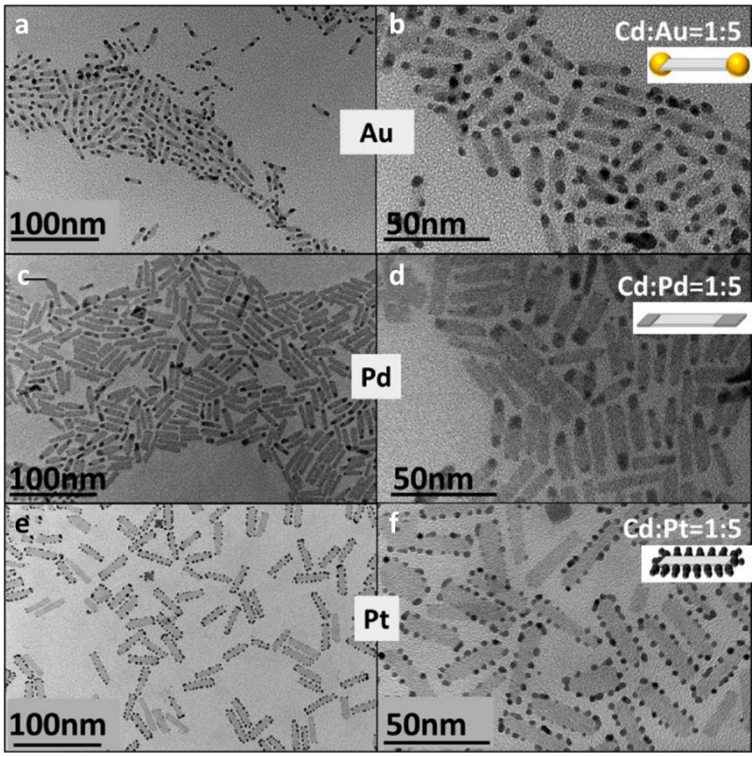

Figure 2.18 (a–f) TEM images indicating the growth of Au, Pd, and Pt noble metal onto 2D CdSe nanoplatelets. Au growth at the room temperature while Pd and Pt growth at an elevated temperature of 130 °C.[24]

In summary, Au/Pt–CdSe/CdS hybrid nanoparticles were massively studied and successfully synthesized with different morphologies and compositions. The most commonly used synthesis route can be described as two main steps. Firstly, semiconductor nanoparticles like CdS nanorods were synthesized with ligand like TOP at high temperatures, and secondly Au or Pt nanoparticles were grown onto clean CdS nanorods in a subsequent low– temperature by reducing Au or Pt precursors like $HAuCl_4$ or $Pt(acac)_2$. The growth of later noble metal can be controlled in the aspect of size and location by controlling the concentration of noble metal precursors, growth time and temperature and so on. Besides the most commonly used method, noble–metal–semiconductor hybrid nanoparticles can also be obtained by using Au nanoparticles as seeds, followed by sulfuration and cation exchange. The combination of noble metal and semiconductor nanoparticles in nanoscale makes these hybrid nanoparticles display interesting properties, such as enhanced charge separation, tunable absorption and photoluminance, which relevance to potential application in photocatalysis and optoelectornics.

2.5 The application of noble metal–II–VI semiconductor heterostructures

2.5.1 Photocatalytic application of noble–metal–II–VI hybrid nanoparticles

The photocatalytic application of transferring solar energy into chemical energy is regarded as a promising approach to relieve the fossil energy crisis. Noble metal–semiconductor hybrid nanoparticles are promising candidates for photocatalytic applications based on the internal electric energy offset between semiconductor and noble metal. Specifically, the Femi energy level of noble metal Au and Pt is within the bandgap of semiconductor materials like CdSe, CdS, ZnSe and ZnS which can strengthen the photo–induced electron–hole pair separation and suppress the charge recombination spatially. The hybrid nanocomposites were used as photocatalysts which displayed catalyst activities using energy from light. For example, CdSe, CdS and ZnSe have a bandgap of 1.8 eV, 2.4 eV and 2.7 eV (for bulk materials), and can absorb the light with a wavelength shorter than 689 nm, 517 nm, 459 nm respectively. As most of the solar radiation that arrives Earth surface is consisted of visible and infrared light and a small portion (~5%) of ultraviolet light, the absorption of visible light (400–700 nm) for photocatalysis is more meaningful. Thus, II–VI nanomaterials like CdSe, CdS and ZnSe semiconductor nanoparticles have size–dependent bandgap in the visible spectral range and have been widely studied on the photocatalysis applications.

2.5.1.1 Pollutant degradation

The early research on photocatalysis by semiconductor hybrid nanoparticles showing that photogenerated electron could be used to degrade pollutant like methylene blue in industry wastewater. Rich in electrons (–) on the noble metal domain, the hybrid Au–CdSe– nanodumbbells was employed as photocatalysts for the reduction of methylene blue to leucomethylene blue, as seen in **Figure 2.19**(a).[98] A series of parallel experiments by using gold nanoparticle, CdSe nanorods or CdSe–Au nanodumbbells separately as photocatalysts at 473 nm for methylene blue reduction showed that 61% of the dye was reduced by using Au–CdSe– nanodumbbells as the catalysts, which was much higher than that of 15% of the dye reduced by individual CdSe nanorods and negligible reduction efficiency of Au particles alone. This founding indicated that with Au growth onto CdSe nanorods, the efficiency of free electron generation which promoted the reduction of methylene blue was obviously enhanced. Pt–CdSe hybrid, as another example of noble metal–semiconductor hybrid nanocomposite was employed to reduce methylene blue to study its photocatalytic application.[99] **Figure 2.19(b)** suggested the scheme of the electron–hole separation and the redox reaction in Pt–CdSe nanorods where methylene blue accepted electrons and methanol accepted holes. Being same

as above mentioned Au–CdSe nanorods, the time trace of the normalized concentration of methylene as shown in **Figure 2.19 (b)** displayed that the nanoscale combined Pt–CdSe nanonets and isolated Pt–CdSe– nanorods showed a reduction reactivity of 46% and 25% respectively which were much higher than that of mechanically mixed CdSe nanorods and Pt dots (2 nm diameter) as catalyst (5%). The underlying catalytic mechanism suggested that the improved performance of Pt–CdSe nanonets compared with Pt–CdSe nanorods can be attributed to the smaller size of the Pt dots and the acidic conditions in which the CdSe was more densely covered by Pt compared with base conditions.

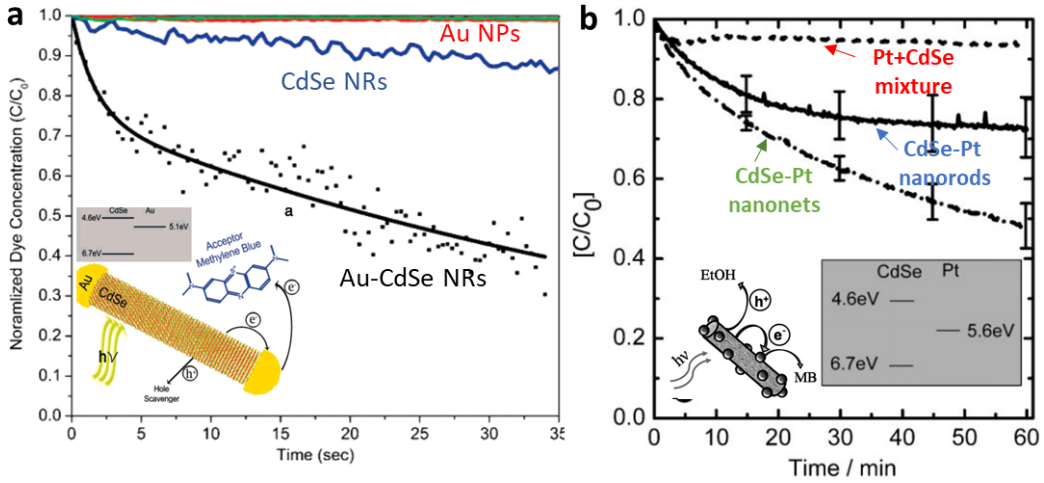

Figure 2.19 (a) The photocatalytic dye degradation rate by using Au nanoparticles, CdSe nanorods and Au–CdSe hybrid nanodumbell separately as catalysts.[98] (b) Time trace of the normalized concentration of methylene dye by employing CdSe–Pt nanonets, CdSe–Pt nanorods and mixture of Pt and CdSe nanoparticles as catalyst. The inset shows the energy band alignment of CdSe and Pt. [99]

2.5.1.2 H_2 evolution reaction. (HER)

Photocatalytic reaction for clean and renewable H_2 energy generation is a hot research topic that could be meet increased energy need of modern society. The study on potential nanomaterials, especially hybrid nanoparticles as catalysts for H_2 generation by water splitting have gained tremendous attention and have achieved great progress. For semiconductors that work as photocatalysts in water splitting, a necessary condition is that the bottom of the conduction band of semiconductor should be positioned more negative than the H^+ to H_2 reduction potential (0 V relative to standard hydrogen electrode at pH=0). Among the various hybrid nanomaterials, Cd–based chalcogenide semiconductors for photocatalytic H_2 generation have been widely studied owing to their suitable band gap for visible light absorption and well–defined synthetic protocols.

The overall water splitting reaction is:

$$H_2O \rightarrow H_2+O_2 \quad (1)$$

which involves two half reactions, O_2 evolution reaction (OER) (Reaction 2) and hydrogen evolution reaction (HER) (Reaction 3)

$$H_2O \rightarrow 2H^+ + 1/2O_2 + 2e^- \quad (2)$$

$$2H^+ + 2e^- \rightarrow H_2 \quad (3)$$

Systematic investigation of the noble metal species, size, site and the photocatalytic reaction regime conditions like the hydrophilic ligand used for phase transfer, and the hole removal chemical for the H_2 generation reaction were reported on noble metal–Cd–based II–VI hybrid nanoparticles.

The role of metal species: Au, Pt and bimetal.

The Femi energy of Au and Pt is 5.1 eV and 5.6 eV respectively which is within the conduction band and valence band of II–VI semiconductor like CdSe, CdS and ZnSe and ZnS. The energy band alignment makes them good candidates for hot electrons capture from semiconductor nanoparticles. The photoinduced charge separation and hot electron transferring behaviours of Au or Pt–Cd chalcogenide hybrid nanoparticles have been extensively studied. For example, Bang and co–workers[100] investigated the effect of metal composition on photocatalytic hydrogen production efficiency, as shown in **Figure 2.20 (a–e)**. By employing Au–CdSe and Pt–CdSe hybrid nanorods as photocatalysts separately for H_2 generation in water splitting, they observed a rate with 145 μmol/h of single Pt–tipped CdSe nanorods and a rate with only 3.3 μmol/h of double Au–tipped CdSe nanorods. The finding indicated a more satisfied performance of Pt than Au for hybrid nanorods in the application of photocatalytic H_2 evolution. The reason contributing to the higher H_2 generation rate of Pt than Au is further revealed by Yu *et.al*[101] who employed single tipped Au–CdSe and Pt–CdSe hybrid nanorods to study the dynamics of photoexcited charge carriers by ultrafast spectroscopy, as seen in **Figure 2.20 (e–h)**. The ultrafast spectroscopy results suggested that both hot and cold electrons could transfer from CdSe to Au or Pt tips, and Au tips showed faster absorption of photoinduced electrons than Pt tips, but the major difference is that only Pt can completely extract the excited electrons from the CdSe nanorod. This founding indicated that the ability to absorb hot electrons from semiconductor is vital for electron transfer. Because of the better ability of Pt in atAtracting electrons from CdSe nanorods, Pt–CdSe hybrid nanorods showed a better performance than Au–CdSe nanorods which was in agreement with the photocatalytic experimental results reported by Bang and co–workers.[100]

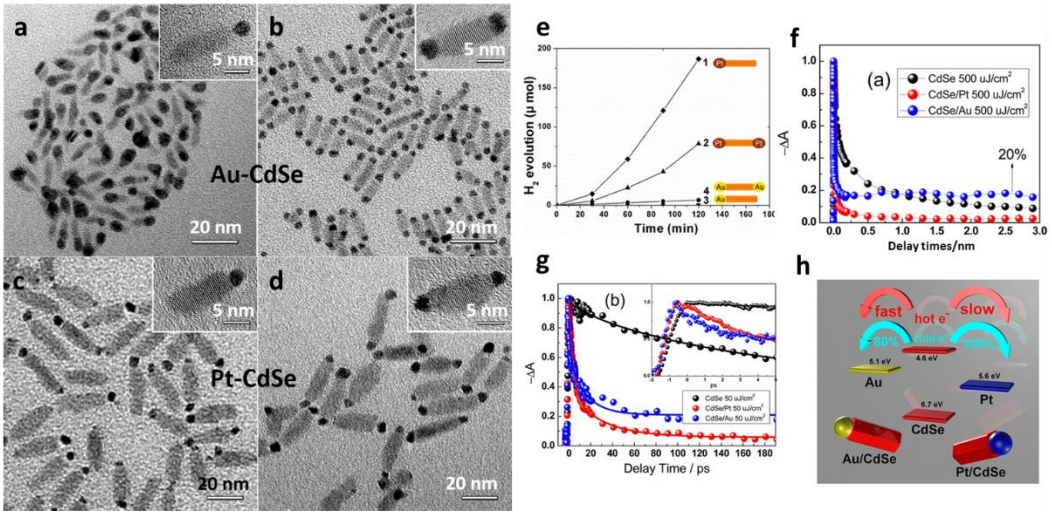

Figure 2.20 (a–d) TEM and HRTEM images of single or double Au–tipped or Pt–tipped CdSe nanorods photocatalysts. (e) H_2 evolution rate of noble metal with varied metal species in (a–d);[100] (e) Normalized transient absorption (TA) time traces of CdSe, CdSe/Au, and CdSe/Pt nanorods (g). (h)Schematic representation of the band alignment of CdSe/Au and CdSe/Pt nanorods and the electrons transfer efficiency.[101]

Except for using the single noble metal hybrid nanoparticles as photocatalyst, bimetal hybrid nanoparticles have also been reported to investigate the photocatalytic H_2 evolution reaction (HER). An interesting report from Kalisman and coworkers[102] indicated that Au–Pt bimetallic cocatalysts showed better performance for water splitting than single metal hybrids. They employed different types of noble metal–semiconductor hybrid for HER. Specifically, Au tiped–CdSe@CdS nanorods, Pt tiped–CdSe@CdS nanorods, Au–Pt core–shell tiped–CdSe@CdS nanorods, and Au core decorated with Pt islands tipped–CdSe@CdS nanorods were used as catalysts for H_2 generation, as seen in **Figure 2.21(a–g)**. The experimental results indicated that Au core decorated with Pt islands tipped–CdSe@CdS nanorods had the highest H_2 generation efficiency. This can be attributed to the combination of Au and Pt metals that have the advantage of fast absorption of hot electrons for Au metal and the complete absorption of hot electrons for Pt metal, enabling both fast and efficient charge transfer and thus efficient hydrogen production. A similar finding was demonstrated by Choi and Song *et al.*[103] who proposed that Pt deposited Au–CdSe–Au nanorods could suppress the electron recombination process. This optimal structure recorded a highest quantum yield of 4.84% which was superior to Au–CdSe–Au nanodumbells with comparable photocurrent as Au–CdSe–Au nanorods, as seen in **Figure 2.21(h–j)**.

The above studies suggested that for single noble metal–semiconductor hybrid nanoparticles, Pt tipped Cd–based heterostructures showed better photocatalytic activity than that of Au tipped ones, and the combination of two species of noble metal in hybrid nanoparticles worked more efficiently than single metal hybrid nanoparticles in the photocatalytic H_2 generation by splitting water.

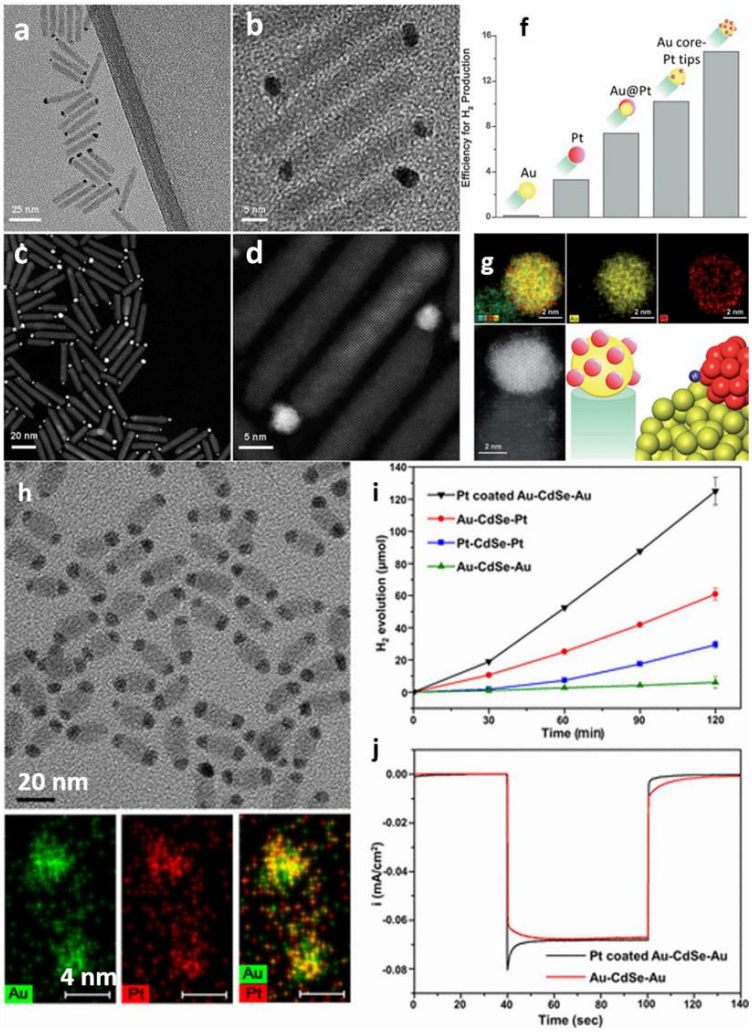

Figure 2.21 (a–d). TEM and STEM images of CdSe@CdS nanorod with Au–Pt bimetallic tips as photocatalysts. (f) H_2 generation efficiency of CdSe@CdS nanorods decorated with Au, Pt, Au@Pt core–shell and Au core–Pt tips as photocatalysts[102] (g). EDS mapping of the Pt islands decorated Au–Pt bimetallic structure.[102] (h) TEM and STEM figures of Pt–coated Au–CdSe–Au nanodumbbells. (i) H_2 generation efficiency and (j) Current–time response curve of Au–CdSe–Au and Pt–coated Au–CdSe–Au nanorods.[103]

The role of metal size.

The size of noble metal plays a critical roles in the photocatalytic reaction as it influence the photo–induced charge separation and recombination. Meyns *et al.*[104] studied the size influence

on the electric transport in Pt–CdSe nanodots. The photocurrent measurement under lase illumination of Pt precisely decorated CdSe nanoparticles with varied Pt domain sizes showed that for CdSe nanodots with a diameter of 10 nm, Pt–CdSe with 3 nm Pt domains exhibited the highest photocurrent among Pt–CdSe with Pt–domains of 1 nm, 2 nm and 3 nm, as seen in **Figure 2.22(a–h).**

Another study on noble metal size effect is reported by Shahar and Banin *et al*.[105] who investigated the influence of the size of Au tip on the photocatalytic performance based on well–defined Au–CdS nanorods by studying the charge transfer dynamics and HER efficiency in the hybrid nanorods. With the diameter of CdS nanorods as 3.9 nm, the optimal Au domain size is found to be 3 nm while the Au tips with a diameter of 1.6 nm, 4.8 nm and 6.2 nm showed lower H_2 generation rate and quantum efficiency because the optimal domain size is the combined result of competing process of electron injection and water reduction on the Au surface. These research founding showed that the optimal diameter of noble metal domains depended on the corresponding the size of CdS or CdSe nanoparticles.

On the other hand, a study reported by Shi and Zhang *et al*. on large Au/CdSe clusters wherein Au nanoparticles were embedded in spherical CdSe nanoparticles suggested a different size dependence of photocatalytic hydrogen evolution rate.[106] As reported, when Au nanoparticles with the size of 2.8, 4.6, 7.2, or 9.0 nm and 3.3 nm CdSe QDs were successfully assembled into large nanocrystal clusters with a diameter of ~100 nm, the plasmonic property of Au nanoparticles played an important role in the H_2 generation reaction, as shown in **Figure 2.22 (i–k)**. As for the Au nanocrystals with a diameter of 7.2 nm, the strong absorption at 575 nm indicated the strong plasmonic absorption of Au NCs which contributed to the formation of more plasmon–induced electron–hole pairs in the cluster. This study demonstrated that the plasmonic generated electron–hole pairs from Au metal nanoparticles could also increase the photocatalytic activity and the H_2 generation efficiency at the interface between plasmonic Au metal nanostructures and CdSe semiconductors.

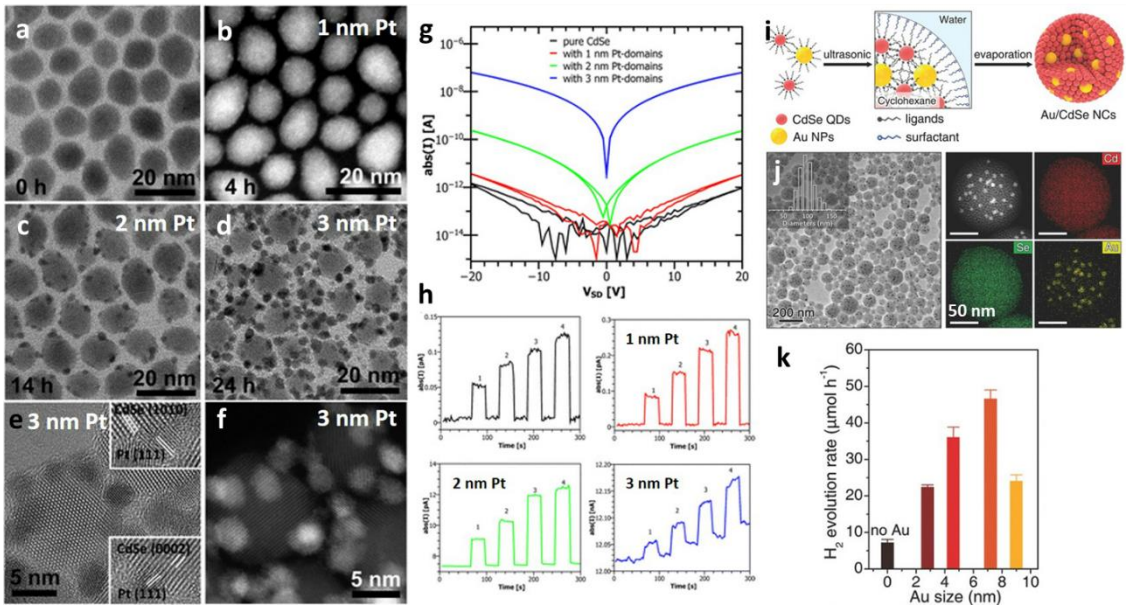

Figure 2.22 (a–f) TEM and STEM images of CdSe NPs and Pt–CdSe hybrid NPs with varied Pt domains size. (g–h) Photocurrent of CdSe NPs and Pt–decorated CdSe NPs.[104](i) Scheme demonstrating the formation of Au/CdSe NCs by self–assembly process. (j) TEM, STEM and EDS images of Au/CdSe NCs. (k) Photocatalytic H_2 evolution rates of Au/CdSe NCs with varied Au NP size. [106]

The role of metal site and quantity.

Several studies reported the geometrical/site and quantity effect of noble metal cocatalyst on the photocatalytic reaction performance. For example, Bang *et al.*[100] compared the H_2 generation rate of single or double Pt–tipped CdSe nanorods. Results showed that the site of Pt growth was very important to HER and the H_2 generation efficiency of single Pt–tipped CdSe nanorods is ~50% higher than that of the double Pt–tipped hybrid nanorods, even with half mass of Pt loading. The improved performance could be attributed to the more effective hole transfer because the unoccupied CdSe nanorods tips were directly exposed to the hole scavenger reagent. The findings were further confirmed by Nakibli and Amirav *et al.* who proposed a "less is more" trend in the case of noble metal as cocatalyst.[107] The hybrid nanorods exhibited a H_2 quantum efficiency of 27% for one Pt tipped nanorods and 18% for two Pt tipped nanorods, while for nanorods with multiple Pt tips, the quantum efficiency is below 1%, as seen in **Figure 2.23**(a–e).[107] The underlying reasons of this phenomenon could be the concentrated electrons amount in one Pt tip than that of departed into two tips as two electrons were needed for one H_2 molecule to be released. The sufficient spatial separation also depressed the recombination of the electron hole pairs.

Beside the hybrid nanorods with tiny noble metal tips, another research on metal site and morphology was reported by Liu and coworkers[108] in relation to the varied conjunction structures between Au and CdSe nanoparticles. Au nanoparticles were synthesized as seeds for later selenization and cation exchange. As pH value for the reaction was controlled at different values, they obtained several different types of Au/CdSe hybrid nanoparticles with varied Au metal sites including Janus nanospheres, heterodimers, symmetric double–headed nanoparticles and multi–headed nanoparticles, as seen in **Figure 2.23**(f–j). The photocatalytic H_2 generation experimental results showed that among these four types of different Au sited hybrid Au/CdSe nanoparticles, the Janus–like nanospheres is proven to be the most active one for photocatalytic H_2 generation, and the Au sites half–shelled CdSe showed the lowest efficiency. These findings were in consistent with the results reported by Nakibli and Amirav[107] who found one side tipped Pt–CdS was more effective than multiple tipped Pt–CdS nanorods for H_2 generation.

In summary, the previous research findings indicate that a high–quality interface between noble metal and semiconductor benefit the photocatalytic H_2 generation and single noble metal tipped nanorods usually work more efficiently than double or multiple tipped nanoparticles as the former provides more efficient spatial charge separation, unoccupied nanorods tip facet for hole removal and more concentrated electrons for H_2 formation and release.

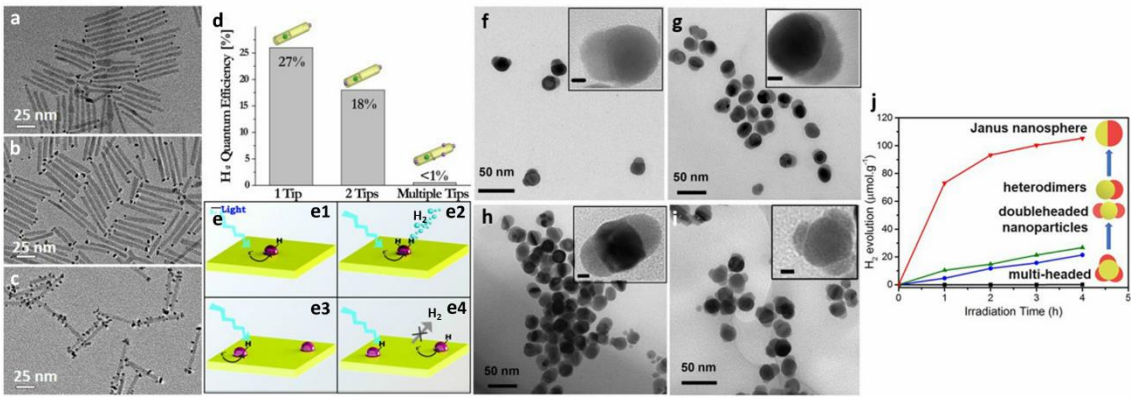

Figure 2.23 (a–c) TEM images CdSe@CdS nanorod with single, double or multiple Pt tips as photocatalysts. (d) Photocatalytic quantum efficiency for H_2 reduction by using the corresponding hybrid nanorods as photocatalysts. (e) Schematic illustration of the formation of H_2 on CdSe@CdS nanorod with a single (top) or a double (down) Au tips catalyst.[107] (f–i) TEM images of Janus nanospheres, heterodimers, symmetric double–headed and multi–headed Au/CdSe hybrid nanoparticles (j) Photocatalytic activity of four different types of Au/CdSe hybrid nanoparticles for hydrogen evolution reactions.[108]

The role of surface coating/phase transfer.

Hybrid nanoparticles are usually synthesized within hydrophobic organic solvent and ligand, surface coating or ligand exchange process is necessary which enable applying the synthesized colloidal nanoparticles for photocatalytic H_2 generation by water splitting. The hydrophilic ligand used for surface coating should help to stabilize the particles in water and maintain good dispensability and accessibility to the active surface site for charge transfer for water splitting. Hydrophilic thiolated–alkyl ligands such as mercaptoundecanoic acid (MUA), mercaptopropionic acid (MPA), 2–mercaptoethanesulfonic acid (MSA), and L–glutathione (GSH) and polymer coatings like Polyethylenimine (PEI) and Poly(styrene–co–maleic anhydride) (PSMA) are usually employed as surface coating ligand before photocatalysis measurement.

Shahar and Banin *et al.*[109] studied the influence of surface coating on the photocatalytic efficiency of Au–CdS nanorods for H_2 generation. Different thiolated–alkyl ligands and polymers were used to transfer Au–CdS nanorods into water phase by surface coatings (**Figure 2.24 a,b**). They found that PEI exhibited the highest H_2 generation rate of 35 ug H_2/h and the highest quantum efficiency of 6.3%. The TA spectra (**Figure 2.24 c**) of MUA, GSH and PEI coated hybrid Au–CdS nanorods all showed a feature of bleach formation at 450 nm from the electron excitation of CdS nanorods and a broad bleach feature at 540 nm from the plasmon response of the Au tip. The normalized TA kinetics (**Figure 2.24d**) of three different surface coated Au–CdS nanorods showed that PEI coated Au–CdS nanorods had the fastest charge transfer dynamics (half–lives of 100 ps), slower for GSH (half–lives of 160 ps) coated samples, and the slowest for MUA (half–lives of 330 ps) passivated particles, respectively. The kinetic measurement suggested that PEI coated Au–CdS nanorods showed the highest efficiency for photocatalystic water splitting, which was consistent with their highest H_2 generation rate and quantum yield.

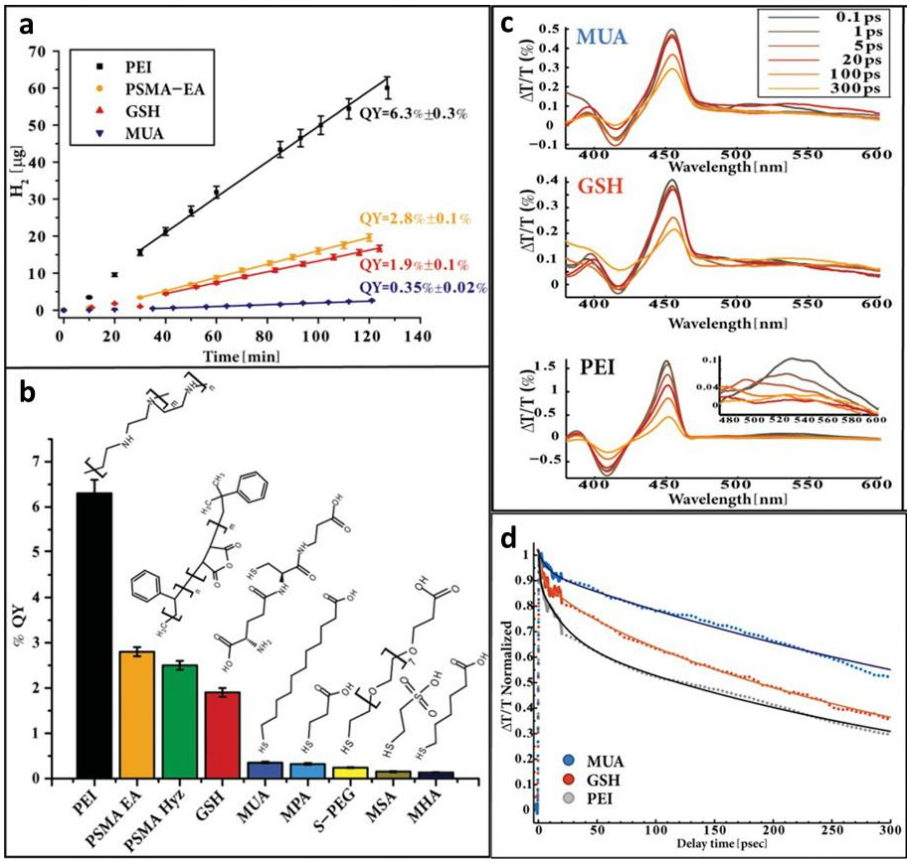

Figure 2.24 (a) Kinetic measurement of H_2 evolution, (b) Apparent photocatalytic quantum yield, (c) Transient absorption spectra at 450nm excitation and (d) Normalized transient absorption kinetics of CdS–Au HNPs with different surface coatings.[109]

The role of holes removal.

H_2 generation is a process that competes with the charge recombination procedure in noble metal semiconductor hybrid nanoparticles. An approach to inhibit photo–generated charge recombination is to irreversibly eliminate the hole by using holes acceptors which can rapidly undergo oxidation reaction. According to the relative energetics of CdSe and CdS semiconductor nanoparticles and noble metal like Au and Pt, photo excited hot electron and hole in the hybrid nanocomposites are separated to different parts of the hybrid nanoparticles. In principle, the long–lived hot electron is transferred to Au or Pt while the hole is kept in the conduction band of semiconductors. As the hole scavenger helps to accumulate the electrons in the Pt tip to reduce two protons for formation of H_2 and compete with the recombination of hole and electron, therefore effective removal of holes is needed to enhance the photocatalytic productivity.

The most common used hole removal or scavenger/sacrificial donor for photocatalysis is methanol or sodium sulphide (Na_2S)/sodium sulfate (Na_2SO_3). These hole removal donates

electrons to the semiconductors to neutralize the photo induced holes. Wu and Lian *et al.*[110] reported that the hole removal to improve the photocatalytic H_2 generation efficiency by using Pt–tipped CdSe/CdS and CdS hybrid nanorods as catalysts. The results showed that compared to methanol, the use of sulfite as the hole removal increased the H_2 generation quantum efficiency and rate for both MUA–capped CdSe/CdS–Pt and CdS–Pt nanorods (**Figure 2.25 a,b**). Besides, the time–resolved fluorescence decay curves (**Figure 2.25 c,d**) showed that in sulphite solution, the CdS and CdSe/CdS nanorods had the shortest average decay lifetime which meant that the fluorescence was heavily quenched. The positive match of the time–resolved fluorescence decay curves with the steady–state H_2 generation quantum efficiency indicated that the hole transfer step might be a key efficiency–limiting step for H_2 generation.
Another factor that affects hole removal is the pH of the solution. Taking the result of Pt decorated two–dimensional Pt–CdS hybrid nanoplateletes (NPLs) for H_2 generation in ethanol/KOH aqueous solution as a samples, as the pH of solution increased between 8.8–14.7, the internal quantum efficiency (IQE) exceeded 40% and increased remarkably with the highest value at pH 14.7, as seen in **Figure 2.25 (e,f)**.[111] It's also worth noting that the pH has no influence on H_2 generation on CdSe based hybrid nanoparticles because the valence band of CdSe is not energetic enough to oxidize OH^-. The detailed studies indicated that at high pH of 14.7, OH^- is the main hole acceptor, which could react fast and irreversibly with ethanol to suppress charge recombination and enable efficient H_2 generation.

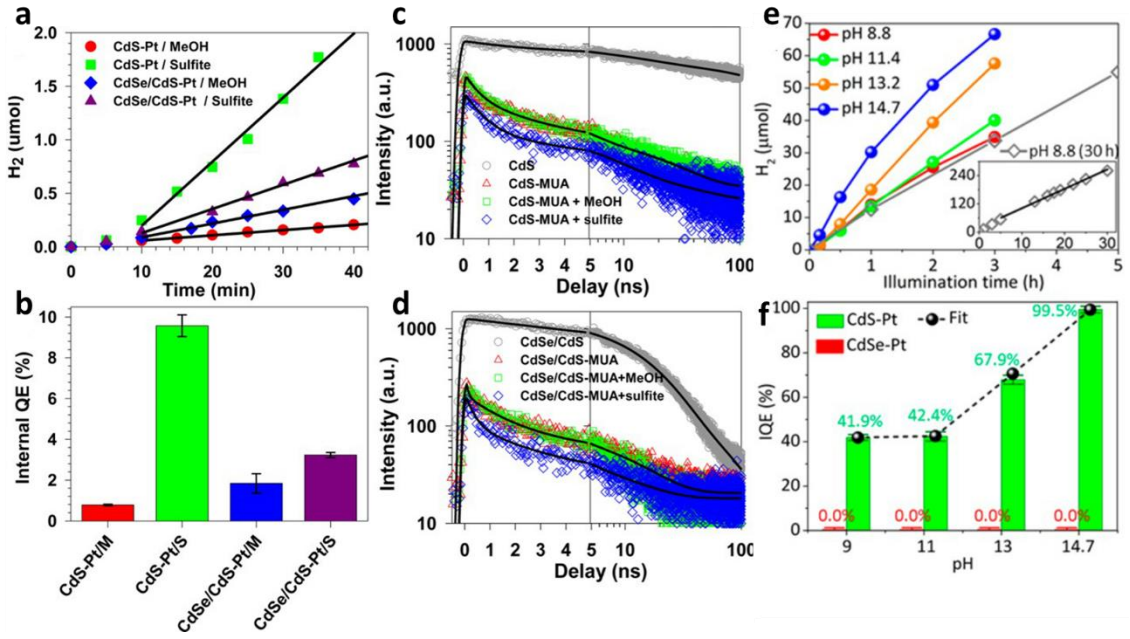

Figure 2.25 (a,b) Photocatalytic H_2 generation rate and quantum efficiency of MUA–capped CdSe/CdS–Pt and CdS–Pt nanorods in methanol or sulphite solution. (c,d) Time–resolved fluorescence decay curves of CdS and CdSe/CdS in different solution, e.g. methanol and sulphide solution.[110] (e) H_2 generation efficiency of Pt–CdS NPLs with pH values from 8.8 to 14.7. (f) pH dependent H_2 generation internal quantum efficiency of Pt–CdS NPLs and Pt–CdSe NPLs.[111]

2.5.2 Other applications of noble metal–II–VI semiconductor nanoparticles

Biomedical applications.

Apart from the widely studied application such as photocatalysts for pollution degradation and clean energy production, noble metal–semiconductor hybrids were also studied in biomedical field owing to its ability to generate reactive oxygen species (ROS), for example photodynamic therapy (PDT). Bare CdSe/CdS nanorods and Au–tipped CdSe/CdS hybrid nanocrystals (HNCs) were used as the photosensitizer for photodynamic tumor therapy reported (**Figure 2.26)**.[112] A report on the *in vitro* detection of ROS generation under visible light irradiation showed that no matter what the surrounding was hypoxic (1% O_2) or not (21% O_2), the ROS generation produced by the Au tipped CdSe/CdS nanorods was more than that of bare CdSe/CdS nanorods (**Figure 2.26c**). The higher amount of ROS led to more effective inhibition during tumor growth as shown in **Figure 2.26 (d, e)** in which a smaller relative tumor volume was observed while the mouse was treated with hybrid nanoparticles–PDT under irradiation. This finding indicated that Au tipped CdSe/CdS nanorods showed a higher efficiency in ROS (singlet oxygen (1O2) and hydroxyl radicals (OH) generation than bare CdSe/CdS nanorods *in vitro* under the visible light irradiation and exhibited good potential as photosensitizer for

oxygen–independent photodynamic tumor therapy.[112] Another interesting research about biological processes application of semiconductor–metal hybrid nanoparticles was reported by Waiskopf and Banin *et al.* [113] where they employed Au–CdS nanorods as efficient photocatalysts to generate ROS like hydrogen peroxide, superoxide, and hydroxyl radicals for controlling biological processes through illumination. In summary, the enhanced capability of producing ROS by illuminating noble metal–semiconductor hybrid nanoparticles provides new ROS–based tools for biological research and lays the foundation for developing novel therapeutic approaches.

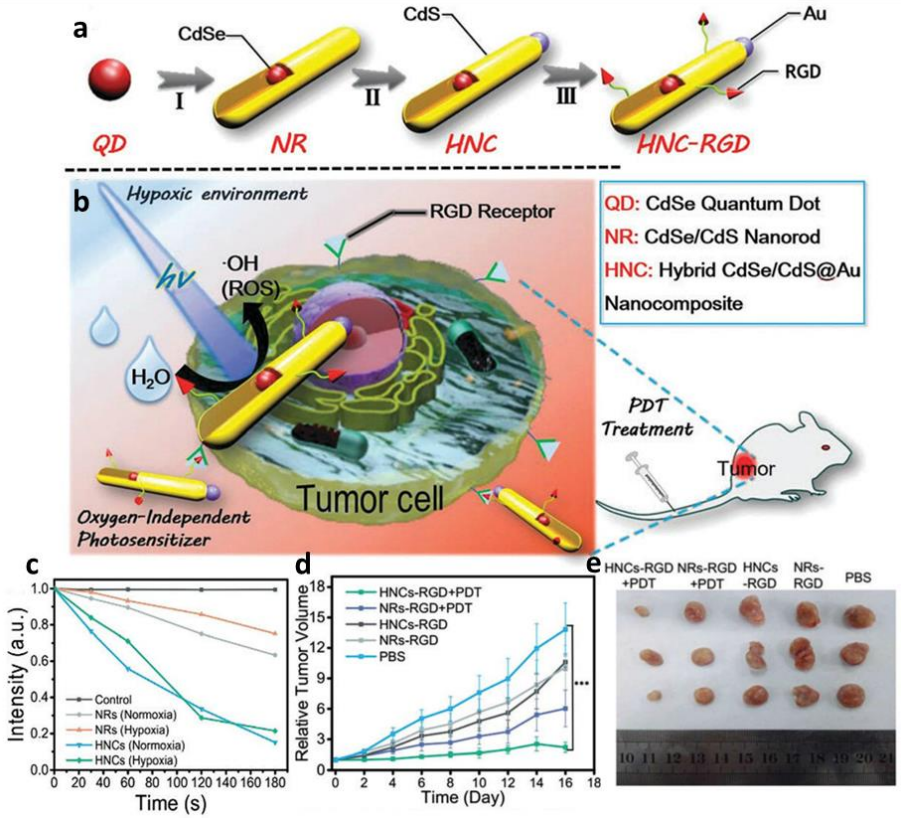

Figure 2.26 (a) Scheme of the HNCs structure growth procedure; (b) Schematic illustration of photocatalytic water splitting to generate ROS for PDT treatment. (c) In vitro evaluation of ROS generation. Absorbance spectra of RNO solution containing HNCs and NRs treated under hypoxia and normoxia; (d) Relative tumor volumes from the different treatment groups; (e) Representative tumor digital photos after various 16 days' treatment. RGD refers to Arg–Gly–Asp. [112]

Photoinitiator in 3D printing.

Besides photocatalytic biomedical applications, semiconductor–metal hybrid nanoparticles were also studied as photoinitiators in 3D printing photopolymerization technique. Pawar and Magdassi *et al.* [114] studied the potential of Au–CdS hybrid nanorods as photoinitiators for 3D printing. They found that the mechanism that was responsible for the formation of radicals

from these hybrid nanoparticles was that Au–CdS hybrid nanorods could generate radicals by a photocatalytic process while traditional photoinitiators were consumed upon irradiation. A scheme of the possible photocatalytic polymerization mechanism of HNPs as photoinitiators was shown in **Figure 2.27a**. Upon light excitation, photocatalytic radicals were formed by HNPs in water, then the hydroxyl radicals generated from hole can work as catalyst for the radical polymerization reaction of acrylamide. [114] The inhibition reaction by oxygen was also presented. As shown in **Figure 2.27 (b,c)**, the polymerization rate could be controlled by introduction of hole scavengers or changing the initial HNPs photoinitiators concentration. By employing the Au–CdS nanorods as the photoinitiator, they successfully printed out a spherical hydrogel C180 ball object containing 73% water and found that this structure cannot be produced by commercial PI (Irgacure 2959) or CdS nanorods without Au tips, which confirmed the essential role of the synergistic effects owing to the hybridization of noble metal onto CdS semiconductors.

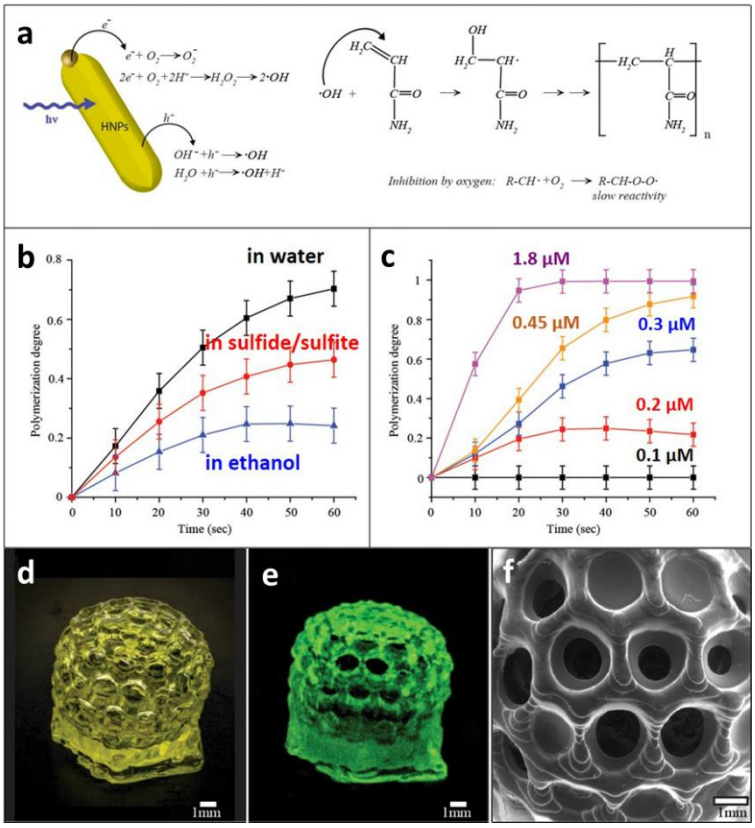

Figure 2.27 (a) Mechanism of using HNPs as photoinitiators for 3D printing. (b) Polymerization dynamic of acrylamide using HNPs as photoinitiators in water, sulfide/sulfite solution, or ethanol. (c) Polymerization dynamic using HNPs with varied concentrations as photoinitiators. (d–f) Pictures of a 3D printed hydrogel ball using CdS–Au HNPs as the photoinitiators, under ambient light and 365 nm excitation respectively. (F) Scanning electron microscopy image of the dried 3D printed ball.[114]

2.6 Conclusions and outlook

In summary, in the past decades, controlled synthesis of Zn–based chalcogenide nanoparticles in terms of size, structure and morphology –have been studied. More progress has been achieved in the synthesis of 0D ZnS, ZnSe and ZnTe nanodots compared with that in the synthesis of 1D and 2D ZnS, ZnSe and ZnTe nanosheets and nanoplatelets. Growth mechanisms including oriented attachment, ligand template growth, cation exchange by using hot–injection or heat–up method were widely reported. As an important type of hybrid nanoparticles, noble metal like Au and Pt were successfully grown onto Cd–based chalcogenide semiconductor nanoparticles which were further employed as photocatalyst for H_2 generation and more. The metal growth mechanisms, influence factors for photocatalytic efficiency were well elucidated. However, compared with Cd–chalcogenide nanoparticles, Zn–chalcogenide nanoparticles produced from synthetic approaches showed low quality, such as low uniformity, poor ligand coverage and abundant surface defects, which affected the performance for application. In addition, Cd–free heterostructure such as noble metal–Zn–chalcogenide were less investigated. Thus, the development of facile approaches for Zn–chalcogenide quantum dots with comparable quality as that of Cd–chalcogenide quantum dots and the expansion of Cd–free Zn–chalcogenide quantum dots to hybrid quantum dots is still a challenge and a worthy project.

2.7 References

1. Henglein A. Photochemistry of colloidal cadmium sulfide. 2. Effects of adsorbed methyl viologen and of colloidal platinum. J. Phys. Chem. 1982;86(13):2291–2293.

2. Rossetti R, Nakahara S, Brus LE. Quantum size effects in the redox potentials, resonance Raman spectra, and electronic spectra of CdS crystallites in aqueous solution. J. Chem. Phys. 1983;79(2):1086–1088.

3. Chemla DS, Miller DAB. Room–Temperature Excitonic Nonlinear–Optical Effects in Semiconductor Quantum–Well Structures. J. Opt. Soc. Am. B. 1985;2(7):1155–1173.

4. Neto JAM, Barbosa LC, Cesar CL, Alves OL, Galembeck F. Quantum Size Effects on Cdtexs1–X Semiconductor–Doped Glass. Appl. Phys. Lett. 1991;59(21):2715–2717.

5. Talapin DV, Lee J–S, Kovalenko MV, Shevchenko EV. Prospects of colloidal nanocrystals for electronic and optoelectronic applications. Chem. Rev. 2010;110(1):389–458.

6. Sun Q, Wang YA, Li LS, Wang DY, Zhu T, Xu J, et al. Bright, multicoloured light–emitting diodes based on quantum dots. Nat. Photonics. 2007;1(12):717–722.
7. Shirasaki Y, Supran GJ, Bawendi MG, Bulovic V. Emergence of colloidal quantum–dot light–emitting technologies. Nat. Photonics. 2013;7(1):13–23.
8. Vaneski A, Schneider J, Susha AS, Rogach AL. Colloidal hybrid heterostructures based on II–VI semiconductor nanocrystals for photocatalytic hydrogen generation. J. Photoch. Photobio. C. 2014;19:52–61.
9. Li XB, Tung CH, Wu LZ. Semiconducting quantum dots for artificial photosynthesis. Nat. Rev. Chem. 2018;2(8):160–173.
10. Wang P, Wang M, Zhang J, Li C, Xu X, Jin Y. Shell Thickness Engineering Significantly Boosts the Photocatalytic H_2 Evolution Efficiency of CdS/CdSe Core/Shell Quantum Dots. ACS Appl. Mater. Interfaces. 2017;9(41):35712–35720.
11. Clifford JP, Konstantatos G, Johnston KW, Hoogland S, Levina L, Sargent EH. Fast, sensitive and spectrally tuneable colloidal–quantum–dot photodetectors. Nat. Nanotechnol. 2009;4(1):40–44.
12. Jin Y, Wang J, Sun B, Blakesley JC, Greenham NC. Solution–processed ultraviolet photodetectors based on colloidal ZnO nanoparticles. Nano Lett. 2008;8(6):1649–1653.
13. Mulder WJM, Koole R, Brandwijk RJ, Storm G, Chin PTK, Strijkers GJ, et al. Quantum dots with a paramagnetic coating as a bimodal molecular imaging probe. Nano Letters. 2006;6(1):1–6.
14. Kim J, Piao Y, Hyeon T. Multifunctional nanostructured materials for multimodal imaging, and simultaneous imaging and therapy. Chem. Soc. Rev. 2009;38(2):372–390.
15. Cheng L, Wang C, Feng L, Yang K, Liu Z. Functional nanomaterials for phototherapies of cancer. Chem. Rev. 2014;114(21):10869–10939.
16. Kumar S, Nann T. Shape control of II–VI semiconductor nanomaterials. Small. 2006;2(3):316–329.
17. Liu W, Lee J–S, Talapin DV. III–V nanocrystals capped with molecular metal chalcogenide ligands: high electron mobility and ambipolar photoresponse. J. Am. Chem. Soc. 2013;135(4):1349–1357.
18. Xie R, Rutherford M, Peng X. Formation of high–quality I− III− VI semiconductor nanocrystals by tuning relative reactivity of cationic precursors. J. Am. Chem. Soc. 2009;131(15):5691–567.

19. Jang Y, Shapiro A, Horani F, Abu–Hariri A, Lifshitz E. Recent Advances in Colloidal IV–VI Core/Shell Heterostructured Nanocrystals. J. Phys. Chem. C. 2018;122(25):13840–13847.

20. Fan J, Chu PK. Group IV nanoparticles: synthesis, properties, and biological applications. Small. 2010;6(19):2080–2098.

21. Zhao Z, Tian J, Sang Y, Cabot A, Liu H. Structure, synthesis, and applications of TiO2 nanobelts. Adv. Mater. 2015;27(16):2557–2582.

22. Mokari T, Banin U. Synthesis and properties of CdSe/ZnS core/shell nanorods. Chem. Mater. 2003;15(20):3955–3960.

23. Diroll BT, Murray CB. High–temperature photoluminescence of CdSe/CdS core/shell nanoheterostructures. ACS nano. 2014;8(6):6466–6474.

24. Naskar S, Schlosser A, Miethe JF, Steinbach F, Feldhoff A, Bigall NC. Site–Selective Noble Metal Growth on CdSe Nanoplatelets. Chem. Mater. 2015;27(8):3159–3166.

25. Berends AC, de Mello Donega C. Ultrathin One– and Two–Dimensional Colloidal Semiconductor Nanocrystals: Pushing Quantum Confinement to the Limit. J. Phys. Chem. Lett. 2017;8(17):4077–4090.

26. Edvinsson T. Optical quantum confinement and photocatalytic properties in two–, one–and zero–dimensional nanostructures. R. Soc. Open. Sci. 2018;5(9):180387.

27. Davidson WL. X–ray diffraction evidence for ZnS formation in zinc activated rubber vulcanizates. Phys. Rev. 1948, 74:116–117.

28. Yeh C–Y, Lu Z, Froyen S, Zunger A. Zinc–blende–wurtzite polytypism in semiconductors. Phys. Rev. B. 1992;46(16):10086.

29. Jumpertz E. Ueber die Elektronendichteverteilung in der Zinkblende. Zeitschrift für Elektrochemie, Berichte der Bunsengesellschaft für physikalische Chemie. 1955;59(5):419–425.

30. Aminoff G. XI. Untersuchungen über die Kristallstrukturen von Wurtzit und Rotnickelkies. Zeitschrift für Kristallographie–Crystalline Materials. 1923;58(1–6):203–219.

31. Jumpertz E. Electron–density distribution in zinc blende. Zeitschrift fuer Elektrochemie. 1955;59:419–425.

32. Karazhanov SZ, Ravindran P, Kjekshus A, Fjellvåg H, Svensson B. Electronic structure and optical properties of Zn X (X= O, S, Se, Te): A density functional study. Phys. Rev. B. 2007;75(15):155104.

33. Lim J, Bae WK, Kwak J, Lee S, Lee C, Char K. Perspective on synthesis, device structures, and printing processes for quantum dot displays. Opt. Mater. Express. 2012;2(5):594–628.

34. Flores EM, Gouvea RA, Piotrowski MJ, Moreira ML. Band alignment and charge transfer predictions of ZnO/ZnX (X = S, Se or Te) interfaces applied to solar cells: a PBE+U theoretical study. Phys. Chem. Chem. Phys. 2018;20(7):4953–4961.

35. de Mello Donega C, Liljeroth P, Vanmaekelbergh D. Physicochemical evaluation of the hot–injection method, a synthesis route for monodisperse nanocrystals. Small. 2005;1(12):1152–1162.

36. Abe S, Capek RK, De Geyter B, Hens Z. Tuning the postfocused size of colloidal nanocrystals by the reaction rate: from theory to application. ACS Nano. 2012;6(1):42–53.

37. van Embden J, Chesman AS, Jasieniak JJ. The heat–up synthesis of colloidal nanocrystals. Chem. Mater. 2015;27(7):2246–2285.

38. Saldanha PL, Lesnyak V, Manna L. Large scale syntheses of colloidal nanomaterials. Nano Today. 2017;12:46–63.

39. Schladt TD, Schneider K, Schild H, Tremel W. Synthesis and bio–functionalization of magnetic nanoparticles for medical diagnosis and treatment. Dalton Trans. 2011;40(24):6315–6143.

40. Park J, Joo J, Kwon SG, Jang Y, Hyeon T. Synthesis of monodisperse spherical nanocrystals. Angew. Chem. Int. Ed. Engl. 2007;46(25):4630–4660.

41. Guidelli EJ, Lignos I, Yoo JJ, Lusardi M, Bawendi MG, Baffa O, et al. Mechanistic Insights and Controlled Synthesis of Radioluminescent ZnSe Quantum Dots Using a Microfluidic Reactor. Chem. of Mater. 2018;30(23):8562–8570.

42. Rossetti R, Hull R, Gibson J, Brus LE. Excited electronic states and optical spectra of ZnS and CdS crystallites in the≅ 15 to 50 Å size range: Evolution from molecular to bulk semiconducting properties. J. Chem. Phys. 1985;82(1):552–559.

43. Li YC, Li XH, Yang CH, Li YF. Ligand–controlling synthesis and ordered assembly of ZnS nanorods and nanodots. J. Phys. Chem. B. 2004;108(41):16002–16011.

44. Thupakula U, Dalui A, Debangshi A, Bal JK, Kumar GS, Acharya S. Shape dependent synthesis and field emission induced rectification in single ZnS nanocrystals. ACS Appl. Mater. Interfaces. 2014;6(10):7856–7863.

45. Pradhan N, Katz B, Efrima S. Synthesis of high–quality metal sulfide nanoparticles from alkyl xanthate single precursors in alkylamine solvents. J. Phys. Chem. B. 2003;107(50):13843–13854.

46. Uehara M, Sasaki S, Nakamura Y, Lee CG, Watanabe K, Nakamura H, et al. Controlled synthesis and structural evolutions of ZnS nanodots and nanorods using identical raw material solution. CrystEngComm. 2011;13(8):2973–2983.

47. Zhu G, Zhang S, Xu Z, Ma J, Shen X. Ultrathin ZnS single crystal nanowires: controlled synthesis and room–temperature ferromagnetism properties. J. Am. Chem. Soc. 2011;133(39):15605–15612.

48. Li D, Hao S, Xing G, Li Y, Li X, Fan L, et al. Solution Grown Single–Unit–Cell Quantum Wires Affording Self–Powered Solar–Blind UV Photodetectors with Ultrahigh Selectivity and Sensitivity. J. Am. Chem. Soc. 2019;141(8):3480–8.

49. Wang Y, Liu Y–H, Zhang Y, Kowalski PJ, Rohrs HW, Buhro WE. Preparation of primary amine derivatives of the magic–size nanocluster $(CdSe)_{13}$. Inorg. Chem. 2013;52(6):2933–2938.

50. Liu Y–H, Wang F, Wang Y, Gibbons PC, Buhro WE. Lamellar assembly of cadmium selenide nanoclusters into quantum belts. J. Am. Chem. Soc. 2011;133(42):17005–17013.

51. Yu JH, Joo J, Park HM, Baik S–I, Kim YW, Kim SC, et al. Synthesis of quantum–sized cubic ZnS nanorods by the oriented attachment mechanism. J. Am. Chem. Soc. 2005;127(15):5662–5670.

52. Fenton JL, Steimle BC, Schaak RE. Tunable intraparticle frameworks for creating complex heterostructured nanoparticle libraries. Science. 2018;360(6388):513–517.

53. Lesnyak V, Brescia R, Messina GC, Manna L. Cu vacancies boost cation exchange reactions in copper selenide nanocrystals. J. Am. Chem. Soc. 2015;137(29):9315–9323.

54. Zhou GT, Wang XC, Yu JC. A low–temperature and mild solvothermal route to the synthesis of Wurtzite–type ZnS with single–crystalline nanoplate–like morphology. Cryst Growth Des. 2005;5(5):1761–1765.

55. Pang Y, Zhang M, Chen D, Chen W, Wang F, Anwar SJ, et al. Why Do Colloidal Wurtzite Semiconductor Nanoplatelets Have an Atomically Uniform Thickness of Eight Monolayers? J. Phys. Chem. Lett. 2019;10(12):3465–3471.

56. Dai L, Lesyuk R, Karpulevich A, Torche A, Bester G, Klinke C. From Wurtzite Nanoplatelets to Zinc Blende Nanorods: Simultaneous Control of Shape and Phase in Ultrathin ZnS Nanocrystals. J. Phys. Chem. Lett.2019;10(14):3828–3835.

57. Chestnoy N, Hull R, Brus LE. Higher excited electronic states in clusters of ZnSe, CdSe, and ZnS: Spin-orbit, vibronic, and relaxation phenomena. J. Chem. Phys. 1986;85(4):2237–2242.

58. Yang L, Xie R, Liu L, Xiao D, Zhu J. Synthesis and Characterization of ZnSe Nanocrystals by W/O Reverse Microemulsion Method: The Effect of Cosurfactant. J. Phys. Chem. C. 2011;115(40):19507–19012.

59. Zhang Q, Li H, Ma Y, Zhai T. ZnSe nanostructures: Synthesis, properties and applications. Prog. Mater. Sci. 2016;83:472–535.

60. Cozzoli PD, Manna L, Curri ML, Kudera S, Giannini C, Striccoli M, et al. Shape and Phase Control of Colloidal ZnSe Nanocrystals. Chem. Mater. 2005;17.

61. Sarkar S, Acharya S, Chakraborty A, Pradhan N. Zinc Blende 0D Quantum Dots to Wurtzite 1D Quantum Wires: The Oriented Attachment and Phase Change in ZnSe Nanostructures. J. Phys. Chem. Letters. 2013;4(19):3292–3297.

62. Acharya S, Panda AB, Efrima S, Golan Y. Polarization Properties and Switchable Assembly of Ultranarrow ZnSe Nanorods. Adv. Mater. 2007;19(8):1105–1108.

63. Jia G, Banin U. A general strategy for synthesizing colloidal semiconductor zinc chalcogenide quantum rods. J. Am. Chem. Soc. 2014;136(31):11121–11127.

64. Zhang LJ, Shen XC, Liang H, Yao JT. Multiple Families of Magic–Sized ZnSe Quantum Dots via Noninjection One–Pot and Hot–Injection Synthesis. J. Phys. Chem. C. 2010;114(50):21921–21927.

65. Ning J, Liu J, Levi–Kalisman Y, Frenkel AI, Banin U. Controlling Anisotropic Growth of Colloidal ZnSe Nanostructures. J. Am. Chem. Soc. 2018;140(44):14627–14637.

66. Park H, Chung H, Kim W. Synthesis of ultrathin wurtzite ZnSe nanosheets. Mater. Lett. 2013;99:172–175.

67. Devami K, Kang D, Lee J–S, Meyyappan M. Synthesis of ZnTe nanostructures by vapor–liquid–solid technique. Chem. Phys. Lett. 2011;504(1–3):62–66.

68. Jang JW, Cho S, Magesh G, Jang YJ, Kim JY, Kim WY, et al. Aqueous–solution route to zinc telluride films for application to CO(2) reduction. Angew. Chem. Int. Ed. Engl. 2014;53(23):5852–7.

69. Lee SH, Kim YJ, Park J. Shape evolution of ZnTe nanocrystals: Nanoflowers, nanodots, and nanorods. Chem. Mater. 2007;19(19):4670–4675.

70. Zhang J, Sun K, Kumbhar A, Fang JY. Shape–control of ZnTe nanocrystal growth in organic solution. J. Phys. Chem. C. 2008;112(14):5454–5458.

71. Zhang J, Jin S, Fry HC, Peng S, Shevchenko E, Wiederrecht GP, et al. Synthesis and characterization of wurtzite ZnTe nanorods with controllable aspect ratios. J. Am. Chem. Soc. 2011;133(39):15324–15327.
72. Wang A, Shen H, Zang S, Lin Q, Wang H, Qian L, et al. Bright, efficient, and color–stable violet ZnSe–based quantum dot light–emitting diodes. Nanoscale. 2015;7(7):2951–2959.
73. Song KK, Lee S. Highly luminescent (ZnSe)ZnS core–shell quantum dots for blue to UV emission: synthesis and characterization. Curr. Appl. Phys. 2001;1(2–3):169–173.
74. Bang J, Park J, Lee JH, Won N, Nam J, Lim J, et al. ZnTe/ZnSe (Core/Shell) Type–II Quantum Dots: Their Optical and Photovoltaic Properties. Chem. Mater. 2010;22(1):233–240.
75. Jang EP, Han CY, Lim SW, Jo JH, Jo DY, Lee SH, et al. Synthesis of Alloyed ZnSeTe Quantum Dots as Bright, Color–Pure Blue Emitters. ACS Appl. Mater. Interfaces. 2019;11(49):46062–46069.
76. Ji B, Panfil YE, Waiskopf N, Remennik S, Popov I, Banin U. Strain–controlled shell morphology on quantum rods. Nat. Commun. 2019;10(1):2.
77. Li H, Brescia R, Krahne R, Bertoni G, Alcocer MJ, D'Andrea C, et al. Blue–UV–emitting ZnSe(dot)/ZnS(rod) core/shell nanocrystals prepared from CdSe/CdS nanocrystals by sequential cation exchange. ACS Nano. 2012;6(2):1637–1647.
78. Ji B, Panfil YE, Banin U. Heavy–Metal–Free Fluorescent ZnTe/ZnSe Nanodumbbells. ACS Nano. 2017;11(7):7312–7320.
79. Bose R, Manna G, Pradhan N. Au–thiol interaction chemistry to influence the structural transformation of semiconductor nanocrystals and formation of giant nanostructures. Small. 2014;10(7):1289–1293.
80. Bose R, Wasey AH, Das GP, Pradhan N. Heteroepitaxial Junction in Au–ZnSe Nanostructure: Experiment versus First–Principle Simulation. J. Phys. Chem. Lett. 2014;5(11):1892–1898.
81. Dunpall R, Lewis EA, Haigh SJ, O'Brien P, Revaprasadu N. Synthesis of biocompatible Au–ZnTe core–shell nanoparticles. J. Mater. Chem. B. 2015;3(14):2826–2833.
82. Mokari T, Rothenberg E, Popov I, Costi R, Banin U. Selective growth of metal tips onto semiconductor quantum rods and tetrapods. Science. 2004;304(5678):1787–1790.
83. Mokari T, Sztrum CG, Salant A, Rabani E, Banin U. Formation of asymmetric one–sided metal–tipped semiconductor nanocrystal dots and rods. Nat. Mater. 2005;4(11):855–863.
84. Saunders AE, Popov I, Banin U. Synthesis of hybrid CdS–Au colloidal nanostructures. J. Phys. Chem. B. 2006;110(50):25421–25429.

85. Carbone L, Jakab A, Khalavka Y, Sonnichsen C. Light–controlled one–sided growth of large plasmonic gold domains on quantum rods observed on the single particle level. Nano Lett. 2009;9(11):3710–3714.

86. Menagen G, Mocatta D, Salant A, Popov I, Dorfs D, Banin U. Selective Gold Growth on CdSe Seeded CdS Nanorods. Chem. Mater. 2008;20(22):6900–6902.

87. Chakrabortty S, Yang JA, Tan YM, Mishra N, Chan Y. Asymmetric dumbbells from selective deposition of metals on seeded semiconductor nanorods. Angew. Chem. Int. Ed. Engl. 2010;49(16):2888–2892.

88. Habas SE, Yang P, Mokari T. Selective Growth of Metal and Binary Metal Tips on CdS Nanorods. J. Am. Chem. Soc. 2008(130):3294–3295.

89. Lambright S, Butaeva E, Razgoniaeva N, Hopkins T, Smith B, Perera D, et al. Enhanced lifetime of excitons in nonepitaxial Au/CdS core/shell nanocrystals. ACS Nano. 2014;8(1):352–361.

90. Ma L, Chen K, Nan F, Wang J–H, Yang D–J, Zhou L, et al. Improved Hydrogen Production of Au–Pt–CdS Hetero–Nanostructures by Efficient Plasmon–Induced Multipathway Electron Transfer. Adv. Fun. Mater. 2016;26(33):6076–6083.

91. Bradley MJ, Read CG, Schaak RE. Pt–Au Nanoparticle Heterodimers as Seeds for Pt–Au–Metal Sulfide Heterotrimers: Thermal Stability and Chemoselective Growth Characteristics. J. Phys. Chem. C. 2015;119(16):8952–8959.

92. van Huis MA, Figuerola A, Fang C, Beche A, Zandbergen HW, Manna L. Chemical transformation of Au–tipped CdS nanorods into AuS/Cd core/shell particles by electron beam irradiation. Nano Lett. 2011;11(11):4555–4561.

93. Haldar KK, Pradhan N, Patra A. Formation of heteroepitaxy in different shapes of Au–CdSe metal–semiconductor hybrid nanostructures. Small. 2013;9(20):3424–3432.

94. Javaid S, Li X, Wang F, Chen W, Pang Y, Wang S, et al. Synthesis of magnetically separable Fe3O4–Au–CdS kinked heterotrimers incorporating plasmonic and semiconducting functionalities. J. Mater. Chem. C. 2019;7(46):14517–14524.

95. AbouZeid KM, Mohamed MB, El–Shall MS. Hybrid Au–CdSe and Ag–CdSe nanoflowers and core–shell nanocrystals via one–pot heterogeneous nucleation and growth. Small. 2011;7(23):3299–3307.

96. Fernàndez–Altable V, Dalmases M, Falqui A, Casu A, Torruella P, Estradé S, et al. Au–Assisted Growth of Anisotropic and Epitaxial CdSe Colloidal Nanocrystals via in Situ Dismantling of Quantum Dots. Chem. Mater. 2015;27(5):1656–1664.

97. Tessier MD, Spinicelli P, Dupont D, Patriarche G, Ithurria S, Dubertret B. Efficient exciton concentrators built from colloidal core/crown CdSe/CdS semiconductor nanoplatelets. Nano Lett. 2014;14(1):207–213.

98. Costi R, Saunders AE, Elmalem E, Salant A, Banin U. Visible light–induced charge retention and photocatalysis with hybrid CdSe–Au nanodumbbells. Nano Lett. 2008;8(2):637–641.

99. Elmalem E, Saunders AE, Costi R, Salant A, Banin U. Growth of Photocatalytic CdSe–Pt Nanorods and Nanonets. Adv. Mater. 2008;20(22):4312–4317.

100. Bang JU, Lee SJ, Jang JS, Choi W, Song H. Geometric Effect of Single or Double Metal–Tipped CdSe Nanorods on Photocatalytic H_2 Generation. J. Phys. Chem. Lett. 2012;3(24):3781–3785.

101. Yu P, Wen X, Lee Y–C, Lee W–C, Kang C–C, Tang J. Photoinduced Ultrafast Charge Separation in Plexcitonic CdSe/Au and CdSe/Pt Nanorods. J. Phys. Chem. Lett. 2013;4(21):3596–3601.

102. Kalisman P, Houben L, Aronovitch E, Kauffmann Y, Bar–Sadan M, Amirav L. The golden gate to photocatalytic hydrogen production. J. Mater. Chem. A. 2015;3(39):19679–19682.

103. Choi JY, Jeong D, Lee SJ, Kang DG, Kim SK, Nam KM, et al. Engineering Reaction Kinetics by Tailoring the Metal Tips of Metal–Semiconductor Nanodumbbells. Nano Lett. 2017;17(9):5688–5694.

104. Meyns M, Willing S, Lehmann H, Klinke C. Metal Domain Size Dependent Electrical Transport in Pt–CdSe Hybrid Nanoparticle Monolayers. ACS Nano. 2015;9(6):6077–6687.

105. Ben–Shahar Y, Scotognella F, Kriegel I, Moretti L, Cerullo G, Rabani E, et al. Optimal metal domain size for photocatalysis with hybrid semiconductor–metal nanorods. Nat. Commun. 2016;7:10413.

106. Shi R, Cao Y, Bao Y, Zhao Y, Waterhouse GIN, Fang Z, et al. Self–Assembled Au/CdSe Nanocrystal Clusters for Plasmon–Mediated Photocatalytic Hydrogen Evolution. Adv. Mater. 2017;29(27):1700803.

107. Nakibli Y, Kalisman P, Amirav L. Less Is More: The Case of Metal Cocatalysts. J. Phys. Chem. Lett. 2015;6(12):2265–2268.

108. Liu XD, Chen K, Ma S, Hao ZH, Liang S, Zhou L, et al. Synthesis of Au/CdSe Janus Nanoparticles with Efficient Charge Transfer for Improving Photocatalytic Hydrogen Generation. Nanoscale Res. Lett. 2019;14(1):349.

109. Ben–Shahar Y, Scotognella F, Waiskopf N, Kriegel I, Dal Conte S, Cerullo G, et al. Effect of surface coating on the photocatalytic function of hybrid CdS–Au nanorods. Small. 2015;11(4):462–471.
110. Wu K, Chen Z, Lv H, Zhu H, Hill CL, Lian T. Hole removal rate limits photodriven H2 generation efficiency in CdS–Pt and CdSe/CdS–Pt semiconductor nanorod–metal tip heterostructures. J. Am. Chem. Soc. 2014;136(21):7708–7716.
111. Li Q, Zhao F, Qu C, Shang Q, Xu Z, Yu L, et al. Two–Dimensional Morphology Enhances Light–Driven H2 Generation Efficiency in CdS Nanoplatelet–Pt Heterostructures. J. Am. Chem. Soc. 2018;140(37):11726–11734.
112. Fan JX, Liu MD, Li CX, Hong S, Zheng DW, Liu XH, et al. A metal–semiconductor nanocomposite as an efficient oxygen–independent photosensitizer for photodynamic tumor therapy. Nanoscale Horiz. 2017;2(6):349–355.
113. Waiskopf N, Ben–Shahar Y, Galchenko M, Carmel I, Moshitzky G, Soreq H, et al. Photocatalytic Reactive Oxygen Species Formation by Semiconductor–Metal Hybrid Nanoparticles. Toward Light–Induced Modulation of Biological Processes. Nano Lett. 2016;16(7):4266–4273.
114. Pawar AA, Halivni S, Waiskopf N, Ben–Shahar Y, Soreni–Harari M, Bergbreiter S, et al. Rapid Three–Dimensional Printing in Water Using Semiconductor–Metal Hybrid Nanoparticles as Photoinitiators. Nano Lett. 2017;17(7):4497–4501.

Chapter 3. Experimental and Characterization Details

3.1 Experimental facilities

3.1.1 Nanoparticles synthesis.

The synthetic experiments were performed using Schleck line techniques, as seen in **Figure 3.1**. With two valves of vacuum and N_2 connection, the surrounding of the reaction system in the flask can be ensured as inert gas protection. The heating mantles were controlled by a thermal controller which determines the reaction temperature. Precursor, ligand and solvent were put into a three–neck flask, evacuated and then filled with N_2 for three times before heating to a pre–determined temperature. A vacuum pump was used to evacuate gas inside the reaction system. The reaction temperature was monitored timely by a thermalcouple which was immersed into the reaction solution. More detailed experimental information could be found in the experimental section of each chapter.

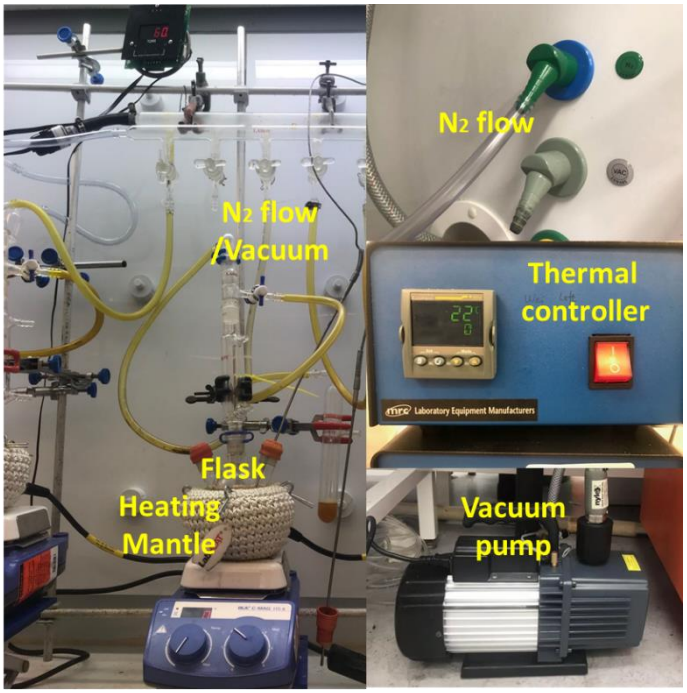

Figure 3.1 A Schleck line set–up for colloidal nanoparticles synthesis.

3.1.2 Nanoparticles purification and storage.

For active precursor preparation, such as the superhydride (air sensitive) reduced Se–oleylamine precursor, a glovebox (**Figure 3.2)** filled with Ar gas was used to for the preparation of the precursor. Typically, Se powder was dissolved in oleylamine by heating in the Schleck line firstly, then the prepared Se–oleylamine solution was cooled down to the room temperature

(~25ºC) and transferred to the Ar-filled glovebox followed by adding superhydride that produced reduced Se–oleylamine precursor.

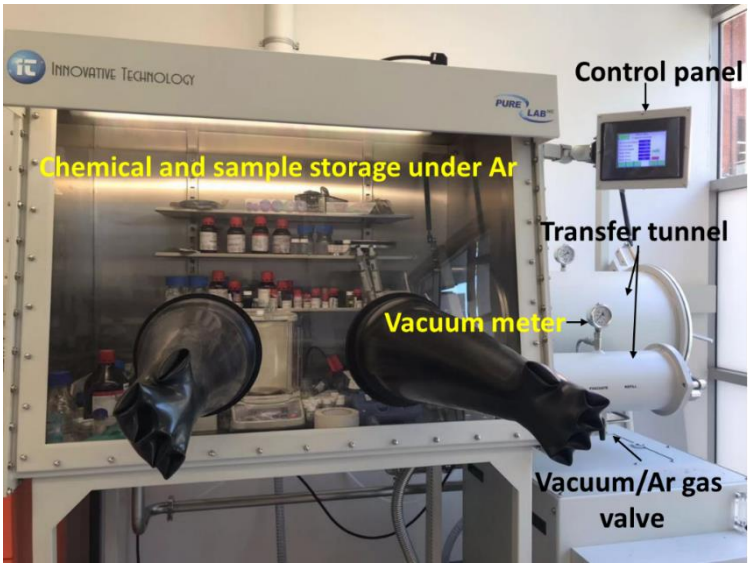

Figure 3.2 A glovebox with Ar protection for reactive chemicals like superhydride addition and purified nanoparticles storage.

The synthesized nanoparticles were purified with toluene/chloroform and ethanol/methanol. Specifically, the nanoparticle synthesized in an organic solvent like oleylamine were transferred to a centrifuge tube and a polar solvent such as ethanol/methanol was added to facilitate the precipitation of the nanopartilces. The purification procedure was repeated for three times by using toluene/chloroform for dispersion and ethanol/methanol for precipitation. A centrifuge was used as shown in **Figure 3.3** and the typical centrifugation speed is set as 5000 round per minute.

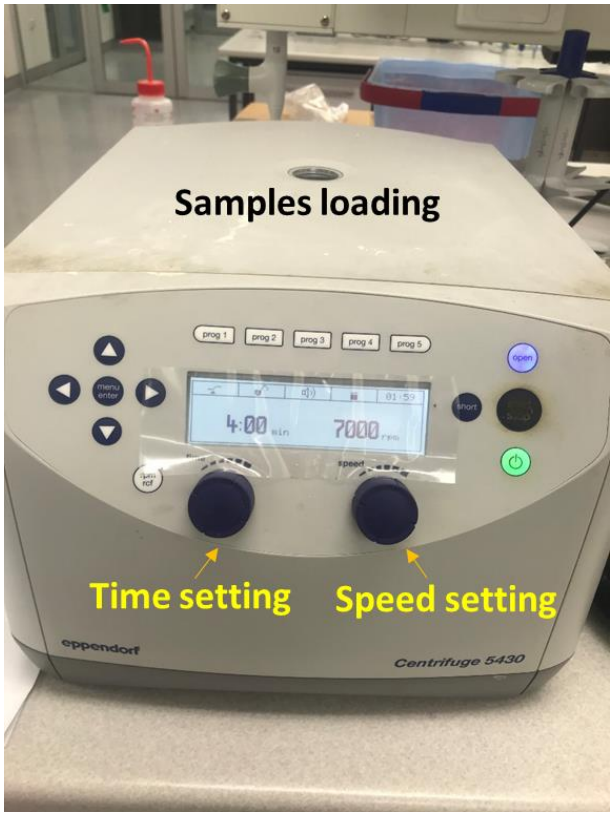

Figure 3.3 A photo of centrifuge used for centrifugation and purification of the nanoparticle samples.

3.2 Characterization.

Ultraviolet–visible spectroscopy (UV–Vis), photoluminescent (PL) spectrograph, transmission electron microscope (TEM), X–ray diffraction (XRD), X–ray photoelectron Sspectroscopy (XPS), inductively coupled plasma source mass spectrometer (ICP–MS) and thermogravimetric analyzer (TGA) were used for nanoparticles characterization in the study. The characterization was performed in School of Molecular and Life Sciences, John de Laeter Centre, Characterization & Analysis Curtin University, Australia, Centre for Microscopy, Characterization & Analysis, The University of Western Australia, a facility funded by the University, State, and Commonwealth Governments, and Chem Centre, Perth Australia. Detailed information about the equipment and operating conditions can be found in **Figure 3.4–3.10.**

3.2.1 Optical measurement (UV–Vis and fluorescence spectrophotometer)

The UV–Vis optical absorption was measured by a Cary 4000 UV–Vis Spectrophotometer equipped with a Xenon light source. Briefly, a proper amount of the synthesized nanoparticles was dispersed in toluene or chloroform in a quartz cuvette for testing. The scanning scale was set between 250nm~800nm depending on the nanomaterial components and size.

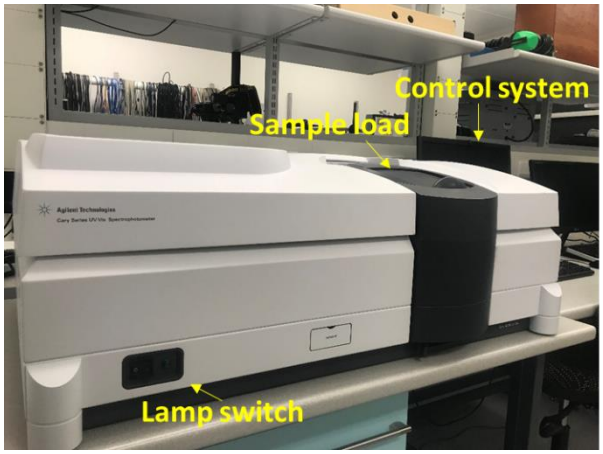

Figure 3.4 A photo of a UV–Vis Spectrophotometer, model Cary series, used for the optical absorption measurement.

The photoluminescence analysis was conducted on a Cary Edipse Photoluminescent (PL) Spectrophotometer where the samples preparation was the same as samples used for above–mentioned UV–Vis optical absorption test. The emission spectra were obtained by exciting the samples at the peak wavelength of the absorption.

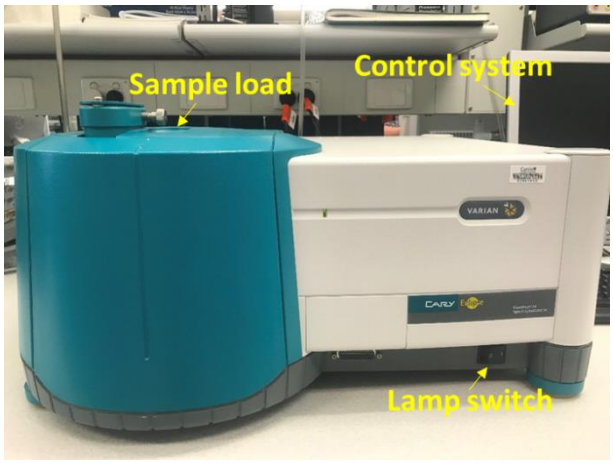

Figure 3.5 Photography of a photoluminescent (PL) spectroscopy.

3.2.2 Transmission electron microscope (TEM)

TEM samples were prepared on carbon-supported copper grids by droping one drop of the solution (e.g. toluene, hexance) which contains dispersed purified nanoparticles. TEM and high–resolution TEM (HRTEM) were performed using a FEI Talos Fs200x G2 FEG transmission electron microscope with a tungsten filament running at an accelerating voltage of 200 kV.

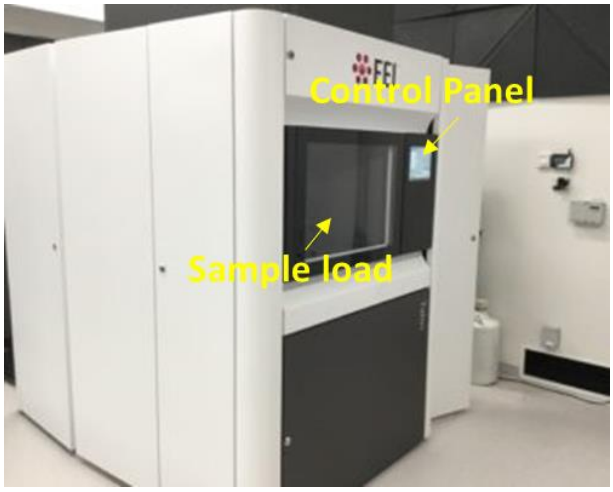

Figure 3.6 FEI Talos Fs200x G2 Feg transmission electron microscope (TEM).

3.2.3 X–ray diffraction (XRD)

The crystal structure analysis was conducted on a Powder X–ray diffraction (XRD) with Cu Kα photons from Bruker AXS D8 Advance operated at 40 kV and 30 mA. Each nanoparticle sample was dispersed in hexane/chloroform to get a condensed solution and then deposited as a thin layer on a low background–scattering silicon substrate. Then the samples were run using a typical scan range from 20° to 70° (2θ) in steps of 0.1° (2θ) with an intergration time of 6 seconds per step, which takes approximately 50 mins each sample.

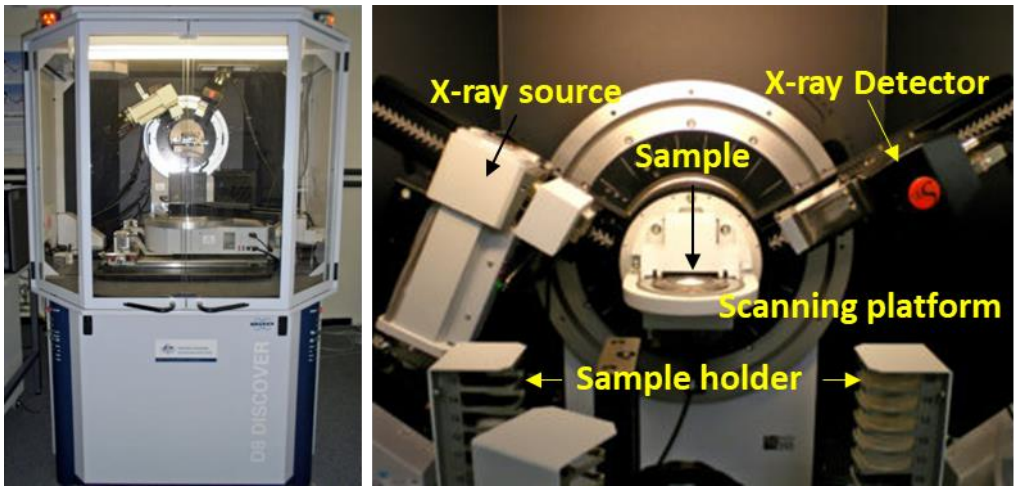

Figure 3.7 Powder X–ray diffraction (XRD) for crystal structure characterization.

3.2.4 X–ray photoelectron spectroscopy (XPS)

XPS measurements were performed on a Kratos Axis Ultra DLD spectrometer equipped with a high intensity monochromated X–ray source Al Kα (1486.6 eV) at 225 W. The electron binding energy scale was calibrated by setting the main line of the C 1s spectrum to 284.8 eV

with the Casa XPS software. For the survey spectra, the pass energy was160 eV and for the high–resolution spectra, the pass energy was 40 eV. For XPS peaks splitting and fitting, each high–resolution spectrum was fitted with a Gaussian shape line in Origin 9.0, the binding energy of each element and the split spin-orbit components were compared with reported research.

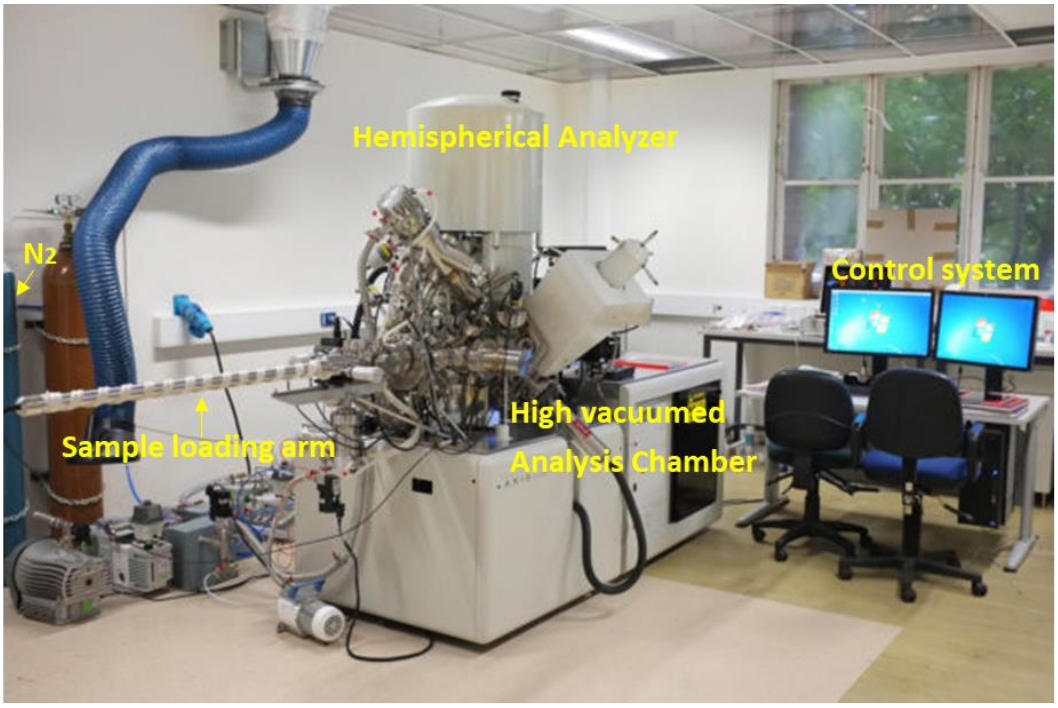

Figure 3.8 X–ray photoelectron spectroscopy (XPS), Kratos Axis Ultra DLD spectrometer, used for elemental composition, chemical state and electronic state analysis of nanoparticles.

3.2.5 Inductively coupled plasma optical emission spectrometry (ICP–OES)

The ion by mass in nanoparticles was measured by ICP–OES on an Agilent 7700 spectrometer with an integrated sample introduction system. For each measurement, taking the measurement range of concentration into account, ~5 mg sample was digested in 2 ml concentrated hydrochloric acid and nitric acid (3:1) at 98°C, then 3% diluted hydrochloric acid and nitric acid in deionized water were added to the above solution to make 25 ml solution for testing.

Figure 3.9 Inductively coupled plasma optical emission spectrometry for elements mass concentration analysis.

3.2.6 Thermogravimetric analyzer (TGA)

A TA Instruments (Model: SDT Q600 simultaneous DTA–TGA) was used for TGA measurement. Typically, around 8 mg of purified and dry nanoparticles sample was weighed into a 110 µL platinum (Pt) crucible with a matched empty crucible as a reference. The sample was heated from 25°C to 500°C with a heating speed of 10°C/min in N_2 flowing at 100 ml/min, after reaching 500°C, it was cooled down to room temperature. The temperature scale of the instrument was calibrated using the melting points of 99.999% indium (156.5985°C), 99.99+% tin (231.93°C), 99.99+% zinc (419.53°C), 99.99% silver (961.78°C), and 99.999% gold (1064.18°C). The balance was calibrated over the temperature range used with alumina mass standards provided by the instrument manufacturer. The heat flow between the pans was calibrated using a sapphire disk provided by the instrument manufacturer. The cell constant was fine–tuned using the heat of fusion of zinc (113 J/g).

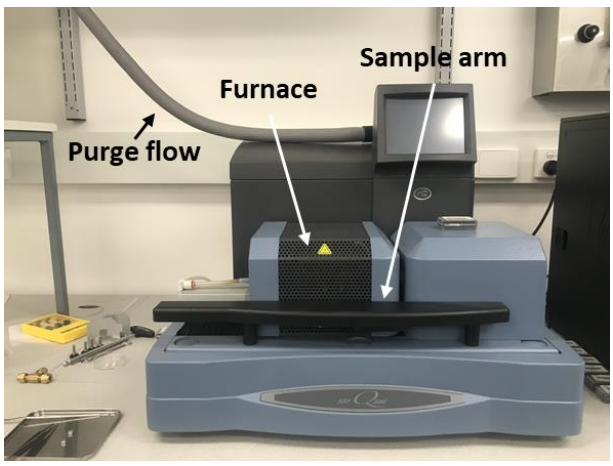

Figure 3.10 Thermogravimetric analyzer (TGA), used for surface ligand mass percentage analysis.

3.2.7 Photocatalytic H_2 evolution reaction (HER).

The equipment for photocatalytic water–splitting experiments is shown in **Figure 3.11**, in which the experiment was conducted in a customized airtight stainless-steel reactor at room temperature. A 300W Xeon lamp (Newport) was employed as a light source (200~2500 nm) and the irradiation intensity of was 120 mW/cm^2. Before irradiation for H_2 generation, the samples (e.g. nanoparticles dispersed in methanol/water) were vigorously stirred for 30 min in dark and the reactor was degassed by purging with N_2 for 30 mins to remove ambient gas. The generated H_2 was in situ measured by a gas chromatography (Agilent 490 Micro GC) using a thermal conductivity detector.

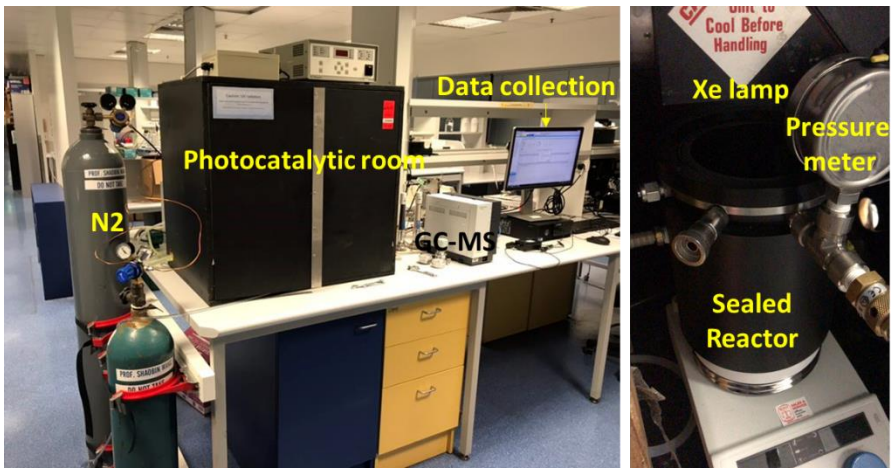

Figure 3.11 Photocatalysis set–up for H_2 evolution reaction measurement.

Chapter 4. Spontaneous shape and phase control of colloidal ZnSe nanocrystals by tailoring Se precursor reactivity

Wei Chen, Amir Karton, Tanveer Hussian, Shaghraf Javaid, Fei Wang, Yingping Pang and Guohua Jia

CrystEngComm, 2019,21, 2955–2961

DOI: https://doi.org/10.1039/C9CE00078J

A copyright permission and author contribution statement could be found in Appendix B.

Summary of Chapter.

In this chapter, we reported the successful and facile shape and size control of ZnSe nanocrystals in a phosphine–free system. By simply tailoring the added ratio of super hydride to selenium precursor, uniform ZnSe nanodots or nanorods with tunable diameter were obtained. We also presented a detailed investigation of the special role of super hydride in the phosphine–free synthesis of ZnSe nanocrystals and proposed a mechanism that was responsible for the formation of ZnSe nanodots and nanorods. By combing the calculated Gibbs free energies of reaction between Se and super hydride and the experiment results, we presented that the selenium precursor in oleylamine can be reduced to Se_2^{2-} or Se^{2-} depending on the amount of super hydride added. With the increase of super hydride, Se^0 was reduced to Se_2^{2-} then Se^{2-}, and the reaction activity of different Se species was determined as $Se^{2-} > Se_2^{2-} > Se^0$. ZnSe nanodots of zinc blende phase were obtained when active Se^{2-} was employed as the Se precursor, ZnSe nanorods of wurtzite phase were obtained when less active Se_2^{2-} was employed as the Se precursor.

The impact and outcomes of the work include a novel synthetic method of shape and phase control of ZnSe nanorods and ZnSe nanodots in a phosphine–free system. A detailed calculation of Se reduction and growth mechanism for the formation of ZnSe nanorods and nanorods were also presented. This method for synthesis of ZnSe nanorods and nanodots was firstly presented and will give insights into the controlled synthesis of other nanomaterials.

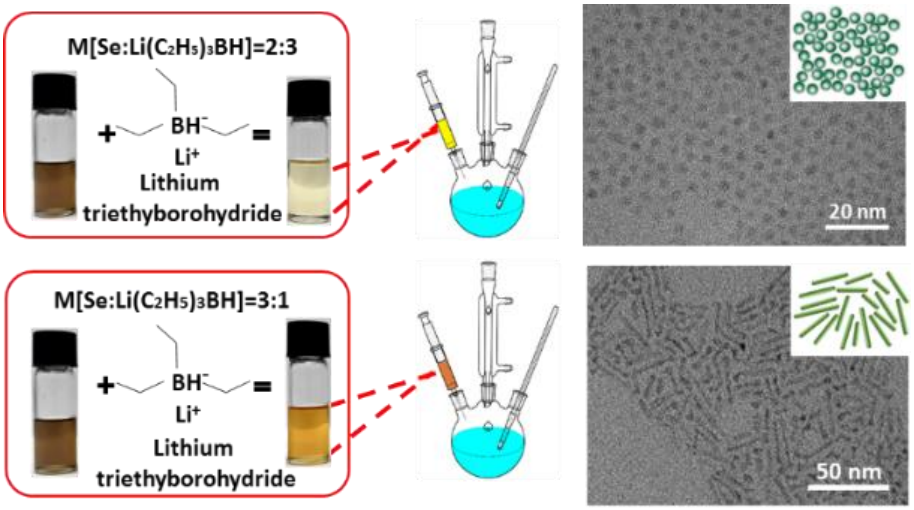

Figure 4.1 A summarized figure of the contents in this chapter. (a, left panel) A photo showing the color change after additon of super hydrid into Se–oleylamine solution. (b, right panel) TEM images and schematic diagtam of ZnSe nanodots and nanorods synthesized using two different precursors, respectively.

Abstract

Herein we demonstrated the shape and phase of colloidal ZnSe nanocrystals can be spontaneously tuned through tailoring the selenium precursor reactivity in a phosphine–free reaction system. Selenium species with diverse reaction activities, i.e. Se_2^{2-} or Se^{2-}, were produced by the addition of difference volume of reductant superhydride (Lithium triethylborohydride). Theoretical calculation of ΔG_r indicated that superhydride–reduced Se_2^{2-} is less active than Se^{2-} for the reaction with Zn precursor. Nanoparticle growth using Se_2^{2-} produces wurtzite ZnSe nanorods whereas the reaction of more reactive Se^{2-} with zinc precursor leads to the formation of spherical zinc blende ZnSe nanodots. This work not only provides a facile synthetic approach for the preparation of high quality ZnSe nanocrystals but also gives insights into the shape and phase control of other colloidal nanocrystals.

4.1 Introduction

Zinc selenide (ZnSe) semiconductor nanocrystal (NC) is regarded as a green material due to its environmental benignity compared with the highly toxic cadmium–based semiconductor NCs[1–7]. With a band gap of 2.82eV of the bulk material, ZnSe NCs or their hybrid nanocrystals can be potentially applied in many applications, such as photodetectors[8], light–emitting diodes (LEDs)[9,10], bio–labelling[11] and solar cells[12–13]. When the smallest dimension of semiconductor NCs is close to or smaller than their Bohr exciton radius, excitons are squeezed and confined in a small space closely, leading to size– and shape dependent properties. This enables the electronic and optical properties of semiconductor NCs being different from their counterparts such as bulk materials[14]. For one dimensional (1D) semiconductor NCs, excitons are quantum confined in two dimensions, and thus they manifest the similar properties as those of bulk material on the length direction. This confinement enables them to have different properties than 0–dimensional spherical nanodots, in terms of electronic structure, linear polarization of photoluminescence and carrier dynamics[15].

A lot of research effort was devoted into the size and shape control of semiconductor NCs, including II–VI[16–20] and III–V[21–22] semiconductors. Effective shape and size control are fulfilled in Cd chalcogenide NCs. Uniform CdX (X=S, Se and Te) nanodots and nanorods or their heterostructures with tunable size have been successfully synthesized by hot injection methods or heat up methods[23–28]. Typically, one dimensional (1D) NCs can be synthesized by oriented attachment[29–31], epitaxial

growth[30, 32], template directed growth[33–34] and cation exchange[35] method. For the shape and size control of 1D zinc based semiconductor NCs, there are some reports on the successful synthesis of neat ZnSe and Mn^{2+} doped ZnSe spherical dots with a diameter range of 2~5 nm by using a hot injection method in which the high reactive zinc precursor or selenium precursor were employed[36–42]. However, the size distribution is much worse than Cd based NCs. Jia[3] *et al*. demonstrated the aspect ratio of ZnSe nanorods can be tuned by a thermodynamically driven ripening process using ZnSe nanowires as the starting material.[2] They also showed that ZnSe nanorod couples, can be produced by the growth of twinning structure on both ends of two parallelly aligned ZnSe nanorods by self–limited assembly mechanism. Most recently, Ning *et al.*[1] synthesized ZnSe nanorods with controlled length by introduction of $[Zn_4(SPh)_{10}](Me_4N)_2$ molecular clusters which interrupt the template formed by inorganic–organic magic size clusters. Among these reports, the synthetic procedures involve tedious steps and are not easy to control. Some of them used toxic organic phosphines such as trioctylphosphine (TOP), trioctylphosphine oxide (TOPO), DPP (diphenylphosphine), SPh (thiophenol) which are not "green" and not convenient to handle during syntheses[1].

In this work, we reported the successful and facile shape and phase control of ZnSe nanocrystals in a phosphine–free system, by simply changing the ratio of super hydride to selenium precursor, wherein uniform ZnSe nanodots or nanorods with tunable diameter were obtained. We also presented a detailed investigation of the specific role of super hydride in the synthesis of ZnSe nanocrystals and propose a growth mechanism that is responsible for the formation of ZnSe nanodots and nanorods.

4.2 Experimental section

4.2.1 Chemicals.

$Zn(NO_3)_2$•$6H_2O$ (99%), 1–octadecene (ODE, 90%), selenium powder (Se, 99%), lithium trithyborohydride ($LiBH(CH_2CH_3)_3$, super hydride, SHR,) solution in THF (1 M), chloroform (99% anhydrous), and ethanol (99.8% anhydrous) were purchased from Sigma–Aldrich. Oleylamine (OLA, 90%) was purchased from FujiFilm Wako Pure Chemicals Corporation. All chemicals were used as received without further purification.

4.2.2 Synthesis of ZnSe nanoparticles.

All experiments were carried out using standard Schlenk–line techniques under dry nitrogen. Aliquots were taken using an injector with needle through the rubber plug on the three–neck flask.

Preparation of Se stock solution.

A 0.1 M Se stock solution was prepared by dissolve 3 mmol (237 mg) Se powder in 30 ml oleylamine in a three–neck flask. The mixture was degassed and refilled with N2 three times at room temperature and then heated to 110 °C and kept at this temperature for 0.5 h to remove air and water. Then the solution was heated to 220°C and kept at this temperature for 2 h. After cooling down to room temperature, a brown Se stock solution was obtained and then transferred into a glovebox for further use.

Preparation of Se precursor by reducing Se–oleylamine using superhydride.

Superhydride solution and Se oleylamine solution were kept in a glove box. Then a certain volume of superhydride was injected it into the Se stock solution in a 10–mL vial in the glove box. Color change of the Se–oleylamine solution was observed immediately after the superhydride was added. The mixture kept in a vial with a septum was removed from the glove box and injected into the flask for the particle growth.

Synthesis of ZnSe Nanodots.

In a typical synthesis, 0.2 mmol (59.5 mg) $Zn(NO_3)_2 \cdot 6H_2O$, 5 mL 1–octadecene and 1 ml oleylamine were mixed in a three–neck flask. The mixture was degassed and refilled with N_2 three times at room temperature and then heated to 110 °C and kept for 0.5 h. At 160 °C, a mixture of 3 mL of Se stock solution and 0.4 ml superhydride solution was injected into the flask. After the injection, the solution was heated up to 200°C and kept for 10 mins, then was further heated up to 260°C and kept at this temperature for 10–120 mins to obtain nanodots.

Synthesis of ZnSe Nanorods.

In a typical synthesis, 0.2 mmol (59.5 mg) $Zn(NO_3)_2 \cdot 6H_2O$, 5 mL 1–octadecene and 1 ml oleylamine were mixed in a three–neck flask. The mixture was degassed and refilled with N_2 three times at room temperature and then heated to110 °C and kept at this temperature for 0.5 h. At 160 °C, a mixture of 3 mL (0.3mmol) of Se stock solution and 0.1 ml (0.1 mmol) super hydride solution was injected into the flask. After the injection, the solution was heated up to 200°C and kept at this temperature for 10 mins. The reaction solution was further heated up to 260°C and kept at this temperature for 10–120 mins to obtain nanorods with varied diameter.

Synthesis of ZnSe Nanorods from magic small ZnSe dots.

The magic small ZnSe dots were synthesized at 200°C and kept at this temperature for 10 mins as described above, then the reaction was terminated by removing the heating mantle. The magic small ZnSe dots was cleaned out from the remaining precursor by addition of ethanol and centrifugation for 5 mins at 5000 rpm. The cleaned magic small ZnSe dots were dissolved in the mixture of 5ml ODE and 1 ml oleylamine again followed by degas and refill with N_2 at 110°C, then heated up to 260°C for 120 mins to obtain ZnSe nanorods.

4.3Results and Discussions

In this work, the shape and phase control of ZnSe nanocrystals were achieved by tailoring the reaction activity of selenium precursors. Se precursor with different reactivity was obtained by adding super hydride as reducing agent. To study the effect of super hydride on the crystalline phase and the shape control of ZnSe nanocrystals, detailed investigations on the Se precursor with or without the addition of super hydride were conducted.

4.3.1 Se Precursor Characterization.

The activity of selenium precursor has an important effect on the semiconductor nanocrystal growth[43]. **Figure. 4.2a** shows a photograph of the original Se stock solution and those solutions after different volume of super hydride added. After the addition of super hydride, the colour of Se–oleylamine stock solution gradually changed from brown to orange (M[super hydride: Se] = 1:3), luminous yellow (M[super hydride: Se] = 2:3) and pale yellow(M[super hydride: Se] = 1:1, 3:2, 2:1). Normalized UV–Vis optical absorption spectra for the Se–oleylamine solutions with the addition of different volume of superhydride in **Figure. 4.2b** indicated that the absorbance intensity between 300 and 450 nm systematically decreased with the increased dosage of super hydride added, which is consistent with the colour change observed in Figure. 4–2a. The obvious colour change in the Se–superhydride–oleylamine precursor solution could be related to the formation of different selenium species, which is similar to that being observed in treatment of Te–(TOP)–oleylamine precursor by super hydride.[33] It is noted that Te^{2-}, Te_2^{2-}, Te_3^{2-} species obtained from the reduction of Te–TOP oleylamine solution by adding different volume of superhydride also display distinctive colours such as white precipitate, blue/violet solution and red solution, respectively[44].

Reducing reagents including superhydride, $NaBH_4$, SmI_2, and NaH, are mainly used to tune the reactivity of Se and Te precursors[20, 45]. De Mello and co–workers[45] observed that elemental selenium (Se^0) was reduced to diselenide (Se_2^{2-}) or seleniude (Se^{2-}) anion

or their mixed species depending on the $NaBH_4$ stoichiometry used. Similar results were also reported by Raibaut[46]. Like $NaBH_4$, we hypothesize that superhydride can gradually reduce Se to Se_2^{2-} or Se^{2-}, which presents different colours in the Se–super hydride–oleylamine stock precursor solution due to the difference valence states of Se. When excess volume of super hydride was added to the Se–oleylamine stock solution, Se is more likely to be reduced into Se^{2-} species.

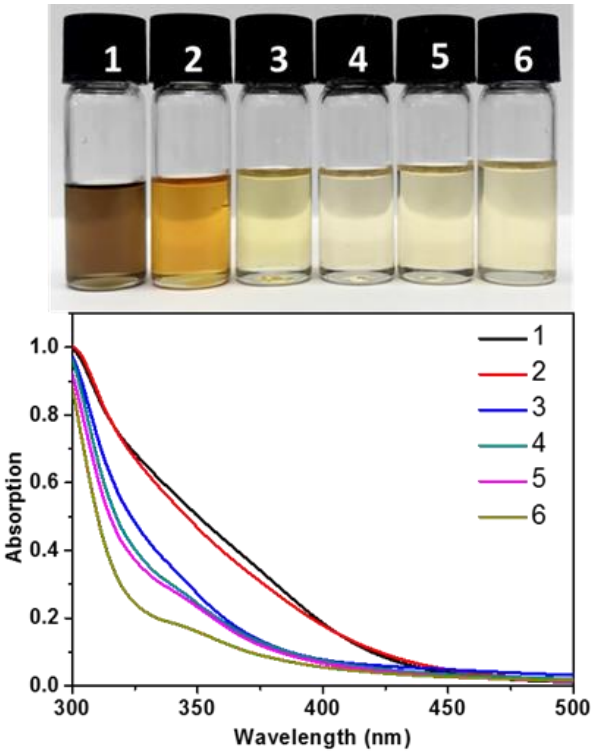

Figure 4.2 A photography (a, top panel) and UV–Vis absorption spectra (b, bottom panel) of Se–oleylamine solution added with different amount of super hydride. (1) M(Super hydride : Se)=0:1; (2) M(Super hydride : Se)=1:3; (3) M(Super hydride : Se)=2:3; (4) M(Super hydride : Se)=1:1; (5) M(Super hydride : Se)=3:2; (6) M(Super hydride : Se)=2:1.

4.3.2 Ab Initio Calculations

Table 4.1 gives the Gibbs free reaction energies for one–electron reduction of Se^0 to Se^{2-} and Se_2^{2-}. As seen from Table 1, the reduction of Se^0 to Se_2^{2-} is highly exergonic with ΔG_{298} = –429.2 kJ/mol (reaction 1), indicating that Se_2^{2-} would form when limited super hydride is available. With the addition of reductant, Se_2^{2-} would be further reduced to Se^{2-} with ΔG_{298} = –145.2 kJ/mol (reaction 2). Overall, the two–electron reduction of Se^0 to Se_2^{2-} is associated with an overall Gibbs free reaction energy of ΔG_{298} = –574.4

kJ/mol (reaction 3). These results indicate that Se is firstly reduced to Se_2^{2-}, then to Se^{2-} with the addition of super hydride.

Table 4.2 Gibbs free reaction energies calculated at the SMD–DSD–PBEP86/Def2–QZVPP level of theory for the reduction of Se^0 to Se^{2-} and Se_2^{2-} (in kJ/mol).

Reaction	ΔG_{298} kJ/mol
(1) $Se^0 + e^- \rightarrow 1/2\ Se_2^{2-}$	–429.2
(2) $1/2\ Se_2^{2-} + e^- \rightarrow Se^{2-}$	–145.2
(3) $Se^0 + 2e^- \rightarrow Se^{2-}$	–574.4

To find out the possible products by employing polyselenide like Se_2^{2-} as precursor, we calculated Gibbs free–reaction energies at 298 K (ΔG_{298}) for the formation of ZnSe, $ZnSe_2$, and $ZnSe_3$ from Zn^{2+} and Se^{2-}, Se_2^{2-}, and Se_3^{2-}, respectively, as seen in **Table 4.2**.

Table 4.3 Gibbs free reaction energies calculated at the SMD–DSD–PBEP86/Def2–QZVPP level of theory for the three possible reactions between Zn^{2+} and the selenium dianions (Se^{2-}, Se_2^{2-}, and Se_3^{2-}) (in kJ/mol).

Reaction	ΔG_{298} kJ/mol
$Zn^{2+} + Se^{2-} \rightarrow ZnSe$	–762.8
$Zn^{2+} + Se_2^{2-} \rightarrow ZnSe_2$	–679.9
$Zn^{2+} + Se_3^{2-} \rightarrow ZnSe_3$	–696.4

As expected, the reactions between Zn^{2+} and the selenium dianions are highly exergonic. The exergonicity of these reactions increases in the order: $Se_2^{2-} < Se_3^{2-} << Se^{2-}$. In particular, the reactions with diatomic and triatomic selenium anions are associated with ΔG_{298} values of –679.9 and –696.4 kJ mol^{-1}, respectively. Fig. 2 shows the clusters formed between the Zn and Se atoms along with the Zn–Se bond distances. The difference of 16.5 kJ mol^{-1} between the two Gibbs free–reaction energies is reflected in a slightly shorter Zn–Se bond distance in the $ZnSe_2$ cluster relative to the $ZnSe_3$ cluster. Namely, the Zn–Se bond distances are 2.376 ($ZnSe_2$) and 2.364 ($ZnSe_3$) Å. On the other hand, the reaction between Zn^{2+} and Se^{2-} is associated with a higher exergonicity of

ΔG_{298} = –762.8 kJ mol^{-1}. This significantly higher Gibbs free–reaction energy is also reflected in a significantly shorter Zn–Se bond distance of 2.219 Å (**Figure. 4.3**).

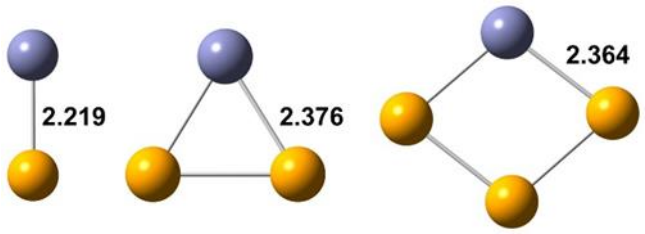

Figure 4.3 SMD–DSD–PBEP86/Def2–QZVPP optimized structures for $ZnSe_n$ clusters (n = 1–3). The Zn–Se bond distances are given in Å. Atomic color scheme: Se, yellow; Zn, purple

4.3.3 Morphological and Structural Characterization.

Based on the results of theoretical calculation and the characterization of Se precursor, we proposed that different Se species might have different effects on the formation of ZnSe nanoparticles since the reactivity of Se precursor plays an important role on the shape control of ZnSe nanoparticles[47]. To this end, we conducted several parallel experiments to synthesize ZnSe nanocrystals using Se stock solution with different ratio of super hydride to Se. UV–Vis absorption, morphological and structural characterization were performed to analyse the growth process while employing different species of Se precursor.

As a result, ZnSe nanodots were obtained with a high molar ratio of super hydride to selenium whereas nanorods were synthesized with a low molar ratio of super hydride to Se.

(a) ZnSe Nanodots.

ZnSe nanodots with good size distribution were obtained by employing a high molar ratio of super hydride to Se (M [Super hydride: Se] = 3:1).

As shown in **Figure 4.4a**, the nanodots with absorption of 340 nm were obtained after the reaction evolved for 10 mins at 200°C. The absorption spectrum of this aliquot shows two distinct peaks at 323 nm and 340 nm, which are typical characteristics of magic size ZnSe nanoclusters.[1, 39] TEM image of this sample shows they are tiny spherical nanoparticles (Appendix C Figure C4–1). As the reaction proceeded for 10 mins at 260°C, the first exciton peak of the UV–Vis spectra of nanodots red–shifted to 361 nm. Further reaction at this temperature for 30 mins, 60 mins and 90 mins led to the absorption exciton peak shifted to 375 nm, 388 nm and 392 nm, respectively, which

indicate the increase of the size of the nanoparticles. X–ray diffraction (XRD) confirmed the obtained ZnSe nanodots are zinc blende phase with diffraction peaks indexed to a cubic zinc–blende structure (**Figure. 4.4b**). The TEM and HRTEM images (**Figure. 4.4c, 4.4d**) shows that the nanodots are single–crystalline, and the lattice plane spacing extracted from the fast Fourier transform (FFT) analysis of selected areas are 0.327 nm for (hkl) = (111), 0.200 nm for (hkl) = (220), which are of a typical zinc blende ZnSe structure.

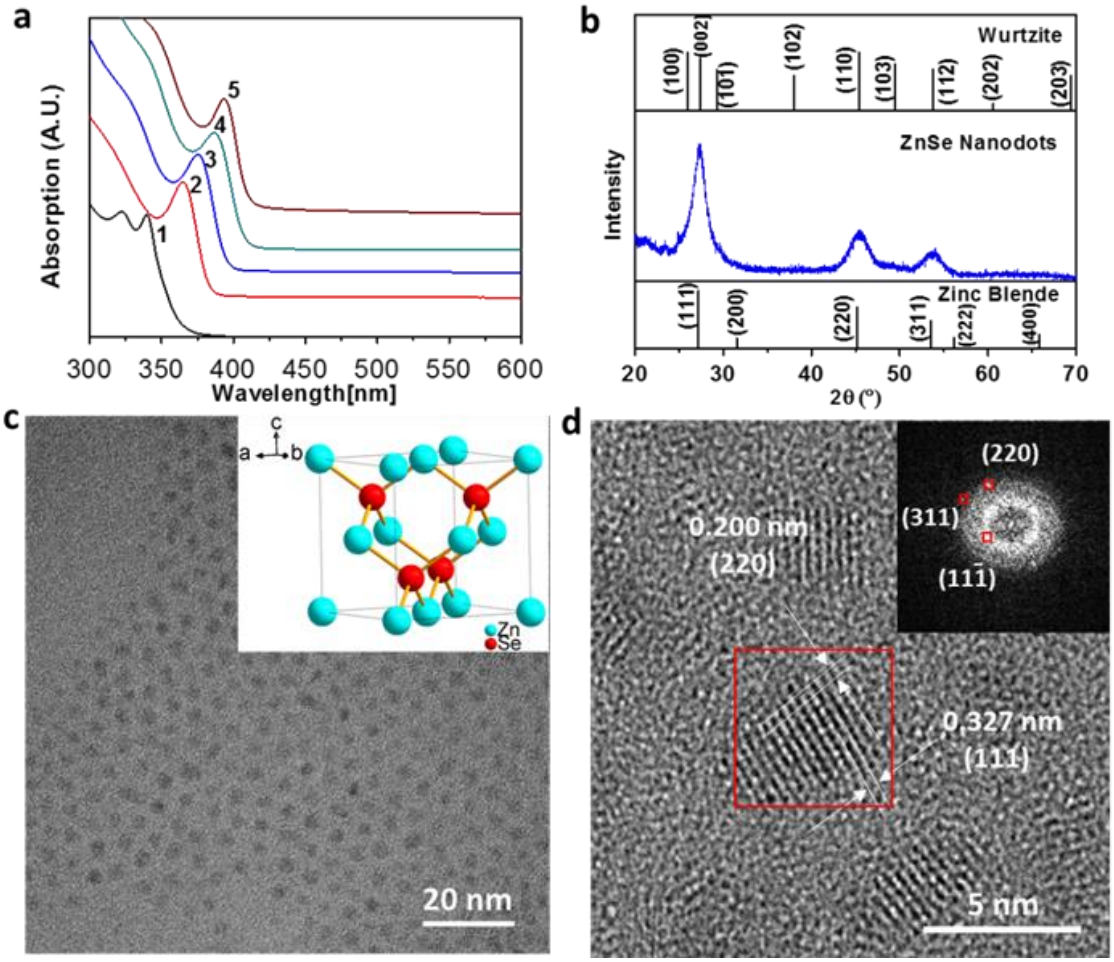

Figure 4.4 Synthesized ZnSe nanodots and structural characterizations. (a) UV–Vis spectra of ZnSe nanodots synthesized at 200ºC, 10min(1), 260ºC,10min(2), 260ºC,30 min(3), 260ºC, 60 min(4); 260ºC, 120 min(5); (b) XRD pattern of ZnSe nanodots synthesized at 260 °C for 60 min; (c) TEM image of ZnSe nanodots synthesized at 260 °C for 60 min. Inset is Zinc blende structure of ZnSe nanodots; (d) HRTEM image of ZnSe nanodots. Inset show the FFT image of a selected area in (d) marked by a red rectangle;

The UV–Vis absorption peaks at 361 nm, 375 nm, 388 nm and 392 nm correspond to ZnSe nanodots with a diameter of 2.62±0.32 nm, 2.77nm±0.31 nm, 2.82±0.34 nm, 2.91±0.34 nm, respectively (**Figure 4.5**).

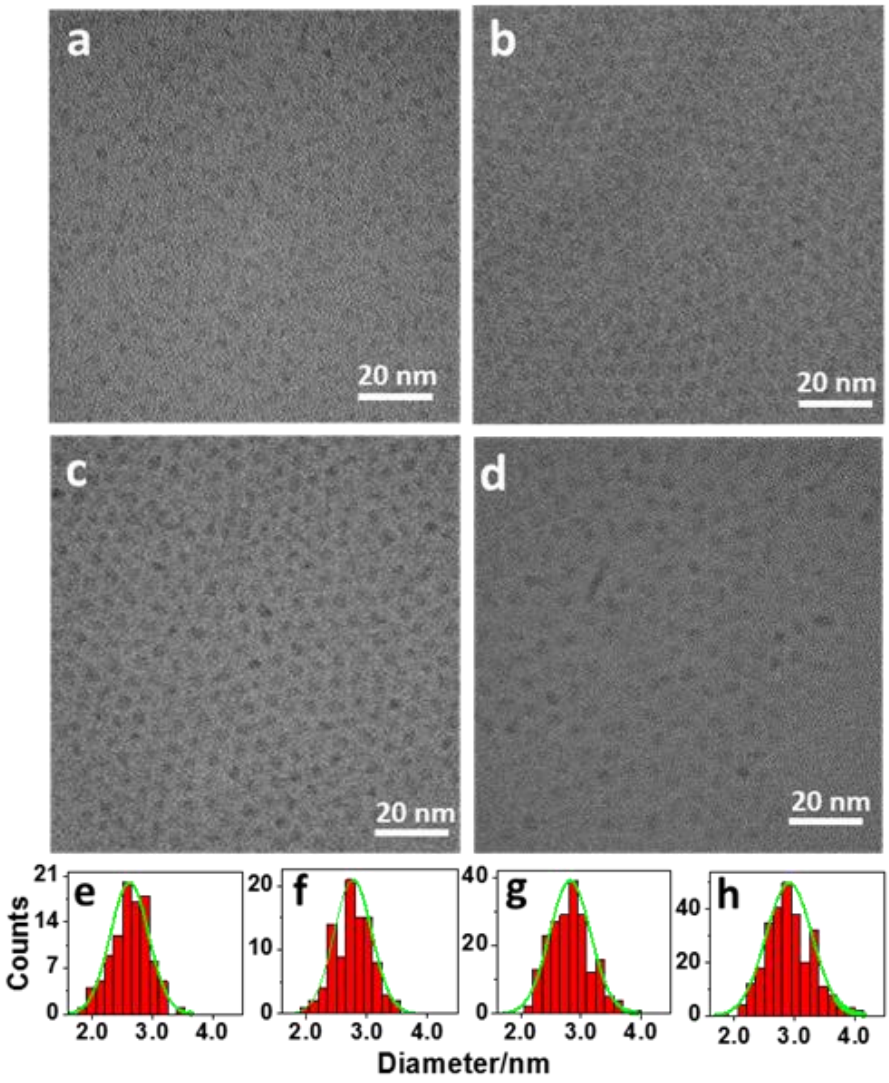

Figure 4.5 TEM images (a–d) and size distribution (e–g) of ZnSe dots.

The above experiment results clearly demonstrate that uniform ZnSe nanodots with a zinc blende phase were obtained when super hydride reduced Se–oleylamine as Se precursor with a M(super hydride : Se) of 3:2 was used. The nucleation of ZnSe nanoparticles occurred immediately after the injection of Se^{2-} precursor with a high reaction activity at 160°C, and the fast growth led to the formation of ZnSe spherical nanodots with a zinc blende structure.

(b) ZnSe Nanorods.

ZnSe nanorods with different length and diameter were obtained by employing a low molar ratio of super hydride to Se (M[Super hydride : Se] = 1:3). In this synthesis, the absorption spectrum (**a** in **Figure 4.6a**) and TEM image (Appendix C Figure C4–2) of the aliquot obtained after 10 min at 200 ^{o}C shows similar features as those of the aliquot taken after the reaction evolved for 10 min at 200 ^{o}C for the synthesis of nanodots. As the reaction proceeded from 200°C for 10 mins to 260°C for 10 mins, the UV–Vis of nanorods red shifted from 340 nm to 373 nm. After the reaction evolved at this temperature for 40 mins, 120 mins, and 200 mins, the exciton peak of absorption spectrum shifted to 381 nm, 387 nm and 396 nm, respectively (**Figure 4.6a**). The broad exciton peak implies that the obtained ZnSe nanorods are not very uniform. The XRD pattern (**Figure. 4.6b**) matches that of wurtzite ZnSe, indicating that the synthesized ZnSe is wurtzite phase. The TEM and HRTEM measurement (**Figure 4.6c, 4.6d**) shows that the nanorods are single–crystalline, and the lattice plane spacing extracted from the fast Fourier transform (FFT) analysis of selected areas are 0.325 nm for (hkl) = (002), 0.343 nm for (hkl) = (100).

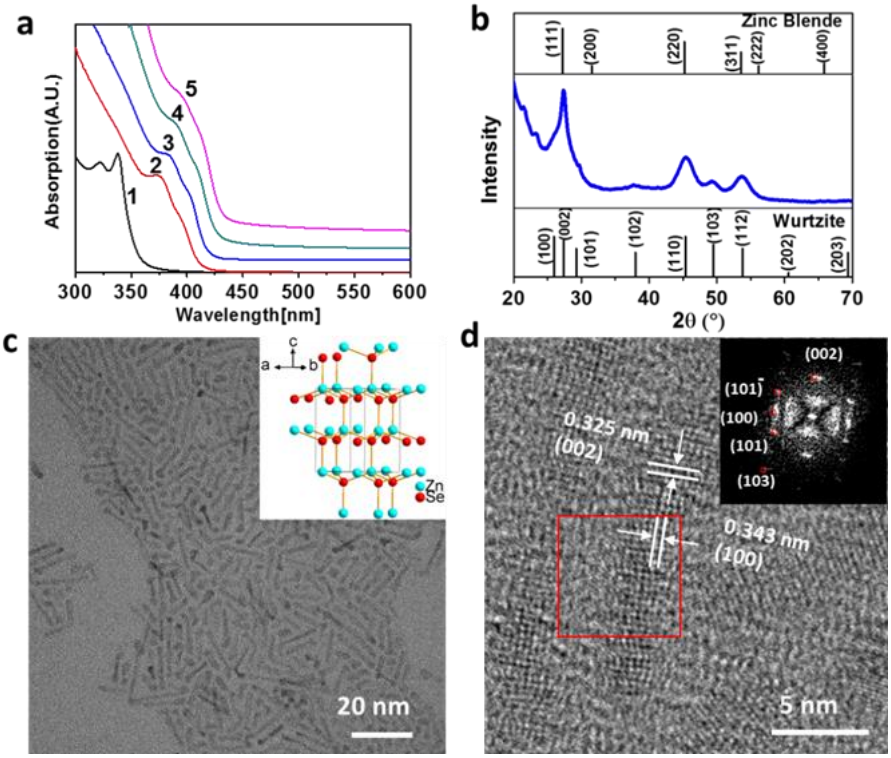

Figure 4.6 Synthesized ZnSe nanorods. (a) UV–Vis spectra of ZnSe nanorods synthesized at 200°C, 10min(1),260°C, 10min(2), 260°C, 30 min(3), 260°C, 60 min(4); 260°C, 120 min(5); (b) XRD pattern of ZnSe nanorods. (c) TEM image of ZnSe nanorods synthesized at 260 °C for 60 min. Inset is the Wurtzite structure of ZnSe nanorods; (d) HRTEM image of ZnSe nanorods. FFT image of a selected area in (d) marked by a red rectangle;

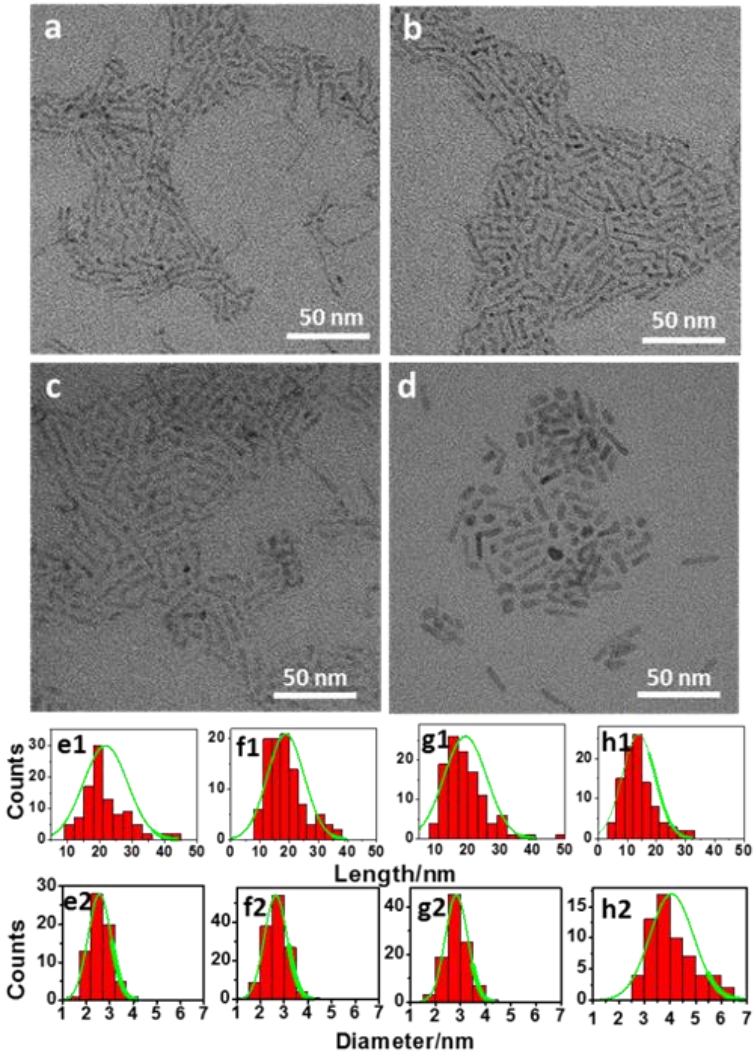

Figure 4.7 TEM images of ZnSe nanorods obtained as the reaction proceeds at 260°C for 10 mins (a); 40 mins (b);120 mins (c); 200 mins (d); length distribution (e1–g1) and diameter distribution (e2–g2) of nanorods corresponding to (a–d), respectively.

As the reaction evolves, the length of nanorods shrinks from 21.7±6.83 nm (260°C, 10 mins) to 19.2±6.60 nm (260°C, 40 mins), 18.8±6.28 nm (260°C, 120 mins), 13.9±5.64 nm (260°C, 200 mins), while the diameter increased from 2.57±0.48 nm to 2.65±0.47 nm, 2.84±0.44 nm to 4.07±0.85 nm, respectively (**Figure 4.7**). A ripening process was observed as the reaction was proceeded at 260°C for a longer time from 120 mins to 200 mins. As the reaction monomers are almost consumed after the reaction evolved for 40 mins at 260°C, the low concentration of the reaction monomers cannot support the kinetics–controlled growth of ZnSe and the reaction will enter a thermodynamic–controlled process.[2] Due to the high surface energy of elongated nanocrystals, long and thin nanowires will thermodynamically shrink to short and thick nanorods at elevated temperatures to minimize the energy of the system.

4.3.4 Growth mechanism of ZnSe nanodots and nanorods using different Se species

Based on the afore–mentioned calculations and characterizations, growth mechanisms that are responsible for the formation of ZnSe nanodots and nanorods were proposed. Selenium precursor in oleylamine can be reduced to Se_2^{2-} or Se^{2-} depending on the amount of super hydride added. With the increase of the addition of super hydride, Se^0 was reduced to Se_2^{2-} then Se^{2-}. The reaction activities of different Se species are in an ascending order of $Se^{2-} > Se_2^{2-} > Se^0$ and energy potentials for reaction of these Se species are in a descending order of $Se^{2-} > Se_2^{2-} > Se^0$. It's worth noting that The reactivity of the anions of Se_2^{2-} and Se^{2-} show different trend for reactivity as that for sulphur species prepared in ODE under non–reducing conditions[48].

When the highly reactive Se^{2-} is added into the reaction system, the reaction that leads the production of ZnSe nanocrystals are too fast for the nucleus to adopt anisotropic growth, leading to the formation of zinc blende ZnSe nanodots. On the other hand, as the less reactive Se_2^{2-} has a high chemical potential, the reaction between Se_2^{2-} and Zn^{2+} may produce the stable phase wurtzite ZnSe nucleus, which then form 1D NCs through oriented attachment [3] (**Figure 4.8**).

A control experimental using purified magic size ZnSe nanoclusters to grow ZnSe nanorods was conducted to further elucidate growth mechanism of ZnSe nanorods (See details and Appendix C Figure C4–3 in the Experimental Section of Appendix C). In a typical synthesis, magic size ZnSe nanoclusters were firstly obtained and separated from the crude solution to effectively remove the unreactive precursors (Appendix C Figure C4–3b). Then the cleaned magic size ZnSe nanoclusters were dissolved in the mixture of ODE and oleylamine again and were heat up to 260°C. After the reaction evolved for 120 mins, wurtzite ZnSe nanorods were produced (Appendix C Figure C4–3c). This suggests that ZnSe nanorods are formed from the magic size ZnSe nanoclusters based on the oriented attachment mechanism. The red shift of the exciton peak in the absorption spectrum in the obtained ZnSe nanorods is associated with the increase of the diameter of ZnSe nanorods (Appendix C Figure C4–3a), which may be attributed to by a ripening process at high temperature.

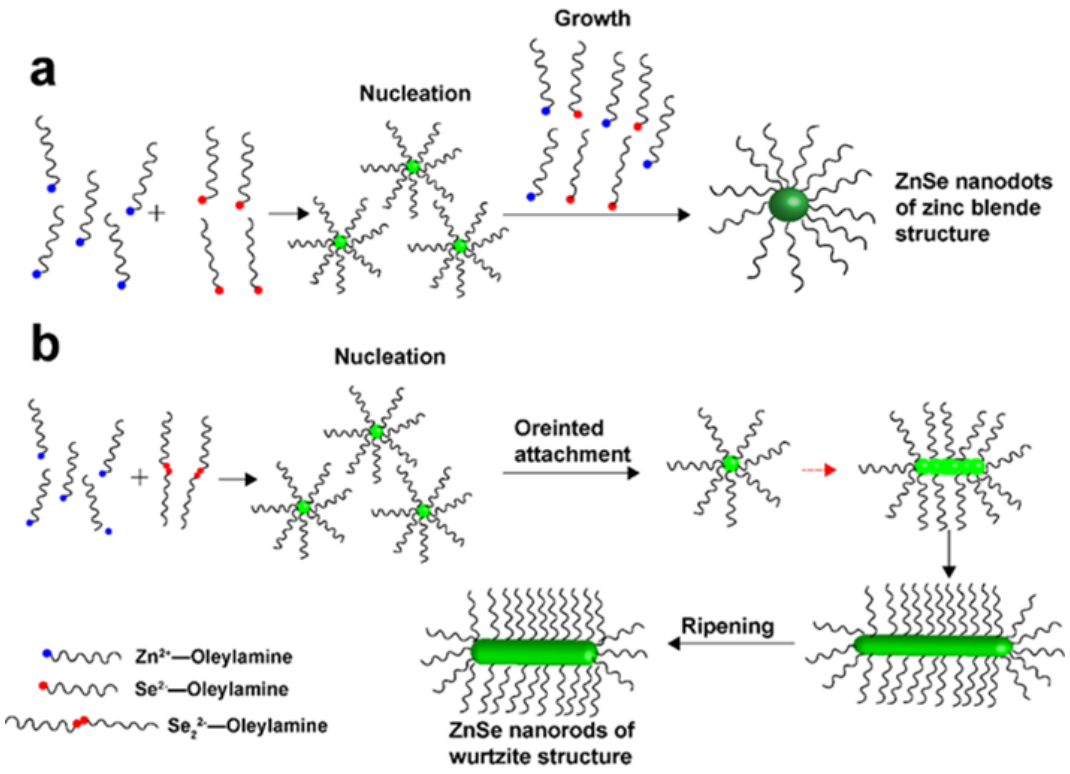

Figure 4.8 Schematic of the growth mechanism of zinc blende ZnSe nanodots employing Se^{2-} as precursor (a); wurtzite ZnSe nanorods employing Se_2^{2-} as precursor (b).

4.4 Conclusions

In summary, uniform ZnSe nanodots and nanorods with controlled morphology and crystal phase were synthesized in a phosphine–free colloidal solution. Shape and phase control of ZnSe nanocrystals can be achieved through directly tailoring the reactivity of Se precursor via the addition of a reducing reagent of super hydride. This new method enables to control the shape and size of ZnSe nanocrystals within the same precursor and ligands by just changing the added ratio of super hydride to Se oleylamine precursor, which also sheds light on the size and shape control of other nanocrystals with high quality.

4.5 References

1. (a) Jia, G, Pang, Y, Ning, J, Banin, U, Ji, B, Heavy–Metal–Free Colloidal Semiconductor Nanorods: Recent Advances and Future Perspectives. Adv. Mater. 2019, 31, 1900781.; (b) Chen, D, Zhang, H, Li, Y, Pang, Y, Yin, Z, Sun, H, Zhang, LC, Wang, S, Saunders, M, Barker, E, Jia, G., Spontaneous Formation of Noble–and Heavy–Metal–Free Alloyed Semiconductor Quantum Rods for Efficient Photocatalysis. Adv. Mater. 2018, 30, 1803351.; (c) Ning J, Liu J, Levi–Kalisman Y, Frenkel AI, Banin U. Controlling Anisotropic Growth of Colloidal ZnSe Nanostructures. J. Am. Chem. Soc. 2018;140(44):14627–14637.
2. (a) Jia G, Banin U. A general strategy for synthesizing colloidal semiconductor zinc chalcogenide quantum rods. J Am Chem Soc. 2014;136(31):11121–11127; (b) Jia G, Xu S, Wang A. Emerging strategies for the synthesis of monodisperse colloidal semiconductor quantum rods. J. Mater. Chem. C 2015;3(32):8284–8293.
3. Jia G, Sitt A, Hitin GB, Hadar I, Bekenstein Y, Amit Y, et al. Couples of colloidal semiconductor nanorods formed by self–limited assembly. Nat. Mater. 2014;13(3): 301–307.
4. Simon T, Bouchonville N, Berr MJ, Vaneski A, Adrovic A, Volbers D, et al. Redox shuttle mechanism enhances photocatalytic H_2 generation on Ni–decorated CdS nanorods. Nat. Mater. 2014;13(11):1013–1018.
5. Hines MA, Guyot–Sionnest P. Bright UV–blue luminescent colloidal ZnSe nanocrystals. J. Phys. Chem. B. 1998;102(19):3655–3657.
6. Acharya S, Panda AB, Efrima S, Golan Y. Polarization properties and switchable assembly of ultranarrow ZnSe nanorods. Adv. Mater. 2007;19(8):1105–1108.
7. Liu S, Zhang Q, Zhang L, Gu L, Zou G, Bao J, et al. Electrochemiluminescence Tuned by Electron–Hole Recombination from Symmetry–Breaking in Wurtzite ZnSe. J. Am. Chem. Soc. 2016;138(4):1154–1157.
8. Oksenberg E, Popovitz–Biro R, Rechav K, Joselevich E. Guided Growth of Horizontal ZnSe Nanowires and their Integration into High–Performance Blue–UV Photodetectors. Adv. Mater. 2015;27(27):3999–4005.
9. Kwon B–H, Jang HS, Yoo HS, Kim SW, Kang DS. White–light emitting surface–functionalized ZnSe quantum dots europium complex–capped hydrid nanocrystal. J. Mater. Chem. 2011;21:12812–12818.

10. Shen H, Cao W, Shewmon NT, Yang C, Li LS, Xue J. High–efficiency, low turn–on voltage blue–violet quantum–dot–based light–emitting diodes. Nano Lett. 2015;15(2):1211–1216.
11. Zhou R, Li M, Wang S, Wu P, Wu L, Hou X. Low–toxic Mn–doped ZnSe@ZnS quantum dots conjugated with nano–hydroxyapatite for cell imaging. Nanoscale. 2014;6(23):14319–14325.
12. Perng DC, Fang JF, Chen JW. Nano–Structured ZnSe/CIS Heterojunction Solar Cells with ZnSe/ZnO Coaxial Nanowires. J. Electrochem. Soc. 2011;158(10):97–101.
13. Cheng DC, Hao HC, Zhang M, Shi W, Lu M. Improving Si solar cell performance using Mn:ZnSe quantum dot–doped PLMA thin film. Nanoscale Res. Lett. 2013;8:291
14. Chen CC, Herhold AB, Johnson CS, Alivisatos AP. Size Dependence of Structural Metastability in Semiconductor Nanocrystals. Science 1997;276(5311):398–401.
15. Shabaev A, Efros AL. 1D exciton spectroscopy of semiconductor nanorods. Nano Lett. 2004;4(10):1821–1825.
16. 16.Choi S–H, Song H, Park IK, Yum J–H, Kim S–S, Lee S, et al. Synthesis of size–controlled CdSe quantum dots and characterization of CdSe–conjugated polymer blends for hybrid solar cells. J. Photochem. Photobiol. 2006;179(1–2):135–141.
17. Yun HJ, Paik T, Diroll B, Edley ME, Baxter JB, Murray CB. Nanocrystal Size–Dependent Efficiency of Quantum Dot Sensitized Solar Cells in the Strongly Coupled CdSe Nanocrystals/TiO_2 System. ACS Appl. Mater. Interfaces, 2016;8(23):14692–14700.
18. Panda AB, Glaspell G, El–Shall MS. Microwave synthesis of highly aligned ultra narrow semiconductor rods and wires. J. Am. Chem. Soc. 2006;128(9):2790–2791.
19. Shieh F, Saunders AE, Korgel BA. General shape control of colloidal CdS, CdSe, CdTe quantum rods and quantum rod heterostructures. J. Phys. Chem. B. 2005;109(18):8538–8542.
20. Zhang J, Jin S, Fry HC, Peng S, Shevchenko E, Wiederrecht GP, Synthesis and characterization of wurtzite ZnTe nanorods with controllable aspect ratios. J. Am. Chem. Soc. 2011;133(39):15324–15327.
21. Lauth J, Strupeit T, Kornowski A, Weller H. A Transmetalation Route for Colloidal GaAs Nanocrystals and Additional III–V Semiconductor Materials. Chem. Mater. 2012;25(8):1377–1383.

22. Brown RP, Gallagher MJ, Fairbrother DH, Rosenzweig Z. Synthesis and Degradation of Cadmium–Free InP and InPZn/ZnS Quantum Dots in Solution. Langmuir. 2018; 34(46): 13924–13934.
23. Cirillo M, Aubert T, Gomes R, Van Deun R, Emplit P, Biermann A, et al. “Flash” Synthesis of CdSe/CdS Core–Shell Quantum Dots. Chem. Mater. 2014;26(2):1154–1160.
24. Oh N, Nam S, Zhai Y, Deshpande K, Trefonas P, Shim M. Double–heterojunction nanorods. Nat. Commun. 2014;5:3642.
25. Oh N, Kim BH, Cho SY, Nam S, Rogers SP, Jiang Y,Double–heterojunction nanorod light–responsive LEDs for display applications. Science. 2017;355(6325):616–619.
26. Wang W, Banerjee S, Jia SG, Steigerwald ML, Herman IP. Ligand control of growth, morphology, and capping structure of colloidal CdSe nanorods. Chem Mater. 2007;19(10): 2573–2580.
27. Li L, Reiss P. One–pot synthesis of highly luminescent InP/ZnS nanocrystals without precursor injection. J. Am. Chem. Soc. 2008;130(35):11588–11589
28. Yang YA, Wu H, Williams KR, Cao YC. Synthesis of CdSe and CdTe nanocrystals without precursor injection. Angew. Chem. Int. Ed. 2005;44(41):6712–6715.
29. Banfield JF, Welch SA, Zhang H, Ebert TT, Penn RL. Aggregation–based crystal growth and microstructure development in natural iron oxyhydroxide biomineralization products. Science. 2000;289(5480):751–754.
30. Zhang Q, Liu S–J, Yu S–H. Recent advances in oriented attachment growth and synthesis of functional materials: concept, evidence, mechanism, and future. J. Mater. Chem. 2009;19(2):191–207.
31. Sarkar S, Acharya S, Chakraborty A, Pradhan N. Zinc Blende 0D Quantum Dots to Wurtzite 1D Quantum Wires: The Oriented Attachment and Phase Change in ZnSe Nanostructures. J. Phys. Chem. Lett. 2013;4(19):3292–3297.
32. Lu Q, Wang AL, Gong Y, Hao W, Cheng H, Chen J, et al. Crystal phase–based epitaxial growth of hybrid noble metal nanostructures on 4H/fcc Au nanowires. Nat. Chem. 2018;10(4):456–461.
33. Pang X, He Y, Jung J, Lin Z. 1D nanocrystals with precisely controlled dimensions, compositions, and architectures. Science. 2016;353(6305):1268–1272.
34. Pileni MP. The role of soft colloidal templates in controlling the size and shape of inorganic nanocrystals. Nat. Mater. 2003;2(3):145–150.

35. Li H, Brescia R, Krahne R, Bertoni G, Alcocer MJ, D'Andrea C, et al. Blue–UV–emitting ZnSe(dot)/ZnS(rod) core/shell nanocrystals prepared from CdSe/CdS nanocrystals by sequential cation exchange. ACS Nano. 2012;6(2):1637–1647.
36. Acharya S, Sarma DD, Jana NR, Pradhan N. An Alternate Route to High–Quality ZnSe and Mn–Doped ZnSe Nanocrystals. J. Phys. Chem. Lett. 2010;1(2):485–488.
37. Groeneveld E, Witteman L, Lefferts M, Ke X, Bals S, Van Tendeloo G, et al. Tailoring ZnSe–CdSe colloidal quantum dots via cation exchange: from core/shell to alloy nanocrystals. ACS Nano. 2013;7(9):7913–7930.
38. Thakar R, Chen YC, Snee PT. Efficient emission from core/(doped) shell nanoparticles: Applications for chemical sensing. Nano Lett. 2007;7(11):3429–3432.
39. Zhang LJ, Shen XC, Liang H, Yao JT. Multiple Families of Magic–Sized ZnSe Quantum Dots via Noninjection One–Pot and Hot–Injection Synthesis. J. Phys. Chem. C. 2010;114(50):21921–21927.
40. Banski M, Afzaal M, Malik MA, Podhorodecki A, Misiewicz J, O'Brien P. Special Role for Zinc Stearate and Octadecene in the Synthesis of Luminescent ZnSe Nanocrystals. Chem. Mater. 2015;27(11):3797–3800.
41. Eilers J, van Hest J, Meijerink A, Donega CdM. Unravelling the Size and Temperature Dependence of Exciton Lifetimes in Colloidal ZnSe Quantum Dots. J. Phys. Chem. C. 2014;118(40):23313–23319.
42. Yu K, Hrdina A, Zhang X, Ouyang J, Leek DM, Wu X, Highly–photoluminescent ZnSe nanocrystals via a non–injection–based approach with precursor reactivity elevated by a secondary phosphine. Chem. Commun. 2011;47(31):8811–8813.
43. Zhang L–J, Chen F–Y, Tong J–Z, Chen G–D, Huang H–J, Shen X–C. Controlled Growth of ZnSe Nanocrystals by Tuning Reactivity and Amount of Zinc Precursor. J. Chem. 2013;2013:1–6.
44. McAfee JL, Andreatta JR, Sevcik RS, Schultz LD. Equilibrium among potassium polytellurides in N,N–dimethylformamide solution. J. Mol. Struct. 2012;1022:68–71.
45. Oliveira ARMd, Piovan L, Simonelli F, Barison A, Santos MdFC, de Mello MBM. A 77Se NMR study of elemental selenium reduction using $NaBH_4$. J. Organomet. Chem. 2016;806:54–59.
46. Raibaut L, Cargoet M, Ollivier N, Chang YM, Drobecq H, Boll E, et al. Accelerating chemoselective peptide bond formation using bis(2–selenylethyl)amido peptide selenoester surrogates. Chem. Sci. 2016;7(4):2657–2665.

47. Bullen C, van Embden J, Jasieniak J, Cosgriff JE, Mulder RJ, Rizzardo E, et al. High Activity Phosphine–Free Selenium Precursor Solution for Semiconductor Nanocrystal Growth. Chem. Mater. 2010;22(14):4135–4143.
48. (a) Ding X, Liow CH, Zhang M, Huang R, Li C, Shen H, et al. Surface Plasmon Resonance Enhanced Light Absorption and Photothermal Therapy in the Second Near–Infrared Window. J. Am. Chem. Soc. 2014;136(44):15684–15693; (b) Zou Y, Su X, Jiang J. Phase–controlled synthesis of Cu_2ZnSnS_4 nanocrystals: the role of reactivity between Zn and S. J. Am. Chem. Soc. 2013;135(49):18377–18384.

Chapter 5. Synthesis of ZnSe, ZnS and ZnS_xSe_{1-x} nanorods using the one–pot heat–up method

Wei Chen, Shaghraf, Jiayi Chen, Fei Wang and Guohua Jia

The content for this chapter is under submission.

The contents of this chapter (pg. 87–108) and Appendix E (pg. 184–189) are confidential as they are under embargo due to current consideration for future publication.

The author contribution statement could be found in Appendix B.

Summary of Chapter.

In the previous chapter, Chapter 4, we developed a method for ZnSe nanodots and nanorods synthesis by tuning the activity of Se precursor with addition of reductant superhydride by a hot injection method. This method has a drawback that only a small amount of final products could be obtained (less than 100 mg) because of the limited volume of the injected Se–precursor for the synthesis. Simply increasing the volume of injection precursor would result in the vast decrease of the temperature of the reaction system, thus would affect the nucleation and growth of nanoparticles in a hot–injection method.

Therefore, in this chapter, we tried to develop facile one–pot heat–up method for large–scale production of ZnSe, ZnS and ZnS_xSe_{1-x} nanorods synthesized in a phosphine–free system. By employing different ligands, we successfully synthesized 0D nanodots and 1D nanorods by employing oleylamine (OLA) or oleylamine and dodecanethiol (DDT) as ligand, respectively. The experimental results indicated that DDT played an important role in the formation of 1D Zn–chalcogenide nanorods by the heat–up method. The control experiments showed that without DDT as the co–ligand, only nanodots of zinc blende structured nanoparticles can be obtained. When OLA and DDT were used as the co–ligand, wurtzite 1D nanorods were obtained. Therefore, we proposed a mechanism to explain the formation of Zn–chalcogenide nanorods while using OLA and DDT as ligand for the synthesis. On the one hand, The binding of the DDT on the surfaces of Zn–chalcogenide nucleus is diverse. Typically, these ligands bind less tightly on the (002) surface of the wurtzite structure which leads to the anisotropic growth of nanowires. On the other hand, DDT could activate S precursor in oleylamine solvent and promote the formation of ZnS monomors along with the heating up procedure, which can gradually increase monomer concentration and result in growth of diameter of nanowires and finally produce thicker nanorods.

This work provided a heat–up method for tailoring the phase and morphology of colloidal ZnS, ZnSe and ZnS_xSe_{1-x} nanoparticles. The synthesized nanorods could be used as the materials for the synthesis of hybrid nanoparticles, such as Au–ZnS or ZnS–Ag_2S, which have potential applications in photocatalytic H_2 generation, UV detector and near–infrared fluorescence imaging.

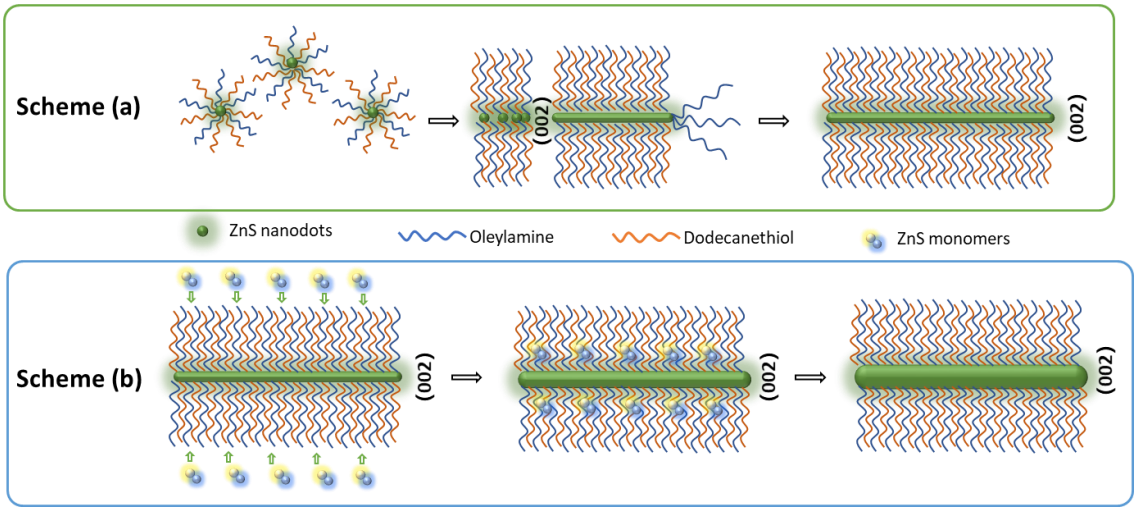

Figure 5.1 Scheme of 1D nanorods synthesis by one–pot heat–up method. (a) Nucleation and ligand-controlled growth (oriented attachment) at low Temperature (<240ºC), thin nanowires obtained. (b) Growth in diameter direction resulted from increased monomers concentration at high Temperature (>240ºC), thicker nanorods obtained from nanowires. ZnS nanorods were used as an illustrative example.

Abstract

Herein we reported a heat–up method for synthesis of ZnSe, ZnS and ZnS_xSe_{1-x} nanorods and nanodots. The studies of the effect of 1–dodecanethiol (DDT)'s on the synthesis of ZnSe, ZnS and ZnS_xSe_{1-x} nanorods indicated that DDT could improve the reaction activity of Se or S powder precursor in oleylamine which is responsible for the formation of one–dimensional nanorods. Without using DDT as ligand, only nanodots can be obtained by the heat–up synthesis of ZnSe, ZnS and ZnS_xSe_{1-x} nanodots in oleylamine. This heat–up method could be used as general approach for ZnSe, ZnS and ZnS_xSe_{1-x} nanorods, and can be used for the scale–up synthesis of spherical dots. A brief demonstration of synthesis of Au–ZnS and Ag_2S–ZnS hybrid nanostructure showed that the synthesized nanorods could be applied as raw materials for compositing heterostructures such as noble–metal–semiconductor hybrids which might find applications in UV detectors and photocatalysis.

5.1Introduction

As one of the most important types of II–VI semiconductors[1], Zinc chalcogenides (ZnS, ZnSe and ZnTe) nanocrystals have excellent electronic and optoelectronic properties and were regarded as good candidates in a wide range of application such as LED[2, 3], photocatalysis[4, 5], solar cells,[6] bioimaging[7] and light detectors[8]. For example, CdS–CdSe/ZnSe core shell nanorods were assembled to highly photoluminescent LEDs with a type I straddling band offset in the core. [9] It is well known that the size and shape of nanoparticles have significant influence on their electronic and optical properties[10]. For example, CdSe nanocrystals can be simply classified to 0–dimensional, 1–dimensional and 2–dimensional nanoparticles based on the quantum confinement effects. For 0–dimensional nanocrystals, such as nanodots, nanotriangles, nano–peanuts, since the size of all dimension of CdSe nanoparticles is smaller than its Bohr radius [11], electrons and holes are confined in three dimensions. For 1–dimensional nanoparticles, such as nanorods, nanowire and nanobelts, since only the diameter of the nanoparitcles is smaller than the Bohr radius of these materials, the electrons and holes are confined in two dimensions except for the length direction[12]. For 2–dimensional nanoparticles[13], such as nanosheets, nanoplates and quantum wells, only the thickness of the nanoparticles is smaller than the Bohr radius of these materials, thus the electrons and holes are confined only in one dimension. Therefore, these distinct features of the confinement of the electrons and holes lead to their specific properties, for example, one dimensional nanorods

have linearly polarized emission and absorption, which makes them ideal materials for the application in LEDs.

The morphology control of Cd–based nanoparticles has been extensively studied. For example, the successful size and morphology control of CdSe[14–16], CdS[17] nanocrystals were reported by many groups and the growth mechanisms were thoroughly investigated. Uniform nanodots, nanorods and nanoplates of CdSe and CdS were synthesized by hot–injection methods separately, the control of the size and morphology were fulfilled by using different ligands in combination with the reaction temperature[16]. On the other hand, however, less progress has been achieved in the size and morphology control ofZn–based chalcogenide nanocrystals.[1] Some synthetic approaches for the controlled synthesis of zinc chalcogenide nanocrystals have been reported[18], such as employing strong reducing agent to enhance the reaction activity of Se or Te precursor[2, 19, 20], a ripening process to gain shorted and thick ZnSe nanorods from long and thin ZnSe nanowires[21], introducing a molecular cluster for ZnSe nanorods growth[22], and synthesize ZnSe/ZnS dot–in–rods by cation exchange from CdSe/CdS nanorods[23]. However, most of these methods were based on hot–injection methods and required tedious experimental procedures. Although there were some reports on the synthesis of ZnSe and ZnSe nanocrystals using the hot injection method[5, 8, 19, 21], toxic and dangerous chemicals such as DPP[22] and superhydride[2, 20] were used and the experiments need to be conducted very cautiously. The injection speed, injection temperature and amount of injection solution should be precisely controlled to produce uniform nanoparticles and the yield of final product from one synthesis is usually less than 50 mg. This hinders the further study and application of such materials. In this regard, the previous studied hot injection methods are not suitable for scale–up manufacture[24].

There are some reports on ZnS nanodots and nanorods based on heat–up methods[25] by changing S precursor species. However, the synthesized nanoparticles were not very uniform, which may deteriorate their optical or electric performance. Thus, the synthesis of ZnSe, ZnS nanocrystals with controlled morphology using by a heat–up method is still challenging. It is known that the precursor reactivity has important influence on nanoparticle growth. For the preparation of the ecofriendly phosphine–free selenium precursor, Se powder was dissolved in 1–octadecene (ODE)[26] or oleylamine (OLA)[21] to prepare Se stock solution for the hot–injection synthesis of ZnSe nanoparticles. For the synthesis of the anisotropic one–dimensional nanowires or nanorods, a high monomer concentration in solution is vital for anisotropic

growth. Therefore, we plan to control the final products morphology by controlling the reaction activity of precursor and ligand solvent in the heat–up system.

In typical syntheses of Zn based semiconductors, OLA and ODE were commonly used as phosphine free ligands and solvent for S and Se precursors. Raston *et al.* reported that Se–ODE precursor had higher reactivity than TOPSe at 220°C[26]. O'Brien *et al.* reported that the coupling reaction between ODE and Se in a one–pot synthesis of ZnSe NCs generated a tetrahydroselenophene derivative which acted as an efficient selenium precursor for the nucleation and growth.[27] Ozin *et al.* reported that heating S in OLA would form alkylammonium polysulfides at a low temperature and then the polysulfide ions reacted with excess amine to generate H_2S, which combineed with the metal precursor to form metal sulfides[28]. Heating sulfur or selenium in oleylamine corresponded to a reaction in whichnew S or Se–Oleylamine species such as H_2S or H_2Se will be formed [29].Yang and coworkers [30] reported a study on alkylthiol–enabled Se powder dissolution in oleylamine at the room temperature with high activity, which could be used for the phosphine–free synthesis of copper–based quaternary selenide nanocrystals.

These results inspired us to conduct more work by tuning the reactivity of precursor for one–pot synthesis of zinc–based chalcogenide nanocrystals by changing the types of solvents and ligands. Since DDT can work as the ligand and also can increase the activity of S and Se precursor, the use of DDT will lead a difference for nanocrystals nucleation and growth. So, we employed DDT as a co–solvent and ligand in combination with OLA for our heat–up method. The influence of DDT on the formation of S or Se–OLA species and nanocrystals growth was studied, and the experiments and discussion were shown below.

5.2Experimental section

5.2.1 Chemicals.

Zinc acetate dihydrate, $Zn(CH_3COO)_2 \cdot 2H_2O$ (≥ 98%), selenium powder (Se, ≥ 99.5%), sulphur powder (Se, ≥ 99%), oleylamine (OLA, 70%), 1–1–dodecanethiol (DDT, ≥ 98%), dodecylamine (DDA, 99%), %), gold (III) chloride ($AuCl_3$, 99.99%), silver acetate (CH_3COOAg, ≥ 90%) , toluene (99% anhydrous), and ethanol (99.8% anhydrous) were purchased from Sigma–Aldrich. All chemicals were used as received without further purification.

5.2.2 Synthesis of ZnS, ZnSe and ZnS_xSe_{1-x} nanorods with OLA and DDT.

The synthetic protocol was referred to a reported heat–up method with some modification[7]. All experiments were done with the standard Schlenk line techniques under N_2 protection. A 50 mL three neck flask was used as a reactor. Aliquots were taken by a syringe with needle through the rubber plug on the three–neck flask.

For ZnS nanorods synthesis, 5 mmol (1337 mg) zinc acetate dihydrate, 6 mmol S (192 mg) powder were added to a mixture of 10 ml OLA and 5 ml DDT in the 50 ml flask. The mixture was degassed and refilled with N_2 for three times at the room temperature and then heated to 110 °C and kept at this temperature for 0.5 h to remove air and moisture. Then the solution was heated to 260°C at a rate of 10°C/min, then kept at 260°C for 30 min. Aliquots were taken at 180°C, 240°C or 260°C according to the need. For ZnSe nanorods synthesis, all the other parameters were kept the same except that 6 mmol Se (474 mg) powder were added to the mixture OLA and DDT. For ZnS_xSe_{1-x} nanorods synthesis, all the other parameters were kept the same except that 3 mmol Se (247 mg) and 3 mmol S (96 mg) powder were added to the mixture of OLA and DDT.

5.2.3 Synthesis of ZnS, ZnSe and ZnS_xSe_{1-x} nanoparticles with OLA.

For the synthesis of ZnS nanodots, 5 mmol (1337 mg) zinc acetate dihydrate, 6 mmol S (192 mg) powder were added to a mixture of 20 ml OLA in the 50 ml flask. The mixture was degassed and refilled with N_2 for three times at the room temperature and then heated to 110 °C and kept at this temperature for 0.5 h to remove air and moisture. Then the solution was heated to 260°C at the rate of 10°C/min, then kept at 260°C for 30 min. Aliquots were taken at 180°C, 240°C or 260°C according to the need. For peanut shaped ZnSe nanoparticles synthesis, all the other parameters were kept the same except that 6 mmol Se (474 mg) powder were added to OLA. For the synthesis of ZnS_xSe_{1-x} nanodots, all the other parameters were kept the same except that 3 mmol Se (247 mg) and 3 mmol S (96 mg) powder were added to OLA.

5.2.4 Synthesis of Au–ZnS hybrid nanorods.

In a typical experiment for the synthesis of Au–ZnS hybrid nanorods, 10 mg clean ZnS NRs were dispersed in 10 mL toluene by sonicating for 5 mins to make a 1 mg/mL ZnS NRs solution. Then, 10 mg $AuCl_3$, 70 mg DDA and 10 mL toluene were mixed and sonicated for 10 mins to make a 1 mg/mL $AuCl_3$ solution. Later, 1 mL ZnS NRs solution and 4 mL toluene were taken into a three–neck flask and kept under N_2 flowing., Then the prepared $AuCl_3$ solution of varied

volumes (0.1, 0.5 and 1 mL) was injected into the ZnSe NRs solution at room temperature for growth for a time duration of 1 hour. The samples were heated up to 100 °C and kept at this temperature for 30 mins, which was labeled as samples growth at 100°C. The final products were separated from toluene by centrifugation with help of acetone.

5.2.5 Synthesis of ZnS–Ag_2S hybrid nanorods by cation exchange.

In a typical experiment for the synthesis of ZnS–Ag_2S hybrid nanorods, 1 mg clean ZnS NRs were dispersed in 5 mL toluene by sonicating for 5 mins to make a 0.2 mg/mL ZnS NRs solution. Then 2 mg silver acetate (CH_3COOAg) and 3 mL methanol were mixed and sonicated for 10 mins to make 0.67 mg/mL silver precursor solution for cation exchange. Later, 0.2 mL ZnS NRs solution and 4 mL toluene were taken into a three–neck flask and kept under N_2 flowing, then the prepared silver precursor solution of varied volumes (0.2, 0.4 and 0.8 mL) was injected into the ZnS NRs solution at the room temperature. The mole ratio of Ag to Zn for these three samples were 0.72:1, 1.45:1 and 2.9:1 based on TGA data (Appendix Figure D5–11) of ZnS nanorods. The colorless solution turned to dark brown immediately after the injection of the silver precursor. Final products were collected after reaction evolved for 1h by centrifugation. The final products were dispersed in toluene for further analysis.

5.3Results and Discussions

5.3.1 Synthesis of ZnS, ZnSe and ZnS_xSe_{1-x} nanorods with OLA and DDT as the ligands

a) ZnS Nanorods

By employing OLA and DDT as the co–ligands, a series of ZnS nanoparticles were obtained by and heating zinc acetate and Se powder to 260°C. The crystals phase of synthesized ZnS nanoparticles was analysed by XRD and the absorption spectroscopy, as shown in **Figure 5.2a**. The synthesized nanorods were identified as the wurtzite structure with referring to the the standard card JSCD #39–1363. The diffraction corresponding to the (002) facet was dominant which indicates that the (002) facets were mainly developed in the crystals. The UV–Vis absorption spectrum (Figure 5.2b) of aliquots taken at 180°C, 220°C, 240°C and 260°C showed a red shift from ~283 nm at 180°C to ~290 nm at 220°C, ~295nm at 240°C and ~315nm at 260°C, indicating the increase of the particles size during the heating up procedure.

The morphologies of synthesized nanoparticles were studied by using TEM, as shown in **Figure 5.2c–f**. For aliquot taken at 220 °C, the nanoparticles were very tiny nanodots and short fragments, with a mean diameter of 1.64 ± 0.33 nm (**Figure 5.2c**). By increasing the

temperature to 240°C, the nanowires grew into longer nanowires with an average length and diameter of 14.18 ± 3.12 nm and 1.67 ± 0.31 nm, respectively. The growth on length was obviously while the diameter kept barely same size as that of the tiny dots obtained at 220°C. This phenomenon could be resulted from oriented attachment of the initial ZnS nanodots[31, 32] and the DDT ligand which usually binds less strongly on the (002) facet of wurtzite nanoparticles [33].

Further increase of the reaction temperature to 260 °C with a time duration of 20 mins, the nanorods turned to thicker nanorods with an average length and diameter of 16.69 ± 4.66 nm and 4.04 ± 0.47 nm, respectively. The size diagram was shown in Appendix Figure D5(1–3). Compared with thin nanorods obtained at 240 °C, the length growth is not obvious while the diameter increased clearly. This phenomenon indicated a different growth habit in comparison to the oriented attachment of the previous stage (200°C to 240°C). The reason accounted for the growth in diameter at the elevated temperature could be the gradually increased monomer concentration. As the supply of the high monomer concentration is necessary for the growth of 1D ZnS nanoparticles in the heat–up procedure. One possible explanation is that the DDT ligand binding on ZnS surfaces also released some S source from –SH when the reaction system was heated to or over 240 °C. Aanother possibility is that since DDT has a lower boiling point (275°C) than OLA (364°C), DDT may gradually strip off from the lattice planes of the ZnS (cylindrical surface) which provided site for monomers deposition on the diameter direction.

The FFT image of the ZnS nanorods synthesized at 260 °C for 20 mins (**Figure 5.2f** and inset) identified the lattice distances of the (100), (002), (101) and (102), which match those of XRD pattern of wurtzite ZnS (**Figure 5.2a**). These results proved that the phase of ZnS nanorods synthesized in the mixture of OLA and DDT were wurtzite and increasing temperature from 180°C to 260°C led to the increase of length and width of the synthesized nanorods, along with a red shift of absorption peak from 283 nm to 315 nm.

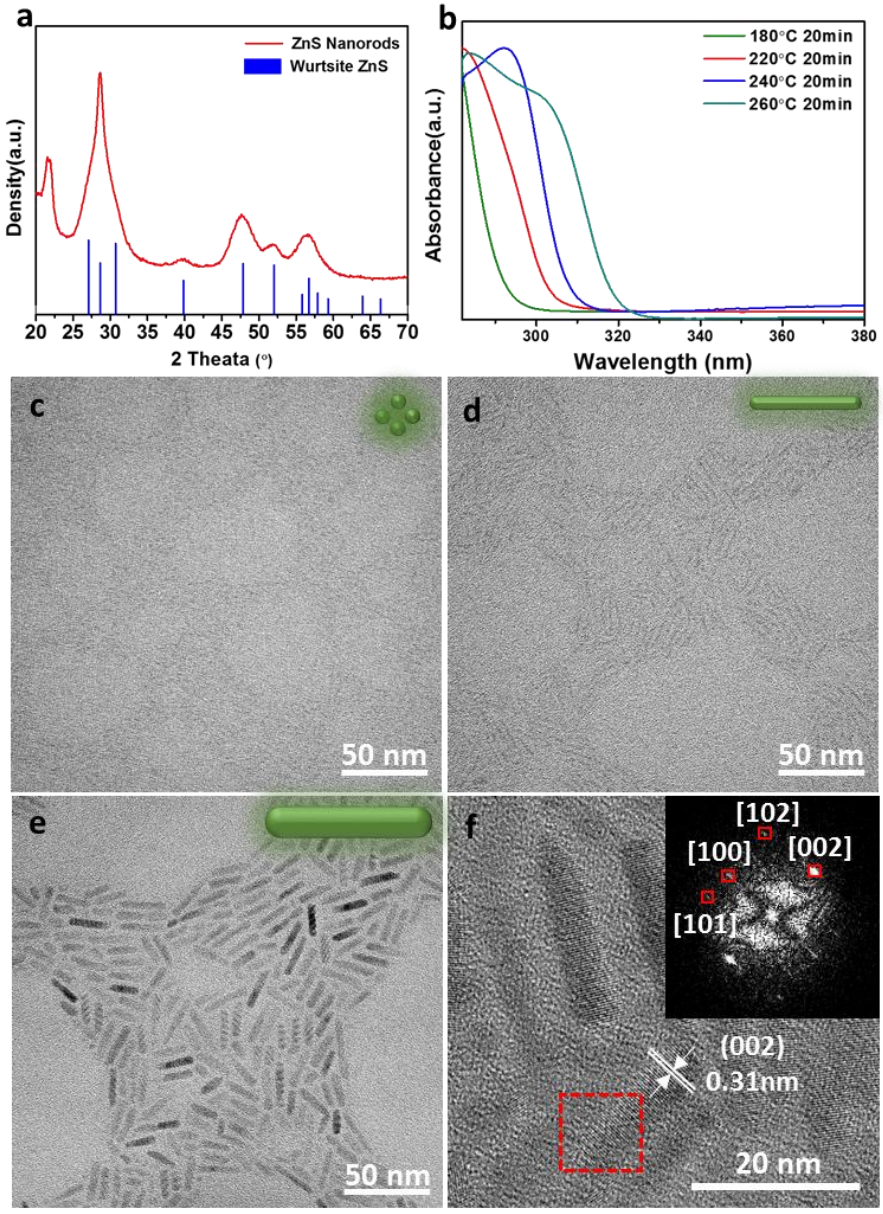

Figure 5.2 (a) XRD pattern and (b) UV–Vis absorption of ZnS synthesized in DDT and OLA. Aliquots were taken at 180°C, 220°C, 240°C and 260°C; (c–e) TEM images of ZnS synthesized in DDT and OLA. Aliquots taken at 220°C, 240°C and 260°C, showing the morphology transfer from tiny nanordots to thin nanowires and thick nanorods. (f) HRTEM images of ZnS NRs in (e), indicating the wurtzite phase with elongation along the (002) direction.

b) ZnSe nanorods

Keeping the ligand and synthetic conditions the same as the abovementioned synthesis of ZnS nanorods, ZnSe nanoparticles can also be produced using the same synthetic conditions of the

abovementioned synthesis of ZnS nanorods except the S powder was replaced by the Se powder. The crystals phase of synthesized ZnSe nanoparticles were analysed by XRD and the diffraction pattern was shown as **Figure 5.3a**, as seen in Figure 5.3a. The synthesized ZnSe nanorods can be indexed to wurtzite phase with referring to the standard JSCD #15–0105 card of wurtzite ZnSe. The diffraction peak corresponding to the (002) plane was dominant which indicates that the (002) facets were mainly developed in the nanocrystals. The UV–Vis absorption spectrum of aliquots taken at 220°C for 60 mins, 250°C for 1 min and 260°C for 8 mins and 15 mins showed a red shift from 355 nm at 220°C to 362 nm at 250°C and 374nm at 260°C for 8 mins and 380 nm for 15 mins. As DDT is stronger ligand than oleylamine, herein the synthesized nanorods with DDT and OLA showed photoluminescence while nanodots synthesized in pure oleylamine had no photoluminescence because of the quenching effect in relation to the surface defects. The corresponding photoluminescence of ZnSe nanorods shifted from 375 nm to 381 nm, 392 nm and 395 nm, respectively.

The morphologies of synthesized ZnSe nanoparticles were studied by using TEM, as shown in **Figure 5.4.**, For aliquot taken at 220°C, the nanoparticles were very thin and short wires with a length and a diameter of 16.9×1.95nm (Figure 5.4a). When the reaction temperature was increased to 240°C, the nanowires grew into thicker and longer nanowires with an average length and diameter of 24.93 ± 5.90 nm and 2.21 ± 0.35 nm, respectively. Further increase of growth temperature to 260°C and growth duration for 30 mins led to the formation of nanorods with an average length and diameter of 19.54 ± 4.80 nm and 2.92 ± 0.49 nm, respectively. The FFT image of the final ZnSe nanorods showed in Figure 5.4d and inset identified the lattice distance of the (100), (002), (101) and (102) of wurtzite ZnS nanocrystals, which was consistent with the XRD results in Figure 5.4a. These results proved that ZnSe nanorods synthesized in the mixture of OLA and DDT were wurtzite structure and increasing temperature from 220°C to 260°C led to the increase of length and width of the synthesized nanorods, along with the red shift of UV–Vis absorption from 355 nm to 380 nm and PL emission from 362 nm to 395 nm. As seen in Figure 5.4c and 3d, after keeping the reaction at 260°C for 30 mins, some short nanorods were obtained. This is because that DDT ligands binding on the surfaces of ZnSe nanorods may detach from the surfaces at high temperatures [5], which initiated a thermodynamic ripening procedure that shortening and thickening of ZnSe nanorods[21]. The size diagrams for ZnSe nanorods synthesized at 220°C, 240°C and 260°C were shown as Appendix Figure D5(4–6).

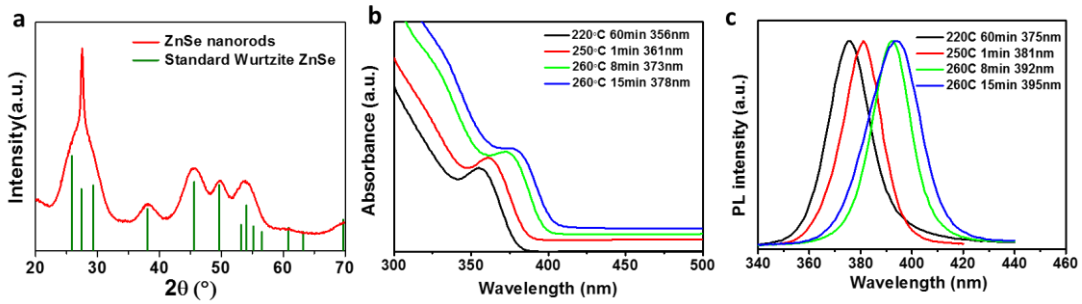

Figure 5.3 (a) XRD pattern, (b) UV–Vis absorption and (c) PL emission of ZnSe nanorods synthesized at different temperatures.

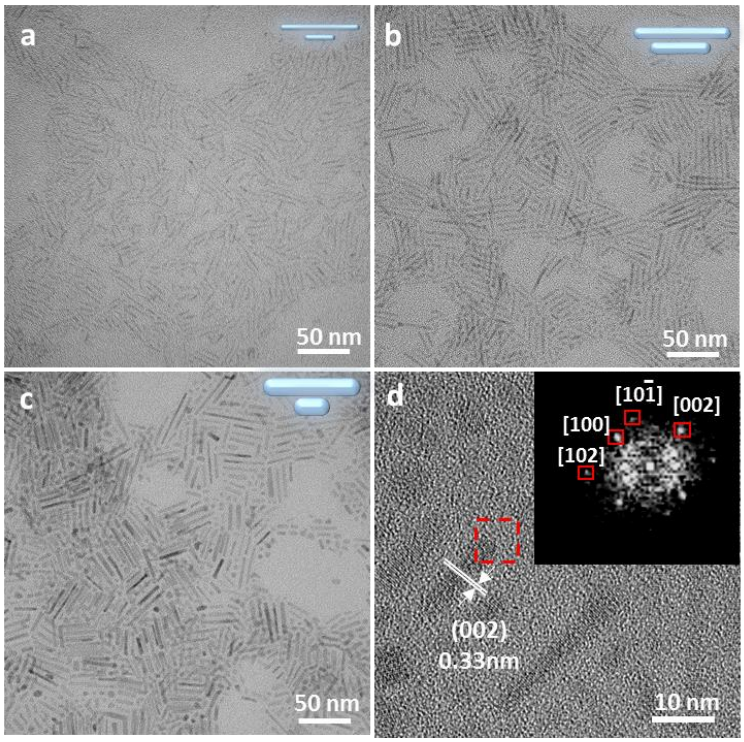

Figure 5.4 TEM images of ZnSe aliquots at (a) 220 °C for 10mins; 16.9×1.95 nm; (b) 240 °C for 30 mins; 24.92×2.21 nm; (c) 260 °C for 30 mins; 19.55×2.92 nm (d) HRTEM and the corresponding FFT pattern of ZnSe nanorods in (c).

c) ZnS_xSe_{1-x} nanorods

Previous studies revealed that alloyed ZnS_xSe_{1-x} nanorods had high efficiency in energy fuel production[5]. Thus it's meaningful to develop facile and robust synthetic method for alloyed ZnS_xSe_{1-x} nanorods. It's interesting to see if this scale–up–accessible method that developed in this work could also be utilized for the synthesis of alloyed $ZnSe_xS_{1-x}$ nanorods. Thus, a mixture of S powder and Se powder was used as the anion precursor to prepare alloyed

ZnS_xSe_{1-x} nanoparticles. The crystals structure, UV–Vis absorption and PL emission spectra of obtained nanoparticles in OLA and DDT were shown in **Figure 5.5**. As seen from **Figure 5.5a**, the diffraction peaks of synthesized ZnS_xSe_{1-x} nanorods din't match the standard XRD patterns of ZnSe or ZnS alone but the position of the diffraction peaks located between that of of ZnSe and ZnS, confirming the produced nanoparticles were alloyed ZnS_xSe_{1-x}. The UV–Vis absorption spectrum (**Figure 5.5b**) of aliquots taken at 220°C, and 260°C for 20 mins showed a red shift from 326 nm at 220°C to 345 nm at 260°C. The red shift of the absorption peaks corresponded to the increase of the particles size during the heating up procedure. The corresponding photoluminescence (**Figure 5.5c**) shifted from 343 nm to 363 nm. The morphology of ZnS_xSe_{1-x} synthesized at 260°C for 20 mins was studied by using TEM, as shown in **Figure 5.5d**. Being different from ZnS or ZnSe, the products synthesized at 260°C for 20 mins were thin and long ZnS_xSe_{1-x} nanorods with a diameter of 2.23 ± 0.40 nm and length of 53.97 ± 12.97 nm. Some nanodots were also found in the final products and the formation of these dots at the high temperature was similar to that observed in a mixture contained ZnSe nanorods and some ZnSe nanodots, as discussed in the previous section. The size diagram for ZnS_xSe_{1-x} nanorods synthesized at 260°C was shown in Appendix Figure D5–7.

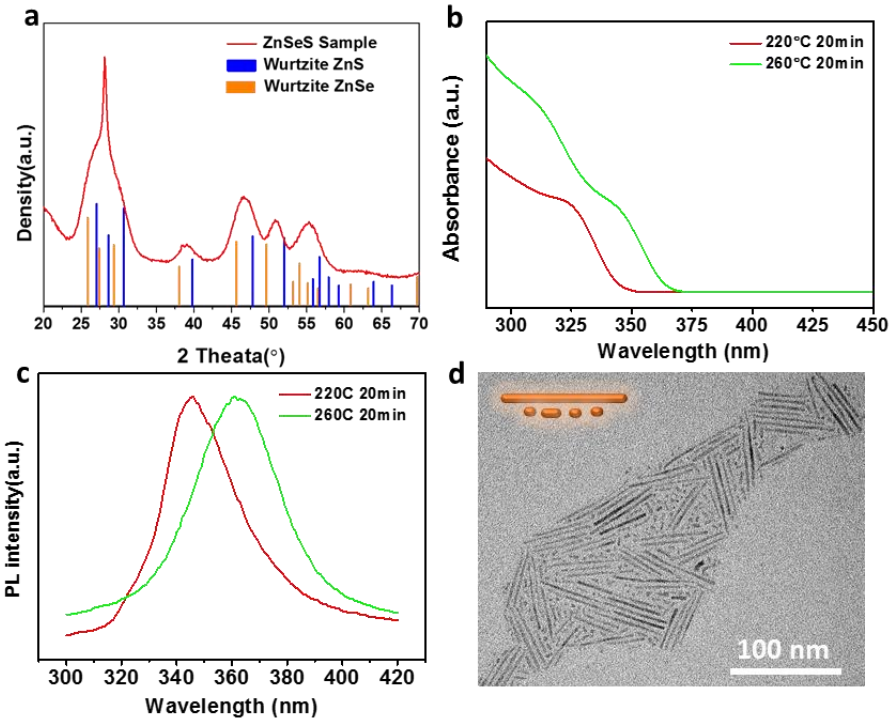

Figure 5.5 (a) XRD pattern, (b) UV–Vis absorption and (c) PL emission spectra and (d) TEM image of ZnS_xSe_{1-x} nanorods, with a diameter of 2.23 ± 0.40 nm and length of 53.97 ± 12.97 nm.

5.3.2 Synthesis of ZnS, ZnSe and ZnS_xSe_{1-x} with pure oleylamine as the ligand

As a comparison, we conducted experiments by employing only OLA as ligand instead of using the mixture of OLA and DDT for heat–up synthesis of ZnS, ZnSe and ZnS_xSe_{1-x} nanocrystals. The TEM images, UV–Vis absorption spectra and XRD patters were shown as **Figure 5.6**. As seen from Figure 5.6, being different from ZnS, ZnSe and ZnS_xSe_{1-x} nanorods synthesized in the mixture of DDT and OLA, the ZnS, ZnSe and ZnS_xSe_{1-x} nanocrystals synthesized in OLA were dots or peanut–shaped particles. After the growth evolved at 260°C for 20 mins, ZnS nanodots with an average diameter of 5.44±1.44 nm were obtained (size histogram can be found in Appendix Figure D5–8) and the XRD pattern confirmed the cubic structure of the obtained ZnS. The synthesized ZnSe nanoparticles in Figure 5.6b showed irregular peanut–shape, and the length and diameter of ZnSe peanut–like nanoparticles is 7.34±1.78 nm and 4.50±0.64 nm, respectively (Appendix Figure D5–9). XRD pattern of the peanut–like nanoparticles can also be indexed to the cubic structured ZnSe. The synthesized ZnS_xSe_{1-x} nanoparticles in Figure 5.6c showed dot–shape, and the diameter of ZnS_xSe_{1-x} nanoparticles is 4.69±0.85 nm (Appendix Figure D5–10). The diffraction peaks in XRD pattern also show a shift with respect to those of standard cubic ZnSe and ZnS, which indicated the formation of alloyed ZnS and ZnSe nanocrystals.

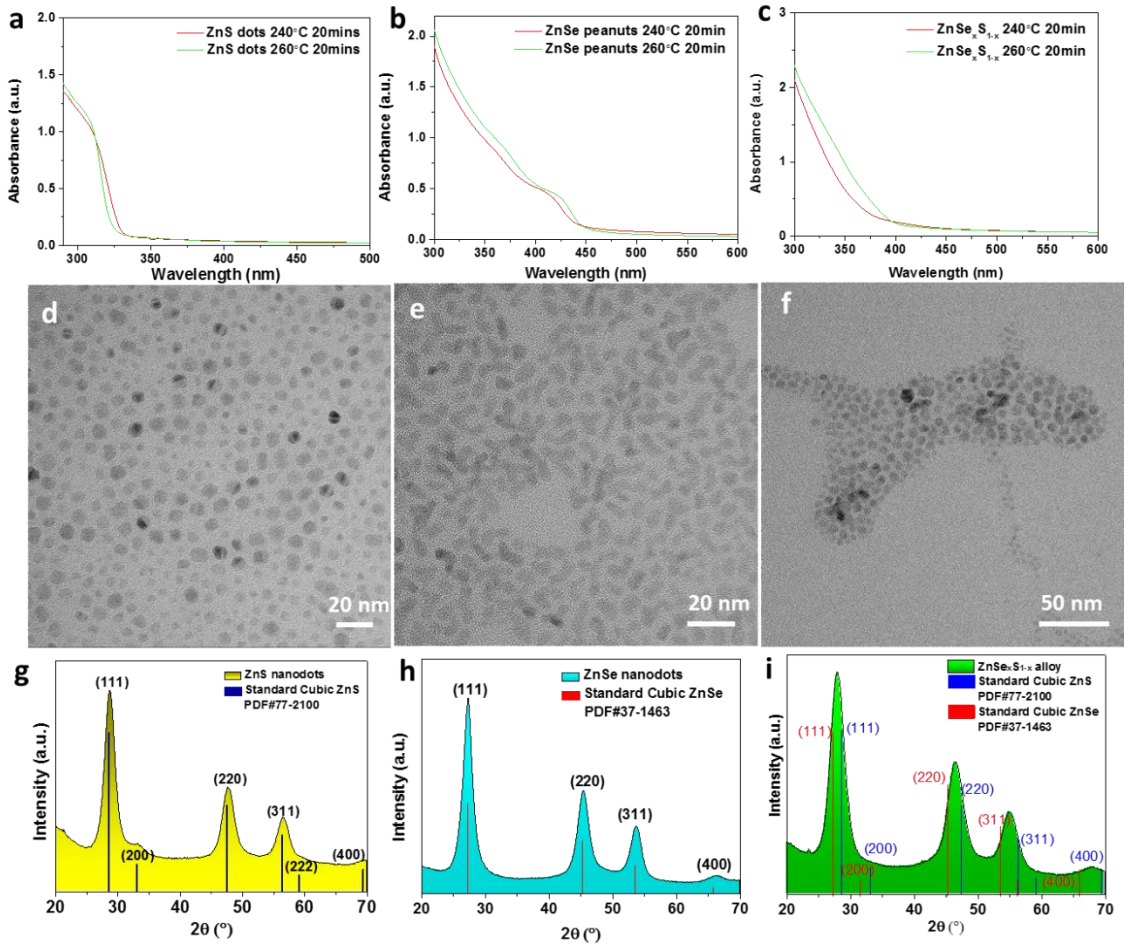

Figure 5.6 (a–c) UV–Vis spectra of ZnS, ZnSe and ZnS_xSe_{1-x} nanocrystals obtained at 240°C to 260°C. (d–e)TEM and (g–i) XRD patterns of ZnS, ZnSe and ZnS_xSe_{1-x} nanocrystals synthesized at 260°C in oleylamine.

5.3.3 Synthetic mechanism of zinc based II–VI nanocrystals with different ligands

In conclusion, a schematic relating to the synthetic mechanism of ZnS, ZnSe and ZnS_xSe_{1-x} nanoparticles with DDT and OLA as ligand or OLA as ligand using the one–pot heat–up synthetic method was shown in **Figure 5.7**. Based on the characterizations of final nanoparticles, we found out that the use of DDT and OLA as ligand produced 1–D ZnS, ZnSe and ZnS_xSe_{1-x} nanorods of wurtzite structure while 0–D ZnS, ZnSe and ZnS_xSe_{1-x} nanodots or nano–peanuts of zinc blende structure were obtained if only OLA was used as the ligand for the growth at 260 ^oC. The final morphology was closely relating to the activation of S or Se precursor by DDT as a high concentration of concentration in solution supported the anisotropic growth.

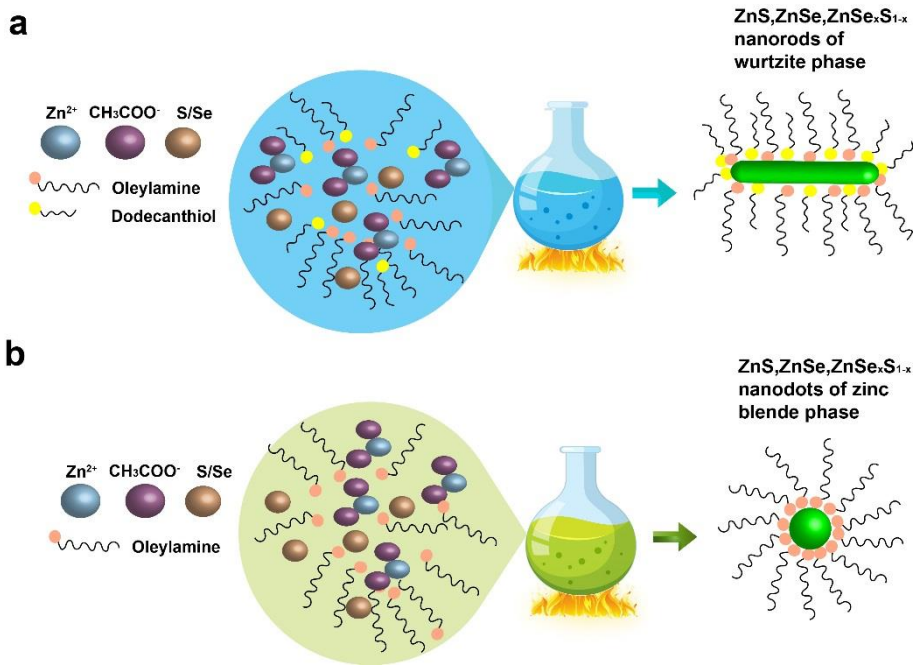

Figure 5.7 Schematic of the synthetic mechanisms of ZnS, ZnSe and ZnS_xSe_{1-x} nanoparticles using DDT and OLA or OLA as the ligand.

5.3.4 Synthesis of hybrid ZnS nanoparticles

Due to the outstanding synergetic properties of combined components in one nanoparticle such as effective electron–hole separation in noble–metal–semiconductor nanoparticles[34], hybrid nanoparticles have been received tremendous attentions in recent years.[35] Herein, we demonstrated the synthesis of hybrid nanorods by employing ZnS nanorods as starting materials.

5.3.4.1 Au growth on ZnS NRs of different ratio at room temperature or 100°C.

Nobel metal–semiconductor hybrid nanoparticles were reported and studied for many applications such as photocatalysis and 3D printer indicator. However, most studies of II–VI semiconductors were based on Cd–containing semiconductors. Compared with Cd containing semiconductors, Zn based II–VI semiconductors are more environment–compatible and less toxic or non–toxic. There was only limited research on this topic, so we studied the growth of Au nanoparticles on ZnS nanorods to form Au–ZnS hybrids, as shown in **Figure 5.8**. As seen from Figure 5.8, with low Au precursor ration, some tiny Au nanoparticles nucleated in the solution at the room temperature when a low molar ratio of Au precursor to ZnS nanorods was used (**Figure 5.8 a1, a2**). By increasing the amount of Au precursor, the Au precursor grew on the edge of ZnSe NRs (**Figure 5.8 b1, b2**) alongside many separated Au nanoparticles formed

by self–nucleation. The further enhancement of Au precursor amount leads to the growth of large Au tips on the body of ZnS NRs (**Figure 5.8 c1, c2**). After keeping Au growth at the room temperature for 1h, then the solution was heated up to 100 °C and kept for 0.5 h (**Figure 5.8 d1–f1, d2–f2**). Under such conditions, ZnS NRs with large Au tipps were obtained without the presence of self–nucleated Au nanoparticles. These results indicated that a higher temperature promotes the aggregation of dissociative Au nanoparticles in solution that is beneficial to the growth of large Au tips on ZnS nanorods.

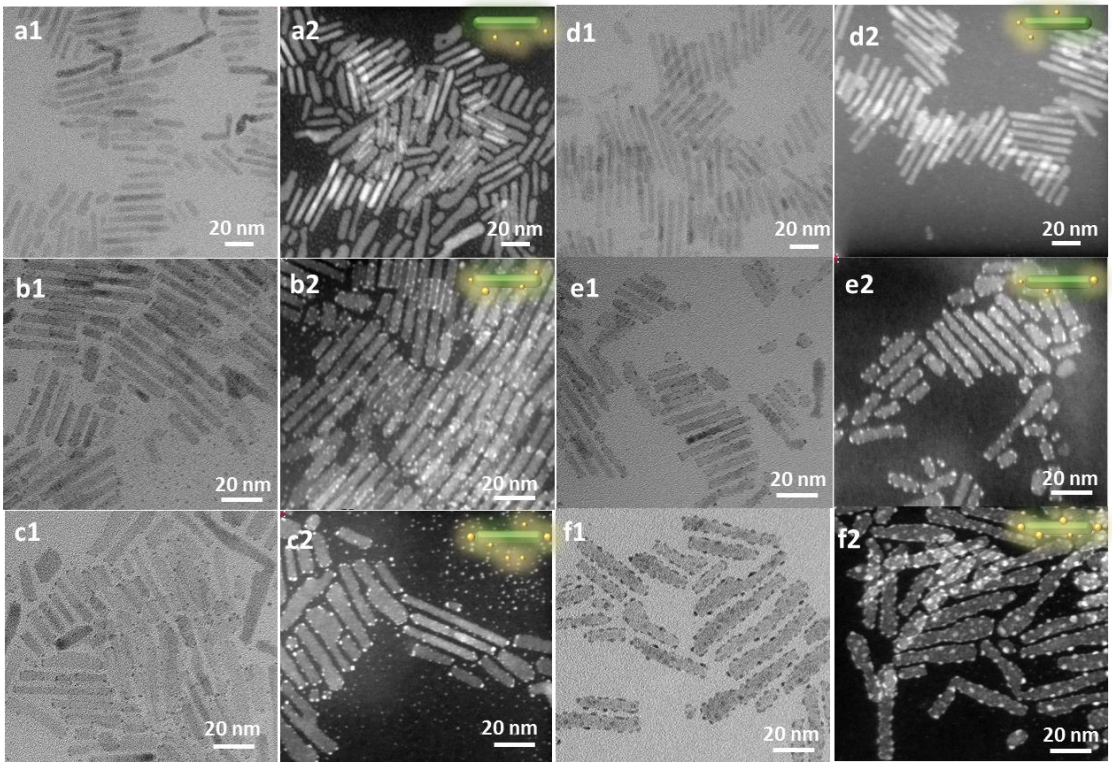

Figure 5.8 TEM and STEM images of Au–ZnS hybrids. (a1–c1) Au grew on ZnS at different ratio at the room temperature, m ($AuCl_3$: ZnS NRs)=1:10, 1:2, 1:1 for (a1–c1) respectively; (a2–c2) STEM images corresponding to (a1–c1); (d1–f1) Au grew on ZnS at different ratio at 100ºC, m ($AuCl_3$: ZnS NRs)=1:10, 1:2, 1:1 for (d1–f1) respectively; (d2 –f2) STEM images were corresponding to (d1–f1), respectively.

5.3.4.2 ZnS–Ag_2S NRs by cation exchange.

Ag_2S nanoparticles find wide applications in biomedicine, such as in cancer imaging and photothermal therapy.[36] Assembling a wide bandgap semiconductor nanocrystal of ZnS with a narrow bandgap semiconductor of Ag_2S to form a heterostructure is interesting, which enable broad band light absorption from UV to near–infrared and makes them ideal for

photocatalysis[37]. So I synthesized ZnS–Ag_2S hybrid NRs by partial cation exchange from ZnS to Ag_2S. As seen from **Figure 5.9**, by adding Ag precursor added to the ZnS solution, partial cation exchange was found and ZnS–Ag_2S hybrid NRs with varied Ag_2S diameter were synthesized. The cation ratio of Ag^+: Zn^{2+} used for cation exchange was calculated based on the TGA data of ZnS NRs (Appendix Figure D5–11). Increased ratio of Ag^+: Zn^{2+} used for cation exchange led to the growth of Ag_2S hump on ZnS NRs, with the increase of the, diameter from 6.26 nm to 7.91 nm. This phenomenon can be explained as that the DDT ligand also worked as S source to promote the growth of Ag_2S humps. Zn, Ag and S element mapping shown in Figure 5.9 (g–i) and XRD pattern (Appendix Figure D5–12) and XPS data (Appendix Figure D5–13) proved the successful partial cation exchange and the formation of ZnS–Ag_2S hybrid NRs. A Schematic diagram of the formation mechanism of ZnS–Ag_2S nanorods by cation exchange is seen as in Appendix Figure D5–14.

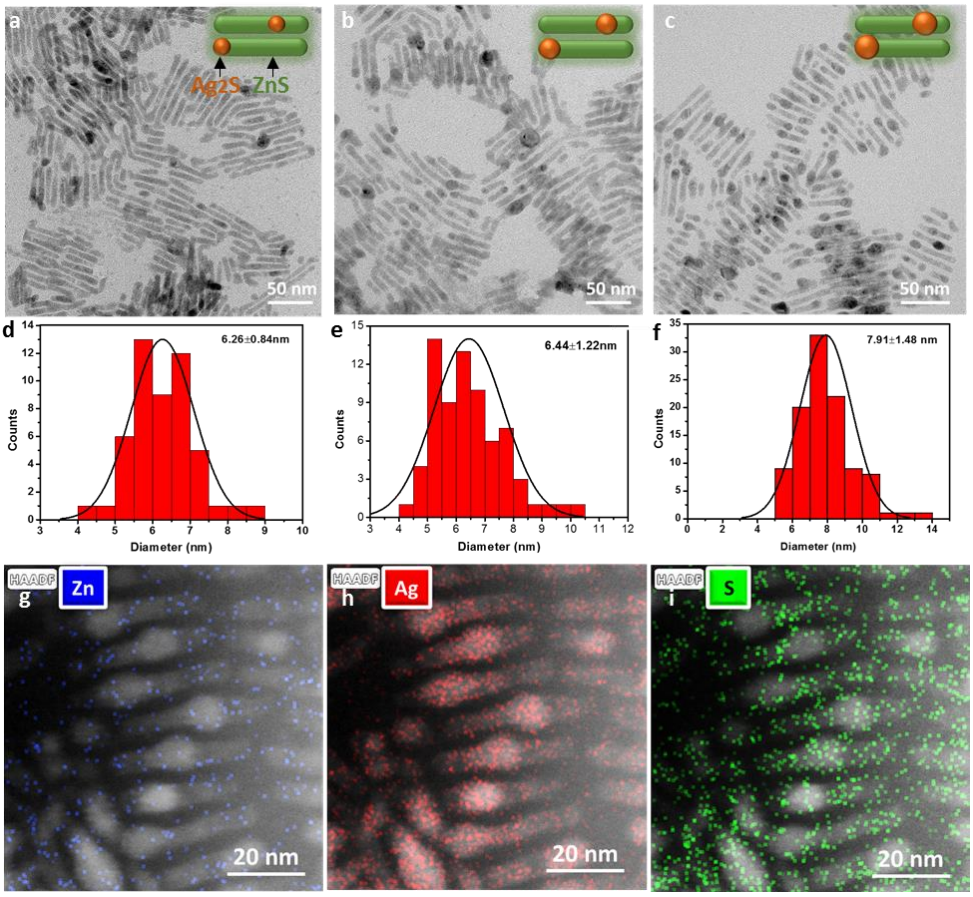

Figure 5.9 TEM images of ZnS–Ag_2S hybrid nanorods prepared with varied Ag to Zn molar ratio. (a–c) n(Ag:Zn)= 0.72:1, 1.45:1 and 2.9:1, respectively. (d–f) Histogram of the diameter of Ag_2S bump corresponding to (a–c). (g–i) STEM and EDS mapping images of (c).

5.4 Conclusion.

In this work, we introduced a simple one–pot heat–up method to synthesize 1–D ZnS, ZnSe, ZnS_xSe_{1-x} nanorods or 0D nanodots by choosing different ligands. Typically, when a mixture containing OLA and DDT was used as the ligand, ZnS, ZnSe and ZnS_xSe_{1-x} nanorods of wurtzite structure were obtained. When only OLA was used as the ligand, ZnS, ZnSe and ZnS_xSe_{1-x} nanodots or nano–peanuts of zinc blende structure were obtained. These results indicated that DDT increased the activity of S or Se powder in OLA which promoted the formation of nanorods. The synthesized nanorods could be used as fundamental materials for hybrid nanoparticles synthesis, such as Au–ZnS or ZnS–Ag_2S. Such hybride nanoparitcles have potential in many applications such as catalytic H_2 generation, UV detector and near–infrared fluorescence imaging.

5.5 References.

1. Jie J, Zhang W, Bello I, Lee C–S, Lee S–T. One–dimensional II–VI nanostructures: Synthesis, properties and optoelectronic applications. Nano Today. 2010;5(4):313–336.
2. Zhang J, Jin S, Fry HC, Peng S, Shevchenko E, Wiederrecht GP, et al. Synthesis and characterization of wurtzite ZnTe nanorods with controllable aspect ratios. J. Am. Chem. Soc. 2011;133(39):15324–15327.
3. Wang A, Shen H, Zang S, Lin Q, Wang H, Qian L, et al. Bright, efficient, and color–stable violet ZnSe–based quantum dot light–emitting diodes. Nanoscale. 2015;7(7):2951–2959.
4. Kuehnel MF, Creissen CE, Sahm CD, Wielend D, Schlosser A, Orchard KL, et al. ZnSe Nanorods as Visible–Light Absorbers for Photocatalytic and Photoelectrochemical H_2 Evolution in Water. Angew. Chem. Int. Ed. Engl. 2019, 58(15): 5059–5063.
5. Chen D, Zhang H, Li Y, Pang Y, Yin Z, Sun H, et al. Spontaneous Formation of Noble–and Heavy–Metal–Free Alloyed Semiconductor Quantum Rods for Efficient Photocatalysis. Adv. Mater. 2018, 30(39): 1803351.
6. Yi L, Liu Y, Yang N, Tang Z, Zhao H, Ma G, et al. One dimensional CuInS2–ZnS heterostructured nanomaterials as low–cost and high–performance counter electrodes of dye–sensitized solar cells. Energy Environ. Sci. 2013;6(3):835–840.
7. Selvaraj J, Mahesh A, Asokan V, Baskaralingam V, Dhayalan A, Paramasivam T. Phosphine–Free, Highly Emissive, Water–Soluble Mn:ZnSe/ZnS Core–Shell Nanorods: Synthesis, Characterization, and in Vitro Bioimaging of HEK293 and HeLa Cells. ACS Appl. Nano Mater. 2017;1(1):371–383.

8. Li D, Hao S, Xing G, Li Y, Li X, Fan L, et al. Solution Grown Single–Unit–Cell Quantum Wires Affording Self–Powered Solar–Blind UV Photodetectors with Ultrahigh Selectivity and Sensitivity. J. Am. Chem. Soc. 2019;141(8):3480–3488.

9. Oh N, Kim BH, Cho SY, Nam S, Rogers SP, Jiang Y, et al. Double–heterojunction nanorod light–responsive LEDs for display applications. Science. 2017;355(6325):616–619.

10. Li LS, Hu JT, Yang WD, Alivisatos AP. Nano Lett Band Gap Variation of Size– and Shape–Controlled Colloidal CdSe Quantum Rods. Nano Lett. 2001;1(7): 349–351

11. Peng X, Manna L, Yang W, Wickham J, Scher E, Kadavanich A, et al. Shape control of CdSe nanocrystals. Nature, 2000, 404(6773): 59–61.

12. Yu H, Li J, Loomis RA, Gibbons PC, Wang LW, Buhro WE. Cadmium selenide quantum wires and the transition from 3D to 2D confinement. J. Am. Chem. Soc. 2003; 125(52):16168–16169.

13. Son JS, Park K, Kwon SG, Yang J, Choi MK, Kim J, et al. Dimension–controlled synthesis of CdS nanocrystals: from 0D quantum dots to 2D nanoplates. Small. 2012;8(15):2394–2402.

14. Liu L, Zhuang Z, Xie T, Wang YG, Li J, Peng Q, et al. Shape control of CdSe nanocrystals with zinc blende structure. J. Am. Chem. Soc. 2009;131(45):16423–16429.

15. Rice KP, Saunders AE, Stoykovich MP. Seed–mediated growth of shape–controlled wurtzite CdSe nanocrystals: platelets, cubes, and rods. J. Am. Chem. Soc. 2013; 135(17): 6669–6676.

16. Li Z, Peng X. Size/shape–controlled synthesis of colloidal CdSe quantum disks: ligand and temperature effects. J. Am. Chem. Soc. 2011;133(17):6578–6586.

17. Shieh F, Saunders AE, Korgel BA. General shape control of colloidal CdS, CdSe, CdTe quantum rods and quantum rod heterostructures. J Phys Chem B. 2005;109(18):8538–8542.

18. Cozzoli PD, Manna L, Curri ML, Kudera S, Giannini C, Striccoli M, et al. Shape and Phase Control of Colloidal ZnSe Nanocrystals. Chem. Mater. 2005;17(6): 1296–1306.

19. Ji B, Panfil YE, Banin U. Heavy–Metal–Free Fluorescent ZnTe/ZnSe Nanodumbbells. ACS Nano. 2017;11(7):7312–7320.

20. Chen W, Karton A, Hussian T, Javaid S, Wang F, Pang Y, et al. Spontaneous shape and phase control of colloidal ZnSe nanocrystals by tailoring Se precursor reactivity. Cryst Eng Comm. 2019;21(18):2955–2961.

21. Jia G, Banin U. A general strategy for synthesizing colloidal semiconductor zinc chalcogenide quantum rods. J. Am. Chem. Soc. 2014;136(31):11121–11127.

22. Ning J, Liu J, Levi–Kalisman Y, Frenkel AI, Banin U. Controlling Anisotropic Growth of Colloidal ZnSe Nanostructures. J. Am. Chem. Soc. 2018;140(44):14627–14637.

23. Li HB, Brescia R, Krahne R, Bertoni G, Alcocer MJP, D'Andrea C, et al. Blue–UV–Emitting ZnSe(Dot)/ZnS(Rod) Core/Shell Nanocrystals Prepared from CdSe/CdS Nanocrystals by Sequential Cation Exchange. Acs Nano. 2012;6(2):1637–1647.

24. Saldanha PL, Lesnyak V, Manna L. Large scale syntheses of colloidal nanomaterials. Nano Today. 2017;12:46–63.

25. Zhai X, Zhang X, Chen S, Yang W, Gong Z. Oleylamine as solvent and stabilizer to synthesize shape–controlled ZnS nanocrystals with good optical properties. Colloid Surface A. 2012;409:126–129.

26. Bullen C, van Embden J, Jasieniak J, Cosgriff JE, Mulder RJ, Rizzardo E, et al. High Activity Phosphine–Free Selenium Precursor Solution for Semiconductor Nanocrystal Growth. Chem. Mater. 2010;22(14):4135–4143.

27. Banski M, Afzaal M, Malik MA, Podhorodecki A, Misiewicz J, O'Brien P. Special Role for Zinc Stearate and Octadecene in the Synthesis of Luminescent ZnSe Nanocrystals. Chem. Mater. 2015;27(11):3797–3800.

28. Thomson JW, Nagashima K, Macdonald PM, Ozin GA. From sulfur–amine solutions to metal sulfide nanocrystals: peering into the oleylamine–sulfur black box. J. Am. Chem. Soc. 2011;133(13):5036–41.

29. van Embden J, Chesman ASR, Jasieniak JJ. The Heat–Up Synthesis of Colloidal Nanocrystals. Chem. Mater. 2015;27(7):2246–2285.

30. Liu Y, Yao D, Shen L, Zhang H, Zhang X, Yang B. Alkylthiol–enabled Se powder dissolution in oleylamine at room temperature for the phosphine–free synthesis of copper–based quaternary selenide nanocrystals. J. Am. Chem. Soc. 2012;134(17):7207–7210.

31. Zhu G, Zhang S, Xu Z, Ma J, Shen X. Ultrathin ZnS single crystal nanowires: controlled synthesis and room–temperature ferromagnetism properties. J. Am. Chem. Soc. 2011;133(39):15605–15612.

32. Yu JH, Joo J, Park HM, Baik S–I, Kim YW, Kim SC, et al. Synthesis of quantum–sized cubic ZnS nanorods by the oriented attachment mechanism. J. Am. Chem. Soc. 2005; 127(15):5662–5670.

33. Singh A, Geaney H, Laffir F, Ryan KM. Colloidal synthesis of wurtzite Cu_2ZnSnS_4 nanorods and their perpendicular assembly. J. Am. Chem. Soc. 2012;134(6):2910–2913.

34. Ben–Shahar Y, Scotognella F, Waiskopf N, Kriegel I, Dal Conte S, Cerullo G, et al. Effect of surface coating on the photocatalytic function of hybrid CdS–Au nanorods. Small. 2015;11(4):462–471.
35. Costi R, Saunders AE, Banin U. Colloidal hybrid nanostructures: a new type of functional materials. Angew. Chem. Int. Ed. 2010;49(29):4878–4897.
36. Yang T, Tang Y, Liu L, Lv X, Wang Q, Ke H, et al. Size–Dependent Ag_2S Nanodots for Second Near–Infrared Fluorescence/Photoacoustics Imaging and Simultaneous Photothermal Therapy. ACS Nano. 2017;11(2):1848–1857.
37. Yang X, Xue H, Xu J, Huang X, Zhang J, Tang YB, et al. Synthesis of porous ZnS:Ag_2S nanosheets by ion exchange for photocatalytic H_2 generation. ACS Appl. Mater. Interfaces. 2014;6(12):9078–9084.

Chapter 6. Non–Epitaxial Gold–Tipped ZnSe Hybrid Nanorods for Efficient Photocatalytic Hydrogen Production

Wei Chen, Xiaojie Li, Fei Wang, Shaghraf Javaid, Yingping Pang, Jiayi Chen, Zongyou Yin, Shaobin Wang, Yunguo Li, Guohua Jia

Small 2020, 16, 1902231

https://doi.org/10.1002/smll.201902231

A copyright permission and author contribution statement could be found in Appendix B.

Summary of Chapter.

In this chapter, we reported a novel synthesis of colloidal gold (Au)–ZnSe hybrid nanorods (NRs) with controlled size and location of Au domains and their application for H_2 production by photocatalytic water splitting for the first time.

Specifically, Au domains were successfully grown onto ZnSe nanorods at controlled site with varied size and quantity. The non–epitaxial growth mechanism of Au tips on wurtzite ZnSe nanorods is revealed experimentally and theoretically. Pure Au nanoparticles (NPs), bare ZnSe and single Au–tipped ZnSe NRs hybrids were employed to study their photocatalytic properties and mechanism. The results indicated that the photocatalytic performance was enhanced effectively after the growth of Au tips and single Au–tipped ZnSe NRs showed higher generation efficiency than double Au–tipped ZnSe NRs. The easier holes transfer and clearance by scavenger after the electron transfer to the Au tips from the untipped apex of single Au–tipped ZnSe NRs than double Au–tipped ZnSe NRs contributed to the better performance. The photocurrent of single Au–tipped ZnSe nanorods hybrids was lightly higher than that of double Au–tipped–ZnSe hybrid nanorods, which was ~1.4 times higher than that of pure ZnSe nanorods. This is also in accordance to the H_2 generation rate results, confirming the effective electron transfer after photoexcitation. The photocatalytic measurement on bare Au particles indicated that with a diameter of ~5.6nm, the plasmon resonance induced hot electrons of Au particles thus led to H_2 production, while the plasmon resonance of tiny Au tips (<2.2nm) on ZnSe NRs was not obvious because of the limitation of its size. We also combined structural analysis of the Au–ZnSe hybrid nanorods with the density functional theory (DFT) simulations to reveal the non–epitaxial growth mechanism of Au on wurtzite ZnSe nanorods.

This work opens an avenue towards Cd–free hybrid nanoparticle–based photocatalysis for efficient clean fuel production.

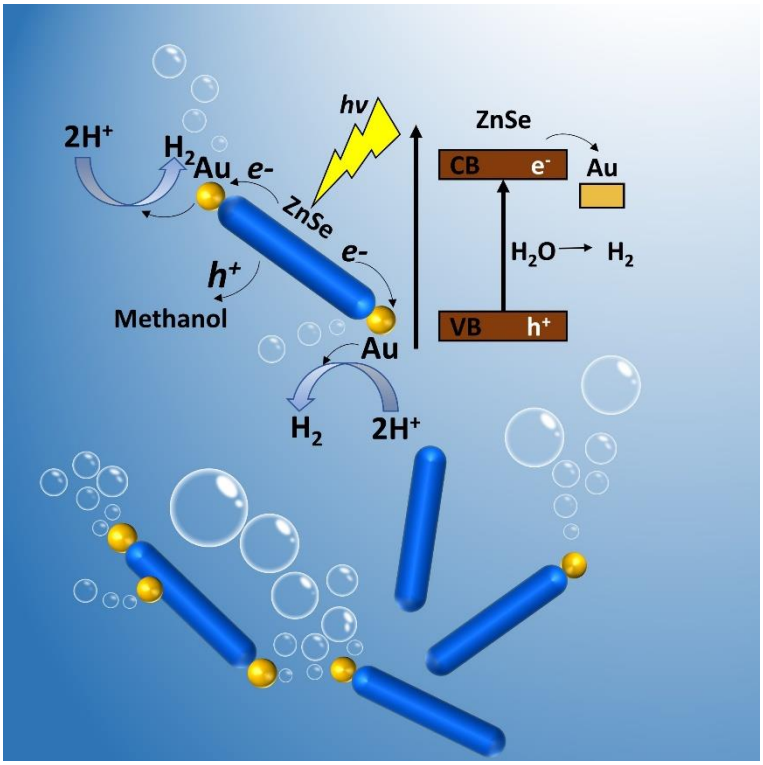

Figure 6.1 Table of content for this chapter Schematic showing the synthesized Au–ZnSe nanorods can be used for photocatalytic H_2 generation.

Abstract

For the first time, colloidal gold (Au)–ZnSe hybrid nanorods (NRs) with controlled size and location of Au domains are synthesized and used for hydrogen production by photocatalytic water splitting. Au tips were found to grow on the apices of ZnSe NRs non–epitaxially to form an interface with no preference of orientation between Au (111) and ZnSe (001). Density functional theory (DFT) calculations reveal that the Au tips on ZnSe hybrid NRs gain enhanced adsorption of H compared to pristine Au, which favors the hydrogen evolution reaction. Photocatalytic tests reveal that the Au tips on ZnSe NRs effectively enhance the photocatalytic performance in hydrogen generation, in which the single Au–tipped ZnSe hybrid NRs show the highest photocatalytic hydrogen production rate of 437.8 $\mu mol \cdot h^{-1} \cdot g^{-1}$ in comparison with a rate of 51.5 $\mu mol \cdot h^{-1} \cdot g^{-1}$ for pristine ZnSe NRs. An apparent quantum efficiency of 1.3% for hydrogen evolution reaction for single Au–tipped ZnSe hybrid NRs was obtained, showing the potential application of this type of cadmium (Cd)–free metal–semiconductor hybrid NPs in solar hydrogen production. This work opens an avenue towards Cd–free hybrid nanoparticle (NP)–based photocatalysis for clean fuel production.

6.1 Introduction

Metal–semiconductor hybrid NPs integrating multiple components into a single nano–object at the nanoscale have received tremendous attention in recent years because they not only possess the properties of individual components but also manifest a synergistic behaviour stemming from the materials interaction.[1–8] This makes the metal–semiconductor hybrid NPs promising in a wide scope of applications ranging from photo–catalysis for hydrogen generation or CO_2 reduction,[9–11] photodynamic therapy,[12,13] wound healing,[14,15] to photoinitiators for 3D printing.[16]

Among these materials, metal–semiconductor NRs, such as Au–CdSe,[17] Pt–CdSe,[18] Au–CdS,[19] Pt–CdS, and Pt–CdSe/CdS[20] are of particular interest. This is because that the hybrid NPs with one–dimensional shape enable more efficient charge separation ability in comparison with hybrid NPs of other morphologies.[20] The noble metal component within the hybrid NPs can work as a co–catalyst by providing the surface active sites for catalytic reaction with a lower activation energy barrier than semiconductors only.[21–23] The lifetime of charge carriers in these materials is also extended because of the enhanced rate of electron–hole separation.[24] Owing to the effective light–induced electron–hole separation, noble metal–semiconductor hybrid NRs such as Pt–CdS,[25] Pd–CdSe@CdS–Au,[26] CdSe/CdS–Pt[20,23] and CdSe/CdS–Pt–

Au[27] have been extensively studied in photo–catalytic water splitting for hydrogen production. Besides hydrogen evolution, CdS nanocrystals with a dinuclear cobalt catalyst[11] or CdS ((Mo–Bi)S_x/CdS)[28] can be used for the selective photocatalytic CO_2 reduction.

Up to now, the research into metal–semiconductor hybrid NRs is mainly focused on Cd–based systems due to the mature synthetic protocols on the precise control of size, shape, composition and metal location and their good performances in photocatalysis.[1,3,4,9,29] However, the high toxicity and the carcinogenicity of Cd–based materials is the main obstacle that restricts their widespread applications.[30,31] Compared with Cd–based materials, Zn–based semiconductor nanocrystals are less or non–toxic and environmental–friendly. Meanwhile, due to the wide band gap of Zn–based II–VI semiconductors (bulk ZnSe: 2.82 eV; bulk ZnS 3.7 eV), these NPs absorb near ultraviolet (UV) and blue light from solar spectrum, unlike the traditional Cd–based nanocrystals absorbing visible light. Given the main purpose for this project is to investigate the positional tipping effect from Au onto ZnSe nanorods on photocatalysis, the complementary absorption of longer wavelength photons to maximize solar harvesting for photocatalysis enhancement is expectable by heterojunction and doping strategies.[32,33] These merits make them potential supplements or alternatives to the Cd–based materials in photocatalytic hydrogen generation and biomedical applications[12]. Recent research on ZnSe and alloyed ZnSeS NRs indicated that these Cd–free NRs can be adopted as efficient photocatalysts for efficient hydrogen generation and oxygen evolution reactions.[34,35]

Metal–ZnSe hybrid NRs have been rarely reported due to the difficulties in the synthesis of ZnSe NRs.[36] To the best of our knowledge, the catalytic properties of these hybrid nanostructures have not been previously investigated. Pradhan *et al.* reported Au tipped wormlike ZnSe hybrid NPs through the growth of a heteroepitaxial junction between cubic Au and zinc blende ZnSe at elevated temperatures.[37] However, the Au–ZnSe hybrids obtained by a wet–chemical approach are not uniform after annealing at a high temperature of 250 ^{o}C, which deteriorates their optical and catalytic properties as these properties are closely relevant to the size, shape and spacial distribution of the metal–semiconductor hybrid NPs. Further studies into the precise control on the size, shape and phase of this new type of Au–ZnSe hybrid NPs, especially NRs, and their catalytic properties are highly demanded and important.

Herein, for the first time, we use a wet–chemical method to obtain Au–ZnSe hybrid NRs with controlled size and location of Au domains on ZnSe NRs. The precisely selective growth of Au tips on the apices of ZnSe NRs was achieved and this new Cd–free metal–semiconductor

hybrid NRs has been demonstrated as excellent photocatalyts for hydrogen generation through water splitting, which are comparable with Cd–based hybrid NPs.

6.2 Experimental section

6.2.1 Reagents.

Zinc acetate dihydrate ($Zn(Ac)_2 \cdot H_2O$, 98%), selenium powder (Se, 99%), gold (III) chloride ($AuCl_3$, 99.99%), dodecylamine (DDA, 99%) oleylamine (OLA, 70%), 1–dodecanethiol (DDT, 98%), polyethylenimine, branched (PEI, average Mw ~25,000 by LS, average Mn ~10,000 by GPC), trioctylphosphine (TOP, 97%), chloroform (99% anhydrous), toluene (99%) and ethanol (99.8% anhydrous) were purchased from Sigma–Aldrich. All the chemicals were used as received without further purification.

6.2.2 Synthesis of ZnSe Nanorods.

The ZnSe nanorods (NRs) were synthesized by using a heat–up method reported in a previous work with some modification.[1] In a typical synthesis, $Zn(Ac)_2 \cdot H_2O$ (2.9 mmol, 632 mg), and Se powder (2.4 mmol, 190 mg) were mixed together with 5 mL of DDT and 18 mL of OLA in a three–necked flask equipped with a thermometer, heating mantle and hot stir plate. This mixed solution was degassed and refilled with nitrogen gas at room temperature for three times. Then the solution was heated to 110 °C under vacuum and kept for 30 mins to remove air and moisture. Under N_2 flow, the reaction mixture was heated to 220 °C, kept at this temperature for 60 mins, and then the temperature of the reaction mixture was raised to 260 °C. After kept at 260 °C for 20 mins, the mixture was cooled down by removing the heating mantle. The products were cleaned with chloroform and ethanol three times before characterization and further used for Au growth.

6.2.3 Growth of Au tips on ZnSe NRs.

In a typical experiment, 10 mg clean ZnSe NRs were dispersed in 10 mL toluene by sonicating for 5 mins to make a 1 mg/mL ZnSe NRs solution. Then, 18 mg $AuCl_3$, 120 mg DDA and 9 mL toluene were mixed and sonicated for 10 mins to make a 2 mg/mL $AuCl_3$ solution. Later, 1 mL ZnSe NRs solution and 4 mL toluene were taken into a three–neck flask and kept under N_2 flowing, then the prepared $AuCl_3$ solution of varied volumes (0.05, 0.1, 0.3, 0.5 and 1 mL)

was injected into the ZnSe NRs solution at room temperature for growth of 1 hour. The final products were separated from toluene by centrifugation with help of acetone.

The size of ZnSe NRs is 24.8×2.1 nm, and the volume of one NR is 85 nm^3. Taking 5.27 g/cm^3 as the density of ZnSe NRs, one NR weight is 4.53×10^{-19} g. The organic ligand on the surface of ZnSe NRs takes up around 30% of mass. So the actual mass of ZnSe NRs at 1 mg ZnSe NRs with the ligand for Au growth is about 0.7 mg, which is equal to 2.60×10^{-3} mmol ZnSe NRs. So the molar ratios of Au: ZnSe NRs are 127:1, 254:1, 762:1, 1270:1 and 2540:1 when 0.05, 0.1, 0.3, 0.5 and 1 mL of 2 mg/L $AuCl_3$ solution were used as the gold precursor, respectively.

6.2.4 Synthesis of Au Nanoparticles.

Au nanoparticles (NPs) were synthesized using $AuCl_3$ as the precursor and oleylamine as the reducing agent according to a literature method.[2] In a typical synthesis, 50 mg $AuCl_3$ was firstly mixed with 5 mL oleylamine and 5ml toluene in a 50 mL flask. After degassing and refilling with N_2, the mixture was heated up to 120 °C under N_2 flow and then kept at this temperature for 45 mins under vigorous stirring. The reaction was quenched by removing the heating mantle. The Au nanoparticles were separated from solution by addition of 10 mL ethanol with the aid of centrifugation.

6.2.5 Ligand exchange with TOP for photoluminescence measurement.

In order to reduce the influence of surface defects of particles on the photoluminescence measurement, a stronger ligand of TOP was used to replace the weak bonding ligands of DDT and OLA passivated on the surfaces of ZnSe NRs and Au–ZnSe hybrid NRs. Typically, 1 mg clean ZnSe NRs and Au–ZnSe hybrid NRs were dispersed in a vial containing 2 mL toluene and 2 mL TOP and kept string for 12 h under N_2 to fulfil ligand exchange. The final NPs dispersed in toluene and TOP were used to measure photoluminescence.

6.2.6 Phase transfer of Au NPs, ZnSe NRs and Au–ZnSe hybrid NRs.

Au NPs, ZnSe NRs and Au–ZnSe hybrid NRs were transferred from toluene to water by coating of PEI. Typically, 5–10 mg clean Au–hybrid NRs were dispersed in toluene (5 mL) and mixed with $CHCl_3$ (5 mL) and PEI (0.25 g). Then the particles were precipitated and washed with hexane (10 mL) and redispersed in pure water (5 mL) for further used as a photocatalyst.[3] For the phase transfer of the mixture containing Au NPs and ZnSe NRs, 5 mg Au NPs and 5 mg ZnSe NRs were dispersed separately in toluene (2.5 mL) and mixed with

$CHCl_3$ (2.5 mL) and PEI (0.13 g) and then the obtained solutions were mixed for photocatalytic tests.

6.2.7 Photocatalytic hydrogen generation experiment.

In photocatalytic water–splitting experiments, methanol was employed as hole scavengers, and the catalyst in 5 mL water, 30 mL methanol were mixed to make a 120 mL suspension (V (methanol: H_2O) =1:4). Photocatalytic H_2 production experiments were carried out in a customized airtight stainless steel cell covered by a quartz window at ambient temperature. A 300W Xeon lamp (Newport) was used as a light source (200~2500 nm) with irradiation intensity centered at 120 mW/cm^2. Before irradiation, the suspensions were mixed under vigorous stirring for 30 min in the dark and the reaction vessel was degassed for anaerobic conditions by purging with N_2 for 30 mins. The produced H_2 was in situ analysed by a gas chromatography (Agilent 490 Micro GC) using a thermal conductivity detector.

6.2.8 Photoelectrochemical Measurements.

Photocurrent was obtained on a Zennium electrochemical workstation (Zahner, Germany) in a standard three–electrode framework with a 0.05 M Na_2SO_4 (pH = 6.8) electrolyte solution, employing a Pt plate as the counter electrode and an Ag/AgCl electrode as the reference electrode. As for the photoanode, the sample film was fabricated on a fluorine–doped tin oxide (FTO) glass, which was ultrasonicated in deionized water (DI) water, acetone and ethanol for 15 min in sequence and dried at 60 °C. Then 5 mg of the catalyst was mixed with 1 mL of absolute methylbenzene and 10 μL of Nafion solution homogeneously. The obtained slurry was dropped onto the pre–treated FTO glass via a spin–coating method, and the prepared electrode was dried at 100 °C for 24 h (catalyst loading ~0.60 mg/cm^2). Photocurrents were obtained using a 300W Xenon arc lamp with light passing through an AM 1.5 G filter into an optical fibre (output I_0 = 100 mW/cm^2).

6.2.9 Apparent Quantum efficiency measurement and calculation.

The apparent quantum efficiency (AQE) was measured under one 365 nm lamp (125 W, Shaoxing Deplux Lighting Co. Ltd. China). The focused intensity was *ca.* 0.31 W/cm^2. The AQE was calculated according to the following equation:

$$\mathrm{AQE}\% = \frac{\text{number of reacted electrons}}{\text{number of incident photons}} \times 100$$

$$= \frac{\text{number of evolved } H_2 \text{ molecules} \times 2}{\text{number of incident photons}} \times 100$$

6.3 Results and Discussions

6.3.1 Synthesis and Characterization of Au–ZnSe Hybrid NRs

Firstly, ZnSe NRs were synthesized by a heat–up method according to a previously reported method with some modifications [38]. In a typical synthesis, zinc acetate and selenium powder were employed as the precursors while oleylamine and 1–dodecanethiol (DDT) were used as the ligand and solvent, respectively, to synthesize ZnSe NRs at 260 °C using standard Schleck techniques.

Transmission electron microscope (TEM) image (Appendix E Figure E6–1) confirms the particles are elongated NRs. The histograms of size distribution show that the length and diameter of the synthesized ZnSe NRs are 24.8 ± 7.7 nm and 2.1 ± 0.3 nm, respectively (Appendix E Figure E6–2). As DDT may act as a S source in the synthesis, powder X–ray diffraction (XRD) (Appendix E Figure E6–3), high resolution TEM (HRTEM) (Appendix E Figure E6–4), UV–Vis absorption (Appendix E Figure E6–5), X–ray photoelectron spectroscopy (XPS) (Appendix E Figure E6–6) and scanning TEM (STEM)–energy–dispersive X–ray spectroscopy (EDS) (Appendix E Figure E6–7) were conducted to verify the composition and crystal phase of the obtained NRs in order to elucidate the sulfur incorporation in ZnSe NRs during their growth. The XRD pattern (Appendix E Figure E6–3) matches well with the standard wurtzite ZnSe and no shift of the diffraction peaks is observed with respect to those of the standard wurtzite ZnSe, confirming the pure phase of wurtzite ZnSe NRs. The sharp peak of the (002) plane corroborates the orientation of the long axis of wurtzite ZnSe NRs. The distance of lattice plane extracted by fast Fourier transform (FFT) analysis of HRTEM is shown in Appendix E Figure E6–4 and Table D6–1 to further identify the crystal structure and composition of synthesized NRs. As seen from Appendix E Figure E6–4 and Table D6–1**,** the lattice distance and angles between planes of synthesized NRs matches the (100), (002), (101) and $(10\bar{1})$ of wurtzite ZnSe structure well, which further proved the composition and structure of ZnSe NRs rather than alloyed ZnSeS. The absorption of synthesized NRs with a diameter of 2.1 ± 0.3 nm (Appendix E Figure E6–5) showed an absorption peak at 368 nm which is in accordance of the excitonic peak of ZnSe with this size. The XPS spectrum of ZnSe NRs synthesized in this work was shown in Appendix E Figure E6–6. As seen from Appendix E Figure E6–6, the Zn element presents solely as Zn(+2). As for

S 2p, it has closely spaced spin–orbit components (Δ=1.16 eV, intensity ratio=0.511) which overlap with those of Se 3p. The XPS spectrum of ZnSe NRs synthesized using dodecanethiol and oleylamine as the surfactant/solvents in this work was dominated by two peaks at 160.3 eV and 166.0 eV, which can be assigned to Se $3p_{3/2}$ and Se $3p_{5/2}$, respectively.[38] The other two weak peaks positioned at 162.4 eV and 163.5 eV correspond to the typical value of metal–thiol binding energy of S 2p.[38]

Element mapping of ZnSe NRs was also conducted to further verify their composition (Appendix E Figure E6–7)**.** EDS mapping of Zn and Se of the obtained ZnSe nanorods shows that Zn and Se elements are distributed evenly throughout the NPs. A weak signal corresponding to S element is also detected on the NPs and the surrounding background. The presence of the S signal can be attributed to the dodecanethiol ligands binding on the surface of the ZnSe NRs and amorphous carbon film, consistent with the results of XPS measurements. Based on the above characterization results, we confirmed that the synthesized nanorods are ZnSe rather than alloyed $ZnSe_xS_{1-x}$ structure, although there might be some thiol ligand binding on nanorods surface and etching could bring in a little bit of S to ZnSe NRs. Thus the main composition should be ZnSe. After the synthesis, the obtained ZnSe NRs were collected, purified and further used to grow Au tips toward Au–ZnSe hybrid NRs.

For Au tips growth on ZnSe NRs, we employed $AuCl_3$ as a gold precursor and dodecylamine as both surfactant and reductant in toluene solution for preparation at room temperature.[18] Typically $AuCl_3$ was firstly dissolved with dodecylamine in toluene by sonication and kept as Au stock solution, and then a predetermined volume of the Au stock solution was injected into ZnSe NRs dispersed in toluene under N_2 protection. The Au tips were allowed for growth for a certain time at room temperature before quenched by addition of acetone.

UV–Vis absorption spectroscopy was carried out to monitor the growth of Au on the ZnSe NRs and to investigate the optical properties (**Figure 6.2**). At a low molar ratio of Au precursor to ZnSe NRs (127:1) (Sample 1 in Figure 6.2), the final solution is colourless. The absorption spectrum of sample 1 also shows a distinct excitonic peak at 368 nm which is similar to that of the original ZnSe NRs (Appendix Figure E6–5). With an increased molar ratio of Au precursor to ZnSe NRs (254:1 to 1270:1, samples 2–4 in Figure 6.2), the absorption exciton peaks of ZnSe NRs become broader and a tail at the longer wavelength appears and gradually becomes prominent. Meanwhile, the color of the product solutions gradually change from light yellow to dark brown. These observations indicate the modified electronic structure of Au–ZnSe hybrid NRs rather than the simple mixture of ZnSe semiconductor and metal tips.[2]

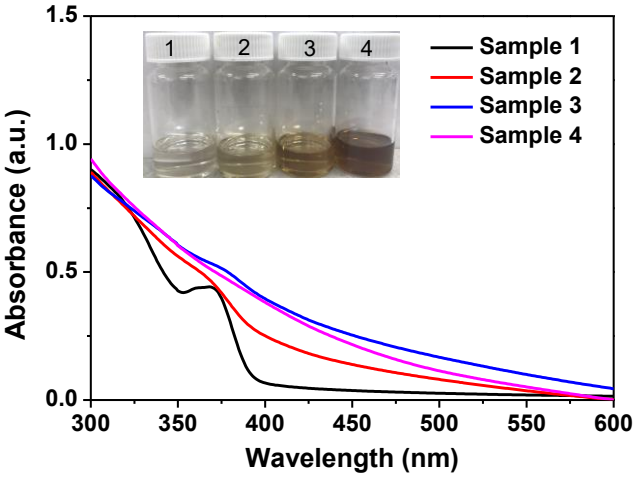

Figure 6.2 Comparison of UV–Vis absorption spectra of Au–ZnSe hybrid NRs obtained by using different molar ratios of Au precursor to ZnSe NRs. (1) n(Au: ZnSe NRs) =127:1; (2) n(Au:ZnSe NRs) =254:1; (3) n(Au:ZnSe NRs) =762:1; (4) n(Au:ZnSe NRs) =1270:1. Inset shows a photograph of Au–ZnSe hybrid NRs dispersed in toluene solution.

The absorption spectra of sample 2–4 present broad features with the tails extending to the low energy region of the spectra. The mixing of the electronic states of metal and semiconductors in hybrid NRs may result in the strong scattering in their absorption spectra, which is previously observed in metal–CdS (CdSe) hybrid NRs. The decreased solubility of Au–ZnSe hybrid NRs after the growth of the Au tips may also enhance the scattering of the absorption spectra.[39]

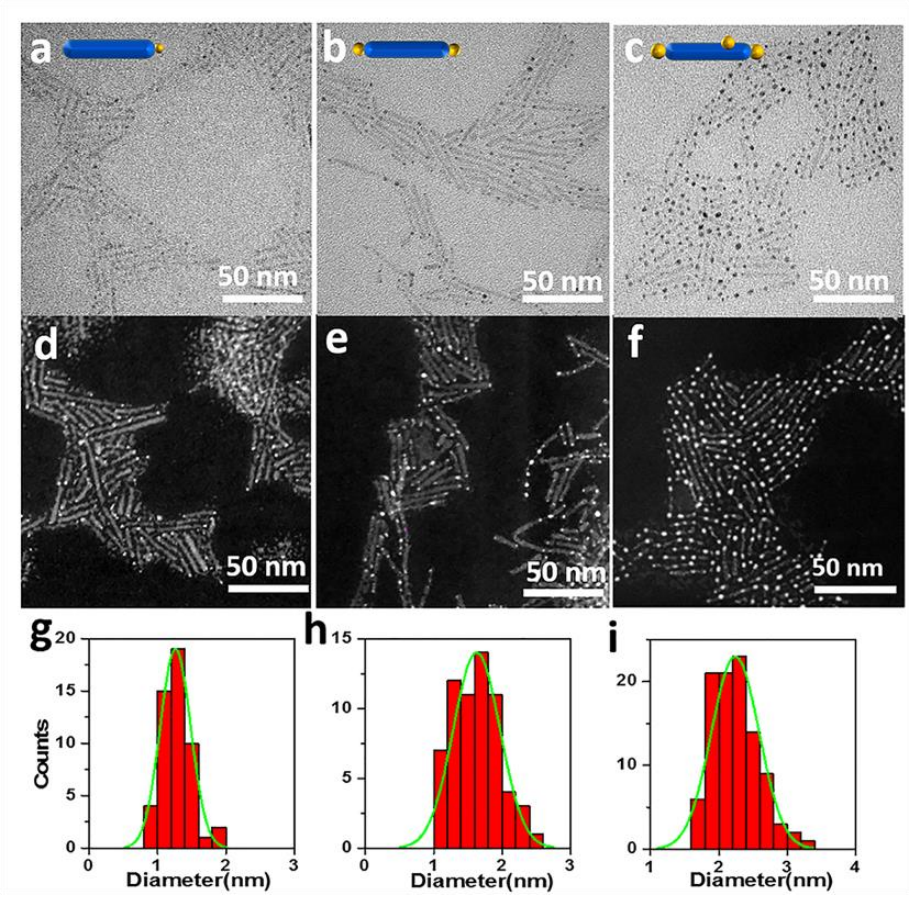

Figure 6.3 TEM images of Au–ZnSe hybrid NRs with Au tips of variable size. (a) 1.3 ± 0.2 nm (Sample 2 in Figure 6.2); (b) 1.6 ± 0.3 nm (Sample 3 in Figure 6.2); (c) 2.2 ± 0.3 nm (Sample 4 in Figure 6.2). (d–e) STEM images corresponding to (a–c). (g–i) Particle size histograms corresponding to (a–c).

TEM measurements were conducted to verify the growth of Au on ZnSe NRs. **Figure 6.3** shows TEM and high–angle annular dark–field–STEM (HAADF–STEM) images of Au–ZnSe hybrid NRs with Au tips at variable sizes. At a low molar ratio of Au precursor to ZnSe NRs (127:1) for the growth of 1 hour, almost no gold was grown on ZnSe NRs (Appendix E Figure E6–8a), which is consistent with the observation that the excitonic peak in UV–Vis absorption spectrum of this sample keeps almost the same as that of the original ZnSe NRs (Appendix E Figure E6–5). When more Au precursor was used for growth (n($AuCl_3$:ZnSe NRs)=254:1), very small gold tips (Dark spots in Figure 6.3a, bright spots in Figure 6.3d) with a diameter of 1.3 ± 0.2 nm (Figure 6.3g) grew onto one of the two apices of the ZnSe NRs. This observation is similar to the Au growth on CdSe NRs reported by Mokari and co–workers in which single Au tip growth is dominant at the low molar ratio of Au to NRs.[40] A further increase of the

molar ratio of $AuCl_3$ to ZnSe NRs to 762:1 (Figure 6.3b, 6.2e) leads to more growth of Au tips. The diameter of the Au tips increases to 1.6 ± 0.3 nm (Figure 6.3h) and apparently the Au tips grew on both apices of the majority of ZnSe NRs. When the molar ratio of $AuCl_3$ to ZnSe NRs was increased to 1270:1 (Figure 6.3c, 6.2f), larger gold tips with a diameter of 2.2 ± 0.3 nm (Figure 6.3i) grew on both apices of ZnSe NRs. In some cases, Au growth on the body of ZnSe NRs was also observed (Figure 6.3c, 6.2f), which can be attributed to the defect–induced growth of Au on the NRs.

The above observations suggested site–selective growth of Au on different facets of the one–dimensional anisotropic wurtzite ZnSe NRs, attributing to the higher reactivity of the end facets with increased surface energy and the imperfect ligand passivation, which is similar to other systems such as Au–CdSe[2] and Au–CdSe/CdS.[40] In other words, there are large differences in surface energy between the side facets of (100) and the end facets of (002) of wurtzite ZnSe NRs.[8] The (002) planes are alternately composed of either Zn or Se atoms, which makes Au growth at earlier stages more favourable on the Se rich facets in single Au tip ZnSe hybrid NRs.[3] Another important factor influencing Au growth is the sparse ligand coverage of the apex region of the NRs with respect to their body.[41] When more Au precursor was used for growth, the increased supersaturation of monomers may overcome the energy barrier that required for the gold growth on ZnSe NRs. Furthermore, when excessive amount of Au precursor was used (n($AuCl_3$:ZnSe NRs)=2540:1), agglomeration of Au tips can be found (Appendix E Figure E6–8b). The Au–ZnSe hybrid NRs with large Au tips may be attributed to the ripening process as the reaction was performed for a prolonged time with low monomer concentrations.[39]

STEM–EDS elemental mapping was used to analyze the composition and distribution of the hybrid NRs. Zn and Se elements are distributed evenly throughout the ZnSe NRs (Appendix E Figure E6–9). Although the location of Au cannot be easily recognized from EDS mapping data, the large contrast of Au with respect to ZnSe in STEM images confirms the Au (brighter spots in STEM images in Figure 6.3d–e) growth on the apices of ZnSe NRs.

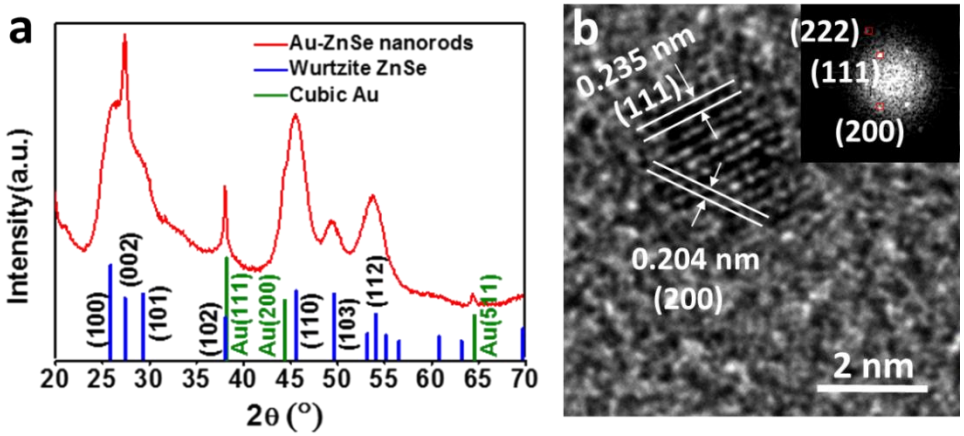

Figure 6.4 (a) XRD pattern, (b) HRTEM image of Au–ZnSe hybrid NRs (Inset shows the corresponding FFT image).

Figure 6.4a presents the XRD pattern of Au–ZnSe hybrid NRs. The main diffraction peaks can be indexed to the (100), (002) and (110) of the hexagonal wurtzite ZnSe (JCPDS card #80–0008), while the other diffraction peaks can be assigned to the (111), (200) and (511) of the face–centered cubic (FCC) Au tips (JCPDS card #99–0056). HRTEM and the associated FFT analysis were used to further reveal the crystal structure of Au tips (Figure 6.4b). The lattice plane spacings of 0.235 nm and 0.204 nm agree well with the (111) and (200) lattice planes of cubic Au, respectively (Figure 6.4b). It is noted that, due to the considerable mass difference among Au, Zn and Se atoms, ZnSe NRs are hard to be visualized at a high magnification while the lattice of Au nanocrystals can be clearly observed. The HRTEM images confirmed that Au tips on ZnSe hybrid NRs are face–centered cubic structure (inset in Figure 6.4b), which is consistent with the XRD results.

TEM, HRTEM, STEM–EDS and XRD characterizations have confirmed the successful growth of cubic phase Au tips on wurtzite ZnSe NRs. We further employed high–resolution XPS to examine the binding environments in the Au–ZnSe hybrid NRs. The survey spectrum of the sample reveals the binding energies for Zn 2p, Se 3d, and Au 3d (**Figure 6.5**a). The main binding energy peaks at ~84 eV and ~87.7 eV of the high resolution XPS spectrum of Au are attributed to Au(0) $4f_{7/2}$ and $4f_{5/2}$ (Figure 6.5b), respectively.[42]

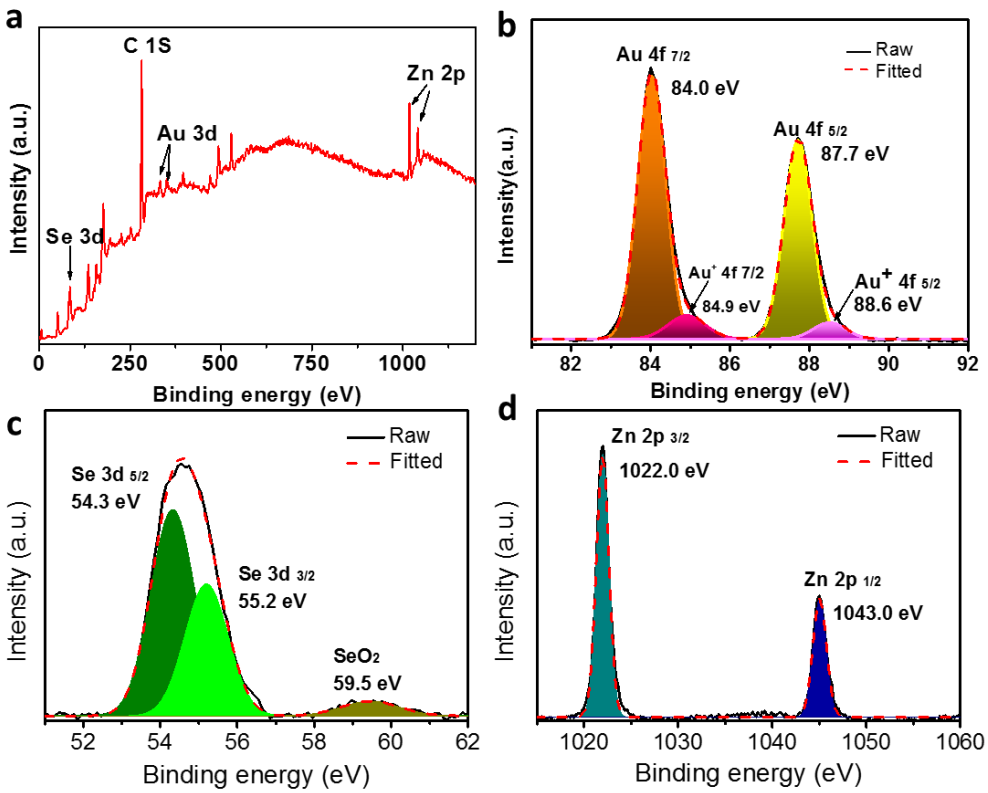

Figure 6.5 XPS spectra of the Au–ZnSe hybrid NRs. (a) Survey spectrum, (b–d) Binding energy peaks of (b) Au 4f, (c) Se 3d and (d) Zn 2p.

The distinct peaks observed at higher energy such as ~84.9 eV and ~88.6 eV can be assigned to $4f_{7/2}$ and $4f_{5/2}$ binding energy peaks of Au(+1).[43] Although the majority of the $AuCl_3$ precursor has been reduced to Au(0), there may be still a small portion of Au^+ not completely reduced to Au (0) under a mild reducing condition. Figure 4c shows two XPS peaks at around 54.3 eV and 55.2 eV, corresponding to the binding energies of Se 3d.[44] A small broaden peak at 59.5 eV indicated a small proportion of SeO_2 impurity formed due to partial oxidation of Se at the surface of the NRs.[8, 45] The two Zn 2p peaks at 1045 eV and 1022 eV in Figure 4d correspond to Zn $2p_{1/2}$ and $2p_{3/2}$, respectively, which confirm the presence of Zn(+2).[46]

6.3.2 Au growth orientation on ZnSe NRs

Based on the above results, we found that Au tips preferentially grow on the Se–rich apex of ZnSe NRs, and then on both apices. To further reveal the growth mechanism of Au–tipped ZnSe hybrid NRs, we analyzed their HRTEM images to determine if the Au tips grow epitaxially onto the apices of the ZnSe NRs. As the predominant lattice planes for Au tips and ZnSe NRs within the Au–ZnSe hybrid NRs are the (111) and (002), respectively, we specifically measured the angles between these two planes to see if there is a fixed angle

between them. As confirmed by the XRD pattern and HRTEM image, the (002) plane is perpendicular to the *c*–axis of the wurtzite ZnSe NRs. As for the Au tips with the cubic structure, the (111) plane can easily be identified in the HRTEM images. So we measured the angle between the (111) plane of Au tips and the length direction of ZnSe NRs, which corresponds to the angle between the (111) plane of Au tips and the (100) plane of ZnSe NRs. Because of the small size of Au tips and the large contrast between ZnSe rods and Au tips, it is difficult to clearly resolve both the lattice planes simultaneously. However, we could verify the length direction of the ZnSe NRs and the (111) plane of Au tips at different magnifications.

The schematic of the angle measurement is shown in Appendix E Figure E6–10. Statistics on the angles between the length direction of the ZnSe NRs and the (111) planes of Au tips of 28 Au–ZnSe hybrid NRs is shown in Figure S10c. If epitaxial growth does occur for this system, we would expect to see a set of discrete, well–defined angles between these sets of lattice planes. For example, from geometrical considerations, if Au (111) aligned with ZnSe (002), the angle between the Au (111) and ZnSe (100) will be 90°. However, statistics show that the angle between Au (111) facet and ZnSe (100) facet of NRs varied between 0° to 90° (Figure S10c), indicating that gold was randomly growth on ZnSe NRs without preferable orientation. Thus, we conclude that the growth of Au tips on wurtzite ZnSe NRs is nonepitaxial.

This finding is different from the reports of Pradhan *et al.* that the formation of the heteroepitaxial junction of the (111) facet of cubic Au on the (111) facet of wormlike zinc blend ZnSe nanocrystals, as well as the epitaxial growth of the (111) facet of gold along the 002 direction of the CdSe NRs.[37,47] In both cases, Au precursor was injected into the pre–synthesized zinc blende ZnSe or wurtzite CdSe nanocrystals at a high temperature of ~190 °C and grew at 250 °C. Another work by Manna and co–workers[17, 19] reveals that annealing of non–epitaxial Au–CdS nanocrystals prepared by wet–chemical synthetic approaches results in the formation of epitaxial Au–CdS hybrid nanocrystals. It is evident that a high temperature is essential for the formation of epitexial Au–semiconductor hybrid nanocrystals while the kinetically controlled wet–chemical synthetic routes at room temperature will generate non–epitaxial Au–ZnSe hybrid NRs.

6.3.3 Density functional theory (DFT) simulations of Au growth

To further establish the proposed non–epitaxial growth mechanism and in particular to elucidate no preferential epitaxial relationship between gold metal and ZnSe domain, we employed the first–principles methods based on DFT to investigate the potential energy surface of ZnSe(001)/Au(111) interface (see details in Appendix E). Although the HRTEM

measurements suggest no preference of a specific orientation relationship between Au and ZnSe, we think the interface between the Au (111) and ZnSe (001) is a typical and representative structure of the hybrid system, as it is composed of the most closely packed planes and resembles the Au–CdSe hybrid system. We calculated the potential energy surface (PES) of interfacing ZnSe (001) and Au (111) (see Appendix E). The initial input structure and calculated PES are displayed in **Figure 6.6**a and 6.5b, respectively. The highest barrier between energy minima is 0.1 eV per Au atom at the interface layer. It can be inferred that the barrier can work at low temperatures like room temperature to induce non–epitaxial growth of Au on the ZnSe (001) surface. At elevated temperatures the small barrier may be overcome and the growth of epitaxial Au or transition into epitaxial Au can be seen.

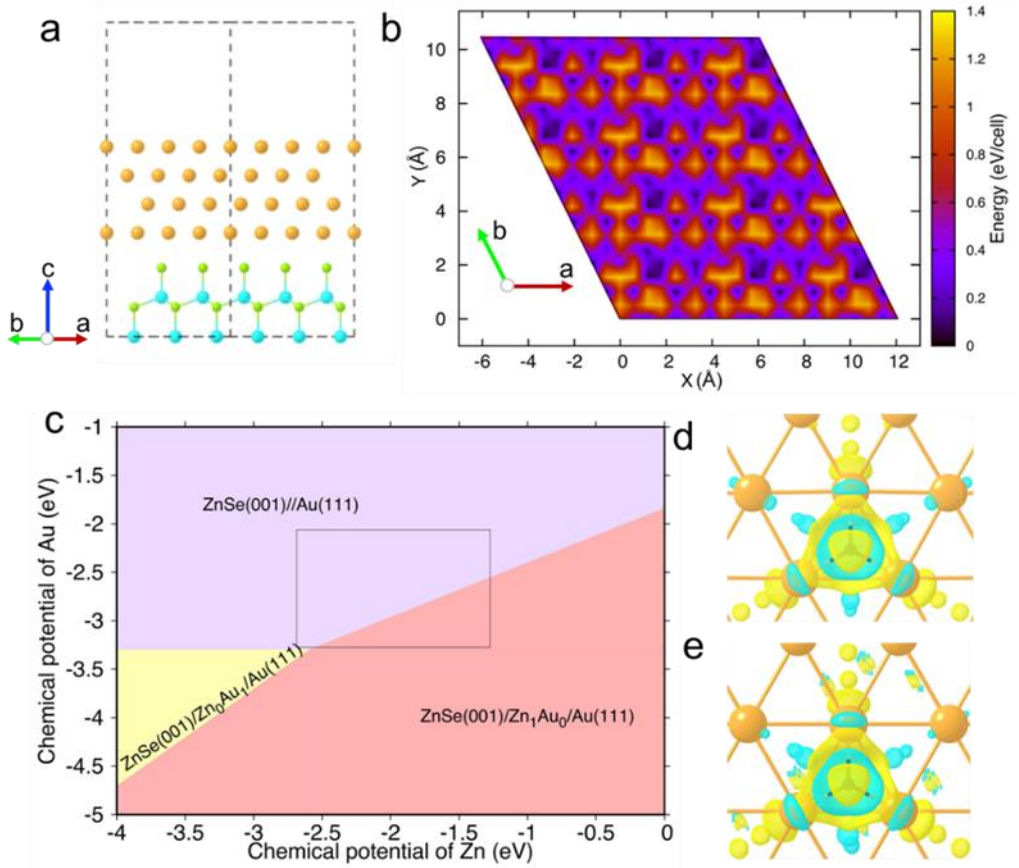

Figure 6.6 (a) Initial input interface structure for potential energy surface calculations of ZnSe(001)/Au(111) interface, which contains 64 Au atoms, 18 Zn atoms and 18 Se atoms; (b) Calculated potential energy surface of ZnSe(001)/Au(111) interface. (c) Phase diagram of ZnSe (001)/Au (111) interface. Five structures were explored, namely, the ZnSe(001)/Au(111), ZnSe (001)/Zn_0Au_1 /Au(111), ZnSe (001)/$Zn_{1/3}Au_{2/3}$ /Au (111), ZnSe(001)/$Zn_{2/3}Au_{1/3}$/Au(111), and ZnSe(001)/Zn_1Au_0/Au(111). The ZnSe(001)/$Zn_{1/3}Au_{2/3}$/Au(111) and ZnSe(001)/$Zn_{2/3}Au_{1/3}$/Au(111) interfaces are not thermodynamically stable. The inset rectangular represents the allowed chemical potentials of Zn and Au. The chemical potential of Zn is bounded by $\mu_{ZnSe} - \mu_{Se} < \mu_{Zn} < \mu_{hcp-Zn}$,

and the chemical potential of Au is bounded by $\mu_{fcc-Au} < \mu_{Au} < \mu_{AuSe} + \mu_{Zn} - \mu_{ZnSe}$. Differential charge density diagrams for hydrogen adsorption onto a fcc site of pristine Au (111) (d) and top Au (111) of ZnSe(001)//Au(111) interface (e). Golden and black balls indicate the Au and H atoms, respectively. Yellow and cyan indicate the charge loss and gain, respectively. Isosurface value is 0.001 e/Å^3.

We then further explored the detailed atomic interface structure. The ZnSe(001)/Au(111) interface structure with the minimum energy was chosen for further studies and relaxed with a Monkhorst–Pack **k**–point set of 2×2×1. Seven Au atoms at the interface layer that are most distant from ZnSe lattice sites were removed to create a ZnSe(001)/Zn_0Au_1/Au(111) interface, namely, an interface with the top layer Zn atoms completely substituted by the interfacing Au layer atoms and no more Au left in the interfacing Au single layer. From the ZnSe(001)/Zn_0Au_1/Au(111) interface, we varied the ratio of Zn to Au at the interfacing single layer to obtain the ZnSe(001)/$Zn_{1/3}Au_{2/3}$/Au(111), ZnSe(001)/$Zn_{2/3}Au_{1/3}$/Au(111), and ZnSe(001)/Zn_1Au_0/Au(111) structures. The phase diagram of the interface can be obtained and is plotted in Figure 5c. Only the ZnSe(001)//Au(111) and ZnSe(001)/Zn_1Au_0/Au(111) interfaces are thermodynamically stable within the allowed chemical potentials of Zn and Au. The other three structures (ZnSe(001)/$Zn_{1/3}Au_{2/3}$/Au(111), ZnSe(001)/$Zn_{2/3}Au_{1/3}$/Au(111), and ZnSe(001)/Zn_0Au_1/Au(111)) are not stable at all. Actuallly, the stable ZnSe(001)/Au(111) and ZnSe(001)/Zn_1Au_0/Au(111) interfaces representing the two hybrids: The interfacing of the Se–terminated ZnSe NR end and the Zn–terminated ZnSe NR end with Au (111), respectively. Therefore, at the low chemical potential of Au (low ratio of $AuCl_3$ to ZnSe), it could only allow the Se–terminated ZnSe NR end to grow Au tips, forming the ZnSe(001)/Au(111) interface. At the increased chemical potential of Au with more added $AuCl_3$, the ZnSe(001)/Zn_1Au_0/Au(111) interface is also allowed. This agrees with experiment results that Au tips first grow on Se–terminated ZnSe(001) NRs.

6.3.4 Au–ZnSe hybrid NRs for photocatalytic hydrogen generation

We investigated the hydrogen evolution reaction (HER) on Au–ZnSe hybrid NRs by using the free energy of hydrogen adsorption (ΔG_{H*}, * denotes the electrode) as a single catalytic descriptor.[48] This descriptor can describe the hydrogen evolution exchange–current density.

$$i_0 = -ek_0 \frac{1}{1 + \exp\left(-\Delta G_{H*}/kT\right)}$$

Where i_0 is the hydrogen evolution exchange–current density, e is the electron charge, and k_0 is a factor that needs to be fitted to experimental data. The best electrode material should have ($\Delta G_{H*} = 0$) for hydrogen evolution reaction

$$H^+ + e^- + * \rightarrow \frac{1}{2} H_2(g)$$

ΔG_{H*}, therefore, can be expressed by

$$\Delta G_{H*} = \Delta E_H + \Delta E_{ZPE} - T\Delta S_H$$

where ΔE_H, ΔE_{ZPE}, and ΔS_H are the potential energy difference, zero–point energy difference and change of entropy, respectively. At 27 °C, it can be simplified as $\Delta G_{H*} = \Delta E_H + 0.24\ eV$.[48]

The calculated HER free energies are summarized in **Table 6.1**. All the stable interfaces show much smaller $|\Delta G_{H*}|$ compared to the pristine Au (111) surface. This is due to the enhanced adsorption of H* by the Au atoms of interface structures. At a close look, the interface structures show an increased charge redistribution upon hydrogen adsorption as can be seen from the differential charge density plot in Figure 6.6c. Hydrogen adsorbed on the hybrid Au–ZnSe (Figure 6.6e) gains more charge than the hydrogen on pristine Au (Figure 6.6d). Besides the enhanced hydrogen adsorption, the unique Au–tipped NR architecture should also allow more efficient charge separation.[37] To this end, we used Au–ZnSe hybrid NRs as photocatalysts for hydrogen production through water splitting.

Table 6.4 Calculated free energy change for hydrogen evolution on different electrodes.

Electrode	$\|\Delta G_{H*}\|$ **(eV)**	
	fcc site	*hcp* site
Au (111)	0.38	0.43
ZnSe(001)//Au(111)	0.28	0.27
ZnSe(001)/Zn_1Au_0/Au(111)	0.15	0.24
ZnSe(001)/Zn_0Au_1/Au(111)	0.10	0.26

To reveal how the selective deposition of Au NPs on the ZnSe NRs affects their photocatalytic activities in hydrogen production, in particular to elucidate the synergistic effect of Au–ZnSe hybrid NRs, we compared photocatalytic performances of single and double Au–tipped ZnSe hybrid NRs with those of pure ZnSe NRs, Au NPs and the mixture containing both the ZnSe NRs and Au NPs (**Figure 6.7**a). Prior to the photocatalytic tests, phase transfer for the NPs was conducted to make them water soluble. The nanoparticles transfer efficiency was calculated by the element concentration tested by ICP–OES. (Appendix E Table D6–2) According to the results, over 90% of samples were successfully transferred to water–soluble

phase and the mass loss percentage of each sample is close to each other. The stability of Au–ZnSe hybrid NRs after phase transfer was characterized by absorption spectroscopy and TEM (Appendix E Figures D6–11 and D6–12). Compared with Au–ZnSe hybrid NRs before the phase transfer, the absorption peak at 368 nm of the Au–ZnSe hybrid NRs in water became slightly broader as the surface of hybrid NRs are coated with bulky PEI ligands (Appendix E Figures D6–11). Au–tipped ZnSe hybrid NRs were observed in the TEM image (Appendix E Figures D6–12a) while the elongated ZnSe NRs with two tips being decorated by Au NPs were clearly seen in the corresponding STEM image (Appendix E Figures D6–12b).

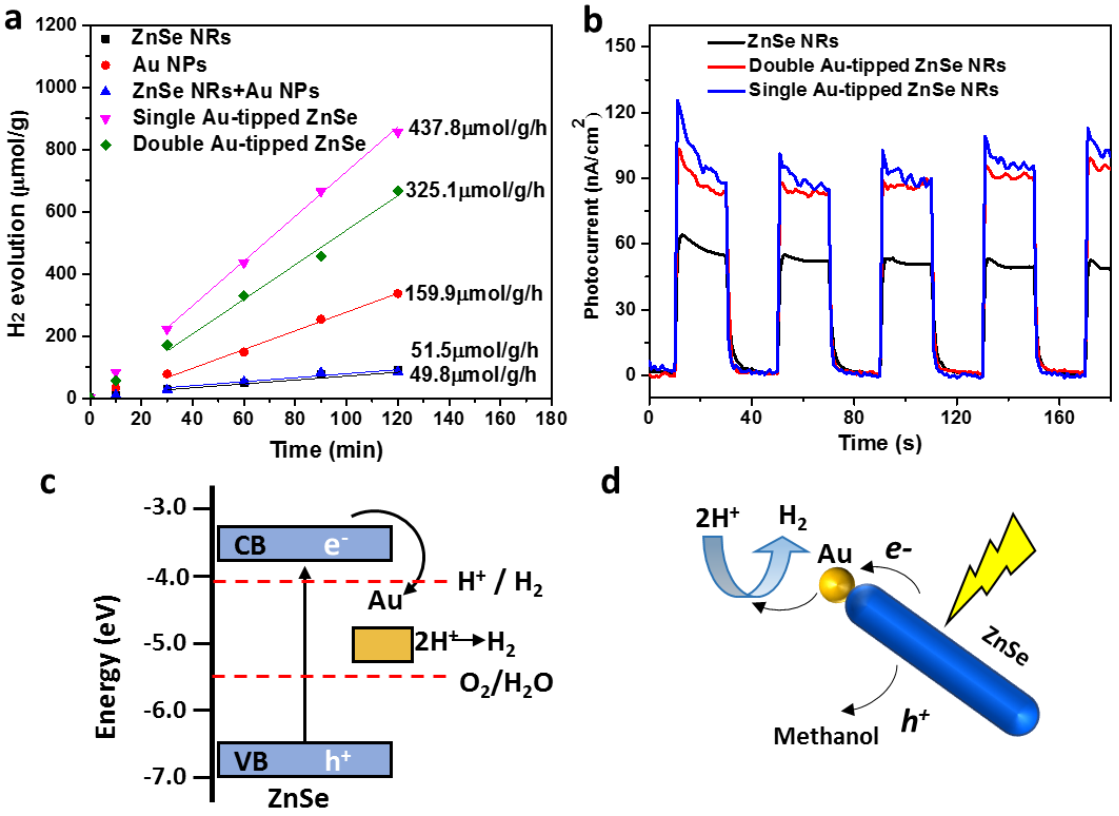

Figure 6.7 (a) Comparison of hydrogen generation rates of pure ZnSe NRs, Au NPs, single Au–tipped Au–ZnSe hybrid NRs and double Au–tipped ZnSe hybrid NRs using methanol as the sacrificial hole scavenger. (b) Transient photocurrent with different working electrodes, i.e. bare ZnSe NRs, single Au–tipped ZnSe and double Au–tipped ZnSe hybrid NRs. (c) Energy band alignment diagram of Au–ZnSe hybrid NRs; (d) Proposed photocatalytic mechanism of Au–ZnSe hybrid NRs for hydrogen production in water splitting.

As hydrogen gas generated from the photocatalytic reaction may dissolve in the water solution, no hydrogen gas will be released to the head space of the reaction vessel until the water solution is saturated, leading to an induction time in such measurements.[10] Therefore, the

hydrogen evolution rates were obtained by a linear fitting after 30 min of induction time during the 2 h illumination (Figure 6.7a). The photocatalytic H_2 evolution experiment was conducted for two hours to measure the stability of the synthesized hybrid Au-ZnSe nanoparticles. The linear fitting of the hydrogen generation rate indicated a stable and good reactivity of the catalyst during the testing period.

As seen from Figure 6.7a, the hydrogen generation rate (49.8 μmol/h/g) of pure ZnSe NRs is the lowest among all NPs. This is reasonable because the recombination rate of light–induced electrons and holes in pure ZnSe NRs is relatively high.[49] In contrast, pure Au NPs with a diameter of 5.56 nm present a higher hydrogen generation rate of 149.9 μmol/h/g. Extinction spectrum of the Au NPs shows a broad plasmon resonance peak at 520 nm (Appendix E Figures D6–13). It is expected that the plasmon resonance induced hot electrons in Au NPs may lead to water reduction for hydrogen production.[50–52] The mixture of Au NPs and ZnSe NRs show a lower hydrogen generation rate of 51.5 μmol/h/g compared with that of pure Au NPs (Figure 6.7a). In the physically mixed sample, the concentration of Au NPs, and hence the plasmon resonance centres, in the water solution is reduced, this decreases the generation of hot reductive electrons, leading to a lower hydrogen generation rate, as compared with pure Au NP sample. Furthermore, because ZnSe NRs have a large absorption cross–section, [36] the incorporation of ZnSe NRs with Au NPs in the water solution can intervene the light absorption of Au NPs and then dampen their plasmon resonance, affecting the generation of hot electrons.

Rather than physically mixing the Au NPs and ZnSe NRs, we have selectively deposited Au NPs on ZnSe NRs, constituting single and double Au–tipped ZnSe hybrid NRs (Figure 6.4). In such a hybrid structure, electron–hole pairs are generated by the light absorption of ZnSe NRs, and are further effectively separated on the metal–semiconductor heterojuncitons, which allows it to act as a photocatalyst to catalyze the redox reaction for hydrogen production via water splitting. As depicted in **Figure 6.7a**, single Au–tipped ZnSe hybrid NRs are more efficient (~437.8 μmol/h/g) in hydrogen generation than double Au–tipped ZnSe hybrid NRs (~325.1 μmol/h/g). In the single Au–tipped ZnSe hybrid NRs, the direct contact of other end of the ZnSe NRs with the solution make it conducive to the hole transfer and consumption by a scavenger after the electron transfer to the Au tip. In the double Au–tipped ZnSe hybrid NRs, the light–induced holes can only be transferred to the scavenger through the less active, defect–free and surfactant passivated side facets, which reduces the efficiency of hole clearance and therefore consequently reduced the hydrogen generation rate.[39,53–54] The apparent quantum

efficiency (AQE) under irradiation for single Au–tipped ZnSe hybrid NRs was measured to be approximately 1.3% (λ=365 nm) (See Supporting Information for details).

It is noteworthy that Au–tipped ZnSe hybrid NRs only show weak plasmon resonance due to the tiny size of the Au domain. Furthermore, as demonstrated in the control experiment, ZnSe NRs can intervene the light absorption of Au NPs which reduces the photocatalytic performance of Au NPs in hydrogen generation. Therefore, the good photocatalytic properties of Au–tipped ZnSe hybrid NRs are mainly attributed to the efficient charge separation enabled by the metal–semiconductor heterojunctions, where Au NPs work as the electron sink to efficiently accept/trap electrons.[55] The plasmon resonance induced hot electron transfer in Au–tipped ZnSe hybrid NRs contributes to the photocatalytic activities only to a small extent due to its tiny size.[56–57]

In order to further verify the photocatalytic mechanism, we compared the photoluminescence spectrum (Appendix E Figures D6–14) and photocurrent (Figure 6.7b) of Au–ZnSe hybrid NRs with that of pure ZnSe NRs. To test photoluminescence spectrum, we have performed surface ligand exchange by using trioctylphosphine (TOP) to ensure Au–ZnSe hybrid NRs and pure ZnSe NRs have same surface conditions. As depicted in Figure S14, the Au–ZnSe coated with either DDT + OLA or TOP shows significantly reduced photoluminescence intensities compared with ZnSe NRs with similar surface conditions. The quenching effect of the photoluminescence can be attributed to the reduced radiative recombination rates induced by the charge separation by the heterojunction between Au tips and ZnSe NRs in the hybrid NRs.[39]

The photocurrent testing was also performed to study the photocatalytic mechanism (Figure 6.7b). As shown in Figure 6b, single Au–tipped ZnSe hybrid NRs show the highest photocurrent of 87.9 nA/cm^2. Even the photocurrent of double Au–tipped–ZnSe hybrid NRs (83.3 nA/cm^2) is slightly lower than that of single Au–tipped ZnSe hybrid NRs, it is ~1.4 times higher than that of pure ZnSe NRs (60.1 nA/cm^2). These results are consistent with the hydrogen generation rate results shown in Figure 6.7a, which confirmed the effective electron transfer after photoexcitation in Au–tipped ZnSe hybrid NRs.

Based on above results, we depict the photocatalytic mechanism of Au–ZnSe hybrid NRs in Figure 6.7c and 6.6d. Upon illumination, excited electrons at the bottom of the conduction band of ZnSe will transfer to Au domain because the Fermi level of Au is lower than the bottom of the conduction band of ZnSe[26,58–60]. The induced holes will stay in the valence band, and thus the electrons and holes are effectively and spatially separated and the probability for

recombination is greatly reduced. Rich in electrons, the Au tips with enhanced capture ability of H can efficiently catalyze proton reduction and hydrogen production while the holes (h^+) in ZnSe NRs are removed by introduction of hole scavengers i.e. methanol (**Figure 6.7d**).

6.4 Conclusions

Novel Au–ZnSe hybrid NRs with controlled size and site selectivity of Au tips have been synthesized using wet–chemical approaches. Au atoms grew non–epitaxially on ZnSe NRs. Au tips growth on ZnSe hybrid NRs show enhanced hydrogen adsorption that improves the HER catalytic properties, and photocatalytic hydrogen production rate of 437.8 $\mu mol \cdot h^{-1} \cdot g^{-1}$ and a APE of 1.3% was obtained by using methanol as sacrificial hole scavenger. Due to the tiny size of Au tips, plasmon resonance induced hot electron transfer in Au–tipped ZnSe hybrid NRs contributes to the photocatalytic activities only to a small extent as most of electron–holes pairs are generated from ZnSe semiconductor NRs. It is worth noting that Au tipped ZnSe hybrid NRs can only absorb UV and blue ranges of the solar spectrum. Further expanding their absorption from blue to visible spectral range through hetero–semiconductors and/or doping aforementioned to realize the full potential of metal–semiconductor hybrid NPs for solar energy application is of significant importance. Furthermore, we anticipate the photocatalytic performances of Au–ZnSe hybrid NRs can be further improved by optimizing the size and type of noble metal species (e.g. Pt or alloyed Au–Pt) as well as number of noble metal domains on the NRs. This work opens an avenue for new Cd–free metal–semiconductor hybrid NP–based photocatalysis for hydrogen generation by water splitting, with relevance to redox reactions in biochemistry.

6.5 Reference

1. Mokari T, Rothenberg E, Popov I, Costi R, Banin U. Selective growth of metal tips onto semiconductor quantum rods and tetrapods. Science. 2004;304(5678):1787–1790.

2. Schlicke, H., Ghosh, D., Fong, L.-K., Xin, H.L., Zheng, H. and Alivisatos, A.P. , Selective Placement of Faceted Metal Tips on Semiconductor Nanorods. Angew. Chem. Int. Ed., 2013,52: 980–982.

3. Habas SE, Yang P, Mokari T. Selective Growth of Metal and Binary Metal Tips on CdS Nanorods. J. Am. Chem. Soc. 2008;130(11):3294–3295.

4. Han Z, Qiu F, Eisenberg R, Holland PL, Krauss TD. Robust Photogeneration of H2 in Water Using Semiconductor Nanocrystals and a Nickel Catalyst. Science. 2012;338(6112): 1321–1324.

5. Zhang J, Tang Y, Lee K, Ouyang M. Tailoring light–matter–spin interactions in colloidal hetero–nanostructures. Nature. 2010;466(7302):91–95.

6. Zhang J, Tang Y, Lee K, Ouyang M. Nonepitaxial growth of hybrid core–shell nanostructures with large lattice mismatches. Science. 2010;327(5973):1634–1638.

7. Cozzoli PD, Pellegrino T, Manna L. Synthesis, properties and perspectives of hybrid nanocrystal structures. Chem. Soc. Rev. 2006;35(11):1195–1208.

8. a) Chen, D, Zhang, H, Li, Y, Pang, Y, Yin, Z, Sun, H, Zhang, LC, Wang, S, Saunders, M, Barker, E, Jia, G., Spontaneous Formation of Noble–and Heavy–Metal–Free Alloyed Semiconductor Quantum Rods for Efficient Photocatalysis. Adv. Mater. 2018, 30, 1803351; b) Javaid S, Li Y, Chen D, Xu X, Pang Y, Chen W, et al. Spontaneous Formation of Heterodimer Au–Fe7S8 Nanoplatelets by a Seeded Growth Approach. J. Phys. Chem. C. 2019;123(16):10604–10613.

9. Ben–Shahar Y, Scotognella F, Kriegel I, Moretti L, Cerullo G, Rabani E, et al. Optimal metal domain size for photocatalysis with hybrid semiconductor–metal nanorods. Nat. Commun. 2016;7:10413.

10. Ben–Shahar Y, Scotognella F, Waiskopf N, Kriegel I, Dal Conte S, Cerullo G, et al. Effect of surface coating on the photocatalytic function of hybrid CdS–Au nanorods. Small. 2015;11(4):462–471.

11. Bi QQ, Wang JW, Lv JX, Wang J, Zhang W, Lu TB. Selective Photocatalytic CO_2 Reduction in Water by Electrostatic Assembly of CdS Nanocrystals with a Dinuclear Cobalt Catalyst. ACS Catal. 2018;8(12):11815–11821.

12. Waiskopf N, Ben–Shahar Y, Galchenko M, Carmel I, Moshitzky G, Soreq H, et al. Photocatalytic Reactive Oxygen Species Formation by Semiconductor–Metal Hybrid Nanoparticles. Toward Light–Induced Modulation of Biological Processes. Nano Lett. 2016;16(7):4266–4273.
13. Fan JX, Liu MD, Li CX, Hong S, Zheng DW, Liu XH, et al. A metal–semiconductor nanocomposite as an efficient oxygen–independent photosensitizer for photodynamic tumor therapy. Nanoscale Horiz. 2017;2(6):349–355.
14. Mao C, Xiang Y, Liu X, Cui Z, Yang X, Yeung KWK, et al. Photo–Inspired Antibacterial Activity and Wound Healing Acceleration by Hydrogel Embedded with Ag/Ag@AgCl/ZnO Nanostructures. ACS Nano. 2017;11(9):9010–9021.
15. Zhang Y, Liu X, Li Z, Zhu S, Yuan X, Cui Z, et al. Nano Ag/ZnO–Incorporated Hydroxyapatite Composite Coatings: Highly Effective Infection Prevention and Excellent Osteointegration. ACS Appl. Mater. Interfaces. 2018;10(1):1266–1277.
16. Pawar AA, Halivni S, Waiskopf N, Ben–Shahar Y, Soreni–Harari M, Bergbreiter S, et al. Rapid Three–Dimensional Printing in Water Using Semiconductor–Metal Hybrid Nanoparticles as Photoinitiators. Nano Lett. 2017;17(7):4497–4501.
17. Figuerola A, van Huis M, Zanella M, Genovese A, Marras S, Falqui A, et al. Epitaxial CdSe–Au nanocrystal heterostructures by thermal annealing. Nano Lett. 2010;10(8):3028–3036.
18. Naskar S, Schlosser A, Miethe JF, Steinbach F, Feldhoff A, Bigall NC. Site–Selective Noble Metal Growth on CdSe Nanoplatelets. Chem Mater. 2015;27(8):3159–3166.
19. Van Huis MA, Figuerola A, Fang C, Beche A, Zandbergen HW, Manna L. Chemical transformation of Au–tipped CdS nanorods into AuS/Cd core/shell particles by electron beam irradiation. Nano Lett. 2011;11(11):4555–4561.
20. Wu K, Chen Z, Lv H, Zhu H, Hill CL, Lian T. Hole removal rate limits photodriven H2 generation efficiency in CdS–Pt and CdSe/CdS–Pt semiconductor nanorod–metal tip heterostructures. J. Am. Chem. Soc. 2014;136(21):7708–7716.
21. Simon T, Bouchonville N, Berr MJ, Vaneski A, Adrovic A, Volbers D, et al. Redox shuttle mechanism enhances photocatalytic H2 generation on Ni–decorated CdS nanorods. Nat. Mater. 2014;13(11):1013–1018.
22. Ma L, Chen K, Nan F, Wang JH, Yang DJ, Zhou L, et al. Improved Hydrogen Production of Au–Pt–CdS Hetero–Nanostructures by Efficient Plasmon–Induced Multipathway Electron Transfer. Adv. Funct. Mater. 2016;26(33):6076–6083.

23. Amirav L, Alivisatos AP. Photocatalytic Hydrogen Production with Tunable Nanorod Heterostructures. J. Phys. Chem. Lett. 2010;1(7):1051–1054.
24. Linic S, Christopher P, Ingram DB. Plasmonic–metal nanostructures for efficient conversion of solar to chemical energy. Nat Mater. 2011;10(12):911–921.
25. Wolff CM, Frischmann PD, Schulze M, Bohn BJ, Wein R, Livadas P, et al. All–in–one visible–light–driven water splitting by combining nanoparticulate and molecular co–catalysts on CdS nanorods. Nat. Energy. 2018;3(10):862–9.
26. Xiang X, Chou L, Li X. Synthesis of PdS–CdSe@CdS–Au nanorods with asymmetric tips with improved H 2 production efficiency in water splitting and increased photostability. Chin. J. Cata. 2018;39(3):407–412.
27. Kalisman P, Houben L, Aronovitch E, Kauffmann Y, Bar–Sadan M, Amirav L. The golden gate to photocatalytic hydrogen production. J. Phys. Chem. A. 2015;3(39):19679–19682.
28. Zhou B, Song J, Xie C, Chen C, Qian Q, Han B. Mo–Bi–Cd Ternary Metal Chalcogenides: Highly Efficient Photocatalyst for CO2 Reduction to Formic Acid Under Visible Light. ACS Sustainable Chem. Eng. 2018;6(5):5754–5759.
29. Shemesh Y, Macdonald JE, Menagen G, Banin U. Synthesis and photocatalytic properties of a family of CdS–PdX hybrid nanoparticles. Angew. Chem. Int. Ed. Engl. 2011;50(5):1185–1189.
30. Rzigalinski BA, Strobl JS. Cadmium–containing nanoparticles: perspectives on pharmacology and toxicology of quantum dots. Toxicol. Appl. Pharmacol. 2009;238(3):280–288.
31. Domingos RF, Simon DF, Hauser C, Wilkinson KJ. Bioaccumulation and effects of CdTe/CdS quantum dots on Chlamydomonas reinhardtii–nanoparticles or the free ions? Environ. Sci. Technol. 2011;45(18):7664–7669.
32. Wu Z, Wang W, Cao Y, He J, Luo Q, Bhutto WA, et al. A beyond near–infrared response in a wide–bandgap ZnO/ZnSe coaxial nanowire solar cell by pseudomorphic layers. J. Mater. Chem. A. 2014;2(35): 14571–14576.
33. Zhuang T–T, Liu Y, Li Y, Zhao Y, Wu L, Jiang J, et al. Integration of Semiconducting Sulfides for Full–Spectrum Solar Energy Absorption and Efficient Charge Separation. Angew. Chem, Int Ed. 2016;55(22):6396–6400
34. Kuehnel MF, Creissen CE, Sahm CD, Wielend D, Schlosser A, Orchard KL, et al. ZnSe Nanorods as Visible–Light Absorbers for Photocatalytic and Photoelectrochemical H_2 Evolution in Water. Angew. Chem. Int. Ed Engl. 2019, 58(15): 5059–5063.

35. Jia, G, Pang, Y, Ning, J, Banin, U, Ji, B, Heavy–Metal–Free Colloidal Semiconductor Nanorods: Recent Advances and Future Perspectives. Adv. Mater. 2019, 31, 1900781.

36. a) Jia G, Banin U. A general strategy for synthesizing colloidal semiconductor zinc chalcogenide quantum rods. J. Am. Chem. Soc. 2014, 136(31): 11121–11127. b) Chen W, Karton A, Hussian T, Javaid S, Wang F, Pang Y, et al. Spontaneous shape and phase control of colloidal ZnSe nanocrystals by tailoring Se precursor reactivity. CrystEngComm. 2019;21(18):2955–2261.c) Chen D, Wang A, Li H, Abad Galán L, Su C, Yin Z, et al. Colloidal quasi–one–dimensional dual semiconductor core/shell nanorod couple heterostructures with blue fluorescence. Nanoscale. 2019;11(21):10190–10197. d) Pang Y, Zhang M, Chen D, Chen W, Wang F, Anwar SJ, et al. Why Do Colloidal Wurtzite Semiconductor Nanoplatelets Have an Atomically Uniform Thickness of Eight Monolayers? J. Phys. Chem. Lett. 2019;10(12):3465–3471.

37. Bose R, Wasey AH, Das GP, Pradhan N. Heteroepitaxial Junction in Au–ZnSe Nanostructure: Experiment versus First–Principle Simulation. J. Phys. Chem. Lett. 2014;5(11):1892–1898.

38. a) Selvaraj J, Mahesh A, Asokan V, Baskaralingam V, Dhayalan A, Paramasivam T. Phosphine–Free, Highly Emissive, Water–Soluble Mn:ZnSe/ZnS Core–Shell Nanorods: Synthesis, Characterization, and in Vitro Bioimaging of HEK293 and HeLa Cells. ACS Appl Nano Mater 2017;1(1):371–383; b) Chang S–H, Chiang M–Y, Chiang C–C, Yuan F–W, Chen C–Y, Chiu B–C, et al. Facile colloidal synthesis of quinary $CuIn_{1-x}Ga_x(S_ySe_{1-y})_2$ (CIGSSe) nanocrystal inks with tunable band gaps for use in low–cost photovoltaics. Energ. Environ. Sci. 2011;4(12):4929–4932.; c) Bourg M–C, Badia A, Lennox RB. Gold−Sulfur Bonding in 2D and 3D Self–Assembled Monolayers: XPS Characterization. J. Phys. Chem. B. 2000;104(28):6562–6567.

39. a) Bang JU, Lee SJ, Jang JS, Choi W, Song H. Geometric Effect of Single or Double Metal–Tipped CdSe Nanorods on Photocatalytic H2 Generation. J. Phys. Chem. Lett. 2012;3(24):3781–3785. b) Shaviv E, Schubert O, Alves–Santos M, Goldoni G, Di Felice R, Vallée F, et al. Absorption Properties of Metal–Semiconductor Hybrid Nanoparticles. ACS Nano. 2011;5(6):4712–4719;c) ten Hove JB, Schijven LMI, Wang J, Velders AH. Size–controlled and water–soluble gold nanoparticles using UV–induced ligand exchange and phase transfer. Chem. Commun. 2018;54(95):13355–13358.

40. a) Mokari T, Sztrum CG, Salant A, Rabani E, Banin U. Formation of asymmetric one–sided metal–tipped semiconductor nanocrystal dots and rods. Nat Mater. 2005;4(11):855–863.

b) Chakrabortty S, Yang JA, Tan YM, Mishra N, Chan Y. Asymmetric dumbbells from selective deposition of metals on seeded semiconductor nanorods. Angew. Chem. Int. Ed. Engl. 2010;49(16):2888–2892.

41. Costi R, Saunders AE, Banin U. Colloidal hybrid nanostructures: a new type of functional materials. Angew Chem. Int. Ed. Engl. 2010;49(29):4878–4997.

42. Pramanik G, Humpolickova J, Valenta J, Kundu P, Bals S, Bour P, et al. Gold nanoclusters with bright near–infrared photoluminescence. Nanoscale. 2018;10(8):3792–3798.

43. Villa A, Dimitratos N, Chan–Thaw CE, Hammond C, Veith GM, Wang D, et al. Characterisation of gold catalysts. Chem. Soc. Rev. 2016;45(18):4953–4994.

44. B. Canavaa, Vignerona J, Etcheberrya A, Guillemolesb JF, Lincot D. High resolution XPS studies of Se chemistry of a Cu(In, Ga)Se_2 surface. Appl. Surf. Sci. 2002;202:8–14.

45. New E, Hancox I, Rochford LA, Walker M, Dearden CA, McConville CF, et al. Organic photovoltaic cells utilising ZnO electron extraction layers produced through thermal conversion of ZnSe. J. Mater. Chem. A. 2014;2(45):19201–19207.

46. Noble–Luginbuhl AR, Nuzzo RG. Assembly and characterization of SAMs formed by the adsorption of alkanethiols on zinc selenide substrates. Langmuir. 2001;17(13):3937–3944.

47. Haldar KK, Pradhan N, Patra A. Formation of heteroepitaxy in different shapes of Au–CdSe metal–semiconductor hybrid nanostructures. Small. 2013;9(20):3424–3432.

48. Nørskov JK, Bligaard T, Logadottir A, Kitchin JR, Chen JG, Pandelov S, et al. Trends in the Exchange Current for Hydrogen Evolution. J Electrochem Soc. 2005;152(3):J23–J6.

49. Wu K, Lian T. Quantum confined colloidal nanorod heterostructures for solar–to–fuel conversion. Chem. Soc. Rev. 2016;45(14):3781–3810.

50. Liu Z, Lu Z, Bosman M, Li N, Frankcombe TJ, Jia G, et al. Photoactivity and Stability Co–Enhancement: When Localized Plasmons Meet Oxygen Vacancies in MgO. Small. 2018;14(48):1803233.

51. Lou Z, Fujitsuka M, Majima T. Pt–Au Triangular Nanoprisms with Strong Dipole Plasmon Resonance for Hydrogen Generation Studied by Single–Particle Spectroscopy. ACS Nano. 2016;10(6):6299–6305.

52. Liu L, Zhang X, Yang L, Ren L, Wang D, Ye J. Metal nanoparticles induced photocatalysis. Natl. Sci. Rev. 2017;4(5):761–780.

53. Nakibli Y, Kalisman P, Amirav L. Less Is More: The Case of Metal Cocatalysts. The J. Phys. Chem. Lett. 2015;6(12):2265–2268.

54. Simon T, Carlson MT, Stolarczyk JK, Feldmann J. Electron Transfer Rate vs Recombination Losses in Photocatalytic H2 Generation on Pt–Decorated CdS Nanorods. ACS Energy Lett. 2016;1(6):1137–1142.

55. a) Subramanian V, Wolf EE, Kamat PV. Catalysis with TiO_2/Gold Nanocomposites. Effect of Metal Particle Size on the Fermi Level Equilibration. J. Am. Chem Soc. 2004;126(15):4943–4950.; b) Murdoch M, Waterhouse GIN, Nadeem MA, Metson JB, Keane MA, Howe RF, et al. The effect of gold loading and particle size on photocatalytic hydrogen production from ethanol over Au/TiO2 nanoparticles. Nat. Chem. 2011;3(6):489–492.; c) Yin, Z., Chen, B., Bosman, M., Cao, X., Chen, J., Zheng, B. and Zhang, H. (2014), Au Nanoparticle-Modified MoS2 Nanosheet–Based Photoelectrochemical Cells for Water Splitting. Small, 10: 3537–3543.

56. a) Scholl JA, Koh AL, Dionne JA. Quantum plasmon resonances of individual metallic nanoparticles. Nature. 2012;483(7390):421–427; b) Wu K, Rodríguez–Córdoba WE, Yang Y, Lian T. Plasmon–Induced Hot Electron Transfer from the Au Tip to CdS Rod in CdS–Au Nanoheterostructures. Nano Letters. 2013;13(11):5255–63.

57. Zhou M, Zeng C, Chen Y, Zhao S, Sfeir MY, Zhu M, et al. Evolution from the plasmon to exciton state in ligand–protected atomically precise gold nanoparticles. Nat. Commun. 2016;7(1):1–7.

58. Oh N, Nam S, Zhai Y, Deshpande K, Trefonas P, Shim M. Double–heterojunction nanorods. Nat. Commun. 2014, 5(1):1–8.

59. Wang A, Shen H, Zang S, Lin Q, Wang H, Qian L, et al. Bright, efficient, and color–stable violet ZnSe–based quantum dot light–emitting diodes. Nanoscale. 2015;7(7):2951–2959.

60. Zhou J, Zhuang HL, Wang H. Layered tetragonal zinc chalcogenides for energy–related applications: from photocatalysts for water splitting to cathode materials for Li–ion batteries. Nanoscale. 2017;9(44):17303–17311

Every reasonable effort has been made to acknowledge the owners of copyright material. I would be pleased to hear from any copyright owner who has been omitted or incorrectly acknowledged.

Chapter 7. Conclusion and Outlooks

7.1 Conclusions

Zinc chalcogenide nanomaterials, including ZnS, ZnSe and ZnTe have emerged as promising Cd–free nanomaterials for light emitting, photocatalytic and biomedical applications. The facile synthesis approach of high–quality zinc chalcogenide nanomaterials is still hilgh demanded. Exquisite control over the size, shape, composition and structure over zinc chalcogenide quantum dots is still a challenge. The mechanisms that underpin nanocrystals nucleation and growth are still not fully understood. In light of this fact, we focused on developing general methods for the synthesis of ZnS, ZnSe nanoparticles and the growth mechanisms were interpreted by combing, the experimental results with theoretical density functional theory (DFT) simulations. The application of photocatalytic H_2 generation by water splitting with Au–ZnSe nanorods as photocatalyst was studied in detail.

The general conclusions have been derived from these studies.

7.1.1 A novel hot–injection method for the synthesis of ZnSe nanodots and nanorods by employing superhydride activated Se precursor.

- Successful and facile shape and size control of ZnSe nanocrystals in a phosphine–free system was accomplished.
- In a hot–injection method, tailoring the added ratio of superhydride to selenium precursor could result in uniform ZnSe nanodots or nanorods with tunable diameter.
- According to the results of Gibbs free energies of reaction between Se and super hydride and the experiment results, the selenium precursor in oleylamine can be reduced to Se_2^{2-} or Se^{2-} depending on the amount of super hydride added.
- With the increase amount of super hydride, Se^0 was reduced to Se_2^{2-} then Se^{2-}, and the reaction activity of different Se species are: $Se^{2-} > Se_2^{2-} > Se^0$.
- ZnSe nanodots of zinc blende phase were obtained when active Se^{2-} was employed as Se precursor, whereas ZnSe nanorods of wurtzite phase were obtained when less active Se_2^{2-} was employed as Se precursor.

7.1.2 A novel one–pot heat–up method for the synthesis of ZnS, ZnSe and ZnS_xSe_{1-x} nanorods by employing DDT and OLA as the co–ligand.

- ZnS, ZnSe and ZnS_xSe_{1-x} nanoparticles with different shape were synthesized by a one–pot heat–up method with different ligands.
- When a mixture of OLA and DDT was used as the ligand, 1D ZnS, ZnSe and

ZnS_xSe_{1-x} nanorods of wurtzite structure were obtained, while 0D ZnS, ZnSe and ZnS_xSe_{1-x} nanodots or nano–peanuts of zinc blende structure were obtained when only OLA was used as the ligand.

- DDT could increase the activity of S or Se powder in OLA during heating up process to form reactive monomers which resulted in the formation of anistropic nanorods.
- DDT may gradually strip off from the lattice planes of the ZnS (cylindrical surface) which provided site for monomers deposition on the diameter direction.

7.1.3 Non–epitaxial gold–tipped ZnSe hybrid nanorods for efficient photocatalytic hydrogen production

- Novel Au–ZnSe hybrid NRs with controlled size and site location of Au nanoparticles have been synthesized using wet–chemical approaches.
- According to structural analysis and DFT calculation results, Au NPs grew non–epitaxially on ZnSe NRs.
- Au tipped ZnSe hybrid NRs show enhanced charge separation that improved the HER catalytic properties and photocatalytic hydrogen production rate. Single–tipped Au–ZnSe hybrid nanorods exhibited better performance than double tipped Au–ZnSe nanorods.
- The better performance of ingle Au–tipped ZnSe NRs in comparison with double Au–tipped ZnSe NRs can attributed to the easier hole transfer and clearance by scavenger after the electron transfer to the Au tips from the untipped apex of single Au–tipped ZnSe NRs.
- Photocatalytic hydrogen production rate of 437.8 $\mu mol \cdot h^{-1} \cdot g^{-1}$ and an APE of 1.3% were obtained by using single–tipped Au–ZnSe hybrid nanorods as catalyst with methanol as sacrificial hole scavenger.
- This work opens an avenue for new Cd–free metal–semiconductor hybrid NP–based photocatalysis for hydrogen generation by water splitting, with relevance to redox reactions in biochemistry.

7.2 Outlooks

Despite some progress being achieved in this thesis, future research in this Cd–free system, especially the research into their multiple applications is still highly demanded.

In Chapter 4 of this thesis, superhydride was used to activate the Se precursor. The reducing reagent might be also employed to increase the reaction activity of other anion precursors such as Te. With the finding that the reactivity of Se precursor could influence the phase and morphology of the final nanoparticles, it is meaningful to extend this strategy to synthesize nanoparticles with varied compositions such as ZnTe, $CoSe_2$, $MoSe_2$, $MoTe_2$, InSe, BiSe, $CuInSe_2$, and $AgInSe_2$ which may find wider applications in lighting and displays, and photo(electro)catalysis.

The research on ligand-controlled growth of Zn–chalcogenide nanorods and nanodots in Chapter 5 presented an insightful perspective on the scale–up production of Cd–free nanoparticles. However, the underlying nucleation and growth mechanisms for heat–up method is still not fully understood. The roles of the reaction conditions such as the reaction temperature, precursor concentration, and heating up rate in regulating of the nucleation and growth processes of nanocrystals using the heat–up method are still not well-understood. Beside zinc chalcogenide nanocatalyst (noble metal-ZnS, ZnS_xSe_{1-x} or ZnSe nanorods) photocatalytic H_2 generation through water splitting, a potential research direction is developing facile approach to synthesize ZnSe/ZnS, ZnS_xSe_{1-x}/ZnS core/shell heterostructures for efficient lighting and displays applications. As ZnS has a larger bandgap than ZnSe, the overgrowth of ZnS shell on the ZnSe core will constitute a heterostructure with Type I band alignment, in which both electrons and holes will be confined in the core of ZnSe, thus enhanced photoluminescence properties such as high luminescence quantum efficiency, longe photo luminance lifetime and good stability are expected because ZnS shell could passivate the surface dangling bonds and eliminate the defects of ZnSe nanocrystals. In addition to their applications in light emitting materials, zinc chalcogenide nanocrystals could be potentially used in UV detector and solar cells. ZnSe and ZnS nanocrystals can be as electron transport layer on top of Si NWs or perovskite solar cells to improve their efficiency by increasing light trapping and photon down-conversion. Furthermore, zinc chalcogenide nanocrystals are heavy-metal free and are non- or less toxic, which makes them more desirable in bio–imaging applications.

As Au–ZnSe hybrid exhibited good performance for photocatalytic H_2 evolution reaction (Chapter 6), an expansion of the type of noble metal should be taken into consideration in future studies to further improve the efficiency of hybrid nanoparticles. For example, platinum (Pt) showed better hydrogen evolution reaction (HER) performance in Cd–based chalcogenide heterostructures, so it is also interesting to develop Pt–ZnSe hybrid nanoparticles for

photocatalytic applications. The selective deposition of bimetals like Au and Pt on alloyed ZnSeS nanorods is also worthwhile. It should also be noted that since this work focuses mainly on developing a new synthetic route for the synthesis of Cd-free Au-ZnSe nanorods with controlled Au domains for the first time, the study on the photocatalytic water splitting application was used as a porotype to investigate its potential in photocatalysis. There is more related research to be done in the future, such as the measurement of the stability of Au-ZnSe hybrid catalysts and the optimal reaction conditions including the choice of sacrificial reagent, the selection of driving light source and capped hydrophilic ligand. An in-depth understanding on the photocatalytic application of this new heterostructure nanoparticle could be gained by the comprehensive investigations on the photocatalytic properties. In addition, as the hybrid zinc chalcogenide nanoparticle are heavy-metal free, the potential of Cd–free Au–ZnSe could be further explored for biomedical applications because of their low toxicity and efficient charge separation ability.

Appendix A

Copyright of reused figures in Chapter 2.

Figure 2.1.

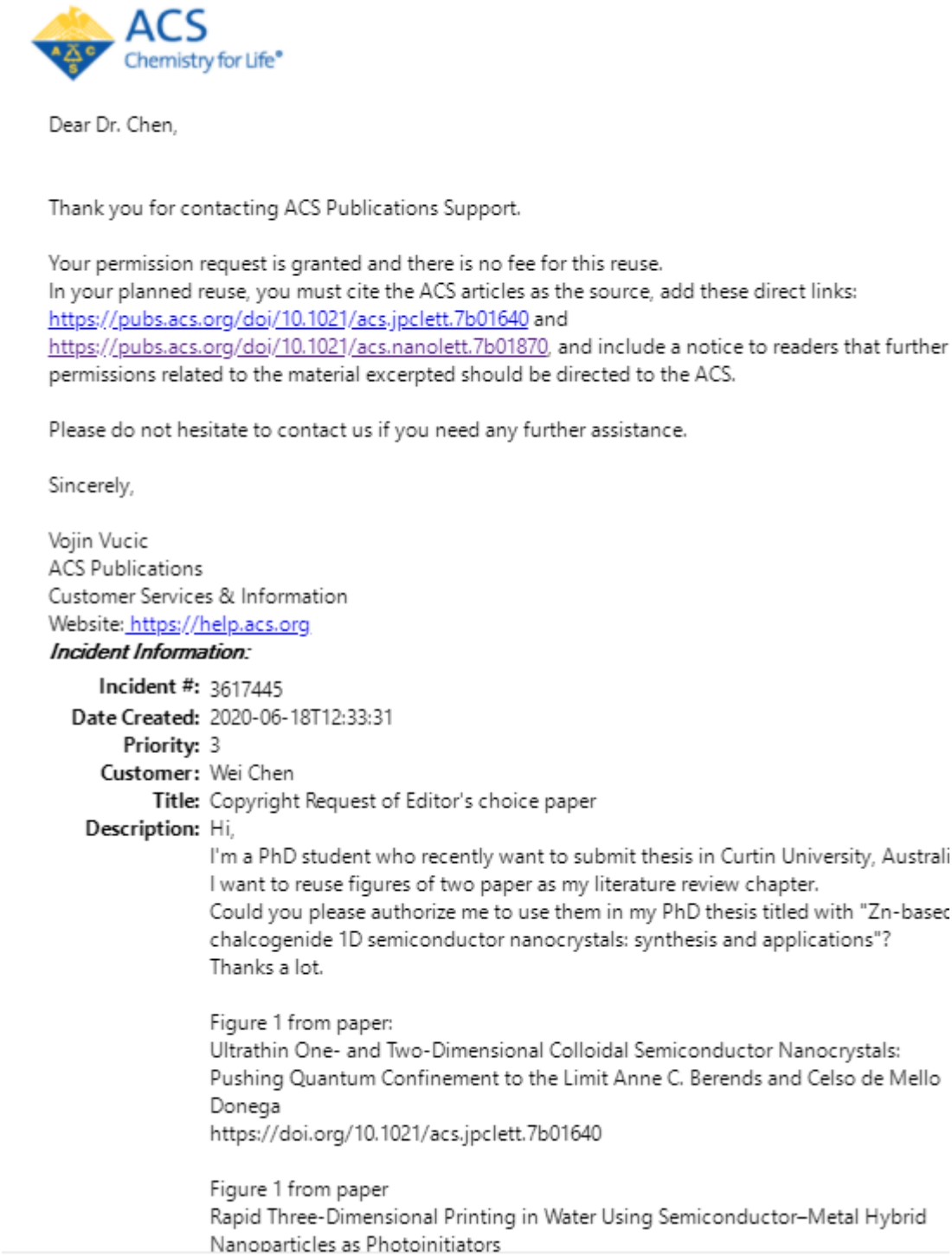

ACS Chemistry for Life®

Dear Dr. Chen,

Thank you for contacting ACS Publications Support.

Your permission request is granted and there is no fee for this reuse.
In your planned reuse, you must cite the ACS articles as the source, add these direct links: https://pubs.acs.org/doi/10.1021/acs.jpclett.7b01640 and https://pubs.acs.org/doi/10.1021/acs.nanolett.7b01870, and include a notice to readers that further permissions related to the material excerpted should be directed to the ACS.

Please do not hesitate to contact us if you need any further assistance.

Sincerely,

Vojin Vucic
ACS Publications
Customer Services & Information
Website: https://help.acs.org

Incident Information:

Incident #: 3617445
Date Created: 2020-06-18T12:33:31
Priority: 3
Customer: Wei Chen
Title: Copyright Request of Editor's choice paper
Description: Hi,
I'm a PhD student who recently want to submit thesis in Curtin University, Australi
I want to reuse figures of two paper as my literature review chapter.
Could you please authorize me to use them in my PhD thesis titled with "Zn-basec
chalcogenide 1D semiconductor nanocrystals: synthesis and applications"?
Thanks a lot.

Figure 1 from paper:
Ultrathin One- and Two-Dimensional Colloidal Semiconductor Nanocrystals: Pushing Quantum Confinement to the Limit Anne C. Berends and Celso de Mello Donega
https://doi.org/10.1021/acs.jpclett.7b01640

Figure 1 from paper
Rapid Three-Dimensional Printing in Water Using Semiconductor–Metal Hybrid Nanoparticles as Photoinitiators

Figure 2.4(a)

Royal Society of Chemistry - License Terms and Conditions

This is a License Agreement between Wei Chen ("You") and Royal Society of Chemistry ("Publisher") provided by Copyright Clearance Center ("CCC"). The license consists of your order details, the terms and conditions provided by Royal Society of Chemistry, and the CCC terms and conditions.

All payments must be made in full to CCC.

Order Date	16-Jun-2020	**Type of Use**	Republish in a thesis/dissertation
Order license ID	1042188-1	**Publisher**	ROYAL SOCIETY OF CHEMISTRY
ISSN	1477-9234	**Portion**	Image/photo/illustration

LICENSED CONTENT

Publication Title	Dalton transactions	**Rightsholder**	Royal Society of Chemistry
Article Title	Synthesis and bio-functionalization of magnetic nanoparticles for medical diagnosis and treatment.	**Publication Type**	e-Journal
		Start Page	6315
Author/Editor	Royal Society of Chemistry (Great Britain)	**Issue**	24
Date	01/01/2003	**Volume**	40
Language	English		
Country	United Kingdom of Great Britain and Northern Ireland		

REQUEST DETAILS

Portion Type	Image/photo/illustration	**Distribution**	Worldwide
Number of images / photos / illustrations	1	**Translation**	Original language of publication
Format (select all that apply)	Print, Electronic	**Copies for the disabled?**	No
Who will republish the content?	Academic institution	**Minor editing privileges?**	No
Duration of Use	Current edition and up to 15 years	**Incidental promotional use?**	No
Lifetime Unit Quantity	Up to 499	**Currency**	USD
Rights Requested	Main product		

NEW WORK DETAILS

Title	Zn-based chalcogenide 1D semiconductor nanocrystals: synthesis and applications	**Institution name**	Curtin University
		Expected presentation date	2020-06-30
Instructor name	Wei Chen		

ADDITIONAL DETAILS

Order reference number	N/A	**The requesting person / organization to appear on the license**	Wei Chen

Figure 2.4(b) Permission from Author.

van Embden, J.; Chesman, A. S.; **Jasieniak, J. J.,** The heat–up synthesis of colloidal nanocrystals. *Chemistry of Materials* 2015, *27* (7), 2246–2285.

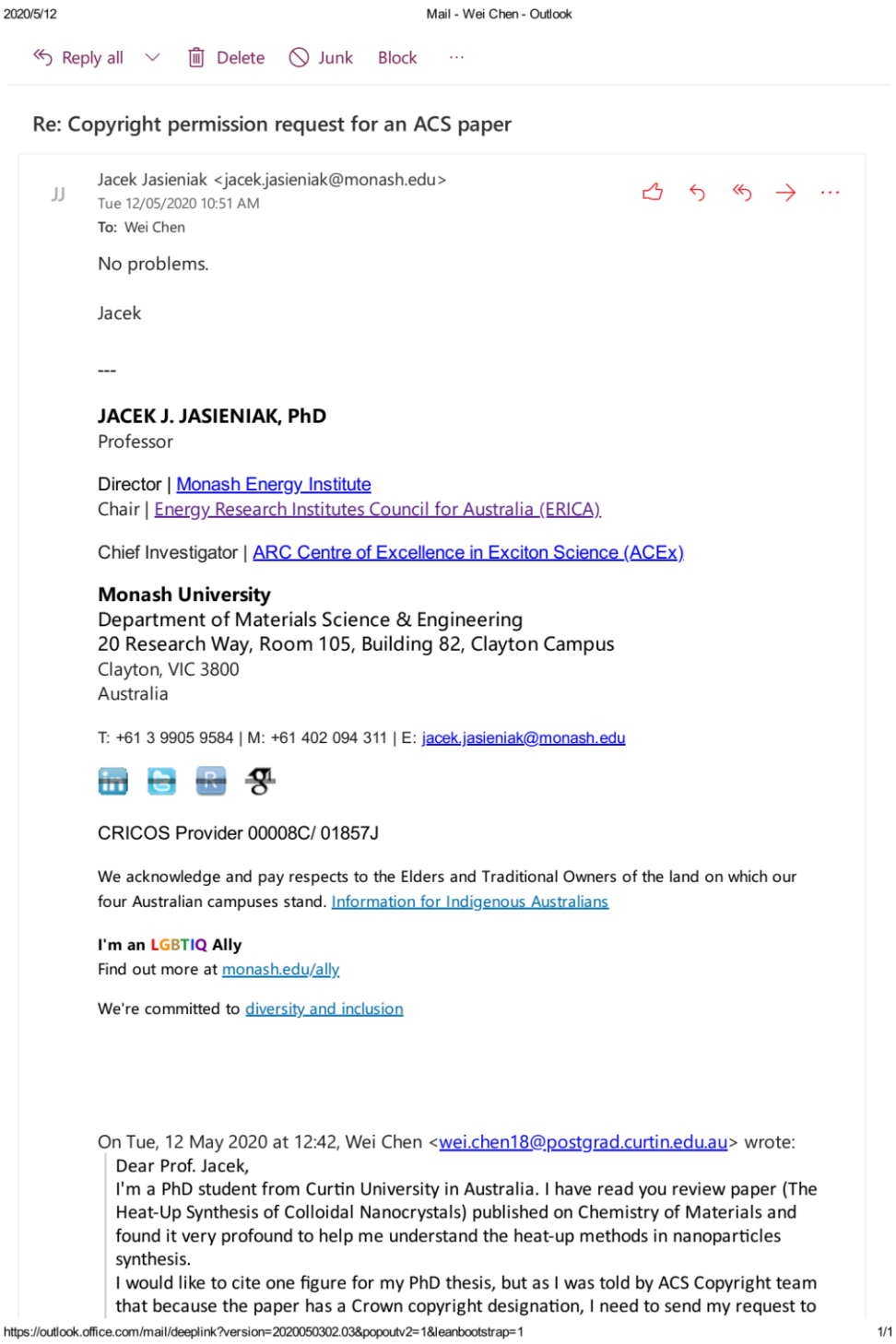

2020/5/12 Mail - Wei Chen - Outlook

Reply all | Delete | Junk | Block | ...

Re: Copyright permission request for an ACS paper

Jacek Jasieniak <jacek.jasieniak@monash.edu>
Tue 12/05/2020 10:51 AM
To: Wei Chen

No problems.

Jacek

JACEK J. JASIENIAK, PhD
Professor

Director | Monash Energy Institute
Chair | Energy Research Institutes Council for Australia (ERICA)

Chief Investigator | ARC Centre of Excellence in Exciton Science (ACEx)

Monash University
Department of Materials Science & Engineering
20 Research Way, Room 105, Building 82, Clayton Campus
Clayton, VIC 3800
Australia

T: +61 3 9905 9584 | M: +61 402 094 311 | E: jacek.jasieniak@monash.edu

CRICOS Provider 00008C/ 01857J

We acknowledge and pay respects to the Elders and Traditional Owners of the land on which our four Australian campuses stand. Information for Indigenous Australians

I'm an LGBTIQ Ally
Find out more at monash.edu/ally

We're committed to diversity and inclusion

On Tue, 12 May 2020 at 12:42, Wei Chen <wei.chen18@postgrad.curtin.edu.au> wrote:

> Dear Prof. Jacek,
> I'm a PhD student from Curtin University in Australia. I have read you review paper (The Heat-Up Synthesis of Colloidal Nanocrystals) published on Chemistry of Materials and found it very profound to help me understand the heat-up methods in nanoparticles synthesis.
> I would like to cite one figure for my PhD thesis, but as I was told by ACS Copyright team that because the paper has a Crown copyright designation, I need to send my request to

https://outlook.office.com/mail/deeplink?version=2020050302.03&popoutv2=1&leanbootstrap=1 1/1

Figure 2.5(a–d)

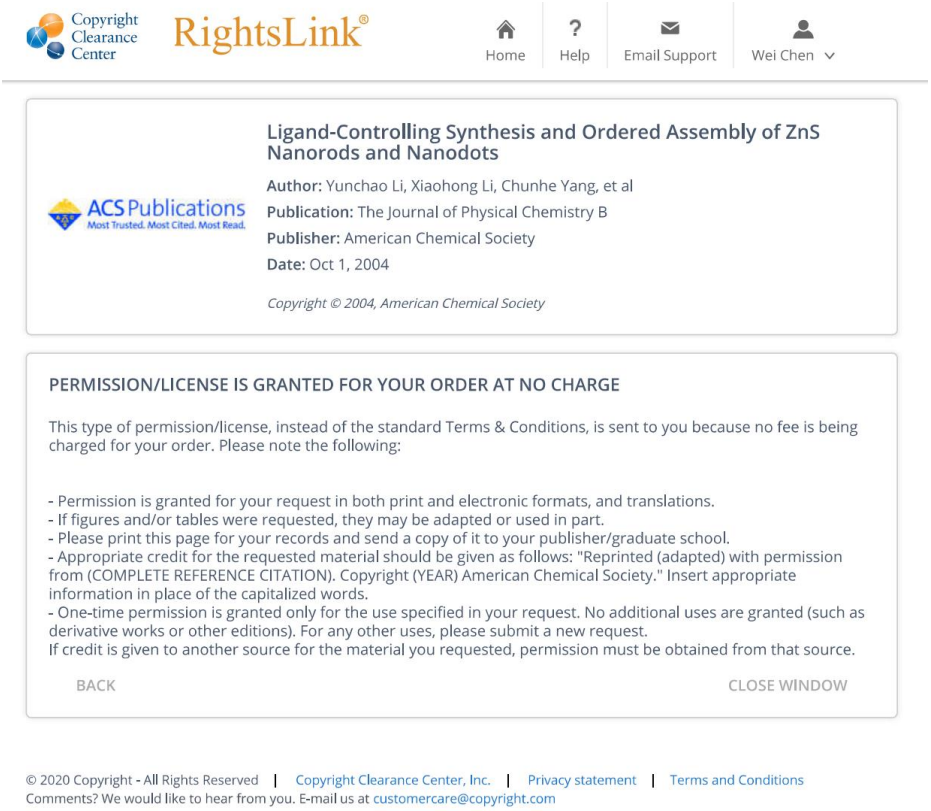

Figure 2.5(e–h)

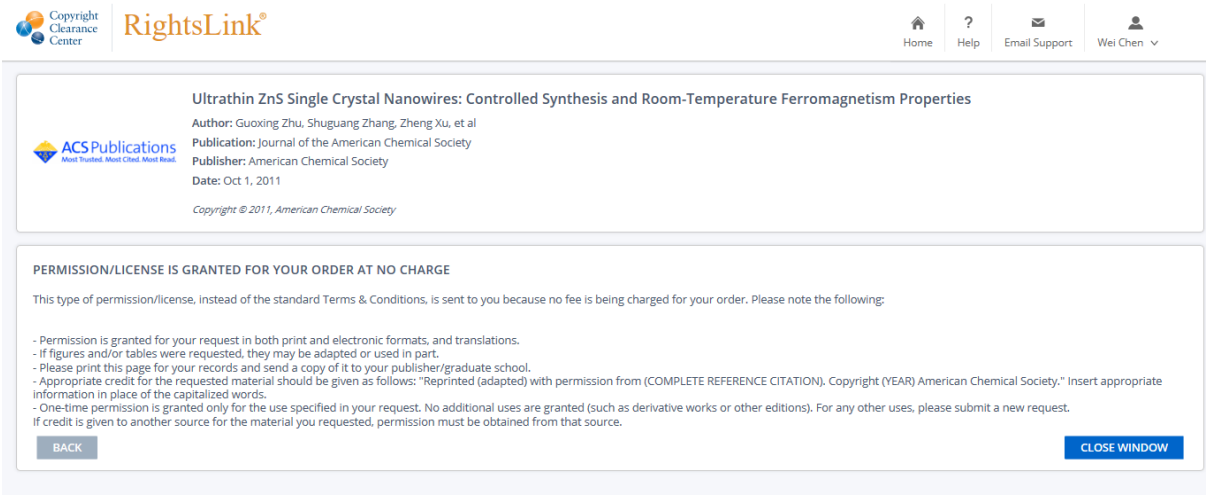

Figure 2.5(i–l)

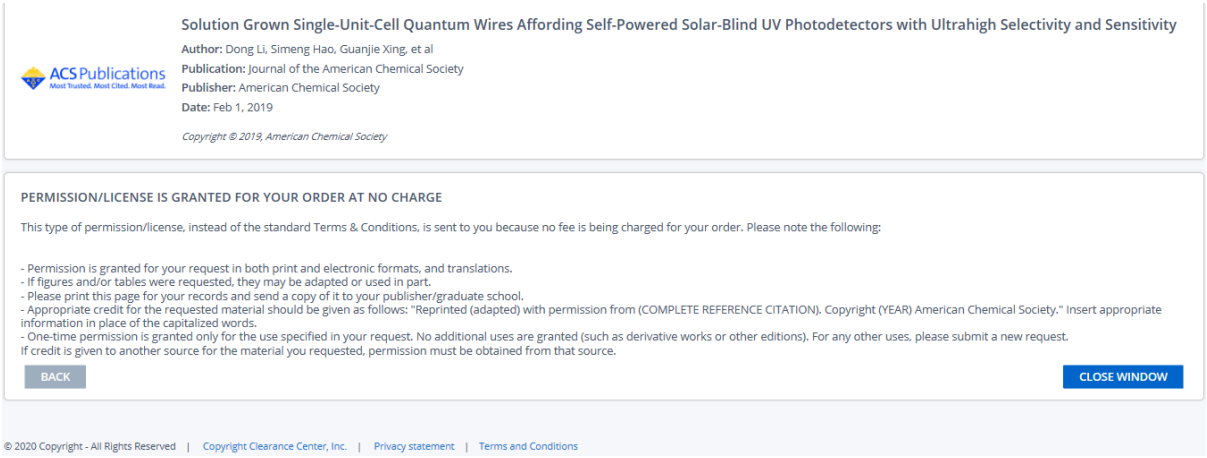

Solution Grown Single-Unit-Cell Quantum Wires Affording Self-Powered Solar-Blind UV Photodetectors with Ultrahigh Selectivity and Sensitivity

Author: Dong Li, Simeng Hao, Guanjie Xing, et al
Publication: Journal of the American Chemical Society
Publisher: American Chemical Society
Date: Feb 1, 2019

Figure 2.6 (a–g)

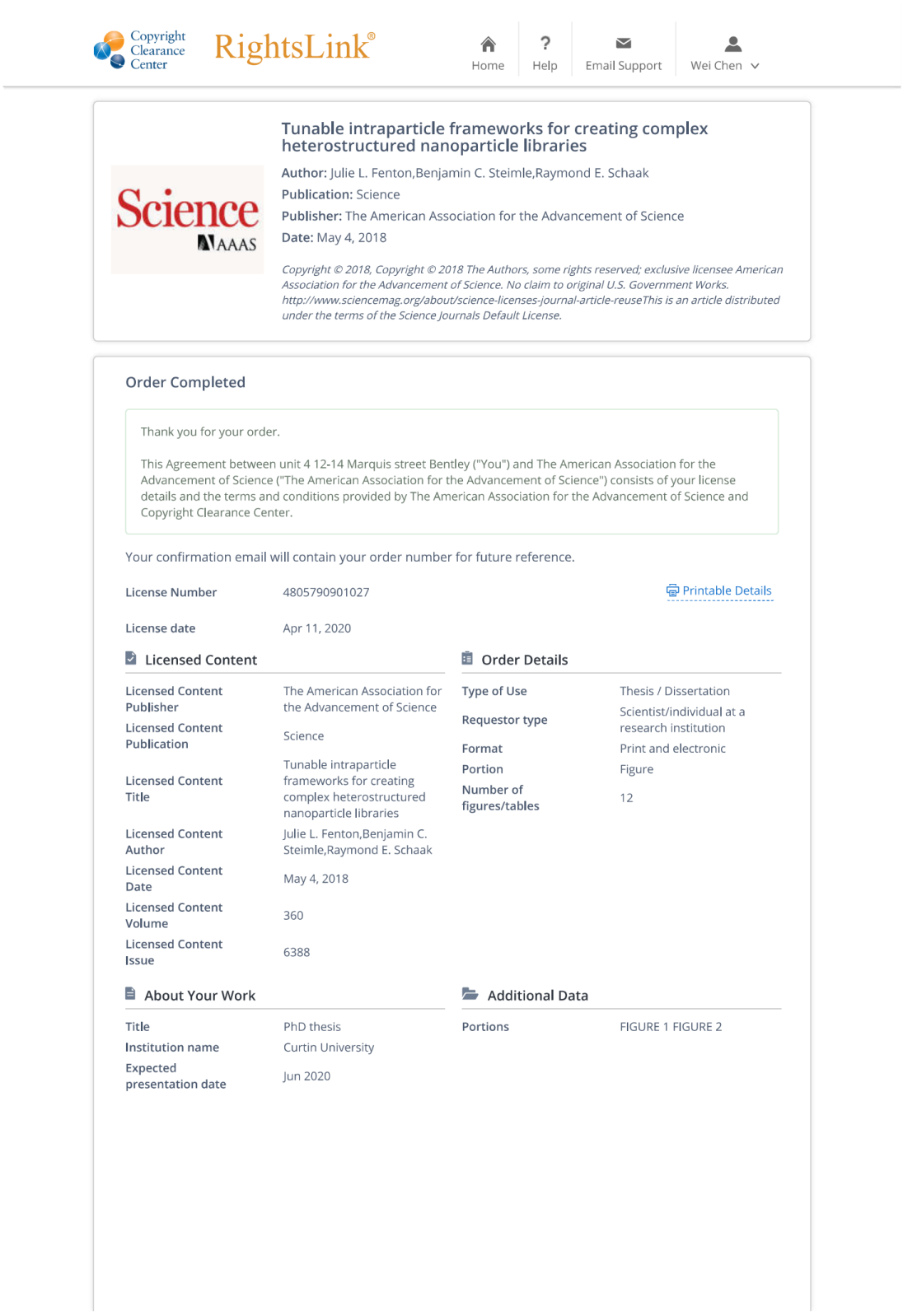

Copyright Clearance Center RightsLink®

Home | Help | Email Support | Wei Chen

Tunable intraparticle frameworks for creating complex heterostructured nanoparticle libraries

Author: Julie L. Fenton,Benjamin C. Steimle,Raymond E. Schaak

Publication: Science

Publisher: The American Association for the Advancement of Science

Date: May 4, 2018

Copyright © 2018, Copyright © 2018 The Authors, some rights reserved; exclusive licensee American Association for the Advancement of Science. No claim to original U.S. Government Works. http://www.sciencemag.org/about/science-licenses-journal-article-reuseThis is an article distributed under the terms of the Science Journals Default License.

Order Completed

Thank you for your order.

This Agreement between unit 4 12-14 Marquis street Bentley ("You") and The American Association for the Advancement of Science ("The American Association for the Advancement of Science") consists of your license details and the terms and conditions provided by The American Association for the Advancement of Science and Copyright Clearance Center.

Your confirmation email will contain your order number for future reference.

Printable Details

License Number	4805790901027
License date	Apr 11, 2020

Licensed Content

Licensed Content Publisher	The American Association for the Advancement of Science
Licensed Content Publication	Science
Licensed Content Title	Tunable intraparticle frameworks for creating complex heterostructured nanoparticle libraries
Licensed Content Author	Julie L. Fenton,Benjamin C. Steimle,Raymond E. Schaak
Licensed Content Date	May 4, 2018
Licensed Content Volume	360
Licensed Content Issue	6388

Order Details

Type of Use	Thesis / Dissertation
Requestor type	Scientist/individual at a research institution
Format	Print and electronic
Portion	Figure
Number of figures/tables	12

About Your Work

Title	PhD thesis
Institution name	Curtin University
Expected presentation date	Jun 2020

Additional Data

Portions	FIGURE 1 FIGURE 2

Figure 2.6 (h–i)

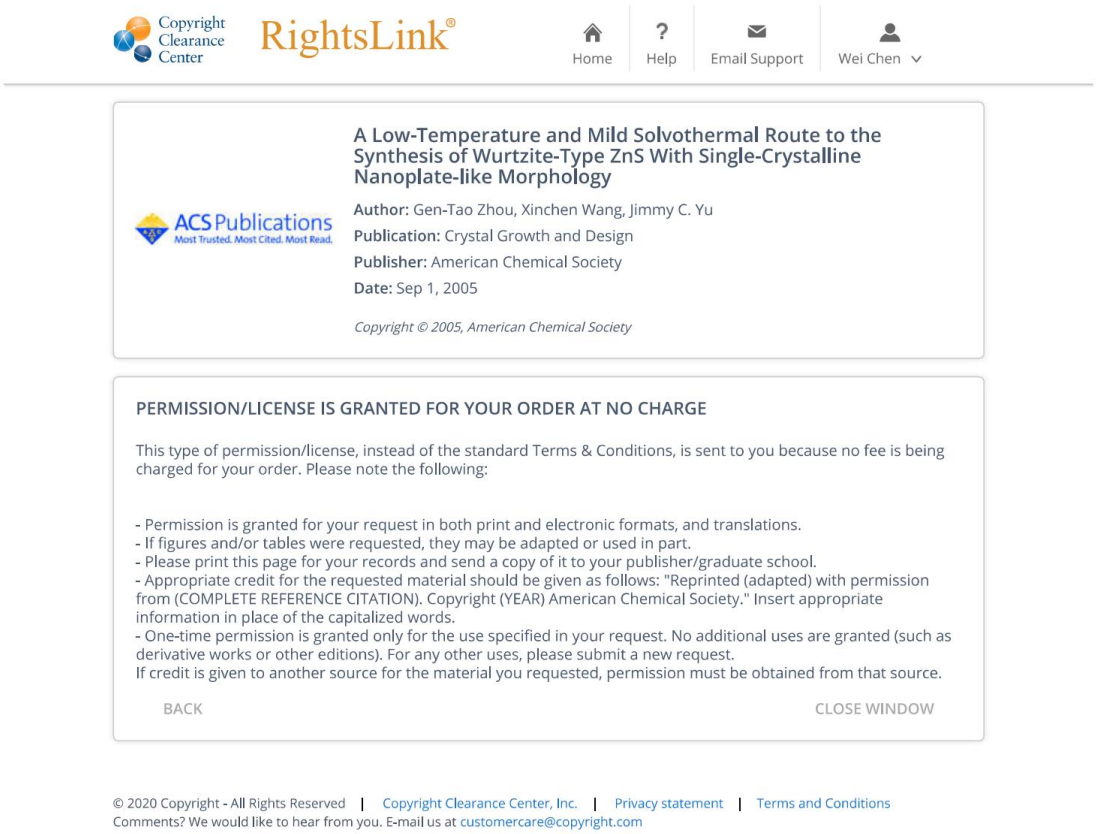

Copyright Clearance Center RightsLink®

Home | Help | Email Support | Wei Chen

ACS Publications
Most Trusted. Most Cited. Most Read.

A Low-Temperature and Mild Solvothermal Route to the Synthesis of Wurtzite-Type ZnS With Single-Crystalline Nanoplate-like Morphology

Author: Gen-Tao Zhou, Xinchen Wang, Jimmy C. Yu
Publication: Crystal Growth and Design
Publisher: American Chemical Society
Date: Sep 1, 2005

Copyright © 2005, American Chemical Society

PERMISSION/LICENSE IS GRANTED FOR YOUR ORDER AT NO CHARGE

This type of permission/license, instead of the standard Terms & Conditions, is sent to you because no fee is being charged for your order. Please note the following:

- Permission is granted for your request in both print and electronic formats, and translations.
- If figures and/or tables were requested, they may be adapted or used in part.
- Please print this page for your records and send a copy of it to your publisher/graduate school.
- Appropriate credit for the requested material should be given as follows: "Reprinted (adapted) with permission from (COMPLETE REFERENCE CITATION). Copyright (YEAR) American Chemical Society." Insert appropriate information in place of the capitalized words.
- One-time permission is granted only for the use specified in your request. No additional uses are granted (such as derivative works or other editions). For any other uses, please submit a new request.

If credit is given to another source for the material you requested, permission must be obtained from that source.

BACK CLOSE WINDOW

Figure 2.6 (j–k)

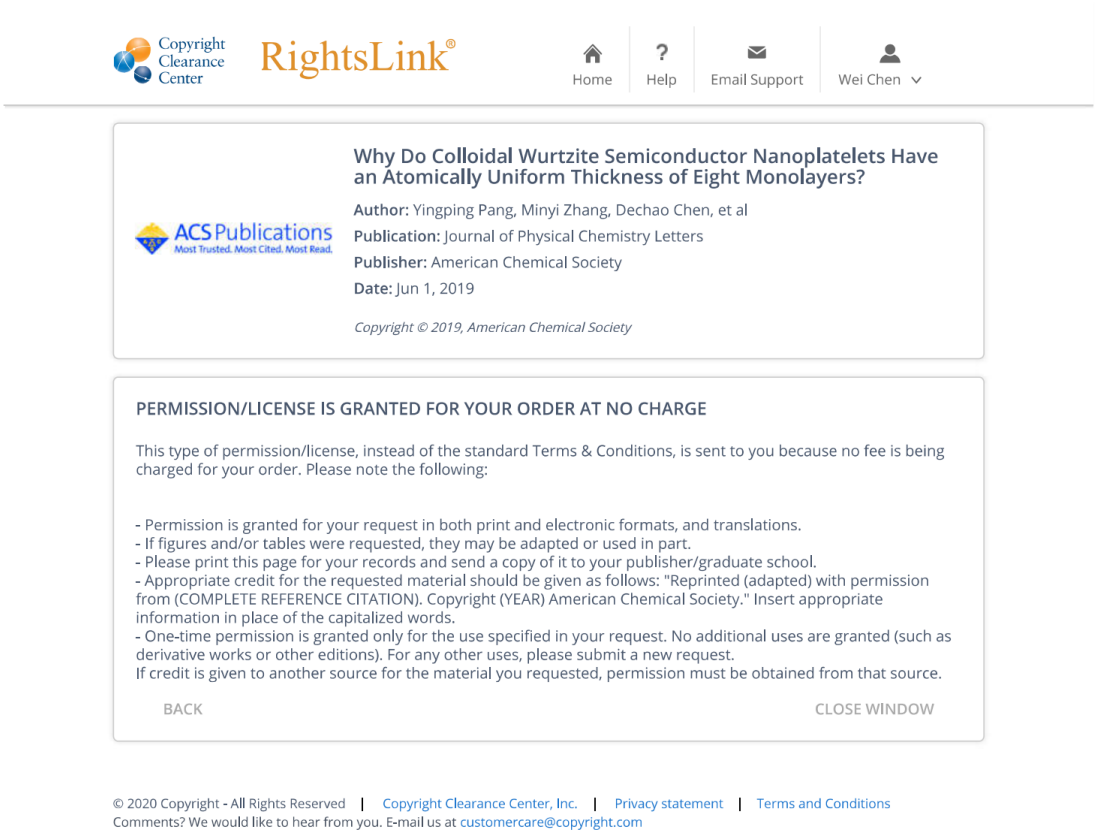
Copyright Clearance Center
RightsLink®
Home
Help
Email Support
Wei Chen
Why Do Colloidal Wurtzite Semiconductor Nanoplatelets Have an Atomically Uniform Thickness of Eight Monolayers?
Author: Yingping Pang, Minyi Zhang, Dechao Chen, et al
Publication: Journal of Physical Chemistry Letters
Publisher: American Chemical Society
Date: Jun 1, 2019
Copyright © 2019, American Chemical Society
ACS Publications
Most Trusted. Most Cited. Most Read.
PERMISSION/LICENSE IS GRANTED FOR YOUR ORDER AT NO CHARGE
This type of permission/license, instead of the standard Terms & Conditions, is sent to you because no fee is being charged for your order. Please note the following:
- Permission is granted for your request in both print and electronic formats, and translations.
- If figures and/or tables were requested, they may be adapted or used in part.
- Please print this page for your records and send a copy of it to your publisher/graduate school.
- Appropriate credit for the requested material should be given as follows: "Reprinted (adapted) with permission from (COMPLETE REFERENCE CITATION). Copyright (YEAR) American Chemical Society." Insert appropriate information in place of the capitalized words.
- One-time permission is granted only for the use specified in your request. No additional uses are granted (such as derivative works or other editions). For any other uses, please submit a new request.
If credit is given to another source for the material you requested, permission must be obtained from that source.
BACK
CLOSE WINDOW
© 2020 Copyright - All Rights Reserved | Copyright Clearance Center, Inc. | Privacy statement | Terms and Conditions
Comments? We would like to hear from you. E-mail us at customercare@copyright.com

Figure 2.6 (l–o)

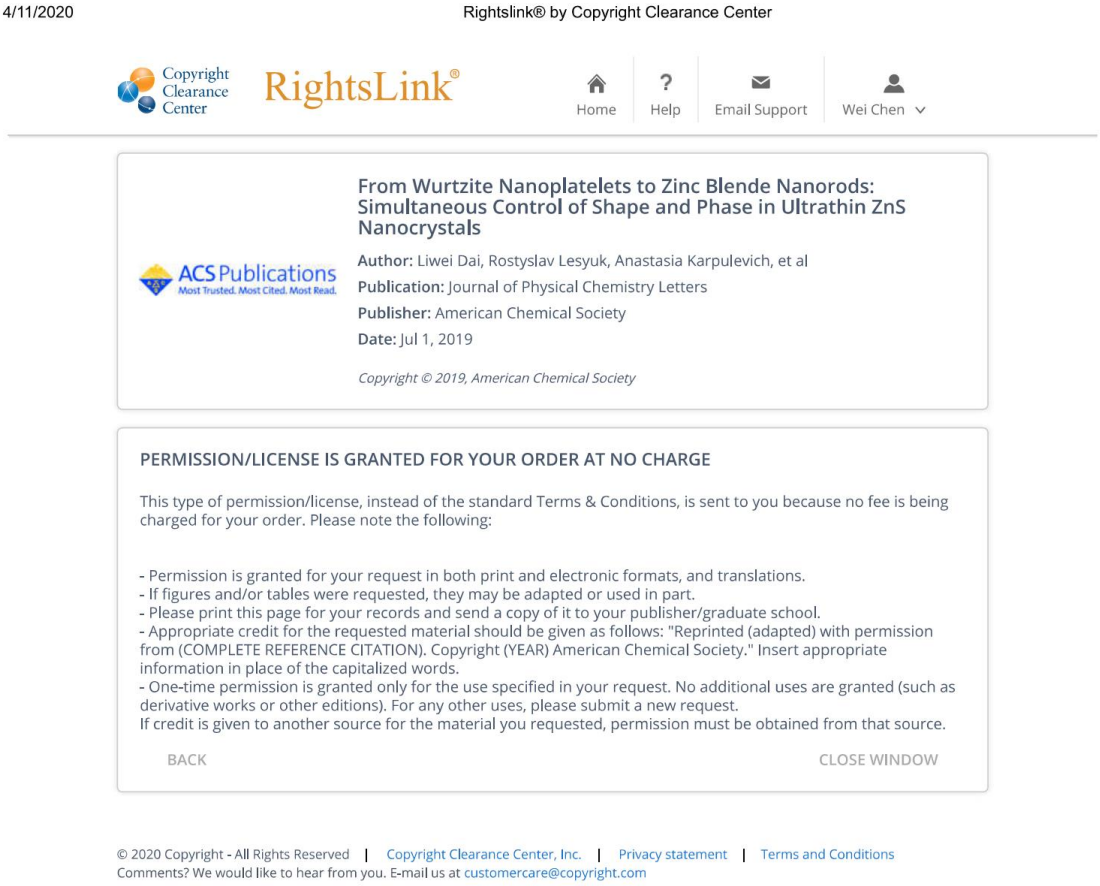

4/11/2020 Rightslink® by Copyright Clearance Center

Copyright Clearance Center RightsLink®

Home | Help | Email Support | Wei Chen

ACS Publications
Most Trusted. Most Cited. Most Read.

From Wurtzite Nanoplatelets to Zinc Blende Nanorods: Simultaneous Control of Shape and Phase in Ultrathin ZnS Nanocrystals

Author: Liwei Dai, Rostyslav Lesyuk, Anastasia Karpulevich, et al
Publication: Journal of Physical Chemistry Letters
Publisher: American Chemical Society
Date: Jul 1, 2019

Copyright © 2019, American Chemical Society

PERMISSION/LICENSE IS GRANTED FOR YOUR ORDER AT NO CHARGE

This type of permission/license, instead of the standard Terms & Conditions, is sent to you because no fee is being charged for your order. Please note the following:

- Permission is granted for your request in both print and electronic formats, and translations.
- If figures and/or tables were requested, they may be adapted or used in part.
- Please print this page for your records and send a copy of it to your publisher/graduate school.
- Appropriate credit for the requested material should be given as follows: "Reprinted (adapted) with permission from (COMPLETE REFERENCE CITATION). Copyright (YEAR) American Chemical Society." Insert appropriate information in place of the capitalized words.
- One-time permission is granted only for the use specified in your request. No additional uses are granted (such as derivative works or other editions). For any other uses, please submit a new request.

If credit is given to another source for the material you requested, permission must be obtained from that source.

BACK CLOSE WINDOW

Figure 2.7(a–c)

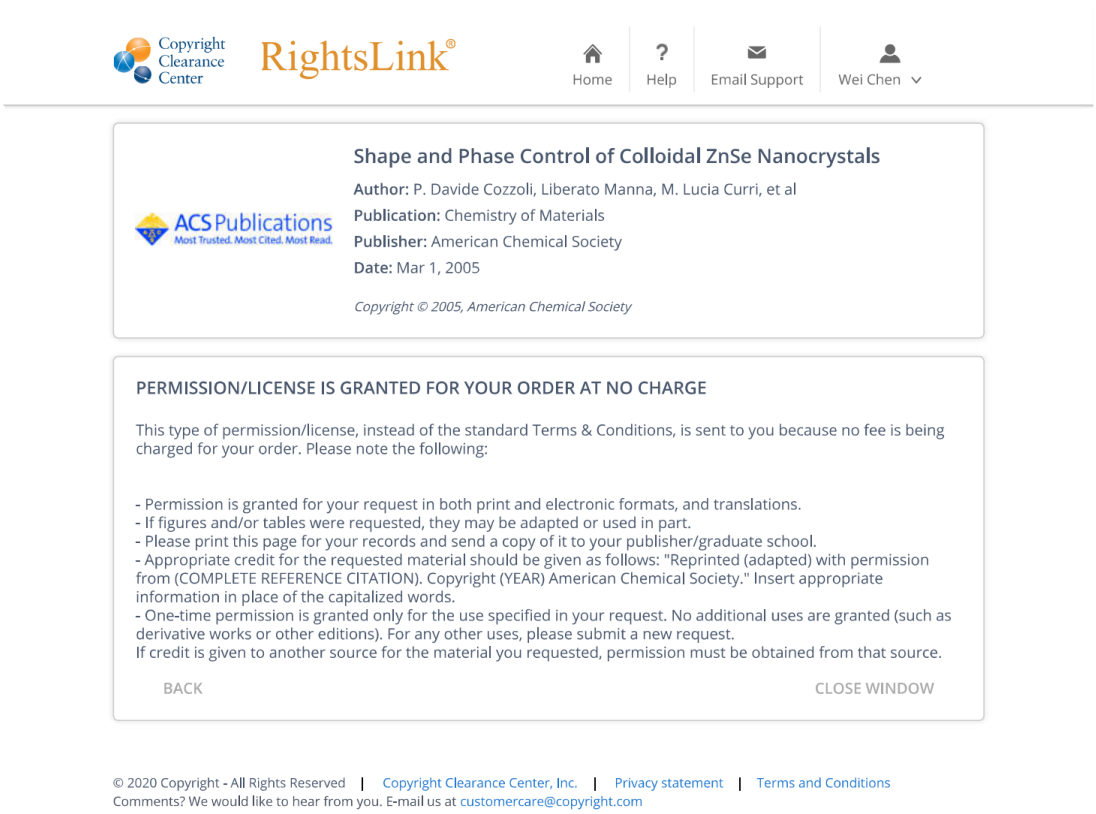

Copyright Clearance Center RightsLink®

Home | Help | Email Support | Wei Chen

ACS Publications
Most Trusted. Most Cited. Most Read.

Shape and Phase Control of Colloidal ZnSe Nanocrystals

Author: P. Davide Cozzoli, Liberato Manna, M. Lucia Curri, et al
Publication: Chemistry of Materials
Publisher: American Chemical Society
Date: Mar 1, 2005

Copyright © 2005, American Chemical Society

PERMISSION/LICENSE IS GRANTED FOR YOUR ORDER AT NO CHARGE

This type of permission/license, instead of the standard Terms & Conditions, is sent to you because no fee is being charged for your order. Please note the following:

- Permission is granted for your request in both print and electronic formats, and translations.
- If figures and/or tables were requested, they may be adapted or used in part.
- Please print this page for your records and send a copy of it to your publisher/graduate school.
- Appropriate credit for the requested material should be given as follows: "Reprinted (adapted) with permission from (COMPLETE REFERENCE CITATION). Copyright (YEAR) American Chemical Society." Insert appropriate information in place of the capitalized words.
- One-time permission is granted only for the use specified in your request. No additional uses are granted (such as derivative works or other editions). For any other uses, please submit a new request.

If credit is given to another source for the material you requested, permission must be obtained from that source.

BACK CLOSE WINDOW

Figure 2.7(d–f)

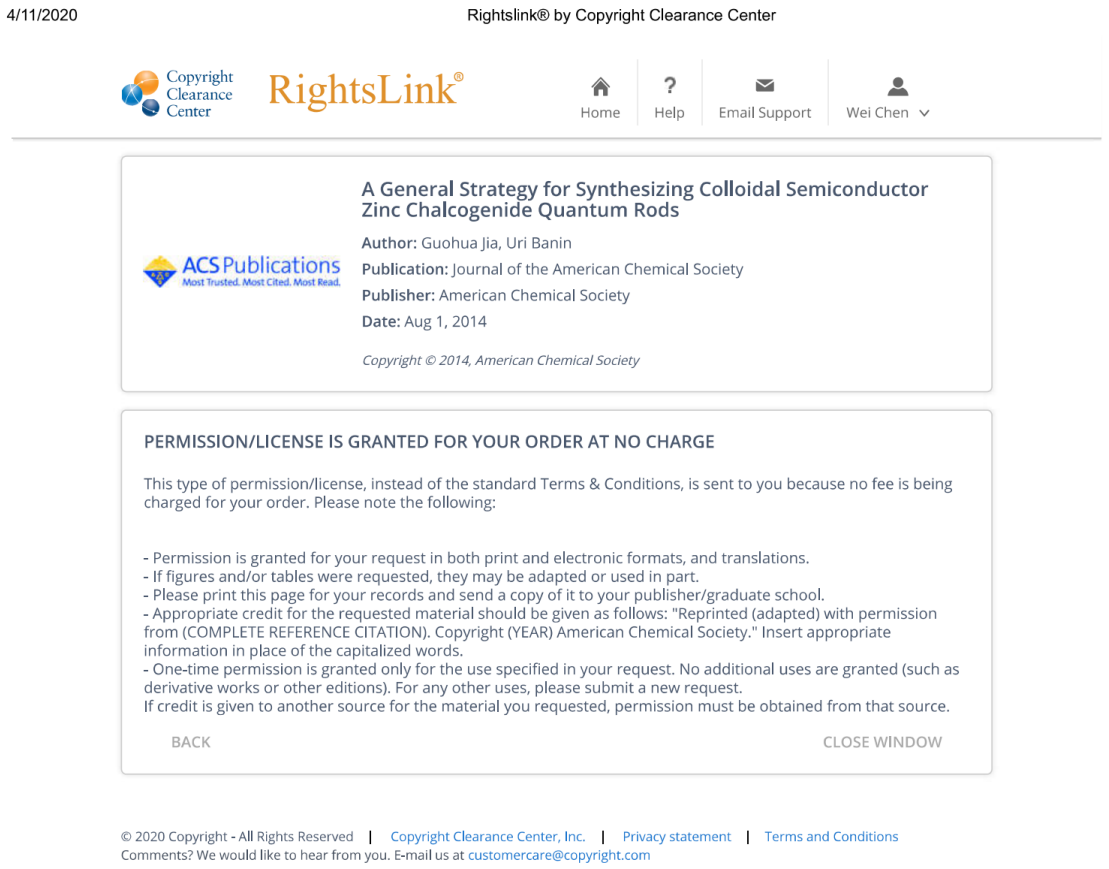

4/11/2020 Rightslink® by Copyright Clearance Center

Copyright Clearance Center RightsLink®

Home | Help | Email Support | Wei Chen

ACS Publications
Most Trusted. Most Cited. Most Read.

A General Strategy for Synthesizing Colloidal Semiconductor Zinc Chalcogenide Quantum Rods

Author: Guohua Jia, Uri Banin
Publication: Journal of the American Chemical Society
Publisher: American Chemical Society
Date: Aug 1, 2014

Copyright © 2014, American Chemical Society

PERMISSION/LICENSE IS GRANTED FOR YOUR ORDER AT NO CHARGE

This type of permission/license, instead of the standard Terms & Conditions, is sent to you because no fee is being charged for your order. Please note the following:

- Permission is granted for your request in both print and electronic formats, and translations.
- If figures and/or tables were requested, they may be adapted or used in part.
- Please print this page for your records and send a copy of it to your publisher/graduate school.
- Appropriate credit for the requested material should be given as follows: "Reprinted (adapted) with permission from (COMPLETE REFERENCE CITATION). Copyright (YEAR) American Chemical Society." Insert appropriate information in place of the capitalized words.
- One-time permission is granted only for the use specified in your request. No additional uses are granted (such as derivative works or other editions). For any other uses, please submit a new request.

If credit is given to another source for the material you requested, permission must be obtained from that source.

BACK CLOSE WINDOW

Figure 2.7(g–l)

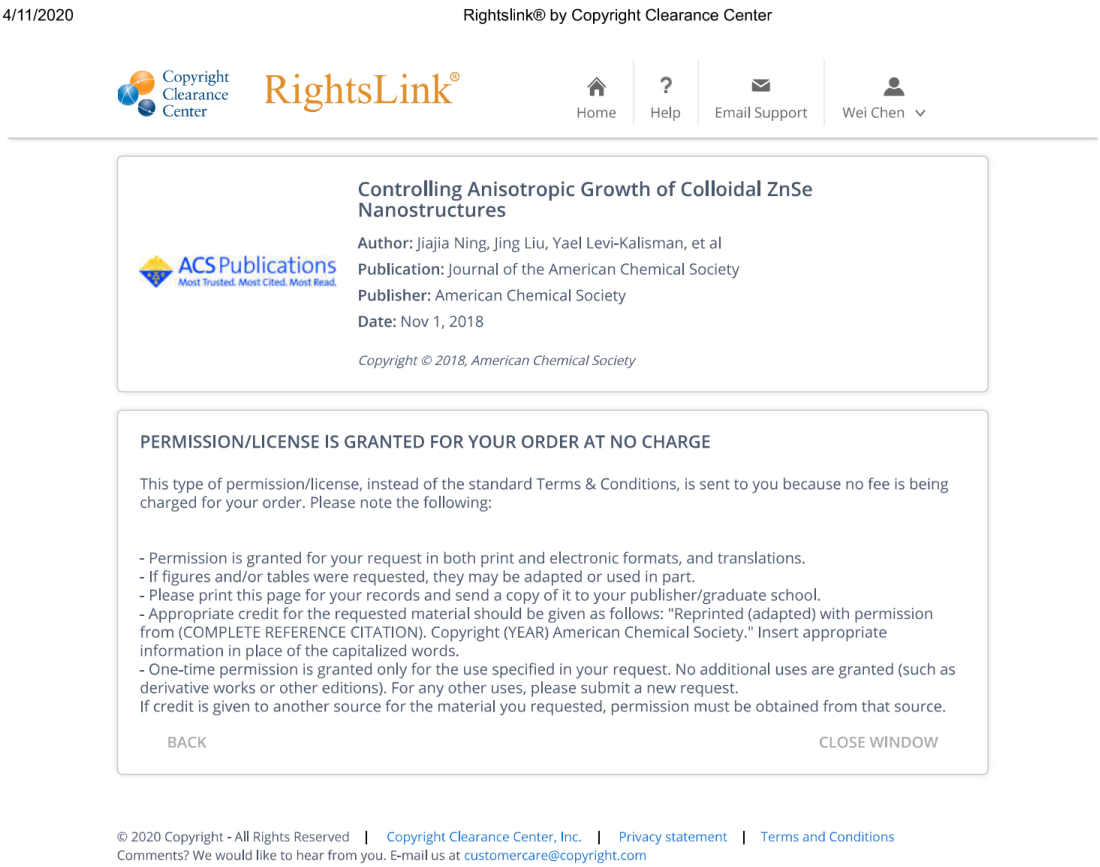
4/11/2020
Rightslink® by Copyright Clearance Center
Copyright Clearance Center
RightsLink®
Home
Help
Email Support
Wei Chen
Controlling Anisotropic Growth of Colloidal ZnSe Nanostructures
ACS Publications
Most Trusted. Most Cited. Most Read.
Author: Jiajia Ning, Jing Liu, Yael Levi-Kalisman, et al
Publication: Journal of the American Chemical Society
Publisher: American Chemical Society
Date: Nov 1, 2018
Copyright © 2018, American Chemical Society
PERMISSION/LICENSE IS GRANTED FOR YOUR ORDER AT NO CHARGE
This type of permission/license, instead of the standard Terms & Conditions, is sent to you because no fee is being charged for your order. Please note the following:
- Permission is granted for your request in both print and electronic formats, and translations.
- If figures and/or tables were requested, they may be adapted or used in part.
- Please print this page for your records and send a copy of it to your publisher/graduate school.
- Appropriate credit for the requested material should be given as follows: "Reprinted (adapted) with permission from (COMPLETE REFERENCE CITATION). Copyright (YEAR) American Chemical Society." Insert appropriate information in place of the capitalized words.
- One-time permission is granted only for the use specified in your request. No additional uses are granted (such as derivative works or other editions). For any other uses, please submit a new request.
If credit is given to another source for the material you requested, permission must be obtained from that source.
BACK
CLOSE WINDOW
© 2020 Copyright - All Rights Reserved | Copyright Clearance Center, Inc. | Privacy statement | Terms and Conditions
Comments? We would like to hear from you. E-mail us at customercare@copyright.com

Figure 2.8(a–d)

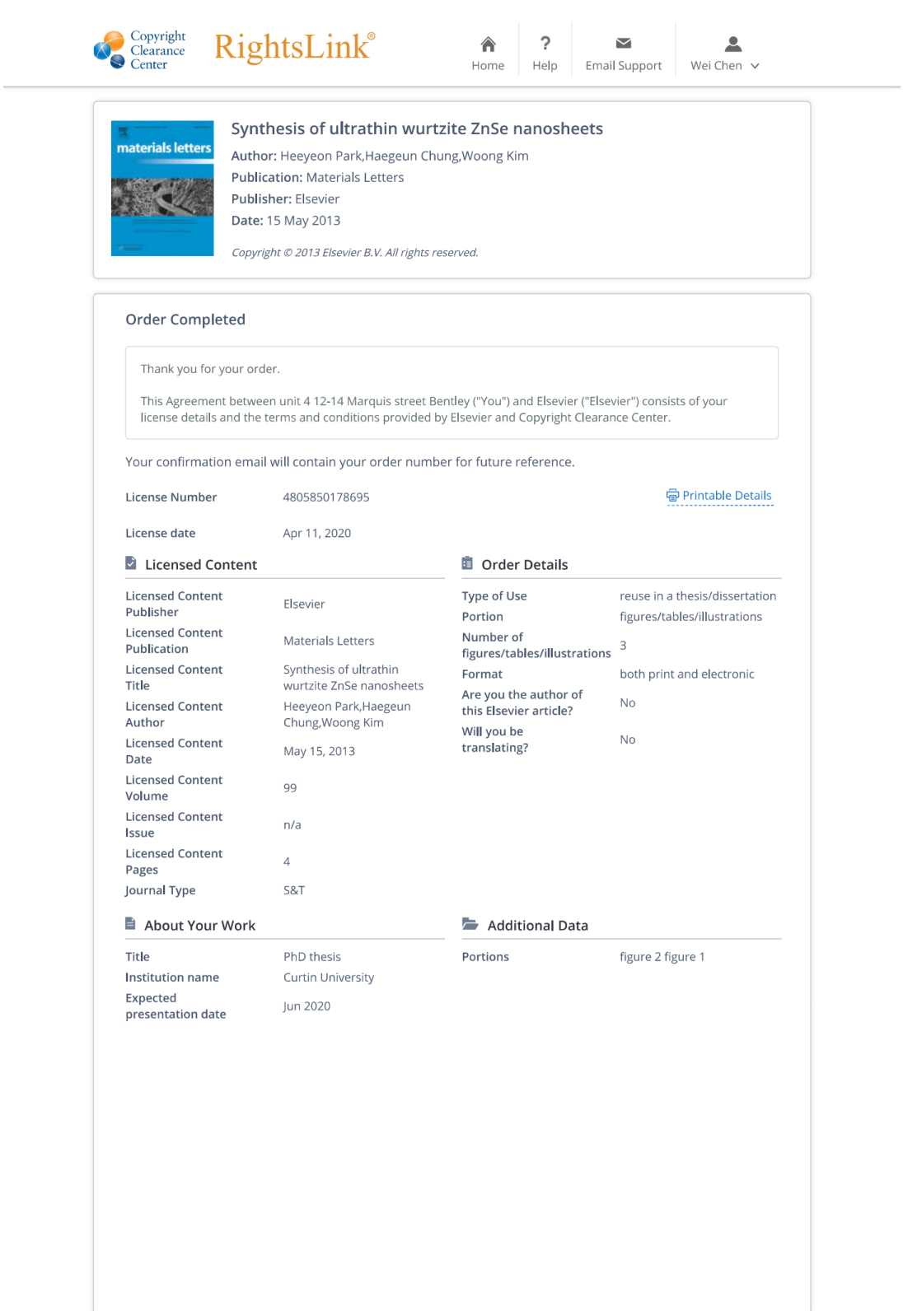

Copyright Clearance Center RightsLink®

Home | Help | Email Support | Wei Chen

Synthesis of ultrathin wurtzite ZnSe nanosheets

Author: Heeyeon Park,Haegeun Chung,Woong Kim
Publication: Materials Letters
Publisher: Elsevier
Date: 15 May 2013

Order Completed

Thank you for your order.

This Agreement between unit 4 12-14 Marquis street Bentley ("You") and Elsevier ("Elsevier") consists of your license details and the terms and conditions provided by Elsevier and Copyright Clearance Center.

Your confirmation email will contain your order number for future reference.

Printable Details

License Number	4805850178695
License date	Apr 11, 2020

Licensed Content

Licensed Content Publisher	Elsevier
Licensed Content Publication	Materials Letters
Licensed Content Title	Synthesis of ultrathin wurtzite ZnSe nanosheets
Licensed Content Author	Heeyeon Park,Haegeun Chung,Woong Kim
Licensed Content Date	May 15, 2013
Licensed Content Volume	99
Licensed Content Issue	n/a
Licensed Content Pages	4
Journal Type	S&T

Order Details

Type of Use	reuse in a thesis/dissertation
Portion	figures/tables/illustrations
Number of figures/tables/illustrations	3
Format	both print and electronic
Are you the author of this Elsevier article?	No
Will you be translating?	No

About Your Work

Title	PhD thesis
Institution name	Curtin University
Expected presentation date	Jun 2020

Additional Data

Portions	figure 2 figure 1

Figure 2.8(e–q)

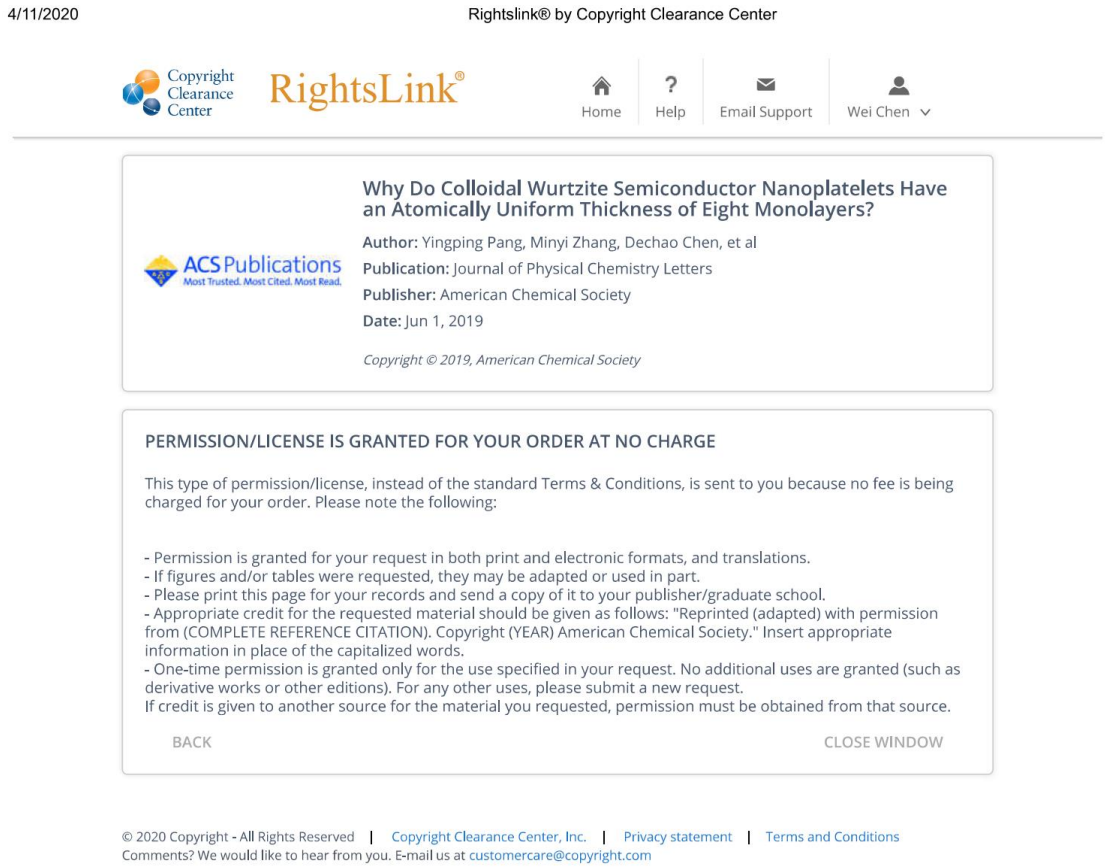

Figure 2.9

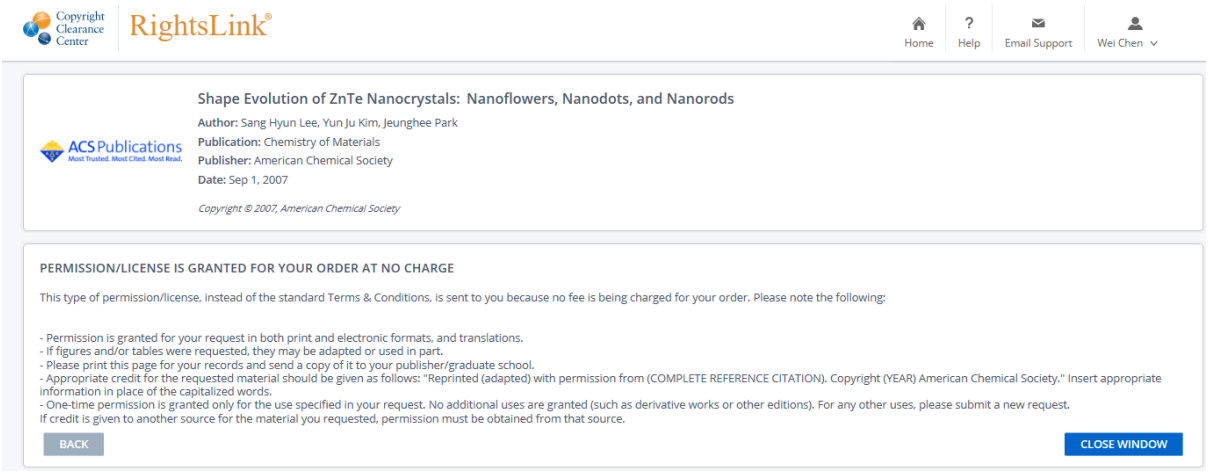

Figure 2.10

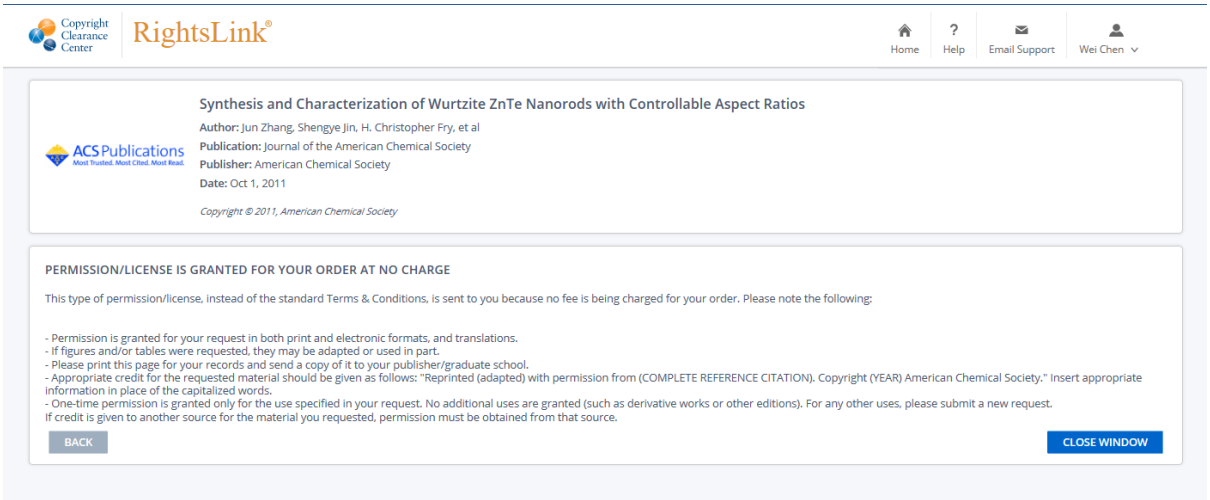

Figure 2.11 (a–d)

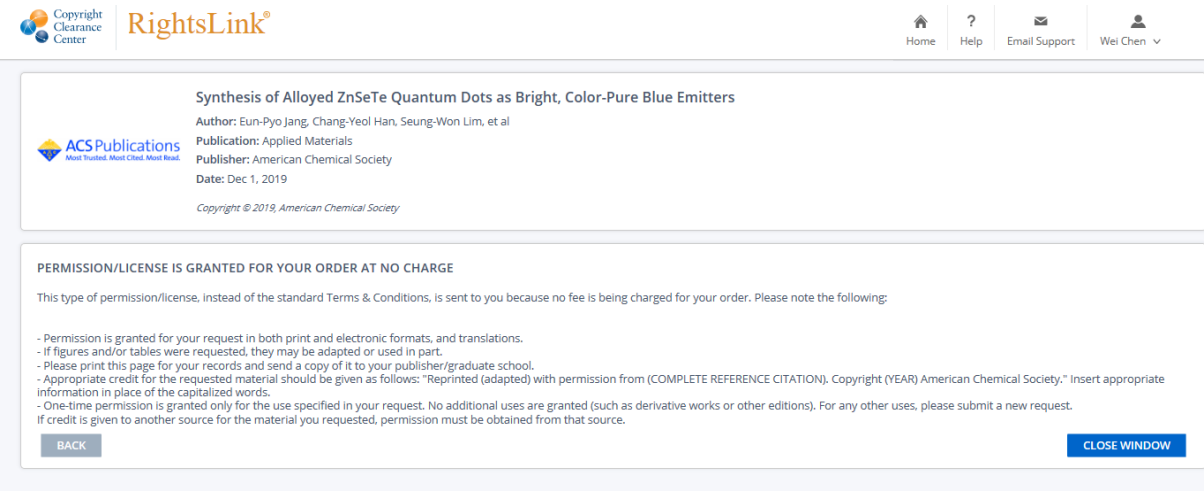

Figure 2.11 (e–h)

This page is available in the following languages:

Creative Commons Licer Deed

Attribution 4.0 International (CC BY 4.0)

This is a human-readable summary of (and not a substitute for) the license.

You are free to:

Share — copy and redistribute the material in any medium or format

Adapt — remix, transform, and build upon the material

for any purpose, even commercially.

The licensor cannot revoke these freedoms as long as you follow the license terms.

Under the following terms:

Attribution — You must give appropriate credit, provide a link to the license, and indicate if changes were made. You may do so in any reasonable manner, but not in any way that suggests the licensor endorses you or your use.

No additional restrictions — You may not apply legal terms or technological measures that legally restrict others from doing anything the license permits.

Notices:

You do not have to comply with the license for elements of the material in the public domain or where your use is permitted by an applicable exception or limitation.

No warranties are given. The license may not give you all of the permissions necessary for your intended use. For example, other rights such as publicity, privacy, or moral rights may limit how you use the material.

Figure 2.12

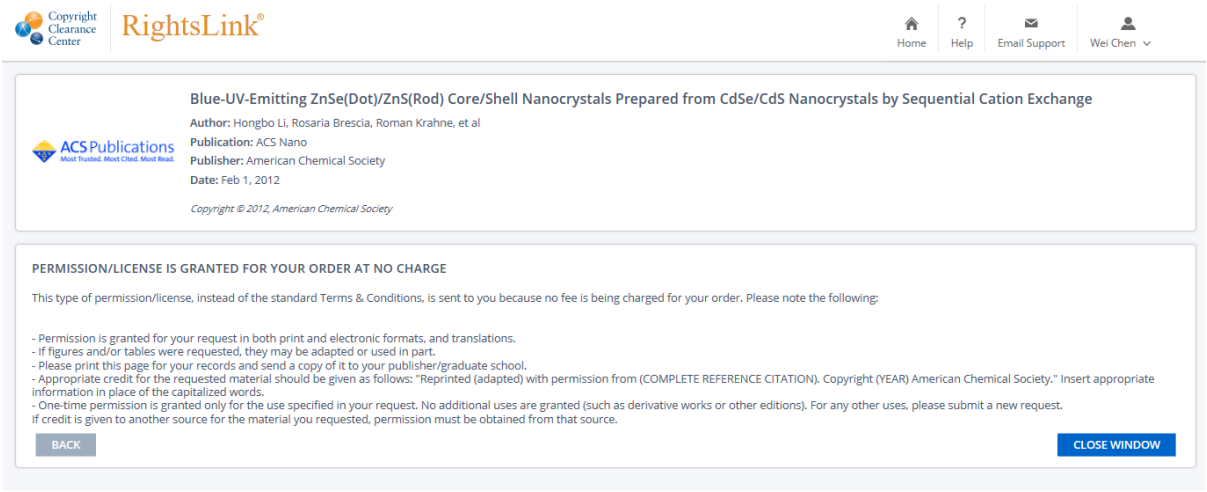

Figure 2.13

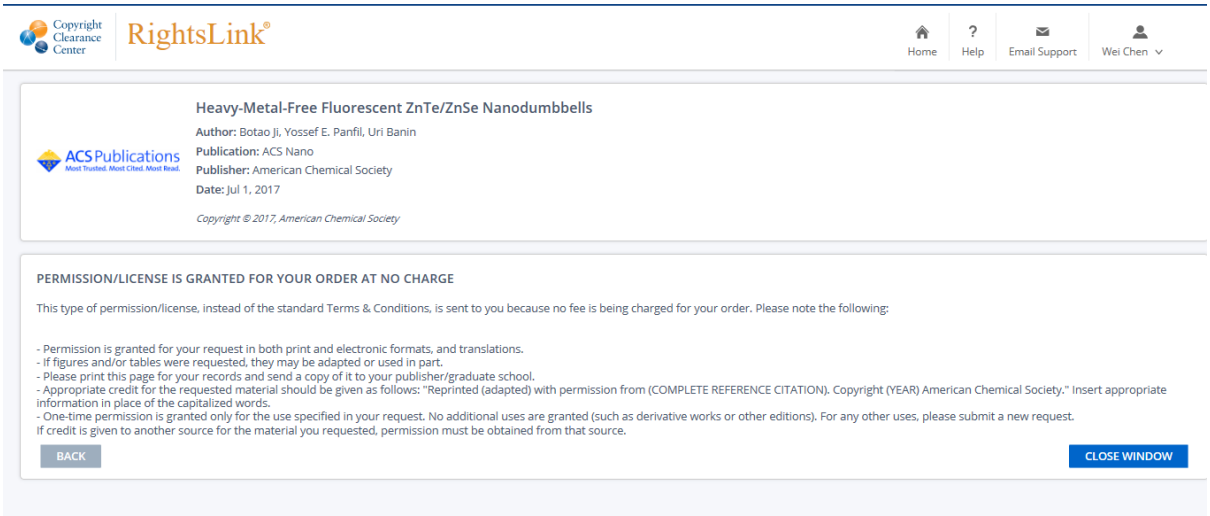

Figure 2.14(a–d)

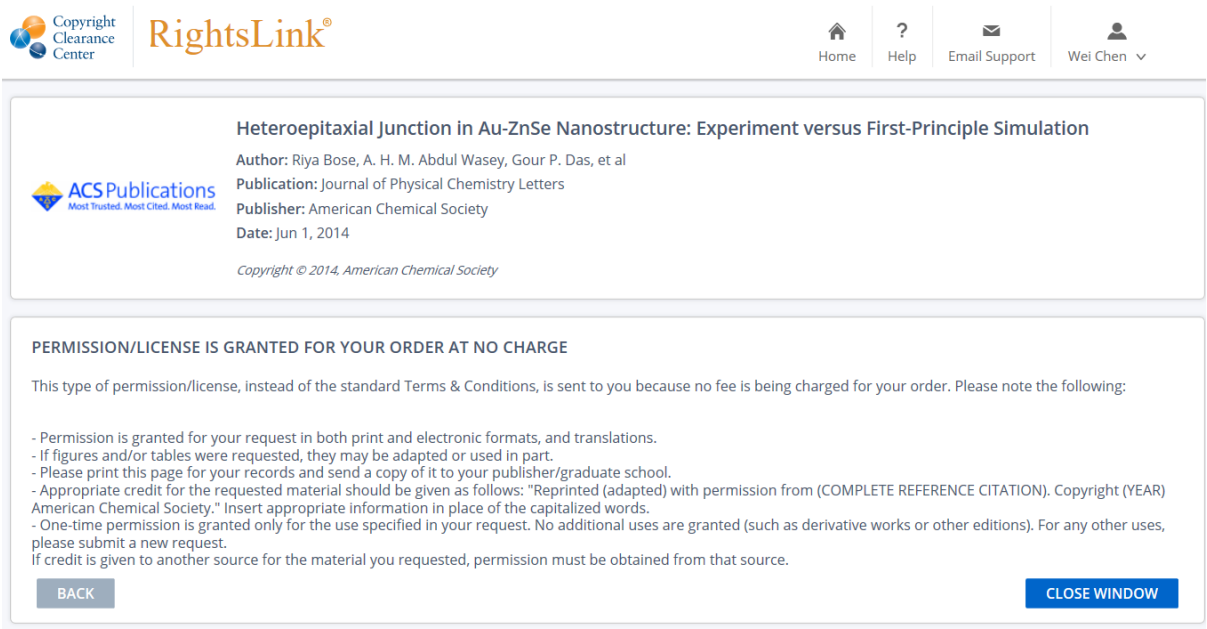

Figure 2.14(e–j)

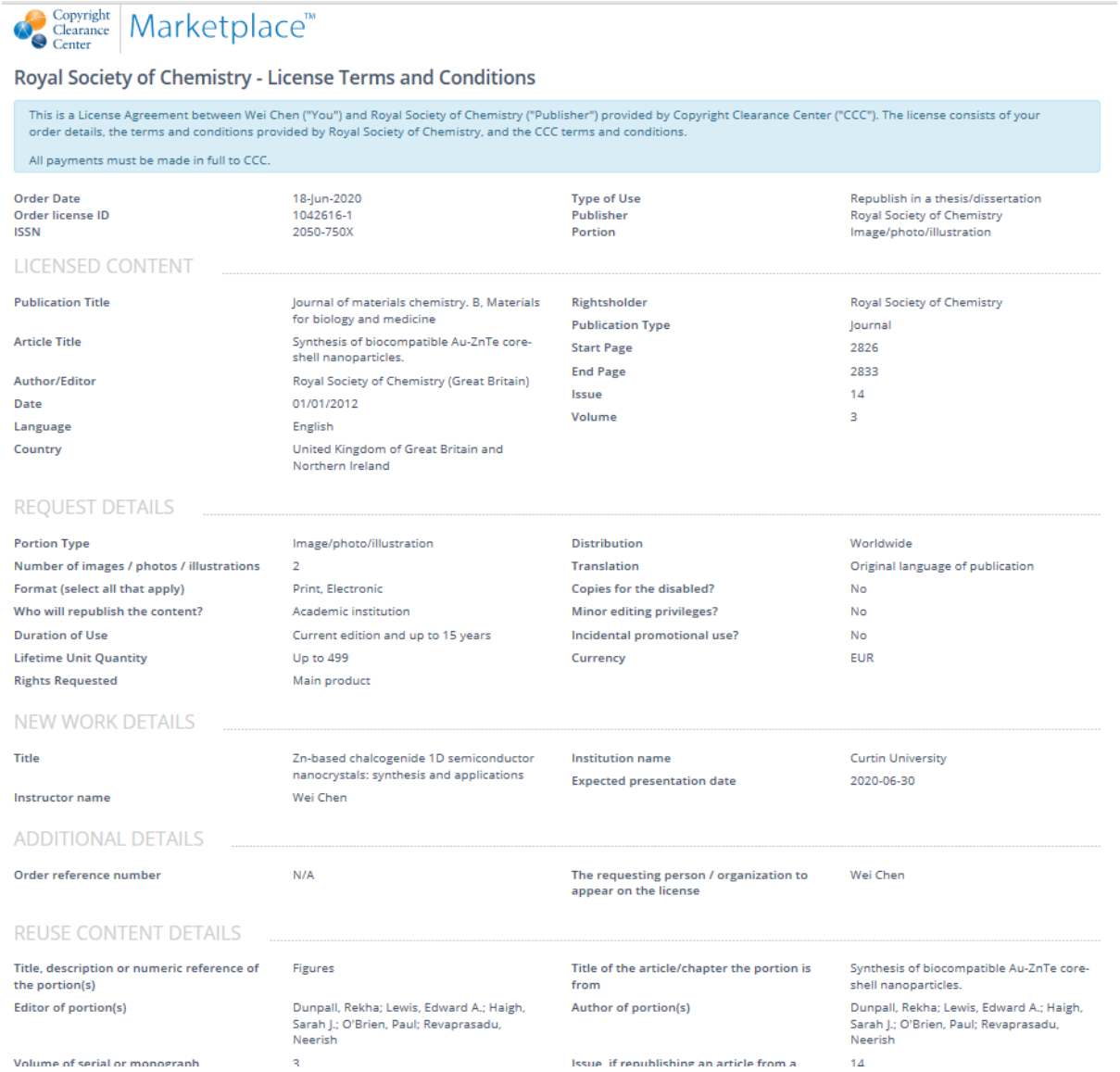

Copyright Clearance Center Marketplace™

Royal Society of Chemistry - License Terms and Conditions

This is a License Agreement between Wei Chen ("You") and Royal Society of Chemistry ("Publisher") provided by Copyright Clearance Center ("CCC"). The license consists of your order details, the terms and conditions provided by Royal Society of Chemistry, and the CCC terms and conditions.

All payments must be made in full to CCC.

Order Date	18-Jun-2020	Type of Use	Republish in a thesis/dissertation
Order license ID	1042616-1	Publisher	Royal Society of Chemistry
ISSN	2050-750X	Portion	Image/photo/illustration

LICENSED CONTENT

Publication Title	Journal of materials chemistry. B, Materials for biology and medicine	Rightsholder	Royal Society of Chemistry
Article Title	Synthesis of biocompatible Au-ZnTe core-shell nanoparticles.	Publication Type	Journal
Author/Editor	Royal Society of Chemistry (Great Britain)	Start Page	2826
Date	01/01/2012	End Page	2833
Language	English	Issue	14
Country	United Kingdom of Great Britain and Northern Ireland	Volume	3

REQUEST DETAILS

Portion Type	Image/photo/illustration	Distribution	Worldwide
Number of images / photos / illustrations	2	Translation	Original language of publication
Format (select all that apply)	Print, Electronic	Copies for the disabled?	No
Who will republish the content?	Academic institution	Minor editing privileges?	No
Duration of Use	Current edition and up to 15 years	Incidental promotional use?	No
Lifetime Unit Quantity	Up to 499	Currency	EUR
Rights Requested	Main product		

NEW WORK DETAILS

Title	Zn-based chalcogenide 1D semiconductor nanocrystals: synthesis and applications	Institution name	Curtin University
Instructor name	Wei Chen	Expected presentation date	2020-06-30

ADDITIONAL DETAILS

Order reference number	N/A	The requesting person / organization to appear on the license	Wei Chen

REUSE CONTENT DETAILS

Title, description or numeric reference of the portion(s)	Figures	Title of the article/chapter the portion is from	Synthesis of biocompatible Au-ZnTe core-shell nanoparticles.
Editor of portion(s)	Dunpall, Rekha; Lewis, Edward A.; Haigh, Sarah J.; O'Brien, Paul; Revaprasadu, Neerish	Author of portion(s)	Dunpall, Rekha; Lewis, Edward A.; Haigh, Sarah J.; O'Brien, Paul; Revaprasadu, Neerish
Volume of serial or monograph	3	Issue, if republishing an article from a	14

Figure 2.15(a–c)

Copyright Clearance Center | Marketplace™

American Association for the Advancement of Science - License Terms and Conditions

This is a License Agreement between Wei Chen ("You") and American Association for the Advancement of Science ("Publisher") provided by Copyright Clearance Center ("CCC"). The license consists of your order details, the terms and conditions provided by American Association for the Advancement of Science, and the CCC terms and conditions.

All payments must be made in full to CCC.

Order Date	18-Jun-2020	Type of Use	Republish in a thesis/dissertation
Order license ID	1042653-1	Publisher	AMERICAN ASSOCIATION FOR THE ADVANCEMENT OF SCIENCE
ISSN	0036-8075	Portion	Chart/graph/table/figure

LICENSED CONTENT

Publication Title	Science	Rightsholder	American Association for the Advancement of Science
Article Title	Chemistry: Selective Growth of Metal Tips onto Semiconductor Quantum Rods and Tetrapods	Publication Type	Journal
Date	01/01/1880	Start Page	1787
Language	English	End Page	1789
Country	United States of America	Issue	5678

REQUEST DETAILS

Portion Type	Chart/graph/table/figure	Distribution	Worldwide
Number of charts / graphs / tables / figures requested	2	Translation	Original language of publication
Format (select all that apply)	Print, Electronic	Copies for the disabled?	No
Who will republish the content?	Not-for-profit entity	Minor editing privileges?	No
Duration of Use	Life of current edition	Incidental promotional use?	No
Lifetime Unit Quantity	Up to 499	Currency	USD
Rights Requested	Main product		

NEW WORK DETAILS

Title	Zn-based chalcogenide 1D semiconductor nanocrystals: synthesis and applications	Institution name	Curtin University
Instructor name	Wei Chen	Expected presentation date	2020-06-30

ADDITIONAL DETAILS

Order reference number	N/A	The requesting person / organization to appear on the license	Wei Chen

REUSE CONTENT DETAILS

Title, description or numeric reference of the portion(s)	Figures	Title of the article/chapter the portion is from	Chemistry: Selective Growth of Metal Tips onto Semiconductor Quantum Rods and Tetrapods
Editor of portion(s)	Banin, U.; Costi, R.; Popov, I.; Rothenberg, E.; Mokari, T.	Author of portion(s)	Banin, U.; Costi, R.; Popov, I.; Rothenberg, E.; Mokari, T.
Volume of serial or monograph	NA		
Page or page range of portion	1787-1789	Issue, if republishing an article from a serial	5678
		Publication date of portion	2004-01-01

Figure 2.15(d–f)

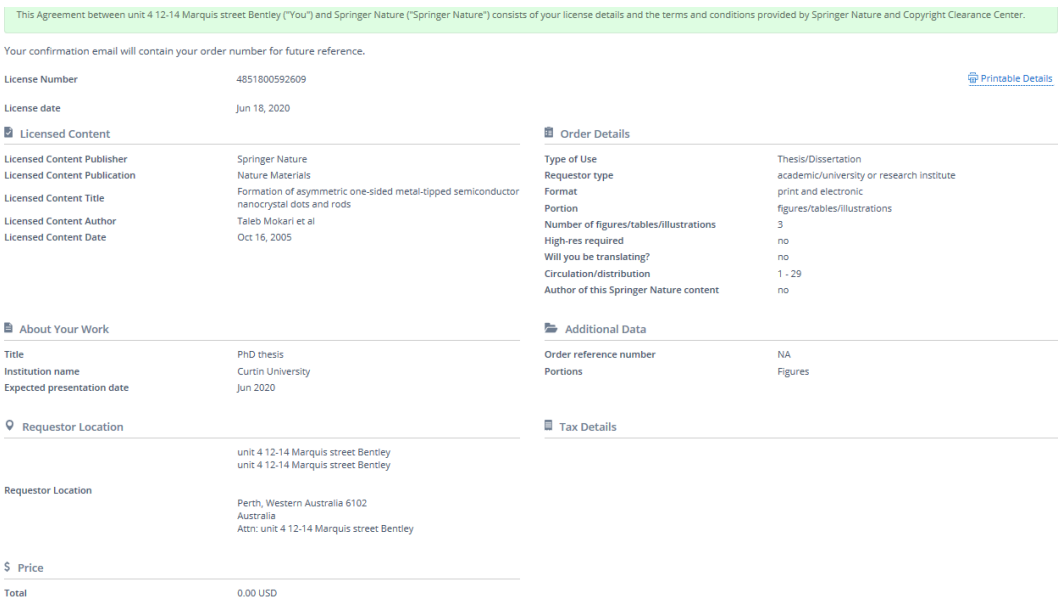

This Agreement between unit 4 12-14 Marquis street Bentley ("You") and Springer Nature ("Springer Nature") consists of your license details and the terms and conditions provided by Springer Nature and Copyright Clearance Center.

Your confirmation email will contain your order number for future reference.

License Number	4851800592609
License date	Jun 18, 2020

Printable Details

Licensed Content

Licensed Content Publisher	Springer Nature
Licensed Content Publication	Nature Materials
Licensed Content Title	Formation of asymmetric one-sided metal-tipped semiconductor nanocrystal dots and rods
Licensed Content Author	Taleb Mokari et al
Licensed Content Date	Oct 16, 2005

Order Details

Type of Use	Thesis/Dissertation
Requestor type	academic/university or research institute
Format	print and electronic
Portion	figures/tables/illustrations
Number of figures/tables/illustrations	3
High-res required	no
Will you be translating?	no
Circulation/distribution	1 - 29
Author of this Springer Nature content	no

About Your Work

Title	PhD thesis
Institution name	Curtin University
Expected presentation date	Jun 2020

Additional Data

Order reference number	NA
Portions	Figures

Requestor Location

Requestor Location	unit 4 12-14 Marquis street Bentley unit 4 12-14 Marquis street Bentley Perth, Western Australia 6102 Australia Attn: unit 4 12-14 Marquis street Bentley

Tax Details

Price

Total	0.00 USD

Figure 2.15(g–l)

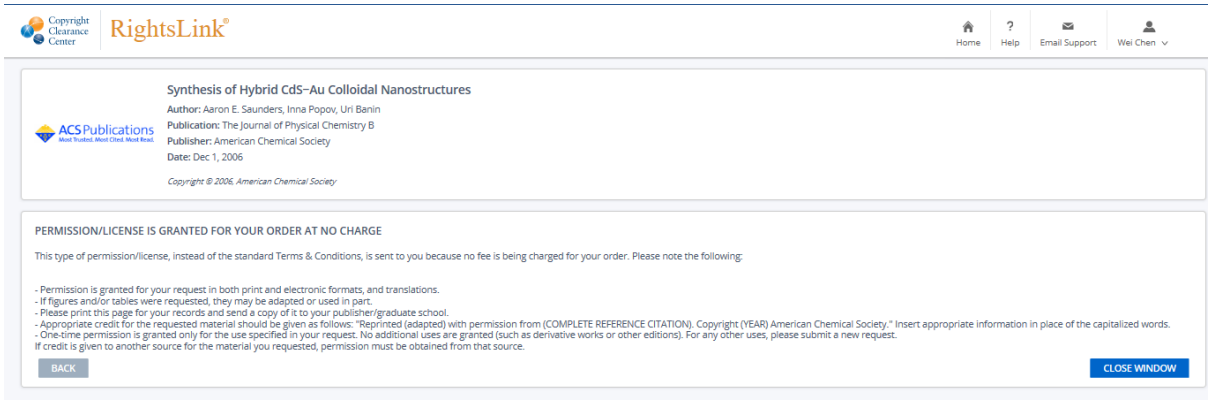

Figure 2.16 (a–i)

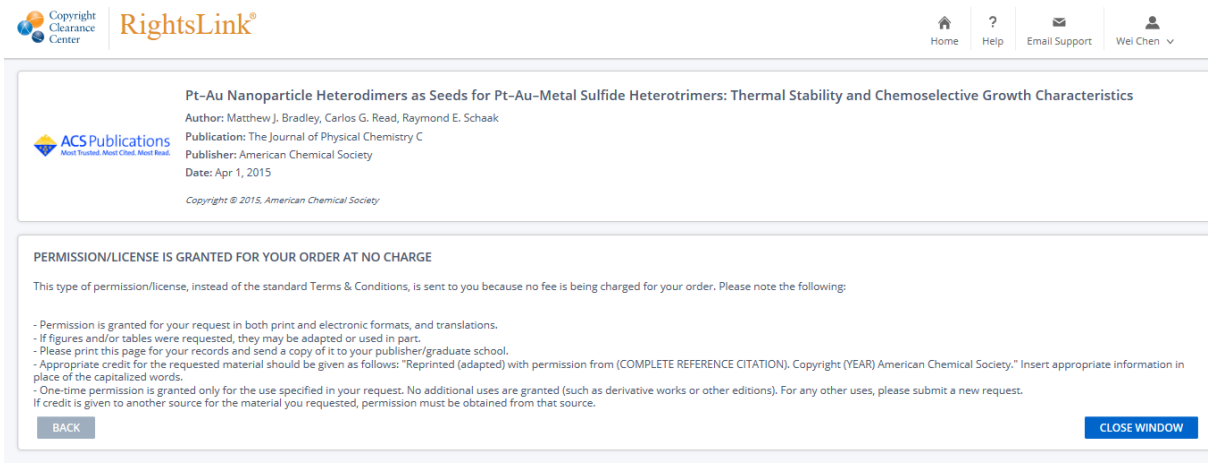

Figure 2.16 (j–n)

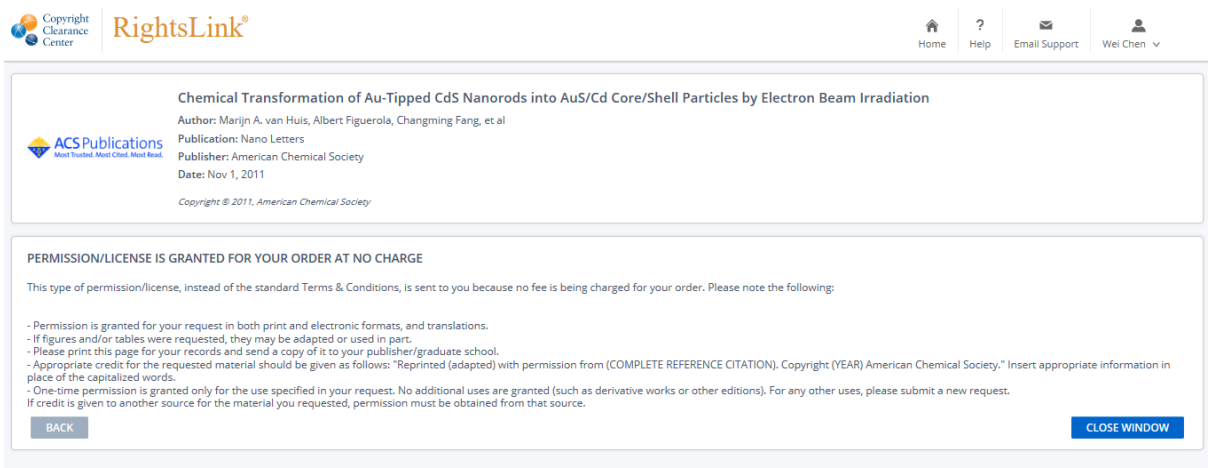

Figure 2.17 (a–d)

This Agreement between unit 4 12-14 Marquis street Bentley ("You") and John Wiley and Sons ("John Wiley and Sons") consists of your license details and the terms and conditions provided by John Wiley and Sons and Copyright Clearance Center.

Your confirmation email will contain your order number for future reference.

Printable Details

License Number	4851810033711
License date	Jun 18, 2020

Licensed Content

Licensed Content Publisher	John Wiley and Sons
Licensed Content Publication	Small
Licensed Content Title	Formation of Heteroepitaxy in Different Shapes of Au–CdSe Metal–Semiconductor Hybrid Nanostructures
Licensed Content Author	Amitava Patra, Narayan Pradhan, Krishna Kanta Haldar
Licensed Content Date	May 10, 2013
Licensed Content Volume	9
Licensed Content Issue	20
Licensed Content Pages	9

Order Details

Type of use	Dissertation/Thesis
Requestor type	University/Academic
Format	Print and electronic
Portion	Figure/table
Number of figures/tables	3
Will you be translating?	No

About Your Work

Title	PhD thesis
Institution name	Curtin University
Expected presentation date	Jun 2020

Additional Data

Order reference number	na
Portions	figures

Requestor Location

	unit 4 12-14 Marquis street Bentley unit 4 12-14 Marquis street Bentley
Requestor Location	Perth, Western Australia 6102 Australia Attn: unit 4 12-14 Marquis street Bentley

Tax Details

Publisher Tax ID	EU826007151

Price

Total	0.00 USD

Figure 2.17 (e–k)

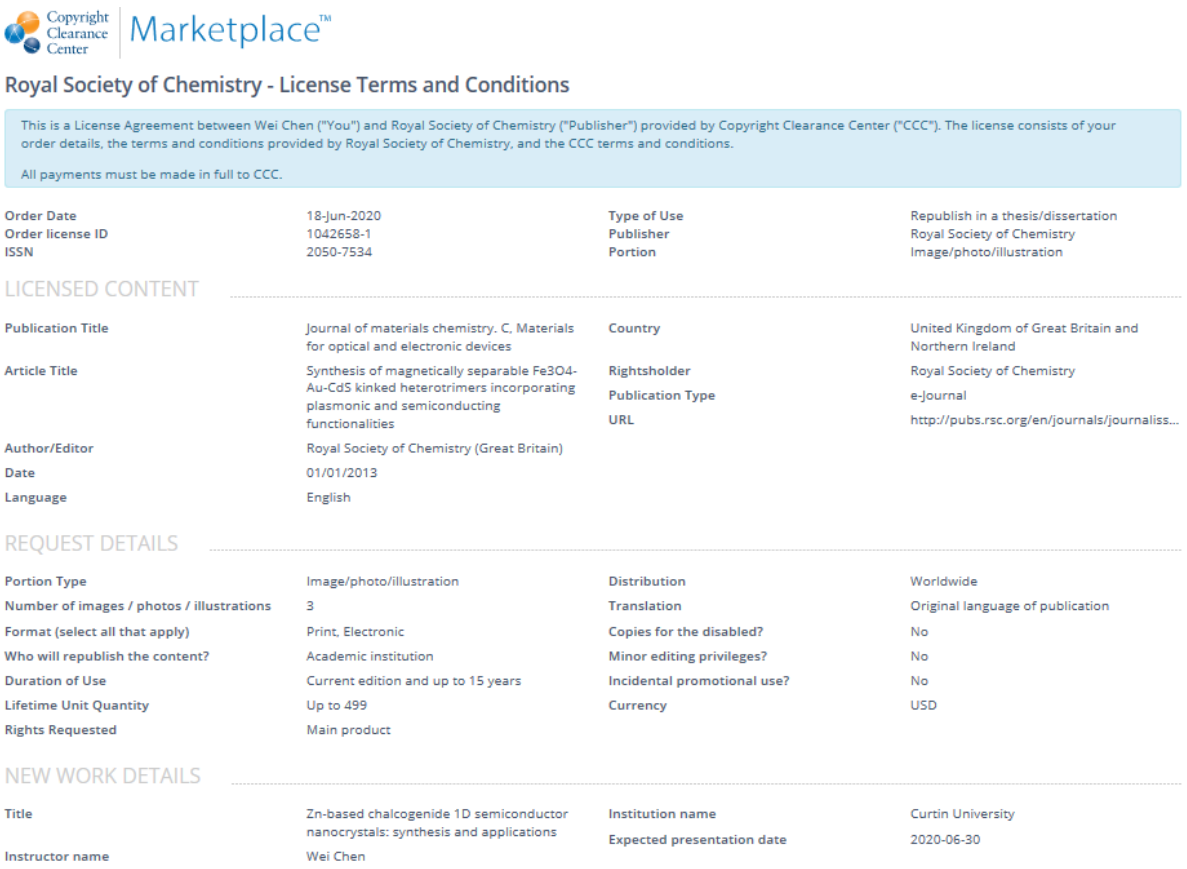

Copyright Clearance Center | Marketplace™

Royal Society of Chemistry - License Terms and Conditions

This is a License Agreement between Wei Chen ("You") and Royal Society of Chemistry ("Publisher") provided by Copyright Clearance Center ("CCC"). The license consists of your order details, the terms and conditions provided by Royal Society of Chemistry, and the CCC terms and conditions.

All payments must be made in full to CCC.

Order Date	18-Jun-2020	Type of Use	Republish in a thesis/dissertation
Order license ID	1042658-1	Publisher	Royal Society of Chemistry
ISSN	2050-7534	Portion	Image/photo/illustration

LICENSED CONTENT

Publication Title	Journal of materials chemistry. C, Materials for optical and electronic devices	Country	United Kingdom of Great Britain and Northern Ireland
Article Title	Synthesis of magnetically separable Fe3O4-Au-CdS kinked heterotrimers incorporating plasmonic and semiconducting functionalities	Rightsholder	Royal Society of Chemistry
		Publication Type	e-Journal
		URL	http://pubs.rsc.org/en/journals/journaliss...
Author/Editor	Royal Society of Chemistry (Great Britain)		
Date	01/01/2013		
Language	English		

REQUEST DETAILS

Portion Type	Image/photo/illustration	Distribution	Worldwide
Number of images / photos / illustrations	3	Translation	Original language of publication
Format (select all that apply)	Print, Electronic	Copies for the disabled?	No
Who will republish the content?	Academic institution	Minor editing privileges?	No
Duration of Use	Current edition and up to 15 years	Incidental promotional use?	No
Lifetime Unit Quantity	Up to 499	Currency	USD
Rights Requested	Main product		

NEW WORK DETAILS

Title	Zn-based chalcogenide 1D semiconductor nanocrystals: synthesis and applications	Institution name	Curtin University
		Expected presentation date	2020-06-30
Instructor name	Wei Chen		

Figure 2.17 (l–o)

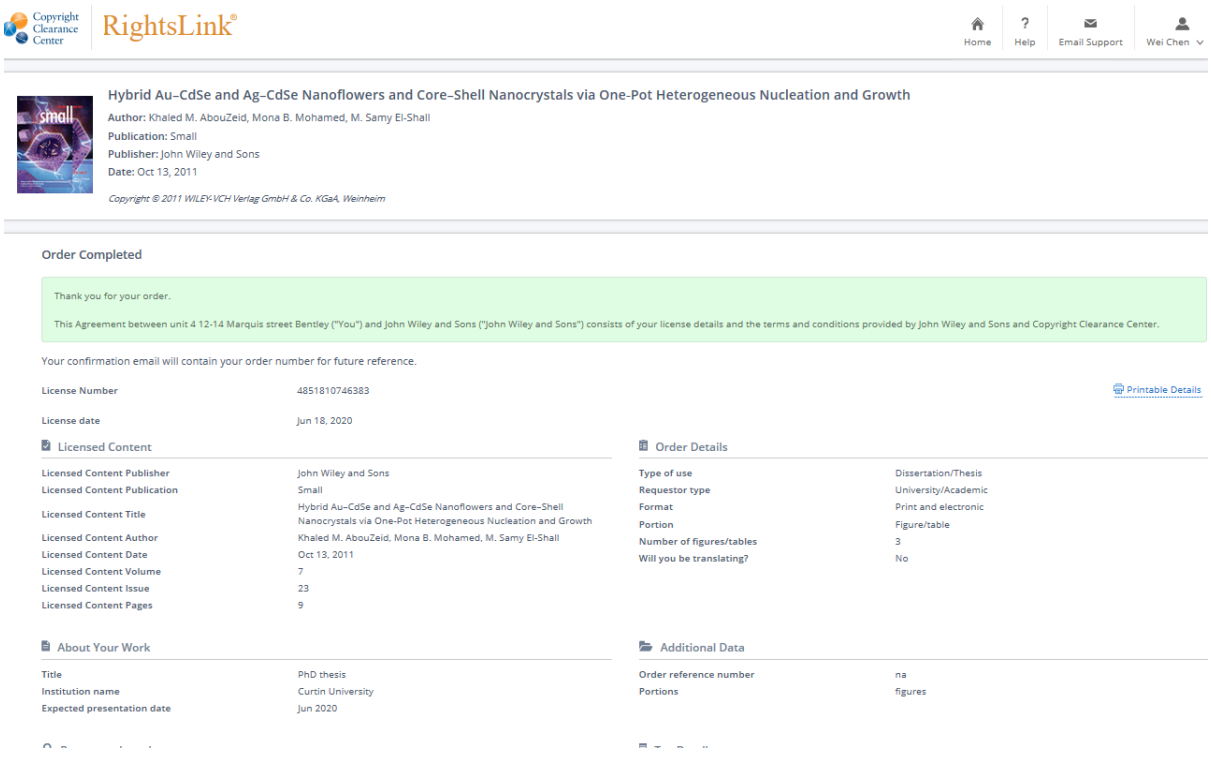

Figure 2.17 (p–s)

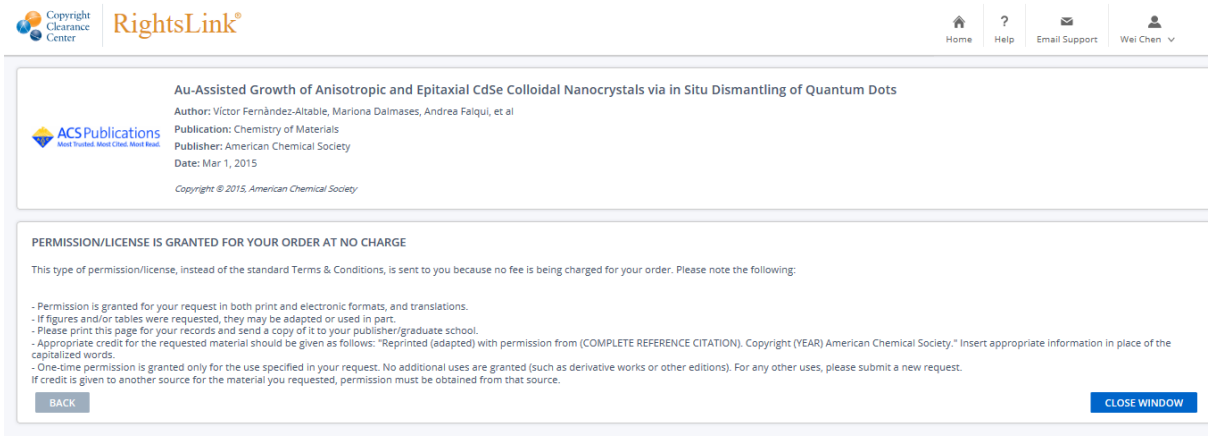

Figure 2.18 (a–f)

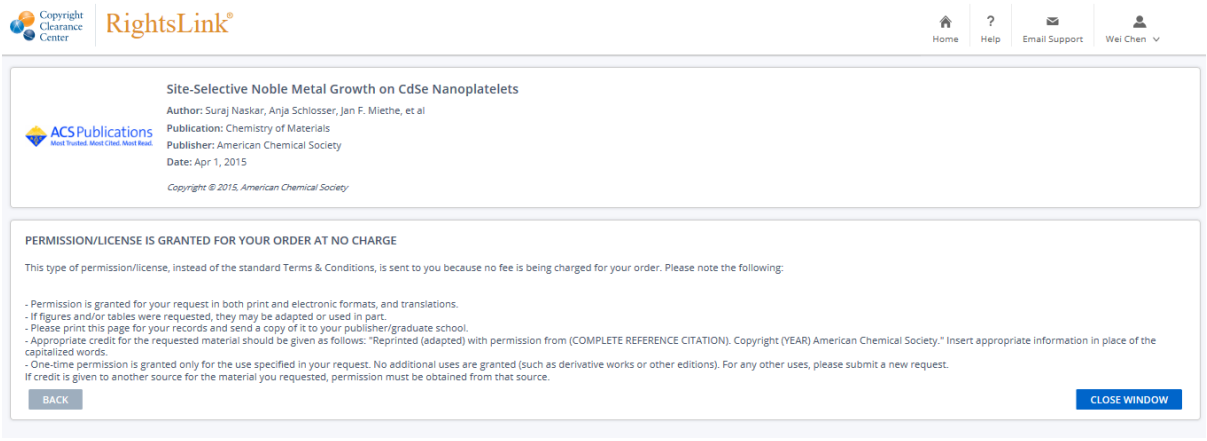

Figure 2.19 (a)

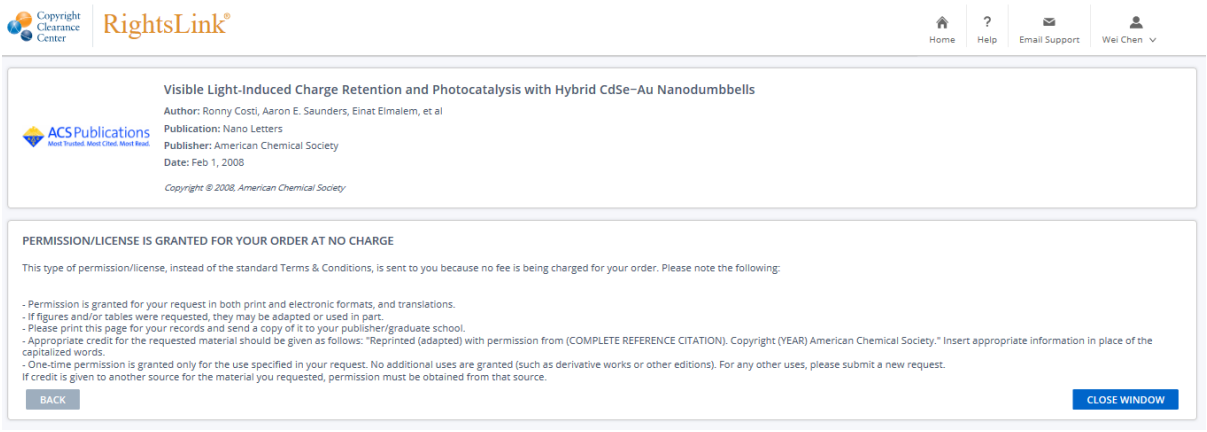

Figure 2.19 (b)

Figure 2.20 (a–d)

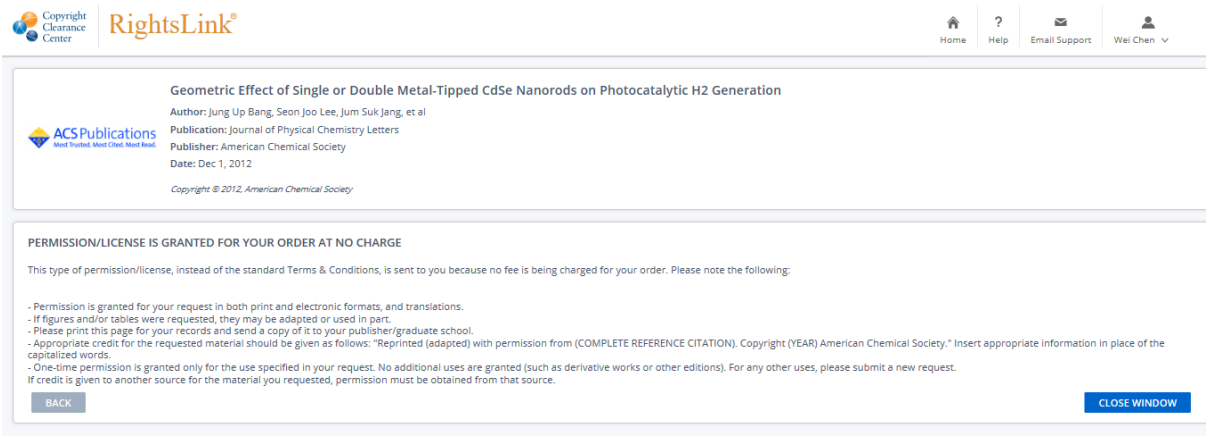

Figure 2.20 (e–g)

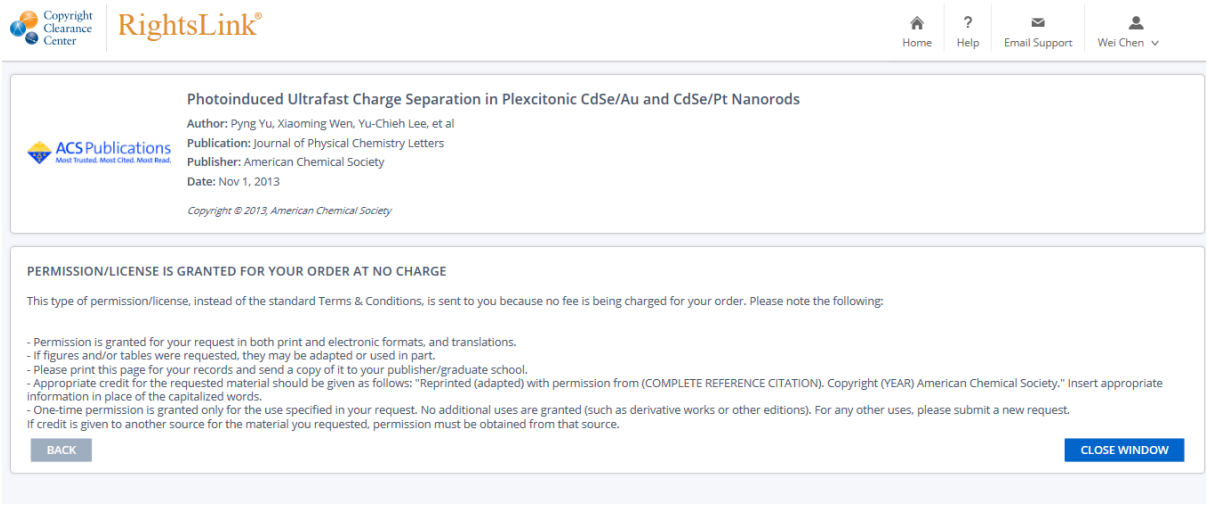

Figure 2.21 (a–d)

Copyright Clearance Center | Marketplace™

Royal Society of Chemistry - License Terms and Conditions

This is a License Agreement between wei chen ("You") and Royal Society of Chemistry ("Publisher") provided by Copyright Clearance Center ("CCC"). The license consists of your order details, the terms and conditions provided by Royal Society of Chemistry, and the CCC terms and conditions.

All payments must be made in full to CCC.

Order Date	18-Jun-2020	Type of Use	Republish in a thesis/dissertation
Order license ID	1042682-1	Publisher	Royal Society of Chemistry
ISSN	2050-7496	Portion	Image/photo/illustration

LICENSED CONTENT

Publication Title	Journal of materials chemistry. A, Materials for energy and sustainability	Publication Type	e-Journal
Article Title	The golden gate to photocatalytic hydrogen production	Start Page	19679
Author/Editor	Royal Society of Chemistry (Great Britain)	End Page	19682
Date	01/01/2013	Issue	39
Language	English	Volume	3
Country	United Kingdom of Great Britain and Northern Ireland	URL	http://pubs.rsc.org/en/journals/journaliss...
Rightsholder	Royal Society of Chemistry		

REQUEST DETAILS

Portion Type	Image/photo/illustration	Distribution	Worldwide
Number of images / photos / illustrations	3	Translation	Original language of publication
Format (select all that apply)	Print, Electronic	Copies for the disabled?	No
Who will republish the content?	Academic institution	Minor editing privileges?	No
Duration of Use	Current edition and up to 15 years	Incidental promotional use?	No
Lifetime Unit Quantity	Up to 499	Currency	USD
Rights Requested	Main product		

NEW WORK DETAILS

Title	Zn-based chalcogenide 1D semiconductor nanocrystals: synthesis and applications	Institution name	Curtin University
Instructor name	Wei Chen	Expected presentation date	2020-06-30

ADDITIONAL DETAILS

Order reference number	na	The requesting person / organization to appear on the license	wei chen

Figure 2.21 (h–j)

Copyright Clearance Center | RightsLink®

Home | Help | Email Support | Wei Chen

ACS Publications
Most Trusted. Most Cited. Most Read.

Engineering Reaction Kinetics by Tailoring the Metal Tips of Metal–Semiconductor Nanodumbbells

Author: Ji Yong Choi, Dahyi Jeong, Seon Joo Lee, et al
Publication: Nano Letters
Publisher: American Chemical Society
Date: Sep 1, 2017

Copyright © 2017, American Chemical Society

PERMISSION/LICENSE IS GRANTED FOR YOUR ORDER AT NO CHARGE

This type of permission/license, instead of the standard Terms & Conditions, is sent to you because no fee is being charged for your order. Please note the following:

- Permission is granted for your request in both print and electronic formats, and translations.
- If figures and/or tables were requested, they may be adapted or used in part.
- Please print this page for your records and send a copy of it to your publisher/graduate school.
- Appropriate credit for the requested material should be given as follows: "Reprinted (adapted) with permission from (COMPLETE REFERENCE CITATION). Copyright (YEAR) American Chemical Society." Insert appropriate information in place of the capitalized words.
- One-time permission is granted only for the use specified in your request. No additional uses are granted (such as derivative works or other editions). For any other uses, please submit a new request.

If credit is given to another source for the material you requested, permission must be obtained from that source.

BACK | CLOSE WINDOW

Figure 2.22 (a–h)

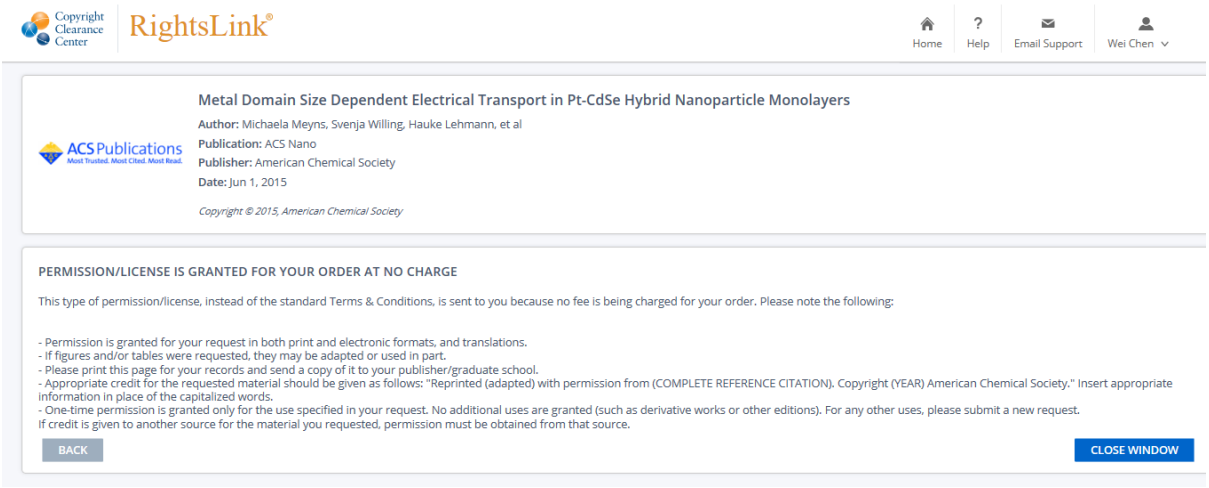

Copyright Clearance Center | RightsLink®

Home | Help | Email Support | Wei Chen

ACS Publications
Most Trusted. Most Cited. Most Read.

Metal Domain Size Dependent Electrical Transport in Pt-CdSe Hybrid Nanoparticle Monolayers

Author: Michaela Meyns, Svenja Willing, Hauke Lehmann, et al
Publication: ACS Nano
Publisher: American Chemical Society
Date: Jun 1, 2015

Copyright © 2015, American Chemical Society

PERMISSION/LICENSE IS GRANTED FOR YOUR ORDER AT NO CHARGE

This type of permission/license, instead of the standard Terms & Conditions, is sent to you because no fee is being charged for your order. Please note the following:

- Permission is granted for your request in both print and electronic formats, and translations.
- If figures and/or tables were requested, they may be adapted or used in part.
- Please print this page for your records and send a copy of it to your publisher/graduate school.
- Appropriate credit for the requested material should be given as follows: "Reprinted (adapted) with permission from (COMPLETE REFERENCE CITATION). Copyright (YEAR) American Chemical Society." Insert appropriate information in place of the capitalized words.
- One-time permission is granted only for the use specified in your request. No additional uses are granted (such as derivative works or other editions). For any other uses, please submit a new request.

If credit is given to another source for the material you requested, permission must be obtained from that source.

BACK | CLOSE WINDOW

Figure 2.22 (i–j)

This Agreement between unit 4 12-14 Marquis street Bentley ("You") and John Wiley and Sons ("John Wiley and Sons") consists of your license details and the terms and conditions provided by John Wiley and Sons and Copyright Clearance Center.

Your confirmation email will contain your order number for future reference.

Printable Details

License Number	4851841328047
License date	Jun 18, 2020

Licensed Content

Licensed Content Publisher	John Wiley and Sons
Licensed Content Publication	Advanced Materials
Licensed Content Title	Self-Assembled Au/CdSe Nanocrystal Clusters for Plasmon-Mediated Photocatalytic Hydrogen Evolution
Licensed Content Author	Tierui Zhang, Yadong Yin, Chen-Ho Tung, et al
Licensed Content Date	May 12, 2017
Licensed Content Volume	29
Licensed Content Issue	27
Licensed Content Pages	7

Order Details

Type of use	Dissertation/Thesis
Requestor type	University/Academic
Format	Print and electronic
Portion	Figure/table
Number of figures/tables	4
Will you be translating?	No

About Your Work

Title	Zn-based chalcogenide 1D semiconductor nanocrystals: synthesis and applications-PhD thesis Wei Chen
Institution name	Curtin University
Expected presentation date	Jun 2020

Additional Data

Order reference number	na
Portions	figures

Requestor Location

	unit 4 12-14 Marquis street Bentley unit 4 12-14 Marquis street Bentley
Requestor Location	Perth, Western Australia 6102 Australia Attn: unit 4 12-14 Marquis street Bentley

Tax Details

Publisher Tax ID	EU826007151

Figure 2.23 (a–e)

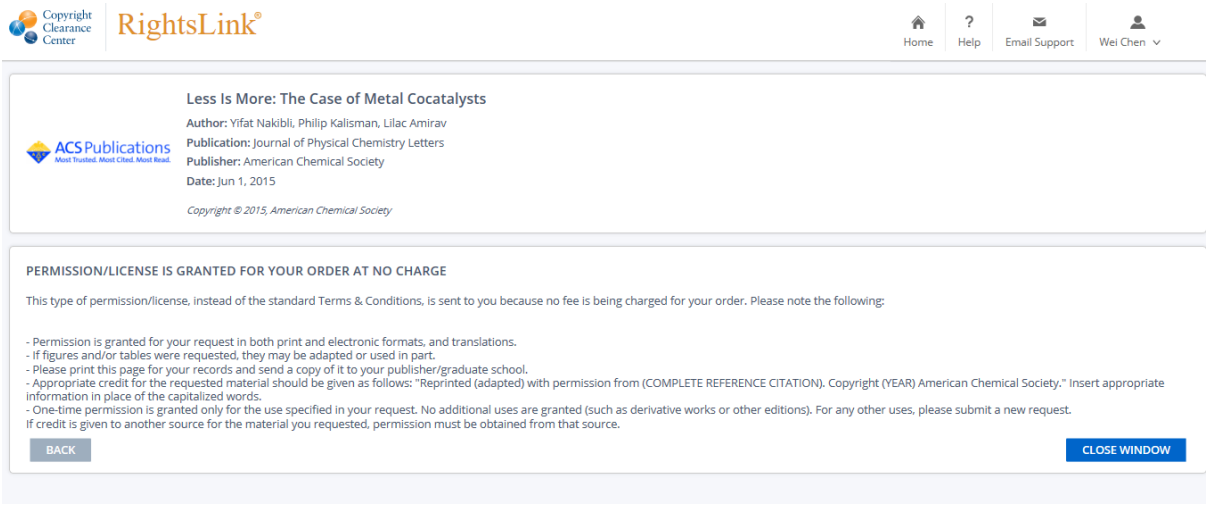

Figure 2.23 (f–j)

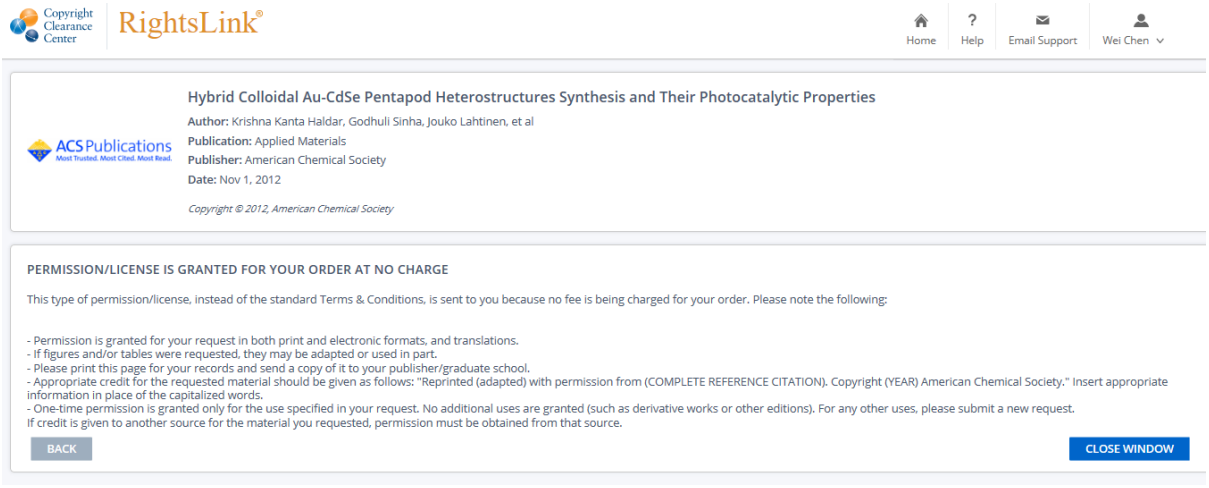

Figure 2.24 (a–c)

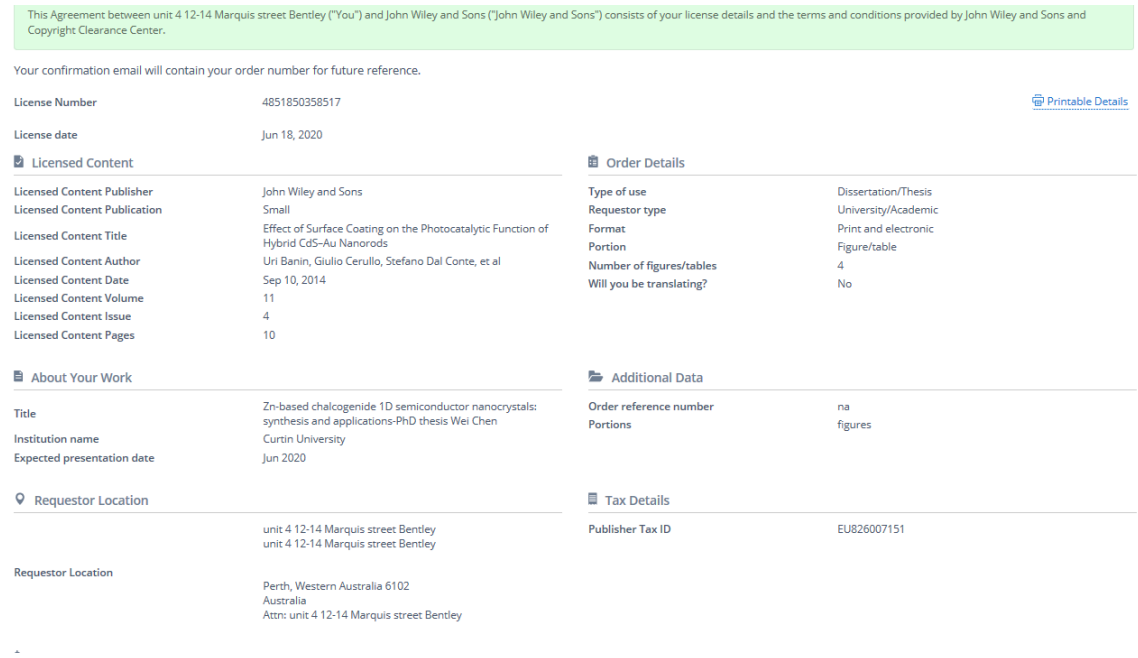

This Agreement between unit 4 12-14 Marquis street Bentley ("You") and John Wiley and Sons ("John Wiley and Sons") consists of your license details and the terms and conditions provided by John Wiley and Sons and Copyright Clearance Center.

Your confirmation email will contain your order number for future reference.

Printable Details

License Number	4851850358517
License date	Jun 18, 2020

Licensed Content

Licensed Content Publisher	John Wiley and Sons
Licensed Content Publication	Small
Licensed Content Title	Effect of Surface Coating on the Photocatalytic Function of Hybrid CdS–Au Nanorods
Licensed Content Author	Uri Banin, Giulio Cerullo, Stefano Dal Conte, et al
Licensed Content Date	Sep 10, 2014
Licensed Content Volume	11
Licensed Content Issue	4
Licensed Content Pages	10

Order Details

Type of use	Dissertation/Thesis
Requestor type	University/Academic
Format	Print and electronic
Portion	Figure/table
Number of figures/tables	4
Will you be translating?	No

About Your Work

Title	Zn-based chalcogenide 1D semiconductor nanocrystals: synthesis and applications-PhD thesis Wei Chen
Institution name	Curtin University
Expected presentation date	Jun 2020

Additional Data

Order reference number	na
Portions	figures

Requestor Location

Requestor Location	unit 4 12-14 Marquis street Bentley unit 4 12-14 Marquis street Bentley Perth, Western Australia 6102 Australia Attn: unit 4 12-14 Marquis street Bentley

Tax Details

Publisher Tax ID	EU826007151

Figure 2.25 (a–d)

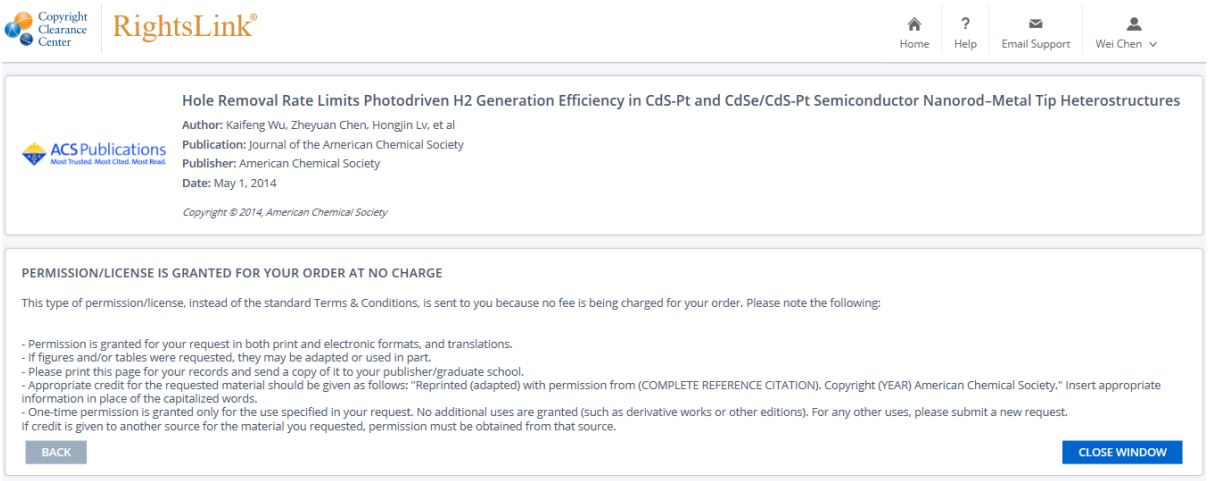

Copyright Clearance Center RightsLink®

Home | Help | Email Support | Wei Chen

ACS Publications Most Trusted. Most Cited. Most Read.

Hole Removal Rate Limits Photodriven H2 Generation Efficiency in CdS-Pt and CdSe/CdS-Pt Semiconductor Nanorod–Metal Tip Heterostructures

Author: Kaifeng Wu, Zheyuan Chen, Hongjin Lv, et al
Publication: Journal of the American Chemical Society
Publisher: American Chemical Society
Date: May 1, 2014

Copyright © 2014, American Chemical Society

PERMISSION/LICENSE IS GRANTED FOR YOUR ORDER AT NO CHARGE

This type of permission/license, instead of the standard Terms & Conditions, is sent to you because no fee is being charged for your order. Please note the following:

- Permission is granted for your request in both print and electronic formats, and translations.
- If figures and/or tables were requested, they may be adapted or used in part.
- Please print this page for your records and send a copy of it to your publisher/graduate school.
- Appropriate credit for the requested material should be given as follows: "Reprinted (adapted) with permission from (COMPLETE REFERENCE CITATION). Copyright (YEAR) American Chemical Society." Insert appropriate information in place of the capitalized words.
- One-time permission is granted only for the use specified in your request. No additional uses are granted (such as derivative works or other editions). For any other uses, please submit a new request.

If credit is given to another source for the material you requested, permission must be obtained from that source.

BACK CLOSE WINDOW

Figure 2.25 (e,f)

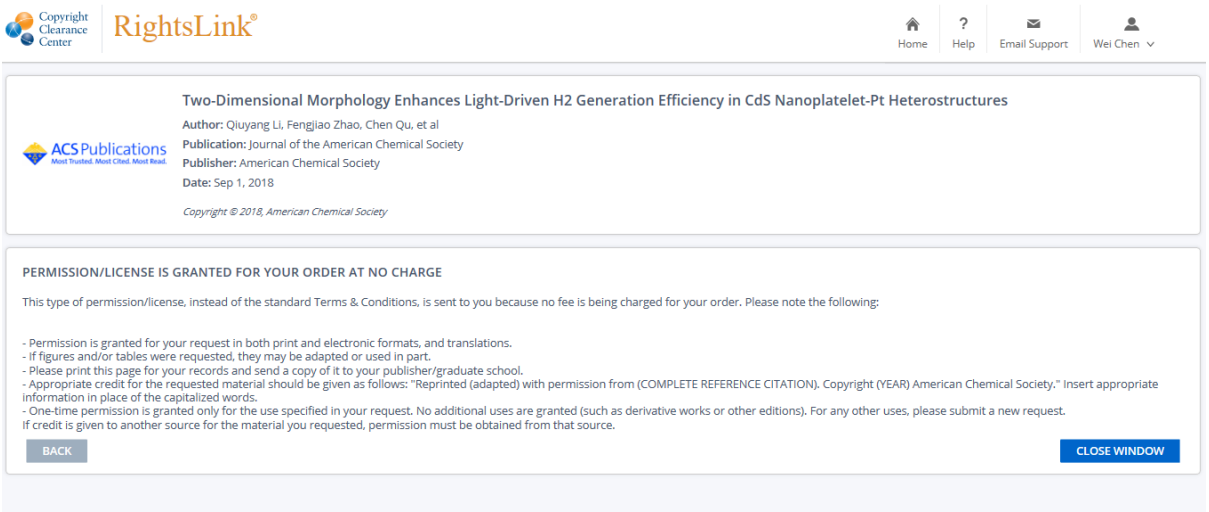

Copyright Clearance Center RightsLink®

Home | Help | Email Support | Wei Chen

ACS Publications Most Trusted. Most Cited. Most Read.

Two-Dimensional Morphology Enhances Light-Driven H2 Generation Efficiency in CdS Nanoplatelet-Pt Heterostructures

Author: Qiuyang Li, Fengjiao Zhao, Chen Qu, et al
Publication: Journal of the American Chemical Society
Publisher: American Chemical Society
Date: Sep 1, 2018

Copyright © 2018, American Chemical Society

PERMISSION/LICENSE IS GRANTED FOR YOUR ORDER AT NO CHARGE

This type of permission/license, instead of the standard Terms & Conditions, is sent to you because no fee is being charged for your order. Please note the following:

- Permission is granted for your request in both print and electronic formats, and translations.
- If figures and/or tables were requested, they may be adapted or used in part.
- Please print this page for your records and send a copy of it to your publisher/graduate school.
- Appropriate credit for the requested material should be given as follows: "Reprinted (adapted) with permission from (COMPLETE REFERENCE CITATION). Copyright (YEAR) American Chemical Society." Insert appropriate information in place of the capitalized words.
- One-time permission is granted only for the use specified in your request. No additional uses are granted (such as derivative works or other editions). For any other uses, please submit a new request.

If credit is given to another source for the material you requested, permission must be obtained from that source.

BACK CLOSE WINDOW

Figure 2.26 (a–e)

Royal Society of Chemistry - License Terms and Conditions

This is a License Agreement between Wei Chen ("You") and Royal Society of Chemistry ("Publisher") provided by Copyright Clearance Center ("CCC"). The license consists of your order details, the terms and conditions provided by Royal Society of Chemistry, and the CCC terms and conditions.

All payments must be made in full to CCC.

Order Date	18-Jun-2020	Type of Use	Republish in a thesis/dissertation
Order license ID	1042690-1	Publisher	Royal Society of Chemistry
ISSN	2055-6764	Portion	Image/photo/illustration

LICENSED CONTENT

Publication Title	Nanoscale Horizons	Country	United Kingdom of Great Britain and Northern Ireland
Author/Editor	Guo jia na mi ke xue zhong xin (China),, Royal Society of Chemistry (Great Britain),	Rightsholder	Royal Society of Chemistry
Date	01/01/2016	Publication Type	e-Journal
Language	English		

REQUEST DETAILS

Portion Type	Image/photo/illustration	Distribution	Worldwide
Number of images / photos / illustrations	1	Translation	Original language of publication
Format (select all that apply)	Print, Electronic	Copies for the disabled?	No
Who will republish the content?	Academic institution	Minor editing privileges?	No
Duration of Use	Current edition and up to 15 years	Incidental promotional use?	No
Lifetime Unit Quantity	Up to 499	Currency	USD
Rights Requested	Main product		

NEW WORK DETAILS

Title	Zn-based chalcogenide 1D semiconductor nanocrystals: synthesis and applications	Institution name	Curtin University
Instructor name	Wei Chen	Expected presentation date	2020-06-30

ADDITIONAL DETAILS

Order reference number	na	The requesting person / organization to appear on the license	Wei Chen

REUSE CONTENT DETAILS

Title, description or numeric reference of the portion(s)	Figures	Title of the article/chapter the portion is from	. A metal-semiconductor nanocomposite as an efficient oxygen-independent photosensitizer for photodynamic tumor therapy
Editor of portion(s)	na	Author of portion(s)	Guo jia na mi ke xue zhong xin (China),; Royal Society of Chemistry (Great Britain),
Volume of serial or monograph	na	Issue, if republishing an article from a serial	na
Page or page range of portion	1-10	Publication date of portion	2016-01-01

Figure 2.27 (a–f)

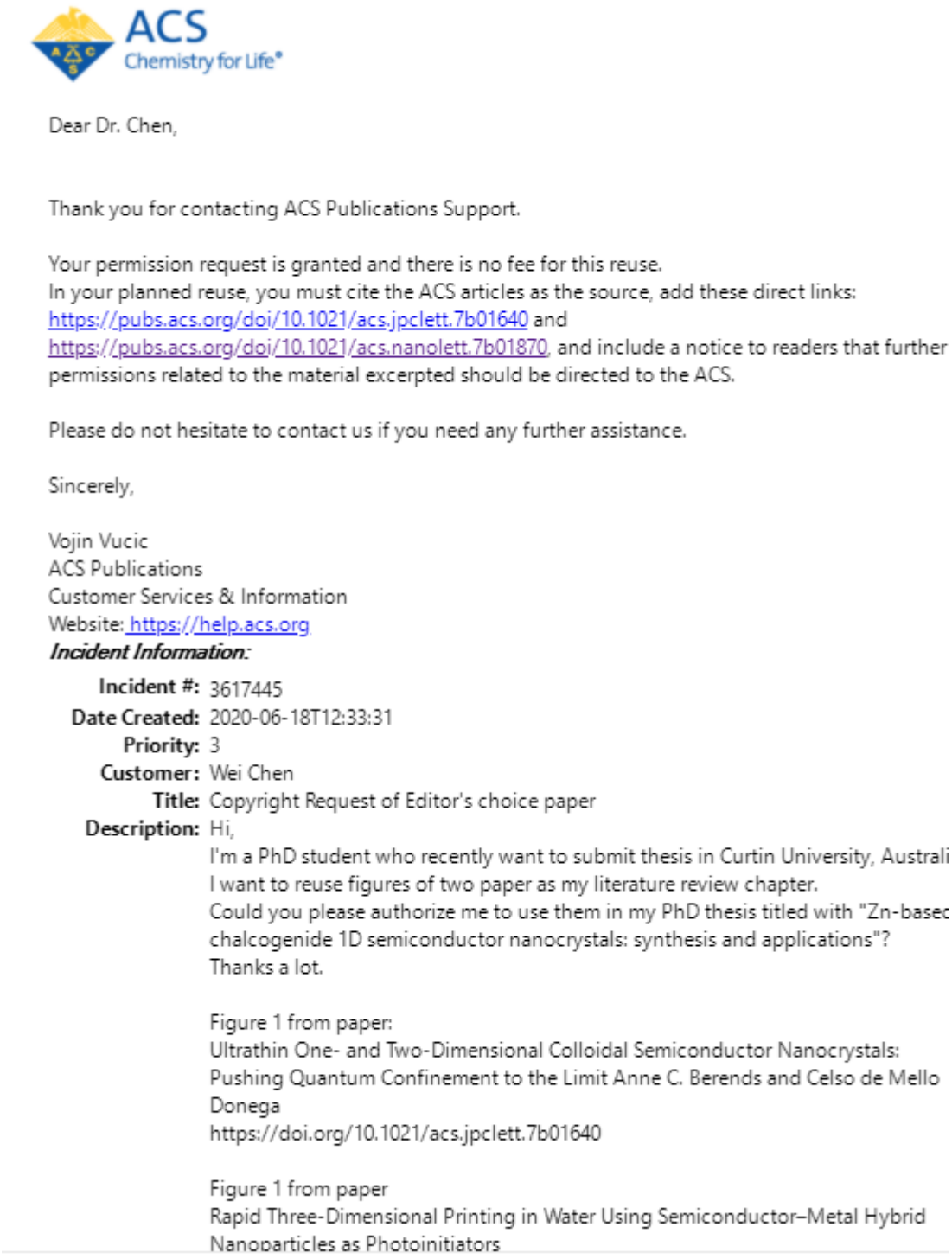

Dear Dr. Chen,

Thank you for contacting ACS Publications Support.

Your permission request is granted and there is no fee for this reuse.
In your planned reuse, you must cite the ACS articles as the source, add these direct links:
https://pubs.acs.org/doi/10.1021/acs.jpclett.7b01640 and
https://pubs.acs.org/doi/10.1021/acs.nanolett.7b01870, and include a notice to readers that further permissions related to the material excerpted should be directed to the ACS.

Please do not hesitate to contact us if you need any further assistance.

Sincerely,

Vojin Vucic
ACS Publications
Customer Services & Information
Website: https://help.acs.org
Incident Information:

Incident #: 3617445
Date Created: 2020-06-18T12:33:31
Priority: 3
Customer: Wei Chen
Title: Copyright Request of Editor's choice paper
Description: Hi,
I'm a PhD student who recently want to submit thesis in Curtin University, Australi
I want to reuse figures of two paper as my literature review chapter.
Could you please authorize me to use them in my PhD thesis titled with "Zn-basec
chalcogenide 1D semiconductor nanocrystals: synthesis and applications"?
Thanks a lot.

Figure 1 from paper:
Ultrathin One- and Two-Dimensional Colloidal Semiconductor Nanocrystals: Pushing Quantum Confinement to the Limit Anne C. Berends and Celso de Mello Donega
https://doi.org/10.1021/acs.jpclett.7b01640

Figure 1 from paper
Rapid Three-Dimensional Printing in Water Using Semiconductor–Metal Hybrid Nanoparticles as Photoinitiators

Appendix B

Statement of contribution to Co–authored paper. (Chapter 4)

To Whom It May Concern I, (Wei Chen), contributed mainly (Wei Chen designed and conducted the experiments, Amir Karton and Tanveer Hussian conducted the Ab calculation. Wei Chen wrote the manuscript and analysed the experimental data including creating figures, tables with support from Guohua Jia. Shaghraf Javaid, Fei Wang, Yingping Pang provided professional comments on manuscript writing and revision.) to the paper/publication entitled (**Wei Chen, Amir Karton, Tanveer Hussian, Shaghraf Javaid, Fei Wang, Yingping Pang and Guohua Jia, Spontaneous shape and phase control of colloidal ZnSe nanocrystals by tailoring Se precursor reactivity, *CrystEngComm,* 2019, 21, 2955**).

(Signature of Candidate)

I, as a Co–Author, endorse that this level of contribution by the candidate indicated above is appropriate.

Wei Chen (Signature of Co–Author 1)

Amir Karton (Signature of Co–Author 2)

Tanveer Hussian (Signature of Co–Author 3)

Shaghraf Javaid (Signature of Co–Author 4)

Fei Wang (Signature of Co–Author 5)

Yingping Pang (Signature of Co–Author 6)

Guohua Jia (Signature of Co–Author 7)

Copyright of published paper.
(Chapter 4)

Spontaneous shape and phase control of colloidal ZnSe nanocrystals by tailoring Se precursor reactivity

W. Chen, A. Karton, T. Hussian, S. Javaid, F. Wang, Y. Pang and G. Jia, *CrystEngComm*, 2019, **21**, 2955
DOI: 10.1039/C9CE00078J

- For reproduction of material from PPS:
  [Original citation] – Reproduced by permission of The Royal Society of Chemistry (RSC) on behalf of the European Society for Photobiology, the European Photochemistry Association, and RSC
- For reproduction of material from all other RSC journals:
  [Original citation] – Reproduced by permission of The Royal Society of Chemistry

If you are the author of this article you still need to obtain permission to reproduce the whole article in a third party publication with the exception of reproduction of the whole article in a thesis or dissertation.

Information about reproducing material from RSC articles with different licences is available on our Permission Requests page.

Statement of contribution to Co–authored paper. (Chapter 5)

To Whom It May Concern I, (Wei Chen), contributed mainly (Wei Chen designed and conducted the experiments, wrote the manuscript and analysed the experimental data including creating figures, tables with support from Guohua Jia, Shaghraf Javaid, Jiayi Chen, Rundong Wang provided professional suggestion on manuscript writing and revision) to the paper (Synthesis of ZnSe, ZnS and ZnSxSe1–x nanorods by a one–pot heat–up method, Wei Chen, Shaghraf, Jiayi Chen, Fei Wang and Guohua Jia).

(Signature of Candidate)

I, as a Co–Author, endorse that this level of contribution by the candidate indicated above is appropriate.

Wei Chen
(Full Name of Co–Author 1) (Signature of Co–Author 1)

Shaghraf Javaid
(Full Name of Co–Author 2) (Signature of Co–Author 2)

Jiayi Chen
(Full Name of Co–Author 3) (Signature of Co–Author 3)

Rundong Mao
(Full Name of Co–Author 4) (Signature of Co–Author 4)

Guohua Jia

(Full Name of Co–Author 6) (Signature of Co–Author 6)

Statement of contribution to Co–authored paper. (Chapter 6)

To Whom It May Concern I, (Wei Chen), contributed mainly (Wei Chen designed and conducted the experiments, Xiaojie Li conducted the photocatalytic experiments, Yuguo Li conducted the DFT calculation. Wei Chen wrote the manuscript and analysed the experimental data including creating figures, tables with support from Guohua Jia. Fei Wang, Shaghraf Javaid, Yingping Pang, Jiayi Chen Zongyou Yin, Shaobin Wang provided professional suggestion on manuscript writing and revision) to the paper/publication entitled (Chen, W., Li, X., Wang, F., Javaid, S., Pang, Y., Chen, J., Yin, Z., Wang, S., Li, Y., Jia, G., Nonepitaxial Gold-Tipped ZnSe Hybrid Nanorods for Efficient Photocatalytic Hydrogen Production. Small 2020, 16, 1902231.).

(Signature of Candidate)

I, as a Co–Author, endorse that this level of contribution by the candidate indicated above is appropriate.

Wei Chen
(Full Name of Co–Author 1) (Signature of Co–Author 1)

Xiaojie Li
(Full Name of Co–Author 2) (Signature of Co–Author 2)

Fei Wang
(Full Name of Co–Author 3) (Signature of Co–Author 3)

Shaghraf Javaid

(Full Name of Co–Author 4) (Signature of Co–Author 4)

Yingping Pang

(Full Name of Co–Author 5) (Signature of Co–Author 5)

Jiayi Chen

(Full Name of Co–Author 6) (Signature of Co–Author 6)

Zongyou Yin

(Full Name of Co–Author 7) (Signature of Co–Author 7)

Shaobin Wang

(Full Name of Co–Author 8) (Signature of Co–Author 8)

Yunguo Li

(Full Name of Co–Author 9) (Signature of Co–Author 9)

Guohua Jia

(Full Name of Co–Author 10) (Signature of Co–Author 10)

Copyright of published paper.(Chapter 6)

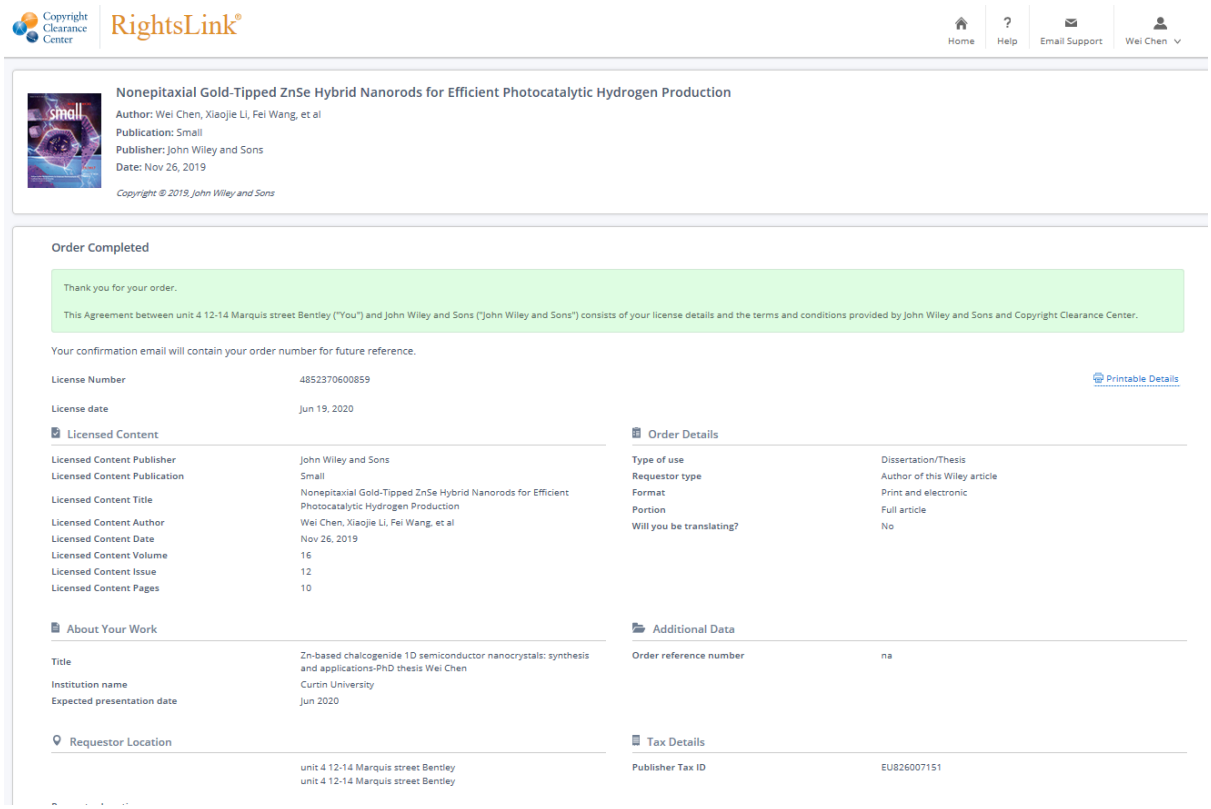

Copyright Clearance Center | RightsLink®

Home | Help | Email Support | Wei Chen

Nonepitaxial Gold-Tipped ZnSe Hybrid Nanorods for Efficient Photocatalytic Hydrogen Production

Author: Wei Chen, Xiaojie Li, Fei Wang, et al
Publication: Small
Publisher: John Wiley and Sons
Date: Nov 26, 2019

Copyright © 2019, John Wiley and Sons

Order Completed

Thank you for your order.

This Agreement between unit 4 12-14 Marquis street Bentley ("You") and John Wiley and Sons ("John Wiley and Sons") consists of your license details and the terms and conditions provided by John Wiley and Sons and Copyright Clearance Center.

Your confirmation email will contain your order number for future reference.

Printable Details

License Number	4852370600859
License date	Jun 19, 2020

Licensed Content

Licensed Content Publisher	John Wiley and Sons
Licensed Content Publication	Small
Licensed Content Title	Nonepitaxial Gold-Tipped ZnSe Hybrid Nanorods for Efficient Photocatalytic Hydrogen Production
Licensed Content Author	Wei Chen, Xiaojie Li, Fei Wang, et al
Licensed Content Date	Nov 26, 2019
Licensed Content Volume	16
Licensed Content Issue	12
Licensed Content Pages	10

Order Details

Type of use	Dissertation/Thesis
Requestor type	Author of this Wiley article
Format	Print and electronic
Portion	Full article
Will you be translating?	No

About Your Work

Title	Zn-based chalcogenide 1D semiconductor nanocrystals: synthesis and applications-PhD thesis Wei Chen
Institution name	Curtin University
Expected presentation date	Jun 2020

Additional Data

Order reference number	na

Requestor Location

unit 4 12-14 Marquis street Bentley
unit 4 12-14 Marquis street Bentley

Tax Details

Publisher Tax ID	EU826007151

Appendix C

Supporting Information for Chapter 4.

Ab Initio Calculations

High–level calculations using double–hybrid density functional theory were performed to probe the reactivity of the Zn^{2+} cation with the possible selenium dianions present in solution (Se^{2-}, Se_2^{2-}, and Se_3^{2-}). Double–hybrid density functional theory (DHDFT) includes non–local correlation from second–order Møller–Plesset (MP2) perturbation theory in addition to the regular ingredients of hybrid DFT[1]. In conjunction with sufficiently large basis sets, [2] DHDFT methods have been found to give structural parameters and reaction energies that are more accurate than those obtained from DFT and MP2 calculations.[1, 3–7] Here we use the spin–component–scaled DSD–PBEP86 DHDFT method of Kozuch and Martin[6, 7] in conjunction with the quadruple–zeta Def2–QZVPP basis set of Weigend and Ahlrichs. [8] Bulk solvent effects were included using the charge–density–based SMD continuum solvation model of Marenich et al. [9] The Gaussian16 suite of programs was used for all the DHDFT calculations[10].

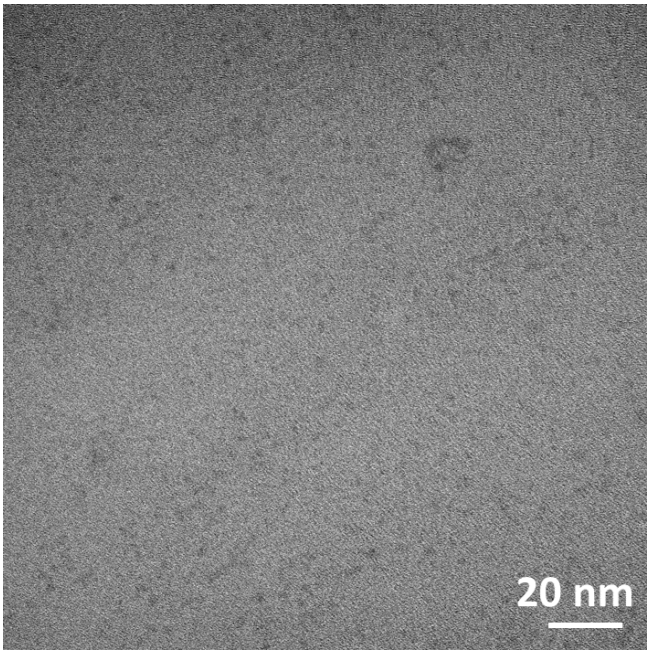

Figure C4-1. TEM image of sample 1 in Figure 4.3

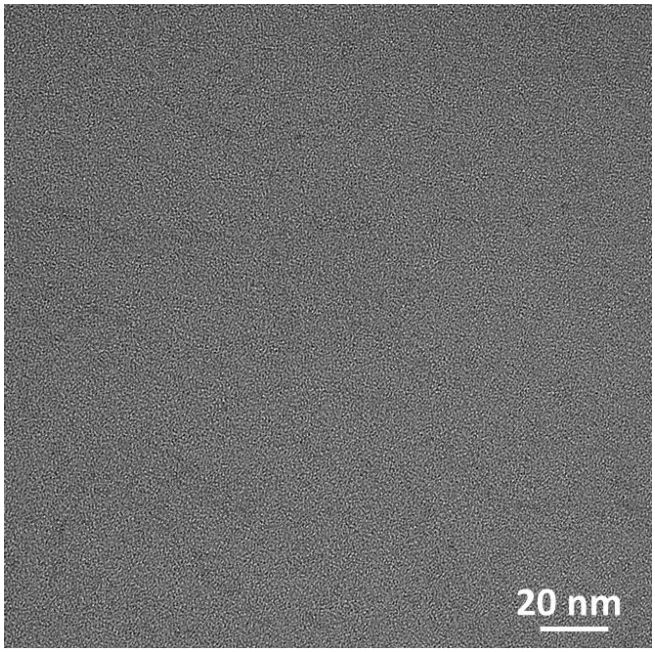

Figure C4-2. TEM image of sample 1 in Figure 4.5

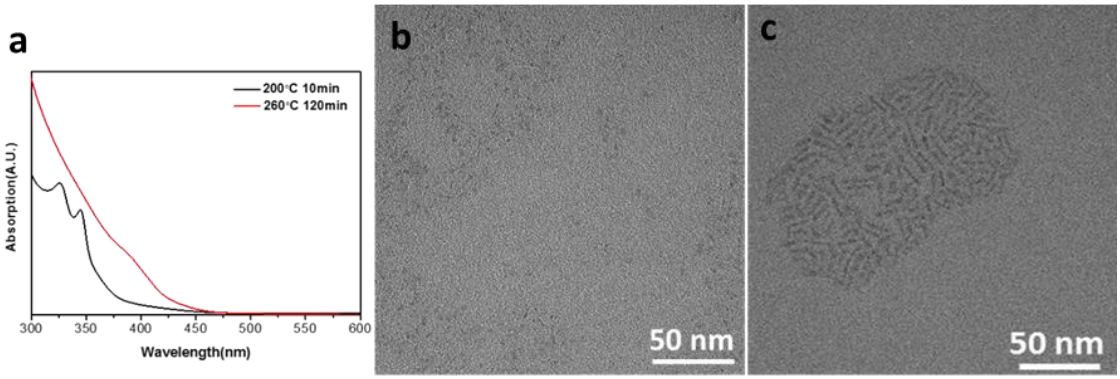

Figure C4-3. ZnSe nanorods synthesized from magic–size small ZnSe nanodots by oriented attachment. (a)Absorbance of ZnSe; (b)Small nanodots at 200ºC; (c) Nanorods at 260ºC from oriented attachment of small nanodots.

Reference:

1. Goerig L, Grimme S. Double–hybrid density functionals. WIREs Comput Mol Sci. 2014;4:25.

2. Karton A, Martin JM. Basis set convergence of explicitly correlated double–hybrid density functional theory calculations. J. Chem. Phys. 2011;135(14):144119.
3. Karton A, Martin JM. Explicitly correlated benchmark calculations on C8H8 isomer energy separations: how accurate are DFT, double–hybrid, and composite ab initio procedures. Mol. Phys. 2012;110:5.
4. Karton A, Sylvetsky N, Martin JML. W4–17: A diverse and high–confidence dataset of atomization energies for benchmarking high–level electronic structure methods. J. Comput. Chem. 2017;38(24):2063–2075.
5. Karton A, Tarnopolsky A, Lamere JF, Schatz GC, Martin JM. Highly accurate first–principles benchmark data sets for the parametrization and validation of density functional and other approximate methods. Derivation of a robust, generally applicable, double–hybrid functional for thermochemistry and thermochemical kinetics. J. Phys. Chem. A. 2008;112(50):12868–12886.
6. Kozuch S, Martin JM. DSD–PBEP86: in search of the best double–hybrid DFT with spin–component scaled MP2 and dispersion corrections. Phys. Chem. Chem. Phys. 2011;13(45):20104–20107.
7. Kozuch S, Martin JM. Spin–component–scaled double hybrids: An extensive search for the best fifth–rung functionals blending DFT and perturbation theory. J. Comput. Chem. 2013;34(27):2327–2344.
8. Weigend F, Ahlrichs R. Balanced basis sets of split valence, triple zeta valence and quadruple zeta valence quality for H to Rn: Design and assessment of accuracy. Phys. Chem. Chem. Phys. 2005;7(18):3297–3305.
9. Marenich AV, Cramer CJ, Truhlar DG. Universal solvation model based on solute electron density and on a continuum model of the solvent defined by the bulk dielectric constant and atomic surface tensions. J. Phys. Chem. B. 2009;113(18):6378–6396.
10. Frisch MJ, Trucks GW. Gaussian 16 Rev. B.01. Wallingford, CT2016.

Appendix D

Supporting information for Chapter 5.

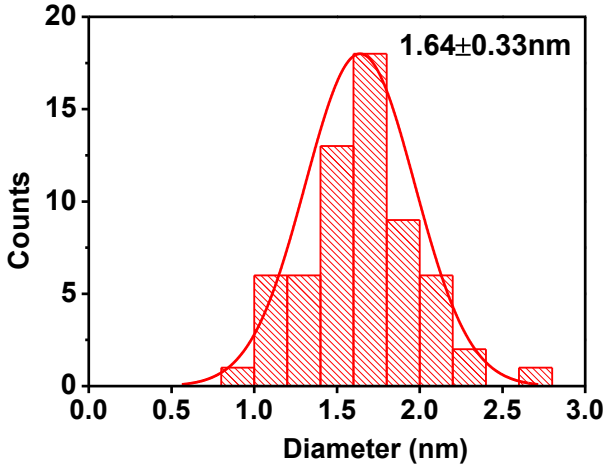

Figure D5-1. Diameter histogram of ZnS nanorods synthesized at 220 ºC for 20 mins ºC

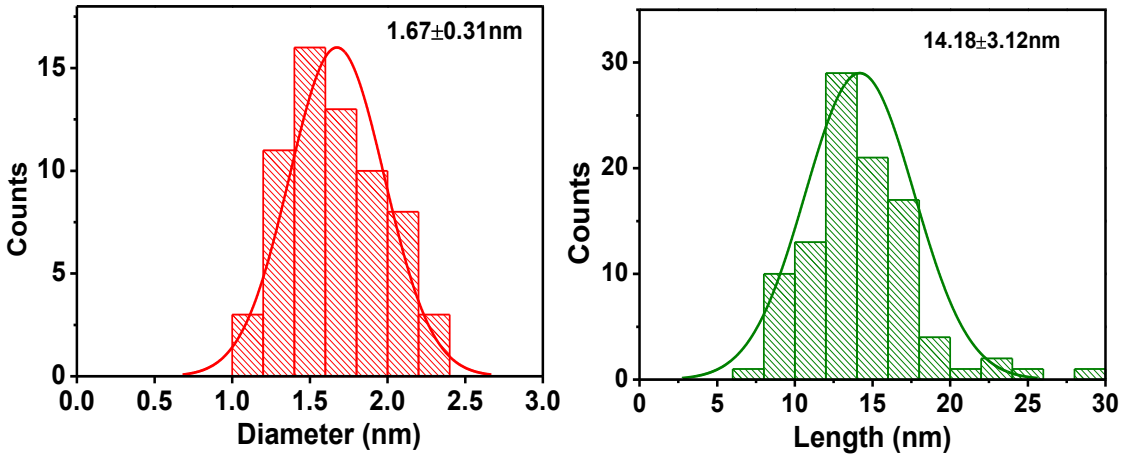

Figure D5-2. Diameter and length hisgram of ZnS nanorods synthesized at 240 ºC for 20 mins

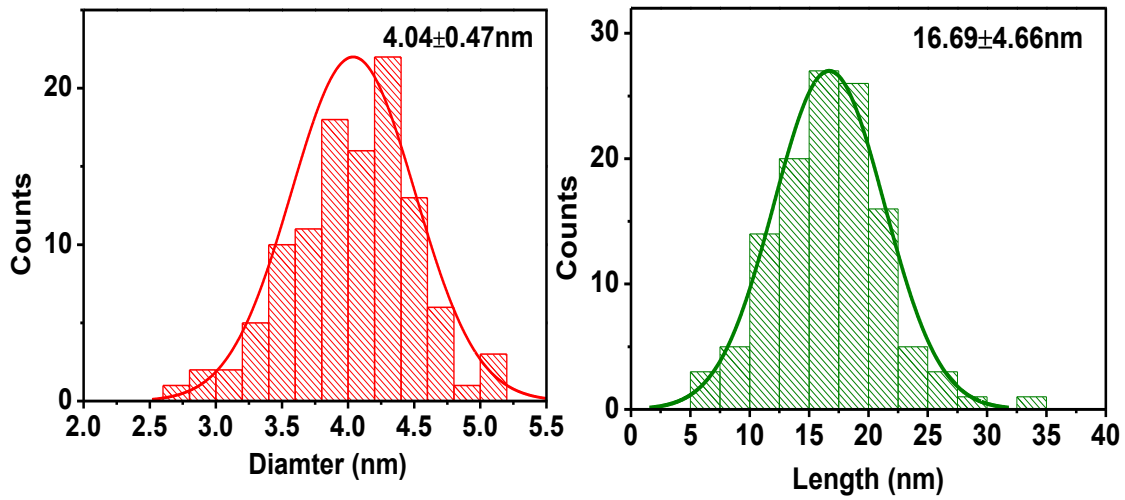

Figure D5-3. Diameter and length histogram of ZnS nanorods synthesized at 260 °C for 20 mins.

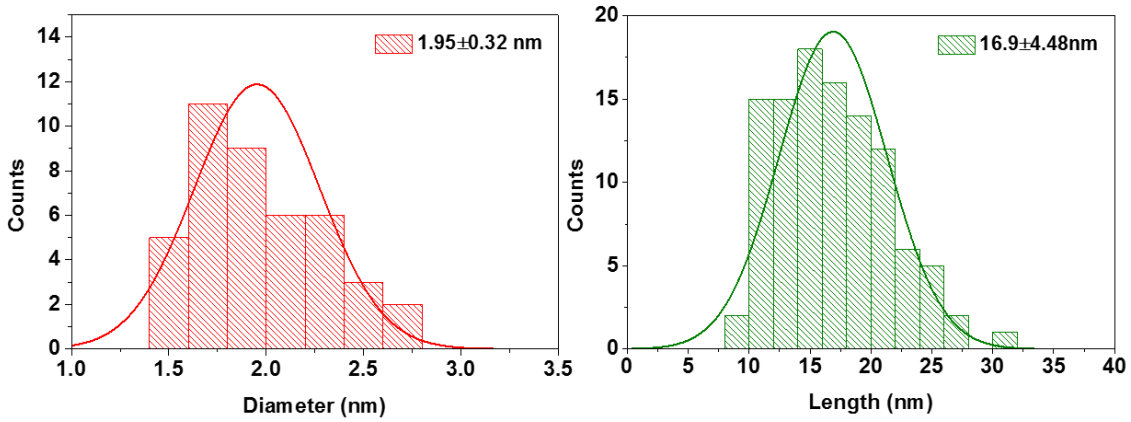

Figure D5-4. Diameter and length histogram of ZnSe nanorods synthesized at 220 °C for 20 mins

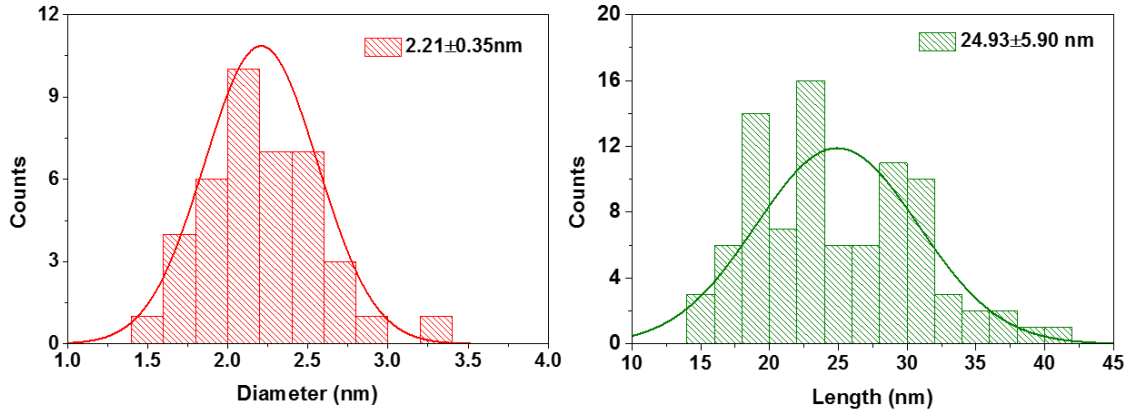

Figure D5-5. Diameter and length histogram of ZnSe nanorods synthesized at 240 °C for 20 mins

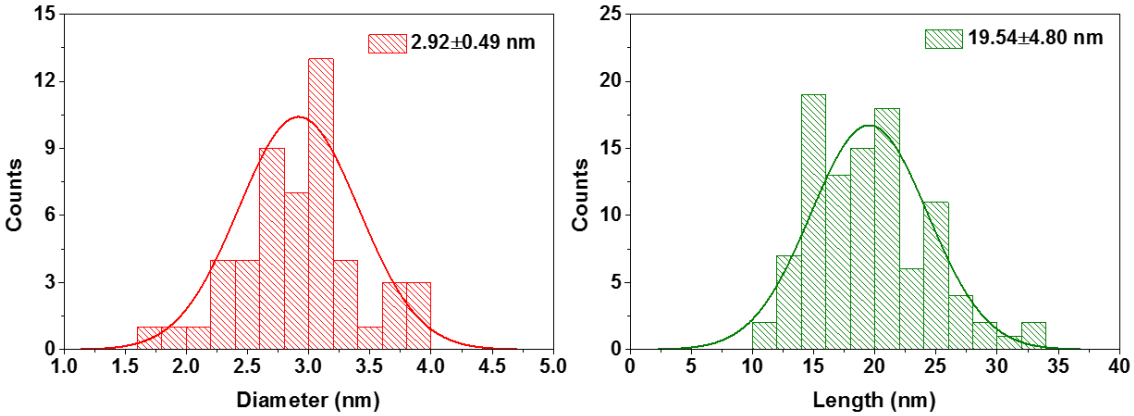

Figure D5-6. Diameter and length hisgram of ZnSe nanorods synthesized at 260°C for 20 mins

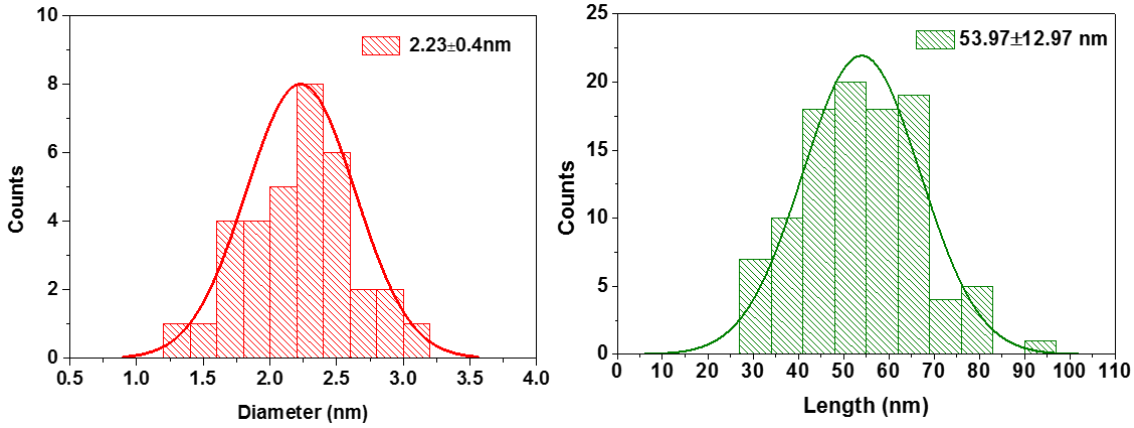

Figure D5-7. Diameter and length histogram of $ZnSe_xS_{1-x}$ nanorods synthesized in DDT and OLA at 260 °C for 20 mins

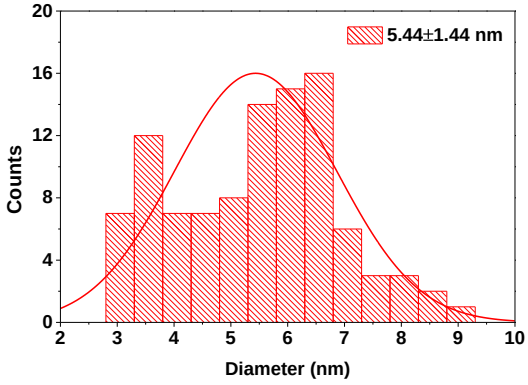

Figure D5-8. Diameter histogram of ZnS nanodots synthesized in OLA at 260 °C for 20 mins

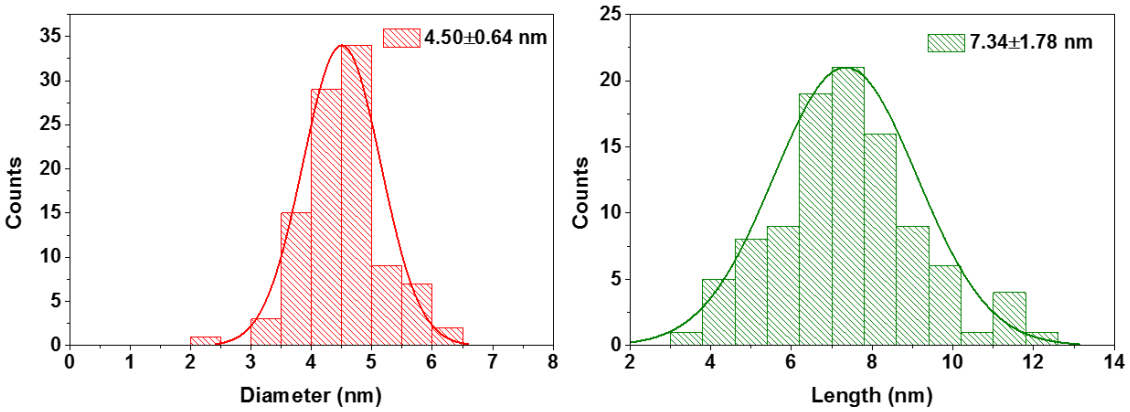

Figure D5-9. Diameter and length histogram of ZnSe peanut–shape nanoparticles synthesized in OLA at 260 °C for 20 mins

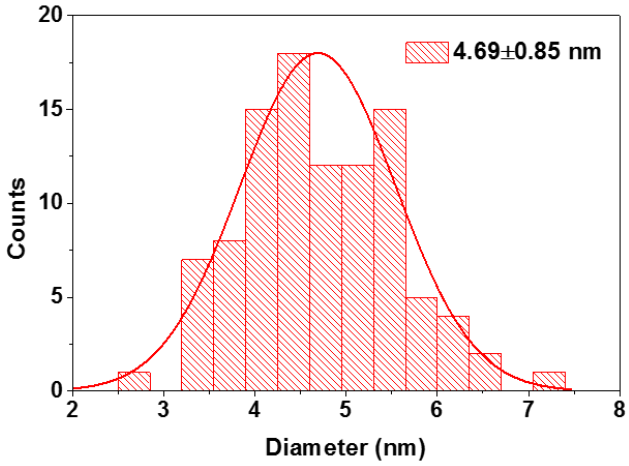

Figure D5-10. Diameter and length histogram of ZnS_xS_{1-x} peanut–shape nanoparticles synthesized in OLA at 260°C for 20 mins

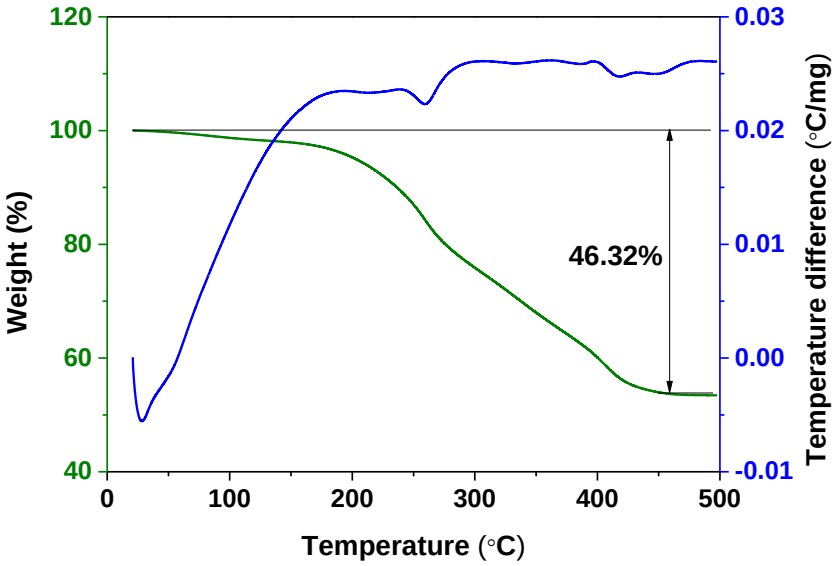

Figure D5-11. Thermal gravimetric analysis (TGA) of ZnS nanorods performed under N_2. The mass loss corresponded to the ligand detachment and the remaining mass was the mass of ZnS nanoparticles.

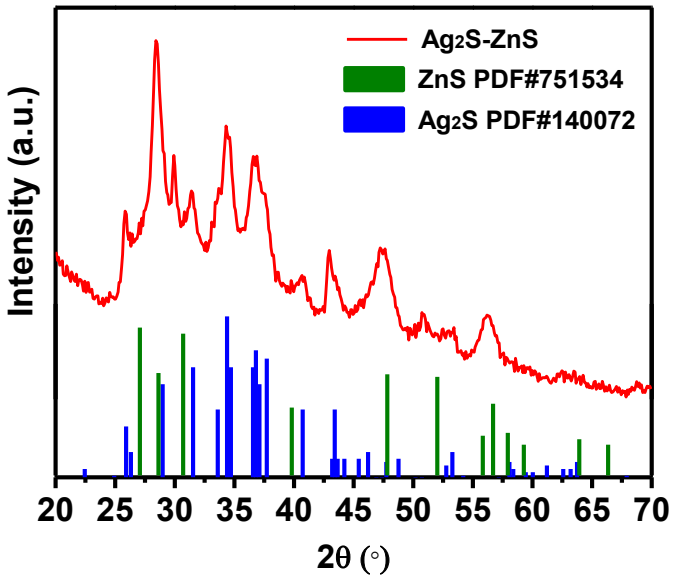

Figure D5-12. XRD pattern of ZnS–Ag_2S hybrid nanorods obtained by cation exchange. The diffraction peaks were indexed to the standard wurtzite ZnS (JCPDS Card File 751534, green column) and monoclinic Ag_2S (JCPDS Card File 140072, blue column).

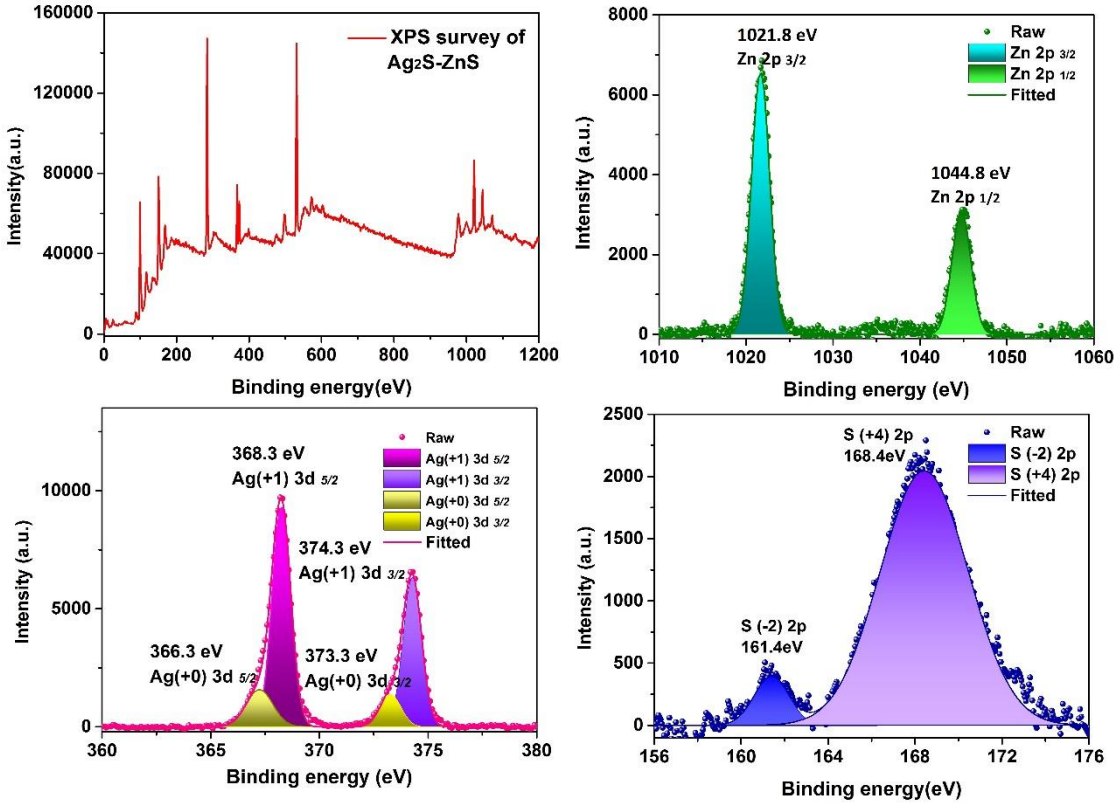

Figure D5-13. XPS spectra of Zn 2p, Ag 3d and S 2p of ZnS–Ag_2S hybrid nanorods.

The binding energies of 1044.4 and 1021.4 eV were assigned to Zn^{2+}. The peaks at 374.3 and 368.8 eV were assigned to Ag $3d_{3/2}$ and Ag $3d_{5/2}$ of Ag^+ ions in Ag_2S, respectively. The peaks at 373.3 and 366.8 eV were assigned to Ag $3d_{3/2}$ and Ag $3d_{5/2}$ of Ag (0) metal, respectively, which could be formed by oxidation of Ag_2S. The binding energies locate at 161.4 eV and 168.4 eV matching well with that of S^{2-} 2p from ZnS–Ag_2S and the 168.4 eV was assigned to S^{4+} 2p which resulted from the oxidation of ZnS or Ag_2S. Overall, the XPS spectra confirmed that a part of ZnS was replaced by Ag_2S during the cation exchange process.

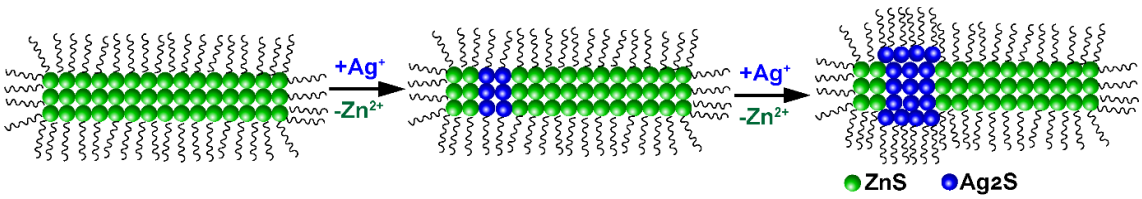

Figure D5-14. Schematic diagram of the formation mechanism of ZnS–Ag_2S nanorods by cation exchange

Appendix E

Supporting information for Chapter 6.

Density functional theory (DFT) calculations

DFT calculations were performed using the Vienna *Ab initio* Simulations Package (VASP)[4,5] and projected augmented wave (PAW)[6–8] method (with $1s^1$, $5d^{10}6s^1$, $4s^24p^4$, $3d^{10}4s^2$ as valence electrons for H, Au, Se and Zn, respectively). The exchange–correlation interaction was treated with generalized gradient approximation (GGA) in the Perdew, Burke and Ernzerhof (PBE)[9] parameterization. The cutoff energy of plane–wave basis was set to 450 eV for ZnSe and 400 eV for Au. Integrations over the first Brillouin zone were calculated using a Gamma–centred **k**–point set of 6×6×4 for wurtzite ZnSe (space group $P6_3mc$, No. 186) and 12×2×12 for fcc Au. With these settings, the total energy was able to converge within 1 meV/atom. The structures were fully relaxed using PBE, and the energy was converged within 10^{-6} eV/cell and the force was converged to less than 10^{-4} eV/Å. We adopted GGA+U (U=8 and J=1)[10,11] to correct the self–interaction and over delocalized *d* states in wurtzite ZnSe.

The detailed interface structure of ZnSe (001) and Au (111) was explored thoroughly. First, we scanned the potential energy surface (PES) of interfacing ZnSe (001) and Au (111). We built a 3x3x4 supercell of ZnSe containing 16 alternating Zn and Se layers along the (001) of which the top 11 layers were removed. The remained layers are terminated by Zn. We then removed the top Zn layer and added four fcc Au (111) layers on the top. The Au fcc lattice is therefore subjected to a strain of 1.4%, which is within the DFT error. We then mapped the PES of this interface structure (denoted as ZnSe(001)//Au (111)) by moving around the Au layers together. The interfacing Se layer and four Au (111) layers were allowed to relax completely. The in–plane coordinates of the top Au (111) layer and the other ZnSe layers were fixed. All the PES calculations for the interface were performed at the PBE level with an energy cutoff of 450 eV and a single Gamma point sampling. This calculation detail is for Figure 5a and 5b.

Supporting Figures

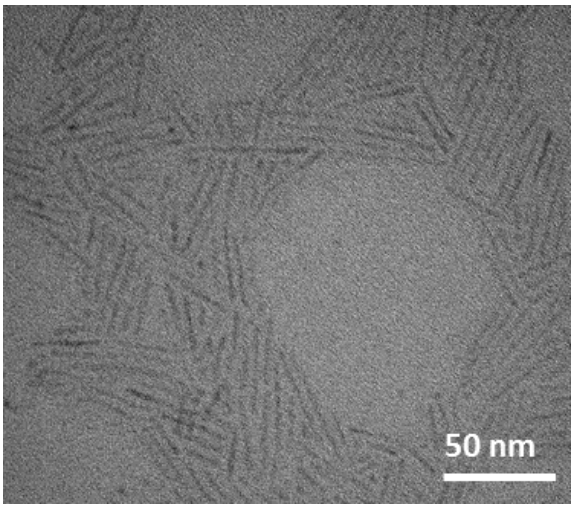

Figure E6-1. TEM image of ZnSe NRs.

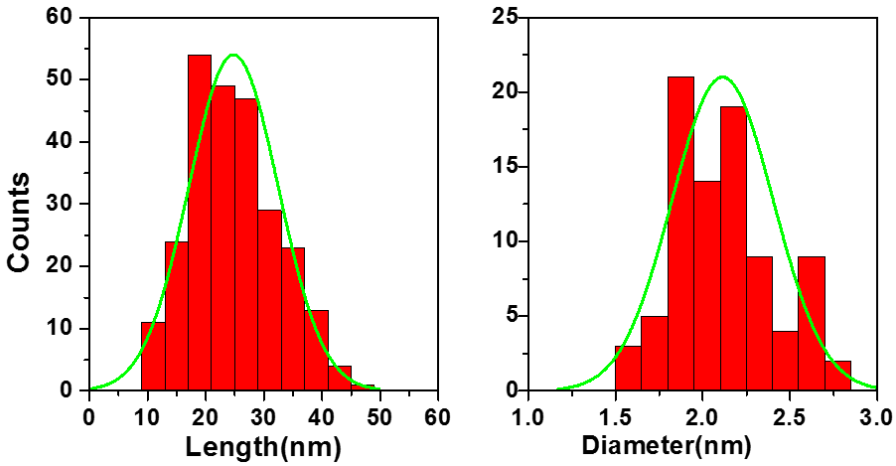

Figure E6-2. Sizing histograms of ZnSe NRs. The average sizes of ZnSe NRs are 2.1 ± 0.3 nm in diameter and 24.8 ± 7.7 nm in length.

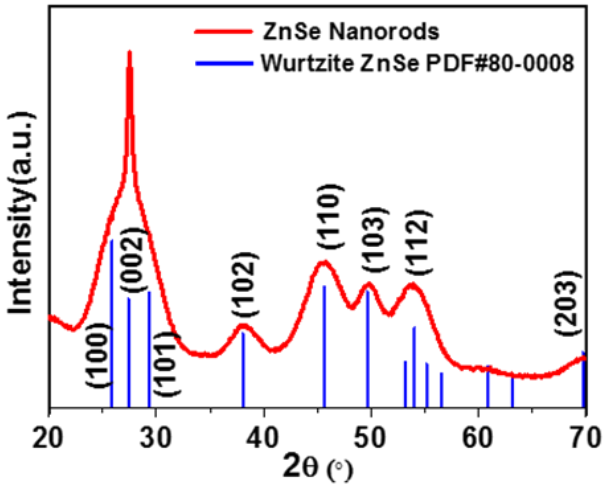

Figure E6-3. XRD pattern of ZnSe NRs. The standard XRD pattern for wurtzite ZnSe was given for reference.

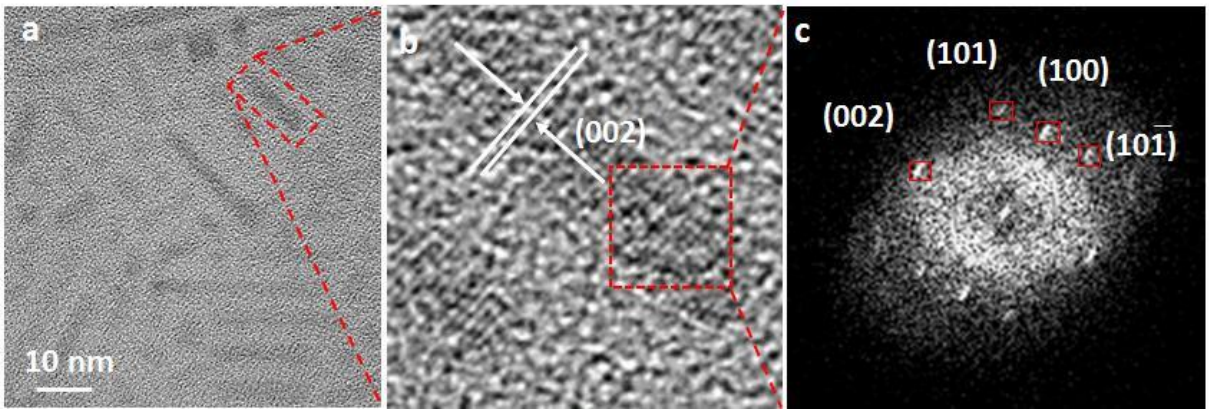

Figure E6-4. Electron microscopic characterizations of ZnSe NRs. (a) TEM image, (b) HRTEM image, (c) FFT of the selected area in (b).

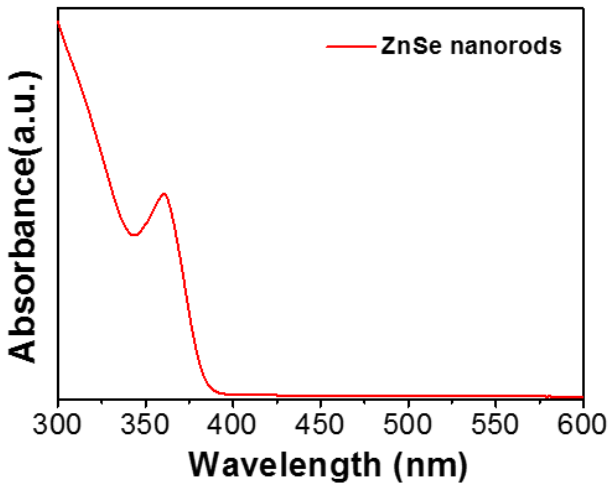

Figure E6-5. UV–Vis absorption spectrum of ZnSe NRs.

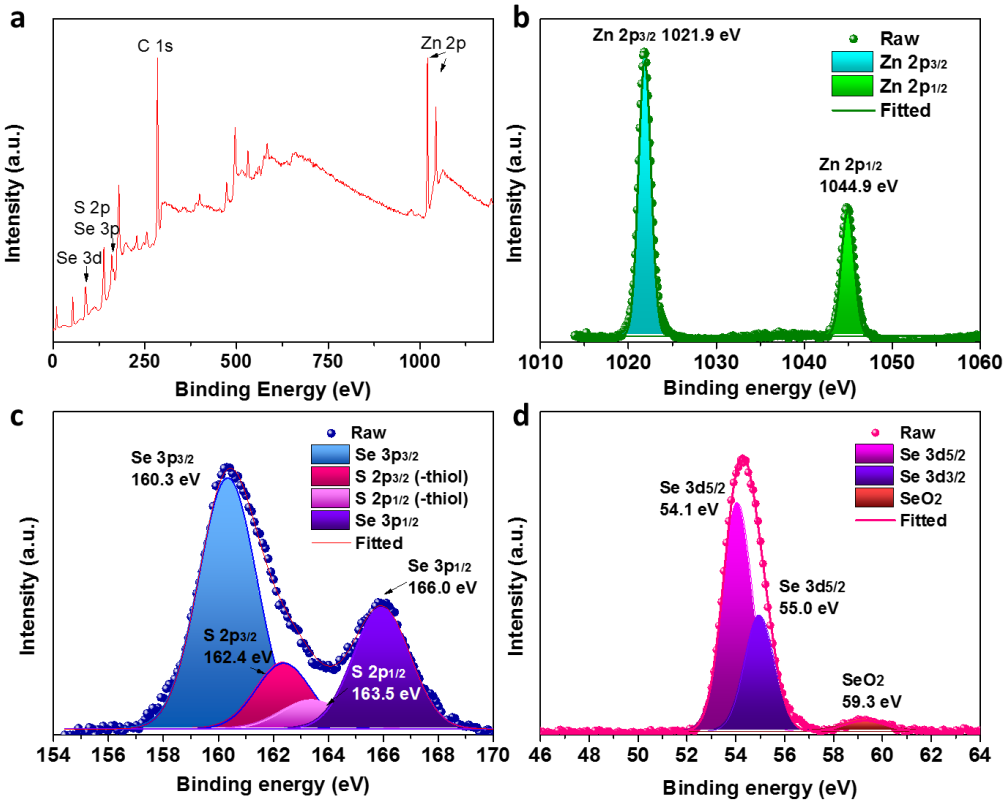

Figure E6-6.XPS spectra of ZnSe NRs synthesized in DDT+OLA; (a) Survey spectrum; (b–d) Binding energy peaks of (b) Zn 2p; (c) Se 3d; (d)Se 3p

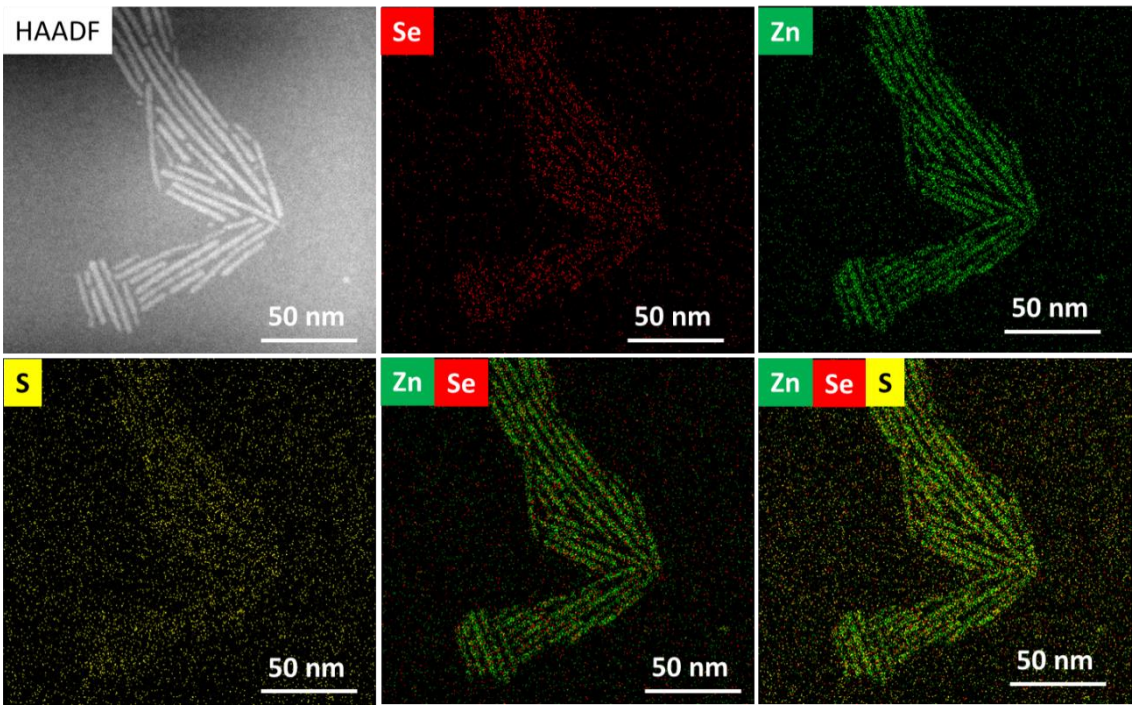

Figure E6-7. HAADF–STEM image and EDS mapping of Se, Zn and S of synthesized ZnSe NRs.

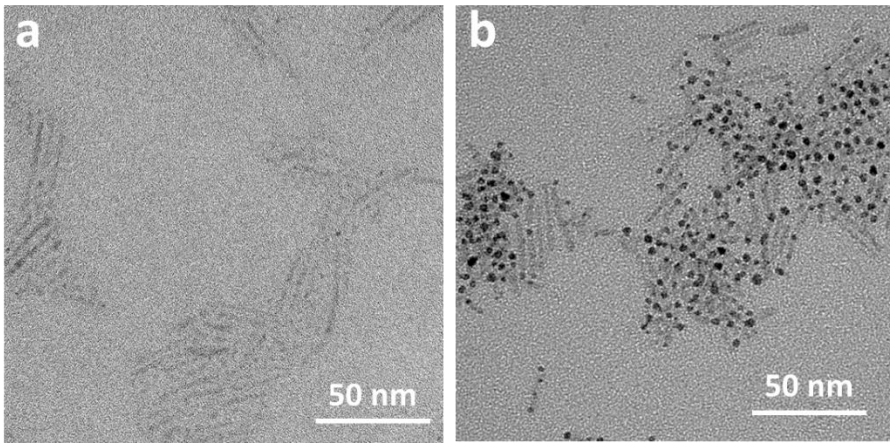

Figure E6-8. TEM images of Au–ZnSe hybrid NRs with variable molar ratios of $AuCl_3$ and ZnSe for growth. (a) 127:1; (b) 2540:1.

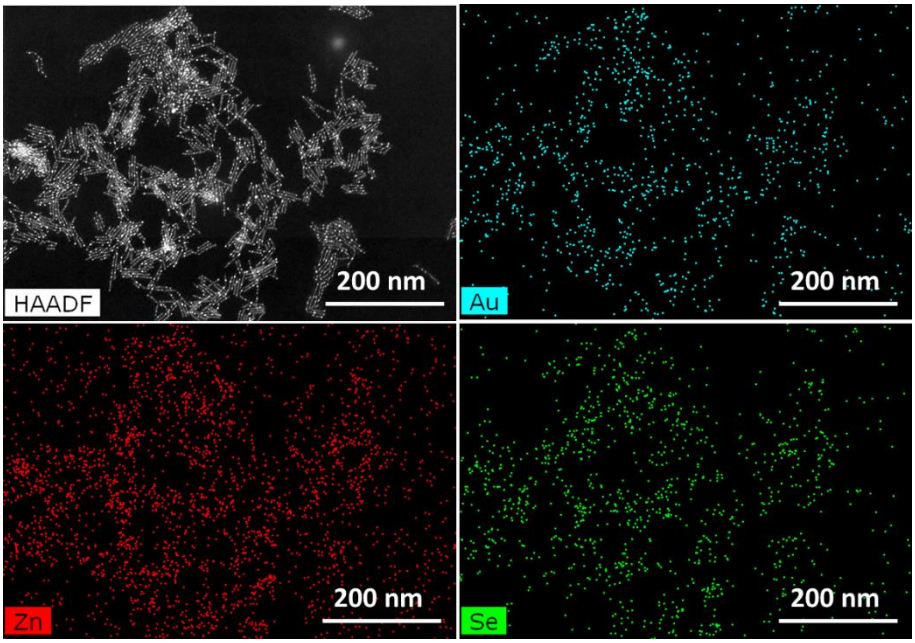

Figure E6-9. HAADF–STEM images of Au–ZnSe hybrid NRs and the corresponding EDS mapping of the elements Au, Se, and Zn.

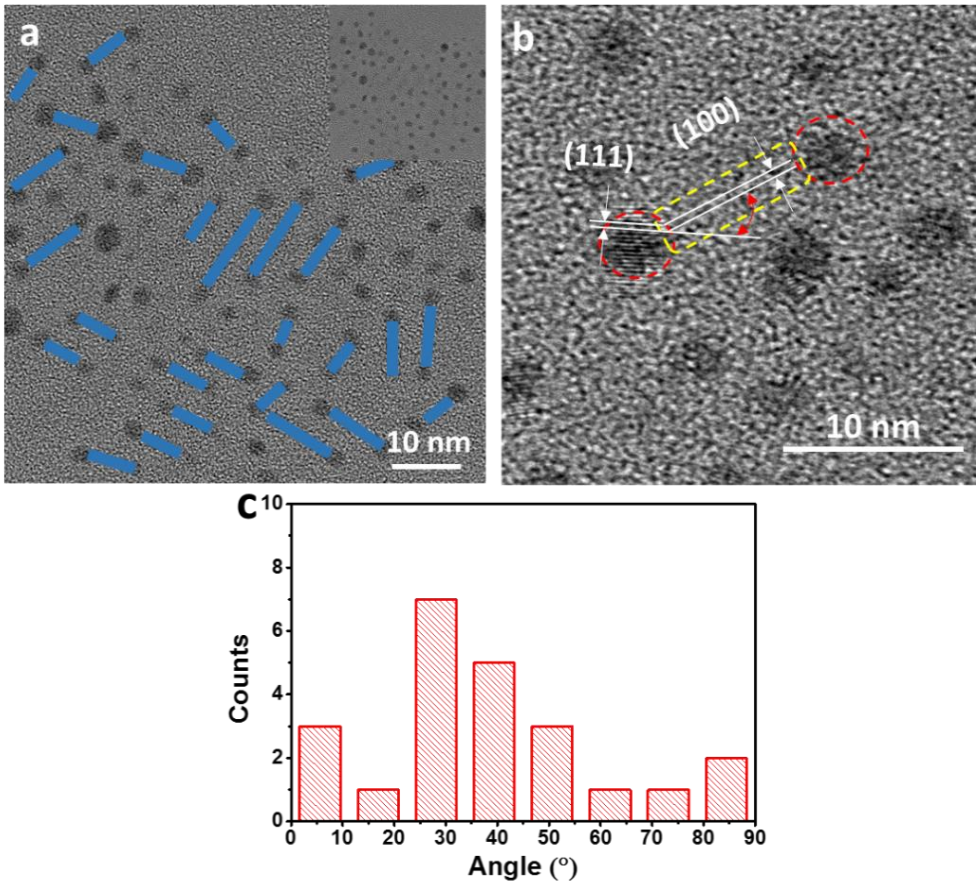

Figure E6-10. (a) TEM images of Au–ZnSe hybrid NRs. Blue lines indicates the orientation of the long axis of ZnSe NRs; (b) HRTEM image of a sample revealing the angle between (111) facet of Au tips and (100) facet of ZnSe NRs; (c)Statistics of the angle between (111) facet of Au tips and (100) facet of ZnSe NRs

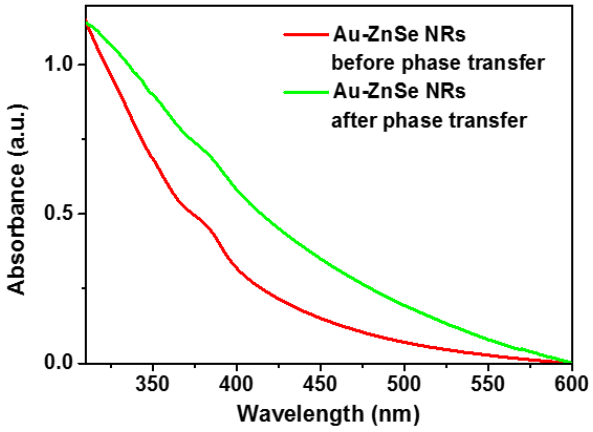

Figure E6-11. Comparision of the absorption spectra of Au–ZnSe hybrid NRNRs before and after the phase transfer in water using PEI.

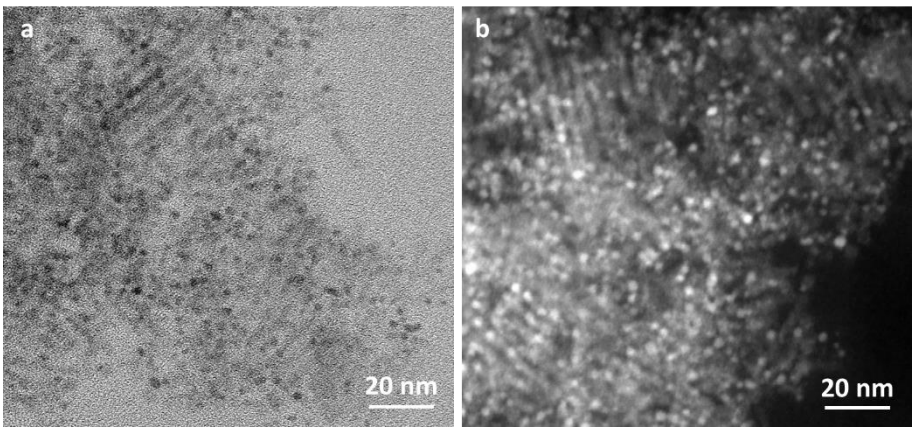

Figure E6-12. TEM and STEM of double Au–tipped ZnSe NRs coated by PEI after phase transfer (in water).

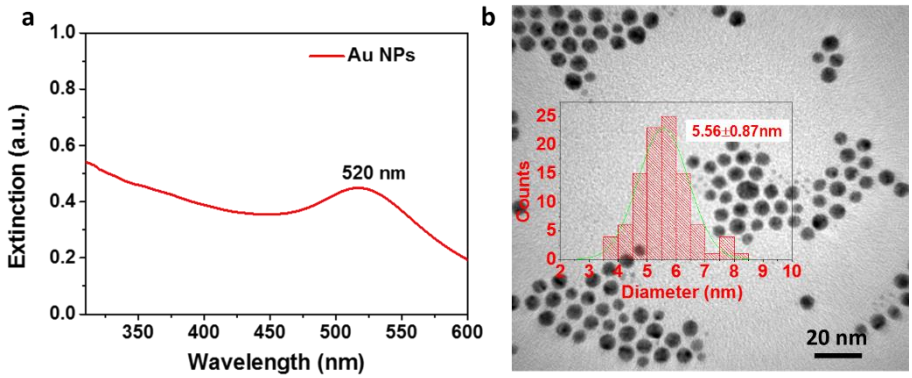

Figure E6-13. (a) Extinction spectrum of Au NPs, (b) TEM image of Au NPs. Inset of (b) shows the sizing histogram of Au NPs with an average diameter of 5.56 ± 0.87 nm.

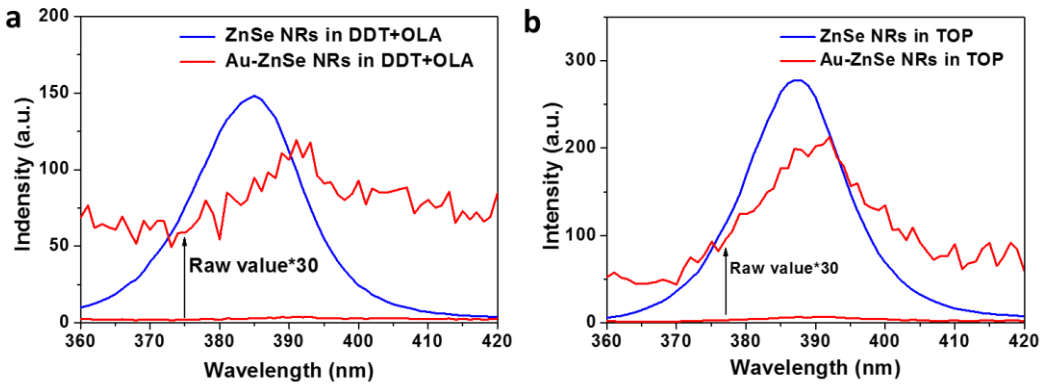

Figure E6-14. (a) Photoluminescence of ZnSe NRs and Au–ZnSe hybrid NRs coated by DDT and OLA; (b) Photoluminescence of ZnSe NRs and Au–ZnSe hybrid NRs coated by TOP.

Table E6-1. The lattice plane spacings of synthesized ZnSe NRs and standard wurtzite ZnSe.

Plane X	Theoretical plane distance (Å) of ZnSe	Theoretical angle (°) between plane X and (002) of ZnSe	Measured plane distance (Å) of ZnSe	Measured angle (°) between plane X and (002) of ZnSe
(100)	3.4416	90	3.4801	89.24
(002)	3.2530	0	3.2483	0
(101)	3.0422	62.15	3.1167	62.69
$(10\bar{1})$	3.0422	117.86	3.0912	120.63

Table E6-2. Comparison of the transfer efficiencies of Zn and Se elements of pure ZnSe NRs, single Au–tipped ZnSe NRs and double Au–tipped ZnSe NRs before and after phase transfer.

	Sample	Mass (mg)	Zn element concentration (mg/L)	Zn content (mg)	Se concentration (mg/L)	Se content (mg)	Transfer efficiency of Zn (%)	Transfer efficiency of Se (%)
Before phase transfer	ZnSe NRs	2.65	32	0.8	35	0.875	–	–
	Single Au–tipped ZnSe NRs	2.62	27	0.675	29	0.725	–	–
	Double Au–tipped Au–ZnSe NRs	2.30	18	0.45	23	0.575	–	–
After phase transfer	ZnSe NRs	2.65	29	0.725	32	0.8	90.6	91.4
	Single Au–tipped ZnSe NRs	2.54	24	0.6	26	0.65	91.6	92.4
	Double Au–tipped ZnSe NRs	2.63	19	0.475	24	0.6	92.3	91.2

Note: For samples after phase transfer, samples mass refers to the weighed mass before phase transfer.

Transfer efficiency is calculated by the following formula:

$$\text{Transfer efficiency for Zn (\%)} = \frac{Zn\ content\ after\ transfer}{Zn\ content\ before\ transfter} * 100$$

$$= \frac{Zn\ content\ after\ transfer}{ZnSe\ NRs\ mass\ before\ transfer * Zn\ percentage} * 100$$

$$\text{Zn percentage of pure ZnSe NRs (\%)} = \frac{Zn\ content\ of\ ZnSe\ NRs\ before\ transfer}{ZnSe\ NRs\ \ mass\ before\ transfter} * 10$$

Taking Zn transfer efficiency of ZnSe NRs for example:

$$\text{Zn percentage of bare ZnSe NRs (\%)} = \frac{0.8}{2.65} * 10 = 30.18\%$$

$$\text{Transfer efficiency for Zn (\%)} = \frac{0.725}{2.65 * 0.3018} * 100 = 90.6\%$$

References

1. Selvaraj J, Mahesh A, Asokan V, et al. Phosphine–Free, Highly Emissive, Water–Soluble Mn: ZnSe/ZnS Core–Shell Nanorods: Synthesis, Characterization, and in Vitro Bioimaging of HEK293 and HeLa Cells. ACS Appl. Nano Mater. 2017; 1(1): 371–383.

2. Hiramatsu H, Osterloh F E. A simple large–scale synthesis of nearly monodisperse gold and silver nanoparticles with adjustable sizes and with exchangeable surfactants. Chem. Mater. 2004; 16(13): 2509–2511.

3. Pang F, Zhang R, Lan D, et al. Synthesis of magnetite–semiconductor–metal trimer nanoparticles through functional modular assembly: a magnetically separable photocatalyst with photothermic enhancement for water reduction. ACS Appl. Mater. Interfaces. 2018; 10(5): 4929–4936.

4. Kresse G, Joubert D. From ultrasoft pseudopotentials to the projector augmented–wave method. Phys. Rev. B.1999; 59(3): 1758.

5. Kresse G, Furhmuller J. Software VASP, Vienna (1999); PE BlöchlJ. . Phys. Rev. B. 1994; 50: 17953.

6. Kresse G, Furthmüller J. Efficiency of ab–initio total energy calculations for metals and semiconductors using a plane–wave basis set. Comput. Mater. Sci. 1996;6(1): 15–50.

7. Kresse G, Furthmüller J. Self–interaction correction to density functional approximation for many electron systems. Phys. Rev. B. 1996; 54: 11169.

8. Kresse G, Hafner J. Ab initio molecular dynamics for open–shell transition metals. Phys. Rev. B. 1993; 48(17): 13115.

9. Perdew J P, Burke K, Ernzerhof M. Generalized gradient approximation made simpleJ. . Phys. Rev. Lett. 1996;77(18): 3865.

10. Dudarev S L, Botton G A, Savrasov S Y, et al. Electron–energy–loss spectra and the structural stability of nickel oxide: An LSDA+ U study. Phys. Rev. B. 1998;57(3): 1505.

11. Miyake T, Zhang P, Cohen M L, et al. Quasiparticle energy of semicore d electrons in ZnS: Combined LDA+ U and G W approach. Phys. Rev. B. 2006;74(24): 245213.